

Mesoproterozoic to Early Devonian Evolution of the Lyderhorn Gneiss (Øygarden Complex, SW Norway)

Constraints from Field Mapping and U-Pb Zircon Geochronology

Master of Science Thesis in Geoscience

Johannes Daniel Wiest



Department of Earth Science

University of Bergen

June 2016

Abstract

The Øygarden Complex and the Bergen Arc System are intriguing large-scale structures in the SW Norwegian Caledonides, but their formation is still incompletely understood. So far, the lack of published U-Pb zircon ages has limited clear interpretations of the geologic evolution of the Øygarden Complex. The Lyderhorn Gneiss is located in the poorly studied eastern part of the Øygarden Complex and forms the core of the Bergen Arc. Detailed field mapping was conducted and seven samples were dated by SIMS U-Pb zircon geochronology, to study the magmatic and structural formation of the Lyderhorn Gneiss.

Igneous protoliths formed during the Mesoproterozoic Gothian-Telemarkian (1504 Ma) and Sveconorwegian (1041 Ma and 1026 - 1022 Ma) orogenic periods. They do not record Sveconorwegian high-grade regional metamorphism. Early Ordovician (483 Ma) thermal resetting of metamict zircons was followed by sustained residence at elevated temperatures that annealed previous radiation damage. The U-Pb zircon system was not affected by Caledonian amphibolite facies metamorphism. The structure of the Lyderhorn Gneiss formed in one single deformation event, recorded in ENE-directed exhumational deformation from amphibolite facies to the brittle-plastic transition. Fluid-assisted strain weakening formed phyllonitic E-dipping detachment shear zones that became finally overprinted by (semi-)brittle deformation.

Based on the Mesoproterozoic protolith ages, the Lyderhorn Gneiss and thereby the Øygarden Complex are correlated with the Telemarkia domain of the Baltican basement. The age of magmatism relates the Øygarden Complex with the Sirdal Magmatic Belt of southern Norway. The correlation suggests a continuous NNW-trend of Sveconorwegian domain boundaries and supports the assertion that Sveconorwegian high-T metamorphism in the Baltican basement was rather local than regional. A rapid temperature increase in the Early Ordovician is interpreted to mark the onset of Caledonian convergence. The structure of the Lyderhorn Gneiss is constrained to have formed by Early Devonian extensional deformation. Bidirectional Devonian extension in the Øygarden Complex is explained by exhumation as a Devonian extensional gneiss dome.

The proposed, symmetrical core complex style of exhumation, resembles previously identified core complexes in central Norway and allows for a more consistent interpretation of basement culminations along the Norwegian margin. Possible onshore-offshore correlations are suggested for the Utsira High in the northern North Sea. Detailed structural and thermochronological studies will be needed to test the proposed model.

Acknowledgements

This work would not have been possible without the help and support of the following persons:

In the first place, I would like to thank my supervisors Prof. Joachim Jacobs, Dr. Anna Ksienzyk and Prof. Haakon Fossen for excellent supervision during my M.Sc. studies at the University of Bergen. I thank Joachim and Anna for giving me the opportunity to study in Bergen, for finding and offering me this exciting project and for outstanding supervision and support during all the different phases of this challenging work. I have learned very much from both of them about systematic scientific work. Numerous discussions and critical but always supportive feedback were of invaluable help. I thank Haakon for sharing his knowledge very openly, for helpful discussions, assistance in the field and that I could participate in the Brasil-Norway summer school, to learn more about the regional geology of SW Norway. Tusen takk, to all of you.

I would like to thank the Department of Earth Science for hosting and supporting my studies. I thank particularly everyone, who contributed kindly and with great effort in the practical work of this project. Irina Dumitru prepared numerous thin sections and helped with the mineral separation. Martian Suppersberger Hamre introduced me to crushing and mineral separation techniques. Egil Erichsen and Irene Heggstad were of great help with cathodoluminescence imaging. Rolf Birger Pedersen and Hamed Fazli Khani contributed with fruitful discussions. Leif-Erik Pedersen helped with thin section photos.

I thank Martin Whitehouse, Lev Ilinsky and Kerstin Lindén at the Nordsim facility in Stockholm for great help with SIMS geochronology. Many thanks to Helge Askvik for introducing me to the geology of Askøy.

Trond Slagstad and Nolwenn Coint are thanked for inviting me to Trondheim, for amazing hospitality and for very helpful discussions together with Per Terje Osmundsen and Tim Redfield. I thank the German Academic Exchange Service (DAAD) for support during the second year of my M.Sc. studies that allowed me to fully concentrate on the project.

Thanks to Sebastian Wolf and Felix Halpaap for helpful discussions on walks in the park. I thank all present and former members of the Bergen Tectonics and Thermochronology Group and the Hjørnerommet for good company during my studies at UiB.

Finally, I want to thank my whole family and Vilde for understanding my passion for rocks.

Bergen, 31.05.2016



Johannes Wiest

Contents

1	Introduction	1
2	Regional Geology	3
2.1	Pre-Caledonian - The Formation of Baltica	3
2.2	The Caledonian Orogeny	9
2.3	Post-Caledonian Development	16
2.4	Geology of the Bergen Arc System	16
3	Principles of U-Pb Zircon Geochronology	25
3.1	U-Pb System in Zircon	25
3.2	SIMS Geochronology	26
4	Methods	28
4.1	Mapping and Sampling	28
4.2	SIMS U-Pb Zircon Geochronology	29
4.2.1	Sample Preparation	29
4.2.2	SIMS Analysis	30
5	Results	32
5.1	Mapping	32
5.1.1	Petrology	33
5.1.2	Structure	39
5.2	U-Pb Zircon Geochronology	56
5.2.1	Sample LYD-197-1	57
5.2.2	Sample LYD-44-1	58
5.2.3	Sample LYD-35-1	60
5.2.4	Sample LYD-169-1	61
5.2.5	Sample LYD-83-1	63
5.2.6	Sample LYD-197-2	64
5.2.7	Sample LYD-163-1	66
5.2.8	Summary of Geochronological Results	68
6	Discussion	70
6.1	Geochronology	70
6.1.1	Interpretation of Acquired Ages	70
6.1.2	Igneous Formation of the Lyderhorn Gneiss and Regional Correlations	75
6.1.3	Significance of Ages for the Regional Geology of SW Norway	77
6.2	Structure	81
6.2.1	Comparison of Structural Data with Selected Previous Studies	81
6.2.2	Structure of the Lyderhorn Gneiss in the Caledonian Orogeny	83
6.2.3	Reinterpretation of the Øygarden Complex as a Devonian Extensional Gneiss Dome	90

7	Conclusion	96
8	Future Work	97
9	Appendix	109

1 Introduction

Geological maps provide regional geological models that are the common ground of diversified geoscientific research disciplines. Most areas of SW Norway are covered by geological maps since several decades. So why conducts a M.Sc. thesis in 2016 basic field mapping within the urban area of the city of Bergen?

The regional geology of Bergen has been investigated since the beginning of the 19th century. Geologists like Naumann, Hiortdahl, Irgens, Kjerulf and Reusch contributed at an early stage. Kolderup and Kolderup (1940) integrated previous works into the results of their own extensive investigations and established a profound geological model of the Bergen area. The principles of their main work, 'Geology of the Bergen Arc System', remain valid until today. Noteworthy is the correct recognition of principal age relationships, without the help of absolute dating methods, even though later geochronological investigations modified some of their conclusions.

Fundamental field mapping in the Bergen area has mainly been carried out between the 1970s and early 90s (see references in Fossen and Ragnhildstveit, 2008), and a refined tectonostratigraphy has been established for the Caledonian nappes. Well-exposed eclogites in the Lindås Nappe have contributed to the modern understanding of the role of fluids in high-grade metamorphism and deformation (e.g Austrheim et al., 1997). The basement in the Western Gneiss Region, north of Bergen, is a spectacularly exposed example of continental subduction and very well studied (Corfu et al., 2014). The basement in the Bergen area itself, on the other hand, received little scientific attention, even though large scale structures like the Bergen Arc System and the Øygarden Complex are incompletely understood.

Lyderhorn is one of seven landmark mountains surrounding the city of Bergen (Fig. 1). The mountain belongs geologically to the easternmost part of the Øygarden Complex and forms the core of the Bergen Arc. Yet, no satisfactory explanation has been found for the peculiar shape of the 100 x 50 km Bergen Arc structure that controls the geology and thereby the geomorphology of the Bergen area (Ramberg et al., 2008).

In the western part of the Øygarden Complex, shear zone structures have been studied in detail (e.g. Fossen and Rykkelid, 1990) and the Devonian cooling history is well constrained by mineral cooling ages (Boundy et al., 1996; Fossen and Dunlap, 1998; Larsen et al., 2003). However, no U-Pb zircon ages have been published to clarify the debated tectonostratigraphic position of the Øygarden Complex and also the exhumation mechanism of the convex basement window is unclear.

The prominent, 396 m high Lyderhorn offers excellent exposures to study magmatic, metamorphic and deformational processes in the poorly researched eastern part of the Øygarden Complex. The aim of this study was to unravel the geologic evolution of the Lyderhorn Gneiss from its magmatic formation until its exhumation to the brittle-plastic transition. New, detailed field mapping was conducted with a focus on petrology and structural geology, to serve as the basis for subsequent U-Pb zircon geochronology. Remote sensing and 3D visualization techniques in ArcGIS were used to identify and illustrate complex, three-dimensional structures. Seven samples were collected and analysed Secondary Ion Mass Spectrometry (SIMS) U-Pb zircon geochronology, to determine precise magmatic ages as well as possible effects of the intense metamorphic overprint on the zircon mineralogy.

The results from this study contribute to the regional geology of SW Norway and have implications for several orogenies. Precise determinations of magmatic ages help to understand the Mesoproterozoic formation of the Baltican basement and bear information about the style of the Sveconorwegian Orogeny. Regional correlations allow to reconstruct the pre-Caledonian structure of the Baltican crust, a key factor for the understanding of Caledonian continental subduction and exhumation. The post-Caledonian structure of the basement, on the other hand, is important for the later tectonic evolution of the northern North Sea and the formation of economically significant rift structures. Finally, the results from this study could be a small step towards understanding the Bergen Arc and show that basic field mapping is still important, even in 2016.



Fig. 1. Lyderhorn (396 m.a.s.l.) seen from the south (Knappen).

2 Regional Geology

The geologic history of Norway spans a time of almost 3 billion years, from the oldest rocks to the most recent post-glacial developments (e.g. Torsvik and Cocks, 2005). The oldest parts of the Norwegian continental crust experienced several supercontinent cycles with major orogenic and extensional phases. The same crust was part of different continent configurations. Thereby, its name as a continental domain changed throughout time (Fig. 2, left column). In the literature these names are used inconsistently, which can lead to confusion. Therefore, I will first give a short clarification of terms. The Paleozoic Caledonian Orogeny was the last event reorganize the entire geology of Norway (e.g. Corfu et al., 2014). Accordingly, three major units can be distinguished (Fig. 3): pre-Caledonian basement, Caledonian units and post-Caledonian (post-Scandian) units. The pre-Caledonian basement was a part of the continent Baltica in the Scandian continent-continent collision. It is therefore called Baltican basement (or Baltic Shield). The Sveconorwegian orogeny formed the principal configuration of the Baltican basement (Bingen et al., 2005). Newly formed Sveconorwegian crust amalgamated with older crust. Distinct Sveconorwegian domains/terrane have been proposed by Bingen et al. (2005). The basement in SW Norway consists largely of the Telemarkia and Idefjorden domains. The pre-Sveconorwegian crust of the basement belonged to the paleocontinent Fennoscandia, which was a part of the East European Craton (Bogdanova et al., 2008). Fennoscandian crust was later incorporated into two supercontinents: first Columbia (also called Nuna) in the Paleoproterozoic and Rodinia in the Neoproterozoic. Paleogeographic reconstructions often label Fennoscandia as Baltica and since significant amounts of Fennoscandian crust formed in the Svecofennian period, the name 'Svecofennian domain' is sometimes used for Fennoscandian crust. In this text, Svecofennian refers to an orogenic period while Fennoscandia refers to a paleocontinent.

2.1 Pre-Caledonian - The Formation of Baltica

The oldest parts of the Baltican crust originated in the Archean. Baltica as an independent continent emerged only in the Late Neoproterozoic. New crust formed in distinct episodes of the long lasting (1.9 - 0.9 Ga) Great Proterozoic Accretionary Orogeny at the active margin of Columbia (Fig. 4; Roberts and Slagstad, 2015). The crustal formation ages in the Baltic Shield show a pronounced trend, getting younger from NE to SW (Fig. 3), reflecting the accretionary history of the basement. The pre-Sveconorwegian history presented here follows the review by Roberts and Slagstad (2015).

Fennoscandia - Archean to Paleoproterozoic

Fennoscandia formed as a continent in the Paleoproterozoic Svecofennian orogenic period (2.0 - 1.8 Ga; Fig. 2). Several cratonal fragments collided to form the core of Fennoscandia during the amalgamation of the supercontinent Columbia. The oldest rocks in Norway are found in basement windows in northern Norway and date back to c. 2.9 Ga (Bingen and Solli, 2009). Most of the Svecofennian crust formed at the active SW margin of Fennoscandia as a part of the convergent western margin of Columbia (Fig. 4D). New crust from volcanic and continental arcs was accreted to the cratonal core. Fennoscandia united with other craton fragments (Volgo-Uralia

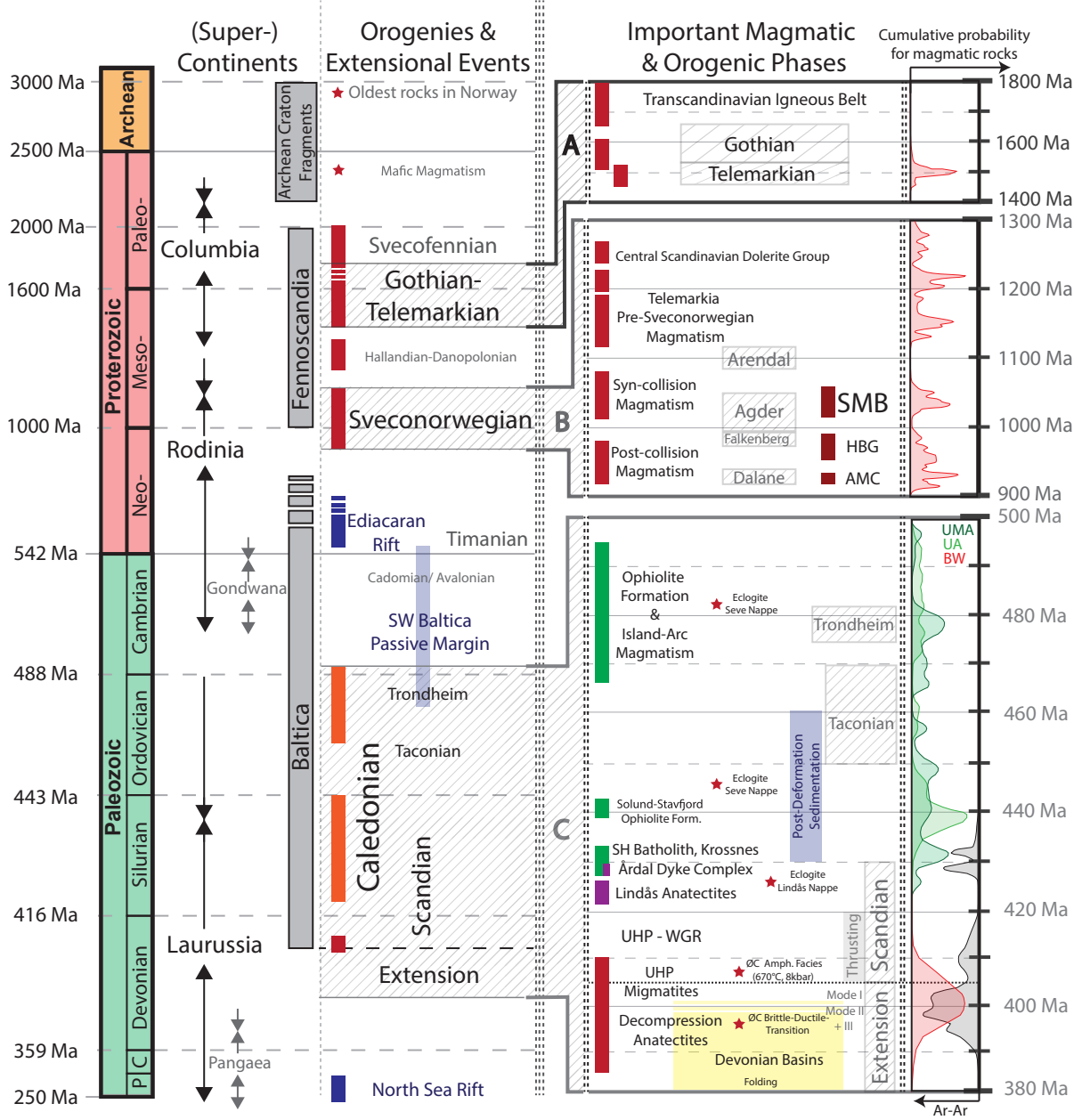


Fig. 2. (Previous page): Non-linear geological time scale, showing the development of (SW) Norway from the Archean to the end of the Paleozoic (left scale). The first column (from the left) shows supercontinent-cycles with major phases of extension and contraction (arrows). The second column contains major tectonic events. Main magmatic episodes are marked by red bars for the basement and orange bars for the Caledonian nappes. Blue bars mark major extensional events. Three phases are important for this work and enlarged on the discontinuous right scale. The Gothian-Telemarkian (A), Sveconorwegian (B) and Caledonian (C) orogenic periods. Coloured bars indicate magmatic activity in the basement (red), Upper and Uppermost Allochthon (green) and Middle Allochthon (purple). The rightmost column shows the cumulative probability for magmatic rocks in the Telemarkia domain from Bingen and Solli (2009), Fig. 4 - 6. For Caledonian times the probabilities are shown separately for the Uppermost Allochthon (UMA), Upper Allochthon (UA) and basement windows (BW). The opposite scale (Ar-Ar, black graph) shows relative probability of mica Ar-Ar cooling ages from the orogenic wedge (Bergen area), modified from Fossen and Dunlap (2006), Fig. 7. Abbreviations: AMC - Anorthosite-Mangerite-Charnockite complex; HBG - Hornblende-Biotite Granite suite; SH - Sunnhordaland; SMB - Sirdal Magmatic Belt; UHP - Ultra-high pressure metamorphism; WGR - Western Gneiss Region; ØC - Øygarden Complex. Based on: Bingen et al. (2005); Bogdanova et al. (2008); Roberts and Slagstad (2015); Bingen et al. (2008b); Pease et al. (2008); Roberts (2003); Torsvik and Cocks (2005); Coint et al. (2015); Slagstad et al. (2013); Slama and Pedersen (2015); Dunning and Pedersen (1988); Pedersen and Dunning (1997); Fossen and Austrheim (1988); Andersen and Jansen (1987); Lundmark and Corfu (2007); Skjerlie et al. (2000); Kühn et al. (2002); Root and Corfu (2012); Bingen et al. (2004); Fossen and Dunlap (1998); Fossen (2000); Fossen (2010a); Boundy et al. (1996); Larsen et al. (2003); Færseth et al. (2011); Gordon et al. (2013); Glodny et al. (2008).

and Sarmatia) to form the East European Craton at around 1.8 Ga (Bogdanova et al., 2008). This continent-continent collision is called the Svecobaltic Orogeny. It was one of many internal mobile belts of Columbia. Besides convergent regimes, temporary and spatially limited extensional regimes occurred as a consequence of migration of the subduction zone (tectonic switching).

Widespread granitoid magmatism occurred between 1.86 and 1.66 Ga in the Transcandinavian Igneous Belt (Fig. 3). This episode of crustal formation marks the transition from the Svecofennian accretion phase (2.0 - 1.8 Ga) in the NE of the orogen to the Gothian-Telemarkian accretion phase (1.66 - 1.48 Ga) in the SW. The part of the Transcandinavian Igneous Belt that was reworked during the Sveconorwegian Orogeny is termed Eastern Segment (Bingen et al., 2005; Fig. 3).

Crustal Growth in the Mesoproterozoic

The Gothian-Telemarkian orogenic period (Fig. 2A) is a discrete phase of continental growth along the active Fennoscandian margin, but is not seen as a distinct orogenic event. This period of regional convergence was contemporary with break-up of Columbia which is poorly constrained to 1.6 - 1.2 Ga. Arc magmatism was accompanied by sedimentation and accretion in a subduction-zone environment. Gothian arc magmatism ranges from 1.66 to 1.52 Ga (Fig. 4A) and defines the Idefjorden domain (Fig. 3). Magmatic ages show a trend, getting younger towards the W. Gothian igneous protolith ages correlate the Western Gneiss Region (WGR; Fig. 3) with the Idefjorden domain (Roffeis and Corfu, 2014). The WGR is the part of the Baltican basement that experienced strong Caledonian reworking.

The subsequent 1.52 - 1.48 Ga Telemarkian magmatic phase (Fig. 4B) defines the Telemarkia domain further W (Fig. 3). Ages of island and continental arc magmatism show a sharp peak at 1.50 Ga (Fig. 2, right column). Formation and accretion of juvenile crust was synchronous with

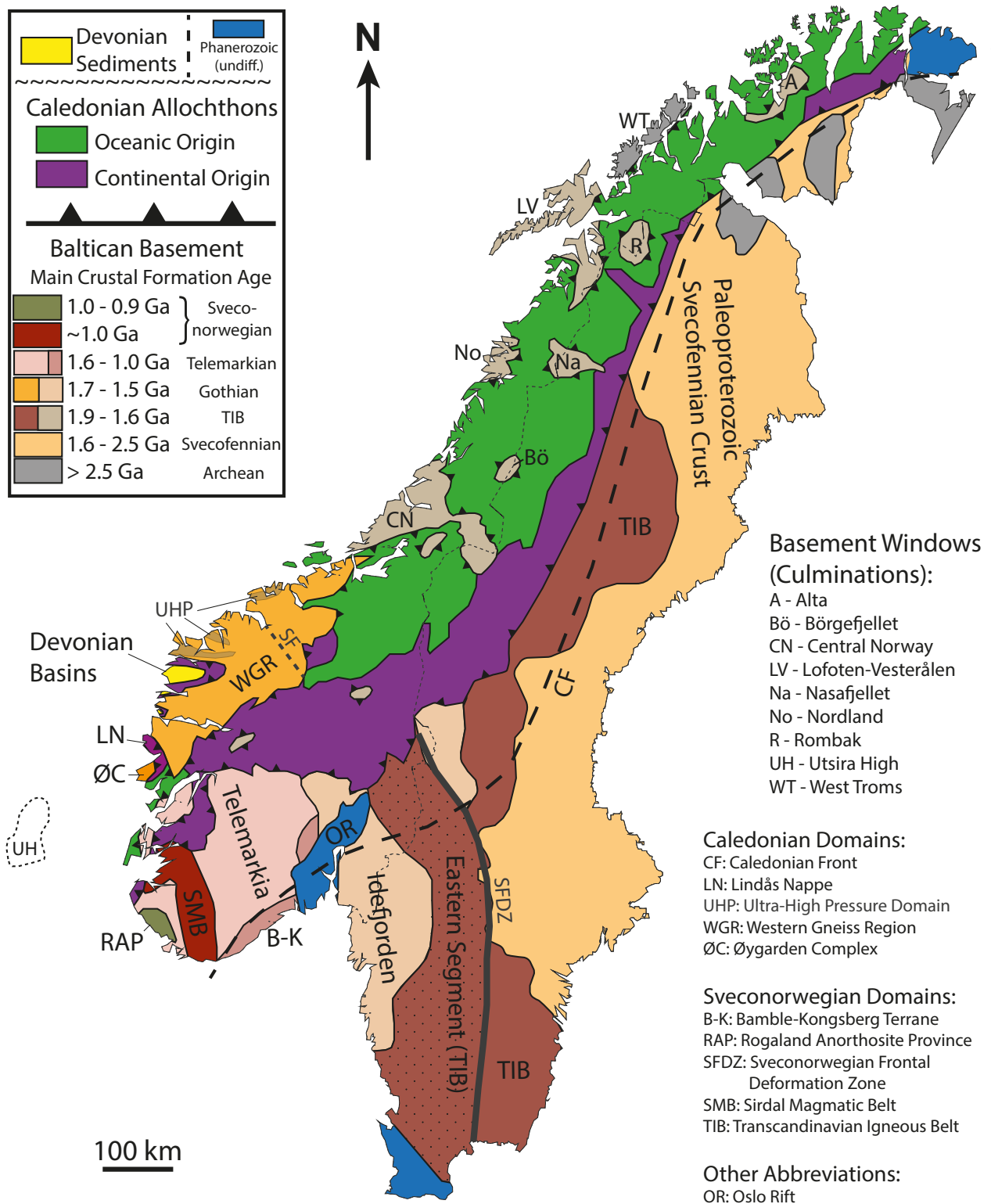


Fig. 3. Geological overview map of Norway and Sweden. The units are divided in three major groups: Pre-Caledonian (Baltican) basement, Caledonian allochthons and post-Caledonian units. The strike of the Caledonian Orogen is roughly NE - SW. Sveconorwegian domain boundaries in the basement strike NNW - SSE. Ages of crustal formation in the Baltican basement show a general trend, getting younger from NE to SW. The study area is part of the Øygarden Complex (ØC; see also Fig. 8). Based on Roberts and Slagstad (2015); Bingen et al. (2008a); Bingen and Solli (2009); Roffeis and Corfu (2014); Bogdanova et al. (2008); Coint et al. (2015) and Fossen (2015).

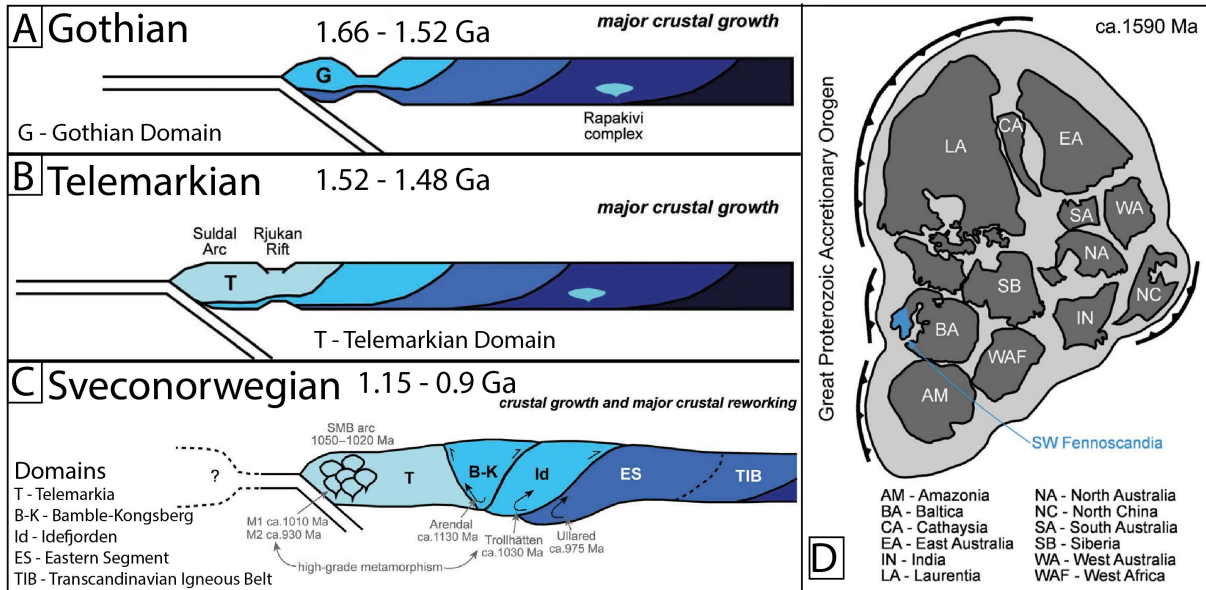


Fig. 4. A - C: Cartoon cross-sections showing major periods of crustal growth at the active SW margin of Fennoscandia in the early Proterozoic. The position of Fennoscandia is shown in the Columbia reconstruction at 1.59 Ga (D). An accretionary setting existed throughout the Proterozoic along the entire western margin of Columbia. It is therefore termed the Great Proterozoic Accretionary Orogen. Modified from Roberts and Slagstad (2015).

continental rifting in the eastern part of the domain (Rjukan Rift) and accompanied by felsic volcanism (Fig. 4C). Telemarkia has been defined as an independent terrane because it contains no magmatic rocks older than c. 1.5 Ga (Bingen et al., 2008b).

The Bamble-Kongsberg domain consists of 1.57 - 1.46 Ga plutonic suites (Bingen and Solli, 2009). It formed as an orogenic wedge during the Sveconorwegian Orogeny, when Telemarkia collided with the Idefjorden terrane (Roffeis and Corfu, 2014).

Reorganization of the subduction zone marks the Hallandian-Danopolonian period (1.47 - 1.38). Related magmatism is found in the Eastern Segment, the WGR and the Caledonian Jotun and Dalsfjord nappes (Bingen and Solli, 2009). Between 1.4 and 1.2 Ga, inboard extensional events affected the Fennoscandian margin and caused episodic and regional magmatism (e.g. Central Scandinavian Dolerite Group) as well as local sedimentary basins.

The Sveconorwegian Orogeny

The Grenvillian orogenic period (1.3 - 1.0 Ga) was one of the most important phases of continental crust formation in earth's history (Rino et al., 2008). The assembly of the supercontinent Rodinia caused worldwide orogenic activity (Li et al., 2008). This time period coincides with the Sveconorwegian orogeny (Fig. 2B). It is currently debated, whether the Sveconorwegian and the Grenvillian Orogenies can be correlated. New findings by Slagstad et al. (2013) have challenged the classical four-phase model by Bingen et al. (2008b) that is based on continent-continent collision. In any case, the Sveconorwegian Orogeny marks the end of the long-lived (1.9 - 0.9 Ga) accretionary history at the Fennoscandian margin and formed the recent structure of the basement through major tectonothermal events.

Collisional Four-Phase Model (Bingen et al., 2008b)

Following terrane accretion, Fennoscandia collided with another major continent (Amazonia?) around 1050 Ma. A major suture zone, that could represent a closed ocean, has not been identified. Four tectonic phases are distinguished:

1) In the Arendal phase (1140 - 1080 Ma) Telemarkia collided with the Idefjorden terrane. High-grade metamorphism and deformation localized in the Bamble-Kongsberg terrane.

2) The Agder phase (1050 - 980 Ma) comprises the main continent-continent collision. Associated metamorphism increases in grade from the Eastern Segment (amphibolite facies) to granulite facies in the Rogaland-Vest-Agder sector. The Sveconorwegian Frontal Deformation Zone (Fig. 3) marks the limit of overprint to the E. The Idefjorden terrane experienced high-pressure (HP) metamorphism at 1050 Ma due to underthrusting. Significant crustal thickening in the Telemarkia terrane caused voluminous syn-collision granite magmatism from 1050 Ma, followed by local high-grade metamorphism from 1035 Ma.

3) The Falkenberg phase (980 - 970 Ma) represents the transition from convergence to divergence. The Eastern Segment is buried to eclogite conditions.

4) Gravitational collapse marks the end of the Sveconorwegian Orogeny in the Dalane phase (970 - 900 Ma). Post-collision magmatism peaks in intrusion of the anorthosite-mangerite-charnockite complex in the Rogaland-Vest-Agder sector

Non-Collisional, Accretionary Model (Slagstad et al., 2013)

Based on the recognition of far more voluminous Sveconorwegian magmatism than previously assumed and the absence of widespread Sveconorwegian metamorphism, Slagstad et al. (2013) proposed a non-collisional, accretionary Sveconorwegian Orogen. Calc-alkaline granitoids (e.g. Feda augen gneiss suite; Bingen et al., 1993; Bingen and Van Breemen, 1998) were previously interpreted as syn-collisional magmatism, caused by crustal melting due to thickening of the Telemarkian crust. Large, weak- or undeformed granite batholiths with intrusion ages confined between 1050 - 1020 Ma were newly discovered in the Sirdal Magmatic Belt (SMB; Fig. 2) that comprises the Feda augen gneiss suite. Geochemically, SMB granites are incompatible with remelting of Telemarkian crust, but indicate formation in a magmatic arc. The period of high-grade metamorphism in the Telemarkia domain (1035 - 970 Ma) overlaps with (1050 - 1020 Ma) SMB magmatism, but Slagstad et al. (2013) recognized the absence of widespread high-grade metamorphism in the SMB. These authors see Sveconorwegian magmatism after 1000 Ma no longer as post-collisional, caused by gravitational collapse of the orogen. Ferroan hornblende-biotite granite (HBG) magmatism (970 - 930 Ma) and anorthosite-mangerite-charnockite magmatism in the Rogaland Anorthosite Province (950 - 920 Ma; Fig. 3) formed by melting of a lower-crustal source (Vander Auwera et al., 2011) that Bybee et al. (2014) explain by a long-lived thermal event. Timing and dynamics of Sveconorwegian magmatism and metamorphism suggest subduction-related processes, typical for Andean-type margins with periodic compression and extension and that no continent-continent collision took place in the Sveconorwegian Orogeny.

Sirdal Magmatic Belt (Coint et al., 2015)

Results from field mapping and geochronology newly define the 200 km x 50 km, NNW-trending

SMB in SW Norway (Fig. 3). The most important lithologies in the belt are porphyritic biotite granites and leucogranites. Their textures grade diffusively from coarse grained to pegmatitic. Magmatic ages range from 1060 to 1020 Ma with two distinct probability peaks at 1050 Ma and 1035 Ma. Gently folded, shallowly E- or W-dipping, sheet like intrusions are bound by characteristic xenolith-rich zones. Xenoliths are granitic gneisses, amphibolites and migmatitic gneisses. The SMB spatially encloses the 1.0 - 0.9 Ga HBG suite (Vander Auwera et al., 2003). SMB-age mafic magmatism is sparse but has been dated (T. Slagstad, personal communication).

Most of the granites in the SMB are undeformed and unmetamorphosed. Weak ductile deformation is localized in xenolith-rich zones. Close to the Rogaland Anorthosite Province, the SMB is overprinted by granulite-facies metamorphism and locally migmatized. This deformation is related to the thermal effect during emplacement of the AMC.

In between Orogenies - Neoproterozoic to Cambrian

Rodinia existed as a supercontinent for c. 150 My after its completed assembly around 900 Ma (Li et al., 2008). Superplume activity triggered a major phase of diachronous extension. Continental rifting started around 750 Ma, but break-up did not succeed before Ediacaran times (600 - 550 Ma; Pease et al., 2008), witnessed by rift-related magmatism (Gee et al., 2008). The birth of Baltica as an independent continent is marked by its segregation from Laurentia and the opening of the Iapetus ocean. The general divergent regime overlaps with assembly of Gondwana and Avalonian-Cadomian-Timanian orogenic activity (Torsvik and Cocks, 2005). While the Timanian orogeny affected NE Baltica, a passive margin formed in (S)W Baltica. Glacial erosion and the absence of a vegetation cover transformed Baltica into the sub-Cambrian peneplain (Gabrielsen et al., 2015; Nielsen and Schovsbo, 2011). Early Cambrian transgression on the Baltoscandian platform is recorded by siliciclastic sediments with characteristic (black) shale beds (Gee et al., 2008). Carbonate deposition followed in the Ordovician. Detrital zircons record a stable source-to-sink system across the entire continent from the Timanian orogen in NE Baltica to the SW passive margin (Slama and Pedersen, 2015). The drainage system existed from early Cambrian to Middle Ordovician (c. 467 Ma). This record contradicts the postulated existence of a hyperextended Baltican margin in the Neoproterozoic and early Paleozoic (Andersen et al., 2012). The hyperextended margin model explains a mantle-peridotite-bearing mélange situated below the crystalline nappes of the Middle Allochthon (see section 2.4). An alternative model relates the mélange to arc-formation in the middle Ordovician (Slama and Pedersen, 2015). The change from a passive to an active Baltican margin marks the onset of the Caledonian Orogeny.

2.2 The Caledonian Orogeny

The Paleozoic Caledonian Orogeny evolved around the closure of the Iapetus ocean and resulted in Scandian continent-continent collision between Laurentia and Baltica (Corfu et al., 2014). The 120 Myr. history involved Avalonia and other continental terranes. Three major phases can be distinguished in the evolution of the Scandinavian Caledonides (Fig. 2C): 1. Early Caledonian (500 - 430 Ma) ophiolite formation, arc magmatism and accretionary events. 2. Scandian continent-continent collision (430 Ma - 405 Ma). 3. Post-orogenic extension. The

traditional tectonostratigraphy distinguishes (par)autochthonous basement and four levels of allochthonous units (Roberts and Gee, 1985). The Lower and Middle Allochthon are Baltica derived. The Upper Allochthon consists of Iapetus-derived oceanic units. The Uppermost Allochthon is of inferred Laurentian origin. Detailed work in the last 30 years has shown that this simplistic division can not be upheld (Corfu et al., 2014). The terminology is still used in this work as it serves very well in explaining the fundamental characteristics of the main units. A more general classification distinguishes between continental nappes with Baltican affinity and outboard/oceanic units (Fig. 3).

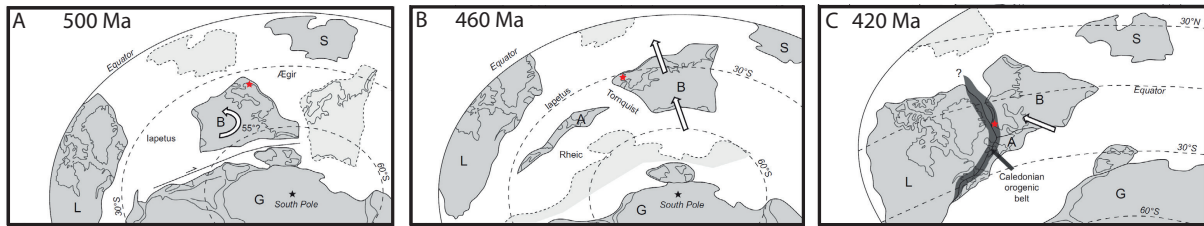


Fig. 5. Paleogeographic reconstructions at 500 Ma (A), 460 Ma (B) and 420 Ma (C). Red stars roughly mark the position of the study area. Alternative positions of the continents are shown in light grey. Modified from Corfu et al. (2014). See text for explanation.

Early Caledonian Orogenic Events

When Baltica separated from Gondwana in the Cambrian its present day western margin faced In the Late Cambrian and Ordovician Baltica underwent major movements. Counter-clockwise rotation by 55° around 500 Ma (Fig. 5A) was followed by drift from 60°S to 30°S until 460 Ma (Fig. 5B). Baltica was soft-docking with Avalonia around 450 - 440 Ma. The Iapetus ocean between Baltica and Laurentia reached its widest extent around 480 Ma. From this time the ocean was closed by westward subduction below Laurentia. This period is coincident with the earliest tectonometamorphic records in the Scandinavian Caledonides. The actual event chronology of early Caledonian development is still disputed. Reconstructions are complicated by the simultaneous but independent evolution of Baltica, Laurentia and Iapetus before all three became juxtaposed in the Scandian collision. A major question is if there were early Caledonian tectonometamorphic events along the Baltican margin or if all early events took place on the Laurentian side of the Iapetus.

A Finnmarkian event around 500 Ma was proposed for northern Norway by Sturt et al. (1978). They interpreted the tectonothermal record in the Kalak-Seve nappes as collision of the Baltican margin with a magmatic arc (Roberts, 2003). More recent work assigned this deformation to the Laurentian margin. The consensus is now that no Finnmarkian event existed at the Baltican margin (Corfu et al., 2014).

It is more commonly accepted that the Trondheim event affected the Baltoscandian margin around 480 Ma (Roberts, 2003). The event is poorly understood. It might represent seaward subduction of a microcontinent that could comprise previously rifted fragments of the Baltican continental margin (Brueckner et al., 2004). HP eclogites in the Seve Nappe Complex give evidence for tectonothermal activity around 482 Ma (Root and Corfu, 2012; Essex et al., 1997). Blueschist facies metamorphism, magmatism and ophiolite emplacement are reported for the

same time in the Köli nappe (Hacker and Gans, 2005). Both nappes have a Baltican affinity but their origin is controversial (Roffeis and Corfu, 2014). A second generation of eclogites in the Seve Nappe has been dated to 446 Ma (Root and Corfu, 2012).

The Trondheim event is contemporaneous with ophiolite formation and arc magmatism at the Laurentian margin (Taconian event; Roberts, 2003). Numerous ophiolites of the Upper and Uppermost Allochthon formed between 490 - 480 Ma and were subsequently obducted onto the Laurentian margin (Dunning and Pedersen, 1988; Slagstad et al., 2014). The Solund - Stavfjord ophiolite complex formed around 440 Ma. It was intruded by the Sogneskollen granite at 434 Ma (Furnes et al., 2012). The geochemical signature of the S-type granite indicates partial melting of Baltican supracrustals. Arc-related magmatism has been dated as young as 430 Ma in the Sunnhordaland nappe (Andersen and Jansen, 1987; Fossen and Austrheim, 1988). Based on geological, isotopic and faunal evidence, the ophiolites are commonly interpreted as peri-Laurentian suprasubduction and marginal basin complexes (Pedersen et al., 1992; Furnes et al., 2012; Roffeis and Corfu, 2014). They were obducted onto the Laurentian margin before they were thrust onto Baltica in the Scandian collision. Many of the deformed ophiolitic units are unconformably overlain by late Ordovician to early Silurian sediments (Corfu et al., 2014). Some of these sediments show a Baltican affinity (e.g. Holdhus Group; Færseth et al., 2011), which is in conflict with the inferred peri-Laurentian origin of the ophiolites. In the northern WGR, Ordovician arc-related intrusives of the Upper Allochthon are tightly infolded into basement gneisses and unconformably overlain by Late Ordovician sediments (Tucker et al., 2004).

The complex early Caledonian record is difficult to unravel and it is still unclear when exactly the shift from a passive to an active Baltican margin occurred (Slama and Pedersen, 2015).

Scandian Continent-Continent Collision

The termination of subduction-related magmatism and marine sedimentation marks the onset of the Scandian phase at 430 Ma (Fig. 2C; Corfu et al., 2014). Baltica's oblique collision with Laurentia from c. 420 Ma (Fig. 5 C; Torsvik and Cocks, 2005) formed the new supercontinent Laurussia. Crustal thickening gave rise to a mountain range comparable in dimensions to the modern day Himalaya (Labrousse et al., 2010).

The Baltican margin was subducted below Laurentia to the NW (Fig. 6A). The negatively buoyant oceanic crust detached probably from the continental slab (Duretz et al., 2012). Early Scandian HP eclogites in the Lindås nappe has been dated to 430 - 423 Ma (Bingen et al., 2004; Glodny et al., 2008). The WGR experienced was buried to ultra-high pressure conditions (UHP) between 425 - 400 Ma (Hacker et al., 2010; Root et al., 2004). The highest pressures are recorded by micro-diamonds and coesite in E-W elongated UHP belts (Fig. 3).

A striking feature of the Scandinavian Caledonides is the sparse record of Scandian magmatism (Bingen and Solli, 2009). The absence of widespread syn-collisional magmatism is attributed to relatively fast subduction and exhumation of the Baltican crust (Roberts, 2003). Early Scandian anatexites in the nappes of SW Norway formed synchronous with early eclogites. At 427 Ma the Årdal dyke complex intruded the Upper Jotun nappe (Lundmark and Corfu, 2007). Anatectic pegmatites and trondhjemites were emplaced in the Lindås nappe at 425 Ma and 418 Ma, respectively (Kühn et al., 2002). Peak UHP metamorphism in the WGR at 420 Ma was

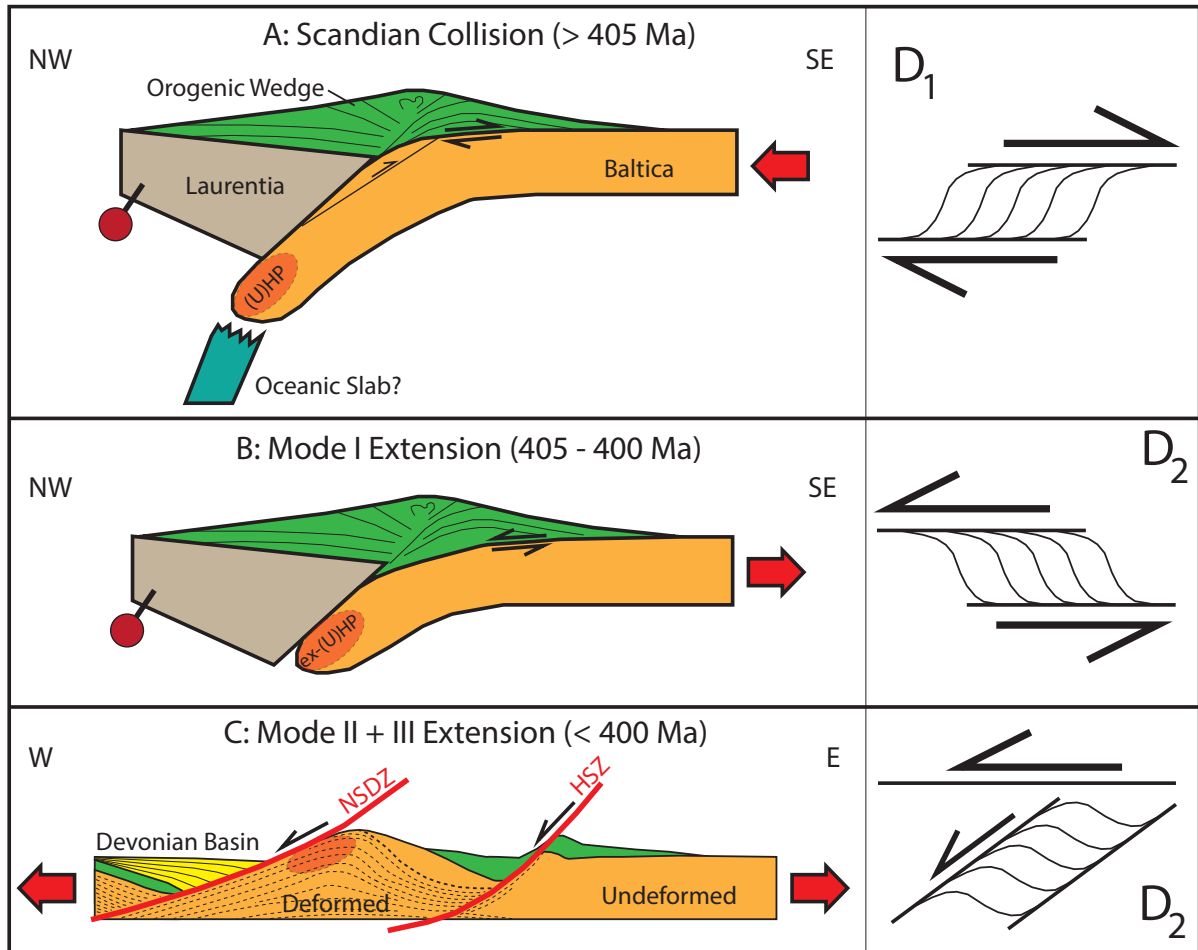


Fig. 6. Cartoon cross-sections for the main stages of Caledonian development with sketches of associated fabrics. Scandian collision involves continental subduction of Baltica, (ultra-)high-pressure ((U)HP) metamorphism at the leading edge of the subducted crust and possible syn-orogenic exhumation of basement slices. The oceanic slab is shown to detach from the continental domain. Post-orogenic extension of the subducted plate in Mode I extension leads to reversal of shear sense at the basal décollement zone. Mode II extension forms hinterland dipping extensional shear zones (HSZ: Hardangerfjord Shear Zone; NSDZ: Nordfjord Sogn Detachment Zone) and Devonian supra-detachment basins. Domains of deformed, viscous Baltican crust are distinguished from cold and undeformed crust. The onset of brittle deformation (Mode III) is dated in the hinterland to 396 Ma (Larsen et al., 2003). Redrawn after Fossen (1992); Fossen (2000); Fossen (2010a); Fossen et al. (2014); Milnes et al. (1997); Roberts (2003) and Butler et al. (2015).

accompanied by partial melting of eclogite-hosting gneisses (Gordon et al., 2013). Anatexis was more abundant during decompression and retrogression through amphibolite facies conditions until c. 385 Ma.

The collision created a wedge-shaped pile of thrust nappes that was thrust to the SE onto the parautochthonous basement. The Neoproterozoic to early Paleozoic sedimentary basement cover, especially weak phyllite layers, acted as the major décollement (Fossen, 1992; Fauconnier et al., 2014). The units higher up in the nappe stratigraphy generally moved the furthest. Apart from the general pattern, there are considerable structural variations along the NE - SW strike of the orogen. Lateral translations reached more than 300 km (Brueckner and Cuthbert, 2013). The Scandian contractional phase is characterized by thin-skinned deformation with extensive imbricate and duplex structures (Fossen, 1992). A penetrative mylonitic fabric with top-to-(S)E kinematic is well developed in the décollement zone and at the base of the thrust nappes (Fig. 6A; D_1). Related mineral stretching lineations show a systematic pattern of nappe translation to the SE and E (Fig. 7A). Mica Ar-Ar cooling ages, associated with contractional fabrics, peak around 410 Ma (Fig. 2; Fossen and Dunlap, 1998). The effect of the Scandian overprint in the basement is variable. From high-T deformation in the WGR (Hacker et al., 2010) it decreases towards the SE. Several basement culminations form windows, evenly distributed along the entire Caledonian belt (Fig. 3). The WGR itself can be seen as the largest of such culminations. Some authors explain these non-planar structures by contractional mechanisms (e.g. Robinson et al., 2014). Alternative models relate them to post-orogenic extension (e.g. Braathen et al., 2000; Osmundsen et al., 2005; see below).

Caledonian Extension

If extension was syn-orogenic or post-orogenic, is an important question in the understanding of the Caledonides. Regional investigations of extensional kinematics have shown that Caledonian extension took place in the Devonian and was mainly post-orogenic (Fossen, 2000). The entire orogenic wedge shows hinterland-directed (top-to-(N)W) transport. At the peak of orogeny, the crust is thickened the most in the hinterland. Thus, hinterland-directed transport strictly implies a switch from plate convergence to plate divergence. This contradicts previously proposed models of largely syn-orogenic Caledonian extension and/or gravitational collapse (e.g. Andersen and Jamtveit, 1990).

In the hinterland (Bergen area), the change from Scandian contraction to extension has been dated to 405 Ma based on cooling ages of extensional fabrics (Fig. 2C; Fossen and Dunlap, 2006). On a regional scale exhumation was more diachronous. This can be seen in the distribution of Ar-Ar cooling ages from white mica shows a trend from older ages (410 - 420 Ma) in the SE (e.g. Fossen and Dunlap, 1998) to younger ages (< 380 Ma) in the NW (e.g. Root et al., 2005). This distribution is in agreement with NW-ward subduction and reverse continental exhumation of the Baltican basement (Andersen et al., 1991). The general trend is disturbed by extensional shear zones at the west coast. Two main phases of post-orogenic extension have been identified by Fossen (1992):

Mode I extension (Fig. 6B) between 405 Ma and 400 Ma is characterized by reactivation of the basal décollement zone with top-to-the-hinterland (W - NW) transport. The general

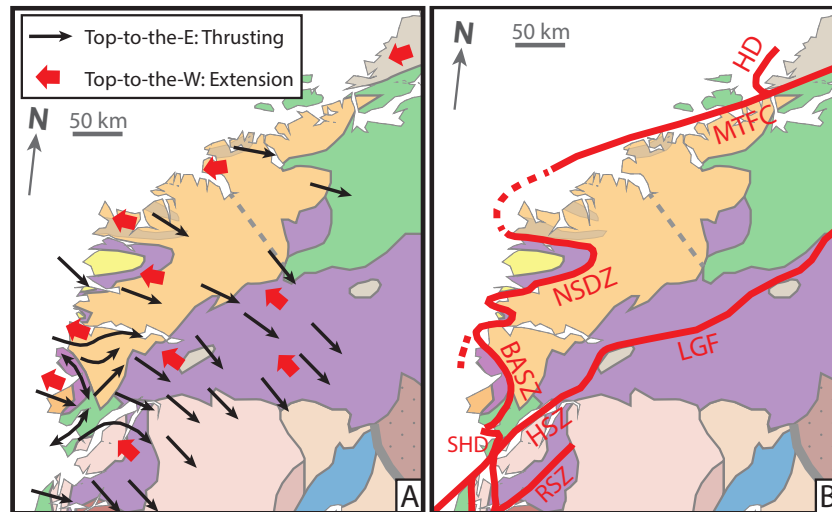


Fig. 7. A: Directions of Caledonian thrusting and Devonian extension in SW Norway based on mineral stretching lineations and their kinematic indicators. Note the deviation from the general SE-trend of thrusting in the Bergen area and the shift from orogen-perpendicular extension in the S to orogen-subparallel extension in the N. Modified from Fossen (1992), Fossen (2000) and Fossen (2010a). **B:** Major Mode II shear zones: HD - Høybakken Detachment, MTFC - Møre-Trøndelag Fault Complex, NSDZ - Nordfjord-Sogn Detachment Zone, BASZ - Bergen Arc Shear Zone, LGF - Lærdal-Gjende Fault Zone, HSZ - Hardangerfjord Shear Zone, SHD - Sunnhordaland Detachment, RSZ - Røldal Shear Zone. Modified from Fossen and Hurich (2005) and Braathen et al. (2000).

transport direction in SW Norway is almost exactly opposed to previous thrusting (Fig. 7A). Therefore, this movement is also called 'back-sliding' of the orogenic wedge. Depending on the chosen reference frame this corresponds to back-movement (eduction) of the subducted slab. The reversal of shear sense is preserved on a regional scale in SW Norway (Fossen, 2010a). Thrusting related D_1 fabrics were overprinted by slightly lower grade extensional fabrics (Fig. 6B, D_2 ; Fossen, 1992). D_2 fabrics are characterized by C-type shear bands, with shallow to sub-horizontal C-surfaces. NW-verging folds with NE-trending fold axes and other asymmetric structures indicate top-to-(N)W movement. The deformation is mainly localized in the décollement zone but affects also the base of the crystalline nappes.

From around 400 Ma the entire crust collapsed. Mode II extension formed hinterland-dipping extensional shear zones (Fig. 6C) that rapidly exhumed the hinterland to brittle conditions (Mode III). A network of Devonian extensional shear zones cross-cuts the orogenic wedge, the décollement zone and cuts down into the basement (Fig. 7B). Extensional structures can be traced along the entire Scandinavian Caledonides, have been identified offshore and might be linked to structures in the Scottish Caledonides (Fossen and Hurich, 2005). Associated D_2 fabrics are characterized by inclined C-planes, forming C'-type shear bands (Fig. 6C). Two types of detachments can be distinguished: NW-dipping shear zones are relatively straight and elongated, while W-dipping detachments at the coast are strongly curved (Fig. 7B).

The coast-'parallel', W-dipping detachments contain Devonian basins in their hanging-wall. The curvature of the interconnected shear zones increases from S towards N, together with the size of the (preserved) supra-detachment basins and the break in metamorphic grade across the shear zone. A spectacular extreme is the Nordfjord-Sogn Detachment Zone. A 5-6 km thick package of mylonites juxtaposes (U)HP eclogites with middle Devonian conglomerates in the

extensive Hornelen Basin (Seranne and Seguret, 1987). The shear zone has an estimated normal displacement of 50 km (Milnes et al., 1997). Metamorphic conditions inside the detachments decreased during exhumation (Braathen et al., 2004). Originally ductile deformation became overprinted by brittle structures. The supra-detachment basins are intermountainous and filled with middle Devonian (398 - 385 Ma) conglomerates and sandstones. The exact age of the earliest strata is poorly constrained and might be even older (Fossen, 2010a). In the Hornelen basin, the stratigraphic thickness of the sediments reaches more than 25 km, while the maximum burial depth did not exceed 10 km (Seranne and Seguret, 1987). East-tilted beds preserve unconformable contacts with Upper Allochthon units to the west. The rest of the basins is bound by tectonic contacts. This is explained by a half-graben supra-detachment model for basin formation, with special cases involving ramp-geometries (Osmundsen and Andersen, 2001; Vetti and Fossen, 2012). Lateral translation of the hanging wall accommodates the space for syn-tectonic sediments.

The NW-dipping Hardangerfjord Shear Zone is a basement shear zone with an assumed pre-Caledonian history (Fossen and Hurich, 2005). Normal displacement of 10 - 15 km resulted in passive folding of the overlying nappes (termed 'Faltungsgraben' by Goldschmidt (1912)). The shear zone continues to the NE at a higher crustal level as the brittle Lærdal-Gjende Fault Zone. The Hardangerfjord Shear Zone delimits thin-skinned Caledonian tectonics in the foreland to thick-skinned tectonics in the hinterland reflecting cold rigid crust and relatively hot, viscously flowing crust, respectively (Fossen et al., 2014).

The Møre-Trøndelag Fault Complex is dominated by sinistral strike-slip movement (Fossen, 2010a). The structure acted as a major transfer structure in an overall transtensional regime (Krabbendam and Dewey, 1998). The trend of Caledonian extension and fold axes rotates from WNW - ESE (perpendicular to the orogen) in the south-west towards NE - SW (orogen-subparallel) closer to the Møre-Trøndelag Fault Complex. Bidirectional extension in the Central Norway Basement Window indicates core complex style exhumation (Braathen et al., 2000). Several basement windows ('gneiss-cored culminations') in central Norway have been explained as Devonian metamorphic core complexes (Osmundsen et al., 2005; Braathen et al., 2002). E-W trending, upright folds control the shape of Devonian basins as well as UHP-domains in the WGR. Fold axes plunge gently to the W. Fold geometries shifts from tight further north towards open in the Bergen area. This folding was active before, during and after the deposition of Devonian sediments (Fossen et al., 2016). It is most commonly explained by transtensional folding (Fossen et al., 2013; Chauvet and Séranne, 1994).

A strongly debated issue remains the actual exhumation mechanism of the WGR. Previously, the exhumation was mostly assigned to extensional shear zones but more recent models suggest an important role of viscous flow in the basement itself (Fossen, 2010a). Coaxial constrictional strain at amphibolite facies conditions has been identified in large parts of the WGR (e.g. Krabbendam and Wain, 1997; Hacker et al., 2010; Barth et al., 2010; Johnston et al., 2007; Young et al., 2007). Different authors relate these fabrics either to Scandian or extensional deformation. Recent studies propose that the intensity of partial melting in the WGR might have been previously underestimated (e.g. Gordon et al., 2015) because only precise in-situ geochronology can reveal if migmatization was Caledonian or Precambrian. Extension-related decompression migmatites

and pegmatites have been dated as young as 385 Ma (Gordon et al., 2013). The presence of melt drastically reduces the viscosity and increases the buoyancy of subducted crust. Based on this, some authors proposed a (partially) buoyancy-driven exhumation of the WGR (Labrousse et al., 2004). On the contrary, Butler et al. (2015) point out that subducted continental crust needs to have an exceptional high strength to remain over a long period at (U)HP conditions as it is observed in the WGR.

The Bergen area reached the transition from ductile to brittle conditions already around 396 Ma (Larsen et al., 2003). At the same time partial melting continued in the WGR. Parts of the WGR reached brittle conditions as late as the Permian (Eide et al., 1997).

2.3 Post-Caledonian Development

Since the switch from Caledonian contraction to post-orogenic extension, SW Norway was in an extensional regime. Devonian extension led to deconstruction of the Caledonian mountain chain. The two-phase Permo-Triassic and Jurassic-Cretaceous North Sea rift transformed SW Norway into today's passive margin (e.g. Doré et al., 1999). Extension culminated in continental break-up and the opening of the North Atlantic in the Paleogene. Inheritance of Caledonian basement structures played an important role in the extensional deformation (Doré et al., 1997). Rift-parallel, Devonian Mode II shear zones were partly reactivated (Fossen et al., 2016). Large, rift-oblique lineaments (e.g. Hardangerfjord Shear Zone) strongly influenced the rift architecture. Devonian metamorphic core complexes controlled Mesozoic fault-evolution at the Mid-Norwegian margin (Osmundsen et al., 2005). Late Paleozoic to early Mesozoic continental deposition was followed by transgressive syn- and post-rift sedimentation (Bell et al., 2014). The structure and thermal history of the rift basins are of large economic interest as they contain Norway's oil deposits. Onshore SW Norway, the post-Devonian exhumation history is poorly constrained (Ksienzyk et al., 2014) because there are no sediments younger than the Devonian basins. The geomorphological evolution of SW Norway, especially the high topography with characteristically flat mountain tops, is strongly debated. Two contrasting models of post-Caledonian landscape evolution exist: One proposes complete erosion of Caledonian topography; peneplanation in the Mesozoic was followed by Cenozoic tectonic uplift (e.g. Gabrielsen et al., 2010). The other assumes incomplete erosion of the Caledonian mountain chain; inheritance of an orogenic root supports high topography under prolonged erosion until today (e.g. Nielsen et al., 2009). In any case, the Norwegian landscape was strongly modified by Quaternary glaciation. Glacial erosion carved deep fjords into the elevated plateaus. Voluminous Quaternary sediments offshore show that important mass movements accompanied this latest episode of the geologic evolution (Steer et al., 2012).

2.4 Geology of the Bergen Arc System

The city of Bergen is located in the center of the large-scale arc structure (Fig. 8). The Bergen Arc System (Kolderup and Kolderup, 1940) is bound outward by the Bergen Arc Shear Zone (BASZ), an oblique lateral detachment shear zone that formed during Devonian Mode II extension (Wennberg et al., 1998). The W-dipping shear zone initiated with a concave shape that

implicates a dextral strike-slip component in the northern part and sinistral-normal displacement in the southern part of the shear zone (Fossen, 1992). The BASZ is seen as a southern branch of the Nordfjord-Sogn Detachment Zone.

The Bergen Arc System contains three major domains: Baltican basement NE of the BASZ belongs to the WGR. The arc itself consists of synclinally folded Caledonian allochthons (Fig. 9). Caledonian nappes also appear SE of the BASZ, overlaying autochthonous basement. The Øygarden Complex forms the core of the Bergen Arc. It is considered parautochthonous Baltican basement and its contact with the nappes in the Minor Bergen Arc is interpreted as the 'basal Caledonian thrust' (e.g. Larsen et al., 2003). Fig. 10 gives an overview over previous geochronological studies in the Bergen Arc System.

Tectonostratigraphy of the Bergen Arc

Post-Caledonian

The youngest rocks in the Bergen Arc are early Late Jurassic sediments that have been found within the Bjørøy fault (Fossen et al., 1997). The Fennsfjorden Devonian Basin in the hanging wall of the BASZ contains coarse conglomerates (Kolderup and Kolderup, 1940; Wennberg et al., 1998). It is thought to represent a southern continuation of the Solund Basin and is the southernmost exposure of Devonian strata in SW Norway.

Caledonian Nappes

The Sunnhordland Nappe (or Hardanger Nappe Complex) consists of various units with oceanic affinity and is belongs to the Upper Allochthon (Roffeis and Corfu, 2014). The nappe occupies the lowest structural position in the Bergen Arc System. Ordovician ophiolitic complexes and arc-related plutons are unconformably overlain by late Ordovician to early Silurian metasediments (Færseth et al., 2011). They show a record of pre-Scandian deformation but have been subsequently overprinted by Scandian and extensional fabrics (Fossen and Dunlap, 2006). The Sunnhordland Nappe comprises the following units within the Bergen Arc:

The Major and Minor Bergen Arc (MaBA/MiBA) consist of Lower Paleozoic ophiolite-related metasedimentary and metaigneous complexes and are commonly correlated (Fossen and Dunlap, 2006). During Scandian thrusting, tectonic fragments of Paleozoic rocks became imbricated with slices of Precambrian (basement) gneisses and their metasedimentary cover (Fossen, 1989). The rocks in the MiBA show higher strains as their equivalents in the MaBA. Scandian regional metamorphism reached upper greenschist to lower amphibolite facies conditions in both arcs (Fossen, 1988a) and formed an intensively folded, pervasive mylonitic foliation (Fossen, 1989). E-dipping low-angle shear zones with 'flinty ultramylonitic mica schists' cut earlier mylonitic fabrics. Heterogenous deformation continued under retrograde conditions. The Upper Ordovician to Silurian metasediments of the MaBA are the sedimentary cover of the Gullfjellet Ophiolite (Fossen and Dunlap, 2006) and folded in upright isoclinal folds (Færseth et al., 2011).

The Gullfjellet Ophiolite Complex is a large constituent of the MaBA. It comprises ophiolitic magmatic rocks (489 Ma; Fig. 10, no. 12) and arc-related granitoids (482 Ma; Fig. 10, no. 14). The Krossnes Granite (430 Ma; Fig. 10, no. 29) and the Sunnhordland batholith (430 Ma; Fig. 10, no. 30) are the youngest arc-related plutons.

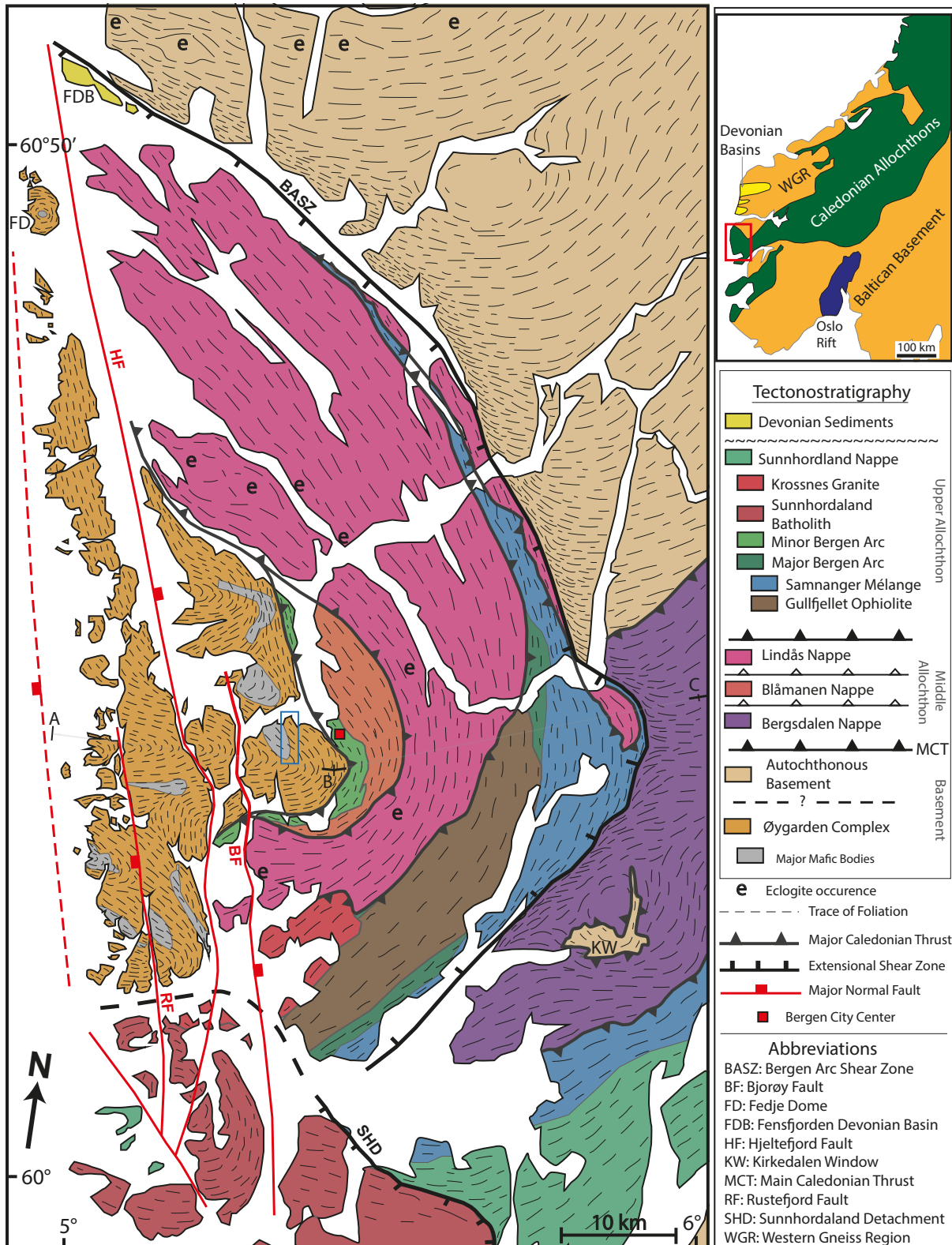


Fig. 8. Simplified geological map of the Bergen Arc System. The location of the map is shown with a red rectangle on the inset map. The established tectonostratigraphy is shown in the right column. Note, that the actual positions of the units in the Bergen Arc deviates from the tectonostratigraphic order. The trace of the Caledonian foliation is indicated by dashes. A,B,C outline the cross section (Fig.9). The working area of this study is marked with a blue rectangle. Based on Kolderup and Kolderup (1940); Askvik (1971); Bering (1984); Andersen and Jansen (1987); Larsen (1996); Boundy et al. (1996); Ragnhildstveit and Helliksen (1997); Larsen et al. (2003); Fossen and Ragnhildstveit (2008); Andersen et al. (2012); Roffeis and Corfu (2014); Centrella et al. (2015) and Winsvold (1996).

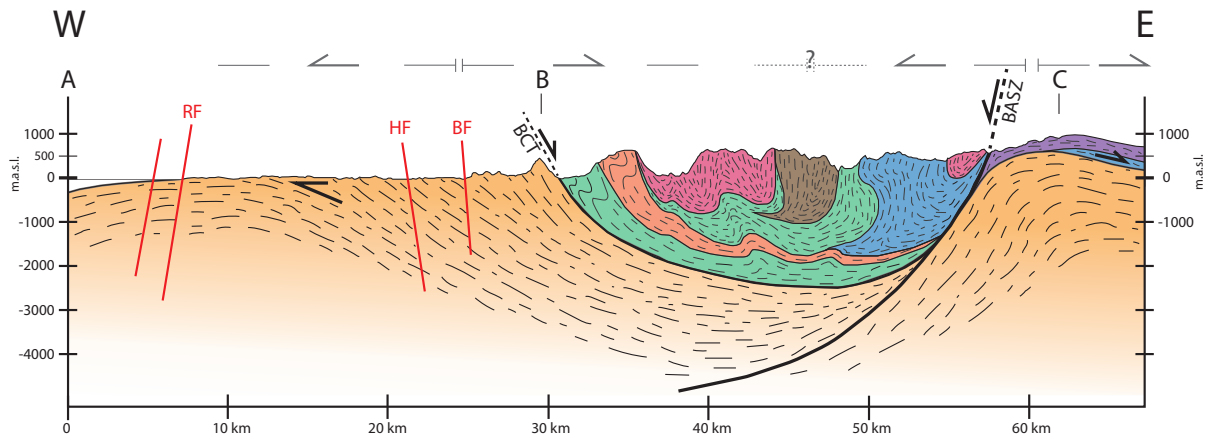


Fig. 9. Schematic cross section through the Bergen Arc. See Fig. 8 for legend and location. Unlike on the map, Øygarden Complex and autochthonous basement are shown with the same color. Grey arrows mark the prevailing sense of shear in different sectors (top-to-E/top-to-W). Dashes indicate the dip of foliation. The synclinally folded allochthons in the Bergen Arc have a steep dip at the surface but how they continue in deeper levels is poorly constrained. Abbreviations: BASZ - Bergen Arc Shear Zone; BCT - Basal Caledonian Thrust. Based on Fossen and Ragnhildstveit (2008); Ragnhildstveit and Helliksen (1997); Fossen and Dunlap (2006); Wennberg et al. (1998); Jolivet et al. (2005); Fossen (1998); Fossen (1989); Fossen (1988b) and Boundy et al. (1996).

The Samnanger mélange contains mantle peridotites, detrital serpentinites and fragments of ophiolitic as well as continental units in a (meta-)sedimentary matrix (Andersen et al., 2012, Slama and Pedersen, 2015). Andersen et al. (2012) interpreted this mélange to have formed during hyperextension of the pre-Caledonian passive margin. Slama and Pedersen (2015) contradicted this model based on an Ordovician zircon population in the detritus of the sedimentary matrix. They see the mélange as an Ordovician arc. Previous workers argued for a formation during emplacement of the Gullfjellet Ophiolite (Dunning and Pedersen, 1988).

The Lindås Nappe represents a slice of lowermost continental crust (Boundy et al., 1996) and belongs to the Middle Allochthon. The nappe consists largely of a Proterozoic anorthosite-mangerite-charnockite-granite suite with intrusion ages between 1237 - 950 Ma (Fig. 10, no. 3, 4, 8, 9, 22). It became overprinted by Sveconorwegian granulite facies metamorphism around 930 Ma (Fig. 10, no. 11). The complex is correlated with similar lithologies in the Jotun Nappe and the Rogaland Anorthosite Province (Bingen et al., 2001). Dry granulites underwent Caledonian, fluid-induced eclogitization along shear zones with top-to-E displacement (Austrheim et al., 1997; Austrheim and Griffin, 1985; Jolivet et al., 2005; Centrella et al., 2015). The exact timing of the eclogite formation in the Lindås nappe is controversial. Previous studies proposed pre-Scandian eclogite formation around 450 Ma (Boundy et al., 1997; Bingen et al., 2001). Re-investigations conclude an early Scandian age between 430 - 423 Ma (Bingen et al., 2004; Glodny et al., 2008). Eclogitization was overlapping with crustal anatexis (425 - 418 Ma; Kühn et al., 2002) and followed by amphibolite facies retrogression (c. 414 Ma; Bingen et al., 2001; Glodny et al., 2008). Controversially, mica Ar-Ar cooling ages from the Lindås nappe (c. 430 Ma; Fig. 10, no. 40) pre-date eclogite formation (430 - 423 Ma; Fig. 10, no. 16 & 17) in the same unit (Fig. 2C, right column; Fig. 10). Exhumation-related eclogite and amphibolite facies fabrics with consistent top-to-E shear sense, anastomize around pre-Caledonian granulite facies fabrics (Jolivet et al.,

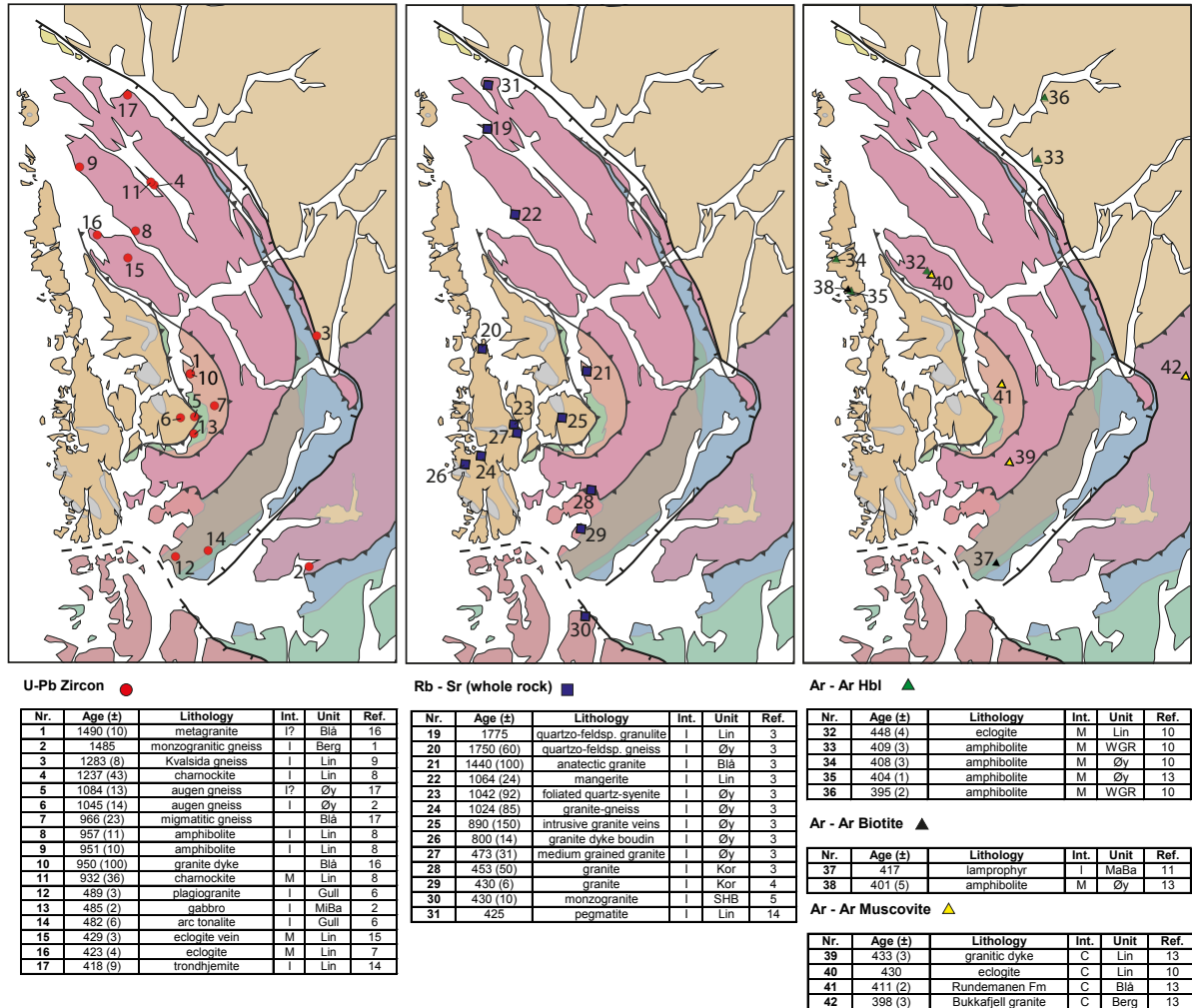


Fig. 10. Previous geochronological age determinations in the Bergen Arc System are shown in separate maps for different methods. See Fig. 8 for legend. Indexes on the maps refer to the corresponding tables where entries are sorted by age. Ages are given with errors in brackets, the dated lithology and the interpretations of the age (Int.): I - igneous (crystallization), M - metamorphism, C - cooling. References (Ref.): 1 - Ragnhildstveit and Helliksen (1997); 2 - Fossen and Ragnhildstveit (2008); 3 - Sturt et al. (1975); 4 - Fossen and Austrheim (1988); 5 - Andersen and Jansen (1987); 6 - Dunning and Pedersen (1988); 7 - Bingen et al. (2004); 8 - Bingen et al. (2001); 9 - Roffeis and Corfu (2014); 10 - Boundy et al. (1996); 11 - Fossen and Dunlap (2006); 12 - Fossen et al. (1997); 13 - Fossen and Dunlap (1998); 14 - Kühn et al. (2002); 15 - Glodny et al. (2008); 16 - Slama & Fossen, unpublished data; 17 - A. Ksienzyk, unpublished data.

2005). This has led to a proposed syn-orogenic exhumation model for the Lindås nappe with very rapid cooling (Brueckner and Cuthbert, 2013; Jolivet et al., 2005; Boundy et al., 1996). The ductile, exhumation-related fabrics follow the arcuate shape of the Bergen Arc (Fig. 8). The Lindås nappe is the only crystalline nappe that does not overlie phyllitic rocks (Roffeis et al., 2012).

The Blåmanen nappe consists of a slice of Precambrian basement and its sedimentary cover (Fossen, 1988b). The Ulriken Gneiss Complex is in mylonitic contact with the MiBA. It consists of migmatitic gneisses with heterogeneous Caledonian deformation. In high-strain zones the migmatites are transformed into banded gneisses. The domain of lowest Caledonian strain is named Biskopshaven Migmatite Complex. The age of migmatization and intrusive granites and pegmatites is commonly seen as Precambrian (Fig. 10: no. 1, 7, 10 & 21). The unconformably overlying Rundemanen Formation consists of Late Precambrian quartzite and diamictite. The entire nappe is strongly folded (Fossen, 1988b).

The SE footwall of the BASZ consists of the Bergsdalen nappes (Wennberg et al., 1998). They are a series of kilometer-thick, lensoid slices of detached Baltican basement, enwrapped in phyllites and micaschists (Fossen, 1993). The nappes experienced significant Caledonian (contractional and extensional) deformation. They are 'sandwiched' between the basement and the overlying Jotun nappe.

Baltican Basement

The basement NE of the arc is part of the WGR. While the (U)HP domains further north received large scientific attention, the southern part of the WGR is very poorly researched. The footwall of the BASZ consists of banded gneisses, migmatites, intrusive granites and pegmatites (Kolderup and Kolderup, 1940; Wennberg et al., 1998; Ragnhildstveit and Helliksen, 1997). Local mafic bodies of different dimensions and composition occur spread over the area. Layers of quartzites can be found locally folded into the gneisses. Based on studies from the Sognefjorden and Eksingedalen areas, it is assumed that this part of the basement is Gothian intruded by Sveconorwegian granites (Skår and Pedersen, 2003). Rohr et al. (2004) published the only U-Pb zircon study from the WGR south of the Sognefjord. They found a Gothian monzonitic protolith (1646 ± 110 Ma) overprinted by Sveconorwegian granulite metamorphism (987 ± 10 Ma) on the island Hisarøya.

The Caledonian overprint in the WGR decreases generally towards the SE, but increases towards the BASZ (Milnes et al., 1997; Wennberg et al., 1998). Winsvold (1996) reported Caledonian eclogites on Byrkenesøy in direct proximity to the BASZ and the Fennsfjorden Devonian basin. Eclogite occurs here within two E-W elongated lenses of 'undeformed migmatitic gneiss and granite', surrounded by banded and mylonitic gneisses. Winsvold interprets the granites and migmatites to be Precambrian. For the eclogites and the deformation of the area he infers Caledonian age. Gneisses show tight to isoclinal folding along WNW-ESE trending fold axes, (sub-)parallel to the mineral stretching lineation. Further east, away from the BASZ the structural trend turns from WNW-ESE to SW-NE. Fossen and Rykkelid (1992) relate NE-SW trending folds in this area (their F2.1) to Mode I extensional back-movement. They see them

kinematically similar to W-verging folds in the décollement zone below the Jotun Nappe (Fossen and Holst, 1995). This interpretation is complicated by the fact that the folds occur in the basement itself. Fossen and Rykkelid (1992) explain it by the parautochthonous state of the basement in this area.

Øygarden Complex

The Øygarden Complex forms the core of the Bergen Arc System. It consists mostly of migmatites and granites, transformed by Caledonian deformation into layered gneiss tectonites (Rykkelid and Fossen, 1992). The migmatites and granites are commonly seen as Precambrian but no U-Pb zircon ages are so far published from the Øygarden Complex. Rb-Sr whole rock ages (Sturt et al., 1975) are mostly between 1750 - 800 Ma (Fig. 10, no. 20 and 23 - 26). A boudinaged granite dyke was dated to 473 Ma (Fig. 10, no. 27). Rb-Sr biotite ages from the same sample were Devonian (398 Ma and 395 Ma). The felsic gneisses contain several mafic bodies. The best studied of those is the norite/gabbro on Askøy (Askvik, 1971). The Precambrian basic pluton intruded into heterogeneous gneisses before it was intruded by a quartz diorite (tonalite). The entire complex was deformed during the Caledonian Orogeny. Large areas in the core of the gabbro escaped deformation and alteration.

The Øygarden Complex shows heterogeneous but strong ductile deformation, which is entirely seen as Caledonian (Larsen et al., 2003; Fossen and Rykkelid, 1990; Bering, 1984). A pervasive, mylonitic L-S fabric formed and strain localized along E-dipping, mid-crustal shear zones (Rykkelid and Fossen, 1992). Non-coaxial deformation produced abundant kinematic indicators with top-to-W shear sense. Top-to-W fabrics prevail in C-S mylonites in the western part of the Øygarden Complex (Fig. 9). Less deformed augen gneisses and gneissic granites in the eastern area show top-to-E sense of shear (Fossen and Rykkelid, 1990, their Fig. 1). The top-to-W fabrics were first assigned to an early Caledonian event (Bering, 1984; Fossen and Rykkelid, 1990). They were later reinterpreted to have formed during post-orogenic extension (Fossen and Rykkelid, 1992; Fossen and Dunlap, 1998). Top-to-E fabrics are assigned to Scandian thrusting (e.g. Larsen et al., 2003).

Mineral stretching lineations in the Øygarden Complex plunge consistently towards E (Rykkelid and Fossen, 1992). Together with generally E-dipping planar fabrics this reflects the eastern limb of a large N-S striking antiform (Fig. 9; Sotra-Fedje culmination by Larsen et al., 2003). The mylonitic fabric is intensely folded along E-plunging fold axes (e.g. Sotra and Sund antiform by Larsen et al., 2003; see also trace of foliation in Fig. 8). These upright folds are associated with the arcuate structure of the Bergen Arc and have the same orientation as the folds of the Devonian basins and the NSDZ. Larsen et al. (2003) argued that the large scale folding postdates ductile top-to-W shearing.

The Fedje Dome (Fig. 8; Larsen, 1996) is located in direct proximity to the Fennsfjorden Devonian Basin (FDB). The gneiss dome is mantled by amphibolitic to quartzitic mylonitic gneisses. The core of the dome consists of migmatitic gneisses and a round lens of amphibolite/metagabbro. Larsen proposed a combined model of diapirism and folding for the formation of the Fedje Dome during Devonian extension.

Ar-Ar mineral ages show rapid cooling of the Øygarden Complex in the Early Devonian from upper amphibolite facies (Boundy et al., 1996) to the brittle-ductile transition at 396 Ma (Larsen

et al., 2003).

Different tectonostratigraphic positions have been proposed for the Øygarden Complex. The most common interpretation sees the Øygarden Complex as (par-)autochthonous Baltican basement (e.g. Larsen et al., 2003). Bering (1984) argued for a allochthonous status due to the pervasive shear deformation. Fossen (1988b) proposed the highest structural position in the Bergen Arc System based on the hypothetical model of a large-scale monocline that would explain the geometry of asymmetric folds in the MiBA and the Blåmanen Nappe (his Fig. 2b and 22).

Lyderhorn is located in the easternmost part of the Øygarden Complex that is geographically referred to as the Laksevåg peninsula. The area has been described by Kolderup and Kolderup (1940) and is covered by the *Berggrunnskart Bergen, M 1:50.000 & M 1:250.000* (Fig. 11A & B). Weiss (1977) published the results of a 'brief reconnaissance study' of the structural features of this area (Fig. 11C). The recent discovery of exceptionally high radiogenic heat production of the 'Løvestakken Granite' (Fig. 11D; e.g. Maystrenko et al., 2015) has sparked new interest in the area. Several master theses were implemented to evaluate the potential of geothermal energy production (Rudlang, 2011; Mathiesen, 2013; Schulze, 2014).

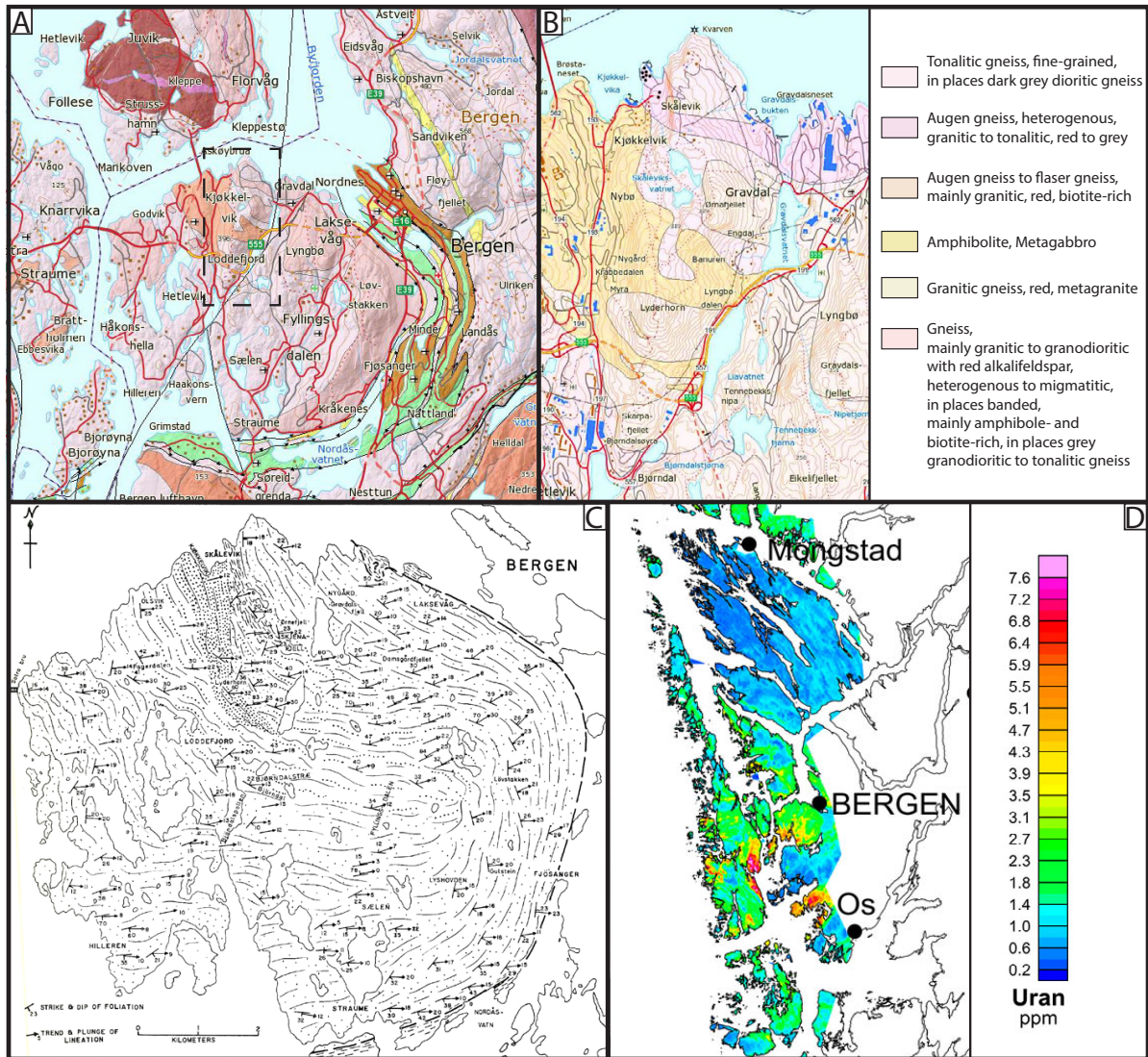


Fig. 11. Published former surveys of the working area. A: The Laksevåg peninsula on the berggrunnskart Bergen - M 1:250.000 (Ragnhildstveit and Helliksen, 1997), the working area is marked by a dashed rectangle and enlarged in B, shown with the berggrunnskart Bergen - M 1:50.000 (Fossen and Ragnhildstveit, 2008). Both maps are downloaded from <http://geo.ngu.no/kart/berggrunn>. C: Structural map of the Laksevåg peninsula from Weiss (1977). D: Map showing airborne geophysical measurements of Uranium concentrations in the Bergen area acquired by NGU. Downloaded from <http://www.ngu.no/nyheter/kart-viser-radioaktivitet-på-vestlandet>.

3 Principles of U-Pb Zircon Geochronology

3.1 U-Pb System in Zircon

Mineralogy of Zircon

Zircon ($\text{Zr}[\text{SiO}_4]$) is a tetragonal orthosilicate mineral with short prismatic habit. Isolated SiO_4 tetrahedra share their edges and corners with ZrO_8 dodecahedra (Harley and Kelly, 2007). Together they form anisotropic sets of chains of alternating SiO_4 and ZrO_8 polyhedra, aligned along the *c*-axis. In pure zircon these chains are separated by unoccupied channels and voids. In natural zircon the voids contain interstitial impurities. The *c*-axis chains furthermore determine the anisotropic physical properties and prismatic habit of the mineral. The remarkably simple structure of zircon results in a moderately high density (4.66 g/cm^3) and its physical robustness. Besides a high hardness (7.5), zircon has especially low thermal expansion and compressibility. This resistance to physical modification is an important characteristic of zircon. Its significance in geosciences stems from the tendency to incorporate a wide range of trace elements through cation substitution mechanisms, while preserving original chemical signatures due to low diffusion rates for most cations (Harley and Kelly, 2007). Furthermore zircon is abundant as an accessory phase in many metamorphic and magmatic rocks.

The ionic radii of Zr^{4+} (0.084 nm) and Si^{4+} (0.026 nm) cations allow the accommodation of up to 5000 ppm U^{4+} (0.026 nm), while Pb^{2+} (0.129 nm) is not incorporated into growing zircon crystals. Radiation damage of the crystal lattice caused by high U can lead to metamictization. Primary zircon crystallizes between 830 - 700 °C (Harrison et al., 2007). Oscillatory zoning and Th/U ratios close to 1 are characteristic for magmatic zircon (e.g. Corfu et al., 2003; Wu and Zheng, 2004). Metamorphic and hydrothermal processes can lead to recrystallization or alteration of zircon. Such processes are commonly associated with characteristic textures and morphologies. Careful pre-analytical assessment of zircon crystals is therefore an inevitable prerequisite for a sound interpretation of U-Pb ages.

U-Pb decay

The U-Th-Pb isotopic system consists of three independent decay series: $^{238}\text{U} \rightarrow ^{206}\text{Pb}$ ($T_{1/2} = 4.5 \text{ Ga}$), $^{235}\text{U} \rightarrow ^{207}\text{Pb}$ ($T_{1/2} = 0.7 \text{ Ga}$) and $^{232}\text{Th} \rightarrow ^{208}\text{Pb}$ ($T_{1/2} = 14.0 \text{ Ga}$). The intermediate products in the decay chains are very short lived, so that they can be neglected in the mathematical decay equations (Allègre, 2008). The greatest strength of the isotopic system are two individual and unconnected U-Pb decay series with half-lives that suite the geologic time scale. They represent two independent radiometric 'clocks' but their respective U and Pb isotopes have the same chemical behaviour and, particularly important, identical diffusion rates (Cherniak and Watson, 2003). An individual radiometric age can be obtained from each of the two U-Pb series (equation (1) & (2)). With the known modern ratio of $\frac{^{238}\text{U}}{^{235}\text{U}} = 137.82$ (Condon et al., 2010) it is further possible to calculate a Pb-Pb age (equation (3)).

$$^{207}\text{Pb} = ^{235}\text{U}(e^{\lambda_{235}t} - 1) \quad (1)$$

$${}^{206}\text{Pb} = {}^{238}\text{U}(e^{\lambda_{238}t} - 1) \quad (2)$$

$$\frac{{}^{207}\text{Pb}}{{}^{206}\text{Pb}} = \frac{(e^{\lambda_{235}t} - 1)}{137.82(e^{\lambda_{238}t} - 1)} \quad (3)$$

Concordia Ages

The concordia age utilizes the whole strength of the U-Pb isotopic system (Ludwig, 1998). Its calculation combines the two individual U-Pb decay series into one single age and evaluates quantitatively concordance as well as age equivalence. Concordia ages can be calculated for both: entire samples with a multitude of analyses (common concordia age) as well as individual analyses (single grain concordia age). Individual analyses are plotted as error symbols in the concordia diagram ($\frac{{}^{206}\text{Pb}}{{}^{238}\text{U}}$ against $\frac{{}^{207}\text{Pb}}{{}^{235}\text{U}}$). In undisturbed systems, both ratios should yield equivalent ages which plot on the concordia line (defined by $y = (e^{\lambda_{238}t} - 1)$ and $x = (e^{\lambda_{235}t} - 1)$). Ages from a system that is not entirely closed, do not plot along the concordia line and are called discordant. If Pb-loss occurs due to diffusion, the ages will plot along a line (discordia) that intersects the concordia twice. These intersections can be interpreted as the primary zircon forming event and a secondary thermal/metamorphic event leading to episodic Pb-loss (Harley and Kelly, 2007).

Diffusion in Zircon

U diffusion in zircon does not occur at subsolidus temperatures (Cherniak and Watson, 2003). Discordant ages reflect the characteristic behaviour of Pb in zircon. That is: robustness to high-grade resetting and weakness to low-grade alteration (Mezger and Krogstad, 1997). The closure temperature for Pb diffusion in pristine zircon is between 800 - 1000 °C (Cherniak and Watson, 2003). Thus, zircon ages are not even reset when they reside for long time scales at temperatures high enough for partial melting. On the other hand, metamict zircons are very vulnerable to diffusional Pb-loss at low temperatures (Mezger and Krogstad, 1997). Zircon can only accumulate radiation damage when residing over long time periods below the 'critical amorphization temperature' of ~ 360 °C (Cherniak and Watson, 2003). More than 1 Gy are necessary for zircon with U around 100 ppm, but the process is faster for high-U zircon. Rapid heating of severely metamict grains can cause significant diffusional Pb-loss and complete resetting. Another cause of discordance are fluid induced diffusion-reaction and coupled dissolution-reprecipitation processes that can re-equilibrate zircons even at surface P-T conditions (Geisler et al., 2007). The counterintuitive behaviour of Pb diffusion in zircon shows that discordia intercept ages need to be interpreted with care.

3.2 SIMS Geochronology

All analytical techniques for measuring isotope compositions in zircon are based on mass spectrometry. Since its development in the early 20th century, mass spectrometry has evolved to a very precise technique with confirmed reliability. Zircon sampling techniques, on the other hand, have long limited the accuracy of the results. In the last 30 years high-precision ion probes have been developed (Davis et al., 2003). SIMS (secondary ion mass spectrometry) geochronology

allows in-situ analyses with a spot size as small as 10 micron (Fig. 12A). In combination with high-resolution images (CL: cathodoluminescence or BSE: backscattered electron) different parts of single zircon grains can be dated individually and zoning can be assigned to multiphase geological histories recorded in a single crystal (Ireland and Williams, 2003).

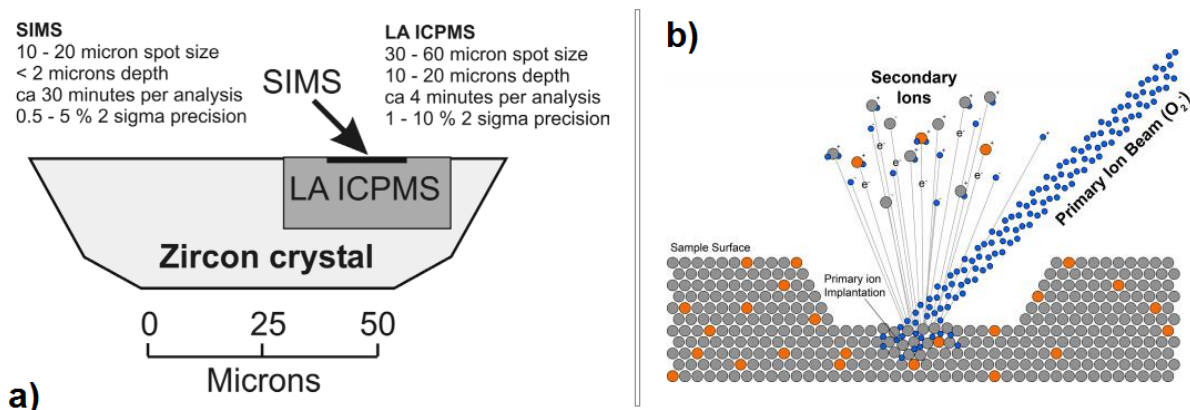


Fig. 12. A: Spatial precision of SIMS zircon geochronology compared with LA ICPMS. Modified from Košler and Sylvester (2003). B: Technical principles of SIMS analysis: a primary ion beam is shot onto the prepared sample surface where it ablates atoms and molecules, ionizing some of them. Modified from <https://shrimprg.stanford.edu/shrimp-rg> (downloaded: 20.05.2015).

A focused beam of high-energy primary ions (O^{2+}) is shot onto polished and gold-coated mineral surfaces to sputter (ablate) atoms and molecules while ionizing some of them (Fig. 12B). The primary beam is either static or dynamic. It cuts a small crater into the surface (usually 10-50 μm in diameter and less than 5 μm deep), making the analysis effectively non-destructive. The secondary ions are accelerated to run through an electrostatic analyser and the magnetic sector. They arrive in the collector units differentially deflected according to their mass and charge. The size of the mass spectrometer unit determines thereby the deflection radius. Together with the spacing of the detectors this controls the achievable mass resolution of the instrument.

To determine the atomic concentration C_A of an atom A in the sample it is necessary to calculate the sensitivity factor $S_{A^+}^M$ of the ion A^+ in the matrix M . Therefore, standard zircons with known atomic concentration C_A and assumed identical matrix composition (as the zircon samples) are analysed simultaneously with the samples. $S_{A^+}^M$ can be calculated after equation 4 from the measured $I_{A^+}^M$ and known C_A .

$$I_{A^+}^M = S_{A^+}^M \times C_A \quad (4)$$

This $S_{A^+}^M$ again can be used to calculate the unknown C_A in the samples, based on the assumption that their matrix composition is identical to the standard.

Data Processing

Raw SIMS data contain systematic analytical uncertainties that need to be corrected for. Accurate determination of interatom ratios is the largest issue in SIMS analysis. Unlike in isotope dilution analysis, SIMS does not measure U, Pb and Th concentrations directly. Therefore, interatom ratios are determined from secondary ion ratios. This U/Pb calibration is done by a

power law, exponential law or linear approximation (Whitehouse et al., 1997). It needs to take into account that different elements have different secondary ionization efficiencies and different tendencies to form multiple oxides (Ireland and Williams, 2003). Initial Pb can be corrected for by the common-Pb correction: Non-radiogenic ^{204}Pb present in the samples is measured. With known ratios of Pb-isotopes in nature, initial ^{206}Pb and ^{207}Pb can be subtracted.

4 Methods

4.1 Mapping and Sampling

Lyderhorn is located exactly 5 km west of the Department of Earth Science at the University of Bergen. The proximity of the working area allowed to conduct this study in a different manner than typical field base studies are implemented. Field work accompanied the entire two years of my M.Sc. program at the University of Bergen and was an iterative process. The Lyderhorn area was investigated by standard outcrop mapping techniques. In preparation, high-resolution orthophotos were used to create a digital map of exposures (Fig. 13). On orthophotos of the working area, bright exposure surfaces are in contrast to the dark vegetation cover. Exposure surfaces were filtered out based on their RGB values and converted into vector file format so that artefacts could be manually deleted and missing outcrops added. During systematic outcrop mapping, 211 individual outcrops were classified and described (Appendix 2 and 3). I use these outcrop numbers as geographic references in the presentation of results.

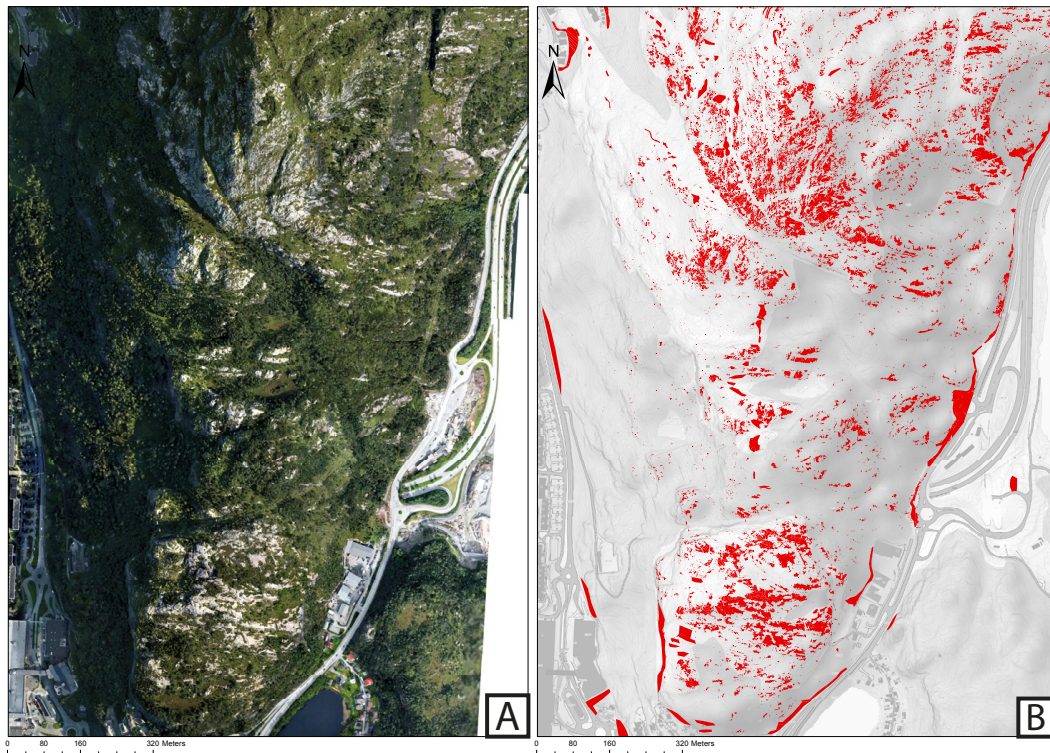


Fig. 13. Representative maps of the southern part of the study area illustrating the creation of a digital exposure map in ArcGIS. Exposure surfaces were filtered out from a collage of high-resolution orthophotos from Google Earth (A). The extracted surfaces were converted into vector file format (B; red polygons). Artefacts (e.g. streets) were manually removed and missing outcrops added.

Thin section samples were collected from chosen localities and prepared at the University of Bergen to allow detailed petrographic descriptions and microfabric analysis. Structural measurements were taken for linear and planar fabrics. Note, that planar structural measurements are reported in this text as 'dip-azimuth'/'dip', different from the standard notation in Norway. Stereonet 9 (Allmendinger et al., 2011) was used for the statistical analysis of structural data and for the creation of stereoplots presented in this work. As fabrics developed under continuous deformation with identical orientation, distinct deformation events or phases were not defined.

After completion of field mapping, seven samples were collected for SIMS U-Pb zircon geochronology from key localities to represent the dominant lithology in each of the units. The samples were crushed on the outcrop into small pieces, to minimize the risk of lab contamination. The first digits of sample numbers refer to outcrop numbers defined during field mapping (Appendix 2 and 3).

4.2 SIMS U-Pb Zircon Geochronology

4.2.1 Sample Preparation

Crushing and Mineral Separation

Crushing and mineral separation was done at the University of Bergen. Samples were crushed with the Fritsch Pulverisette 13 discmill (Fig. 14A) until the bulk of the sample was finer than 315 μm . Larger particles were removed by sieving. The heavy fraction was separated on the Holman-Wilfley shaking table (Fig. 14C) to reduce sample sizes for further processing. Magnetic mineral separation was applied for the heavy fraction. Ferromagnetic minerals were removed with a hand magnet. The Frantz Magnetic Separator (Fig. 14B) was first applied with a current of 0.6 V to extract weak ferromagnetic minerals (e.g. hematite). Afterwards, a current of 1.2 V was used to separate non-magnetic minerals like zircons from very weak ferromagnetic minerals like garnet. For both steps the forward and sideways tilt was 15°.

Depending on size and mineralogy, the non-magnetic fractions were separated with the heavy liquids LST (Low toxicity Sodium heteropolytungstates; density: 2.83g/cm³) and DIM (Di-Iodomethane; density: 3.31g/cm³). LST (Fig. 14D) has been applied to larger samples to remove remaining quartz (2.65g/cm³) and feldspar (2.55 – 2.76g/cm³). These samples were subsequently rinsed with deionized water. For all samples DIM (Fig. 14E) was used to separate zircons (4.60 – 4.70g/cm³) from other heavy minerals. The samples were afterwards rinsed with acetone and dried. Sample LYD-44-1 was once more subjected to the Frantz Magnetic Separator (1.4 V) to remove abundant titanite.

Mount Preparation

Zircons were handpicked from mineral separates. The seven samples contain very distinct zircon populations. The number of picked grains varies between 15 (LYD-35-1) and 140 for samples with strongly metamict zircons (LYD-163-1 and LYD-197-2). Anhedral, colorless and clear zircon fragments in sample LYD-44-1 were picked under cross-polarized lights to allow the identification of zircon. Further mount preparation was carried out at the Nordsim laboratory in Stockholm.

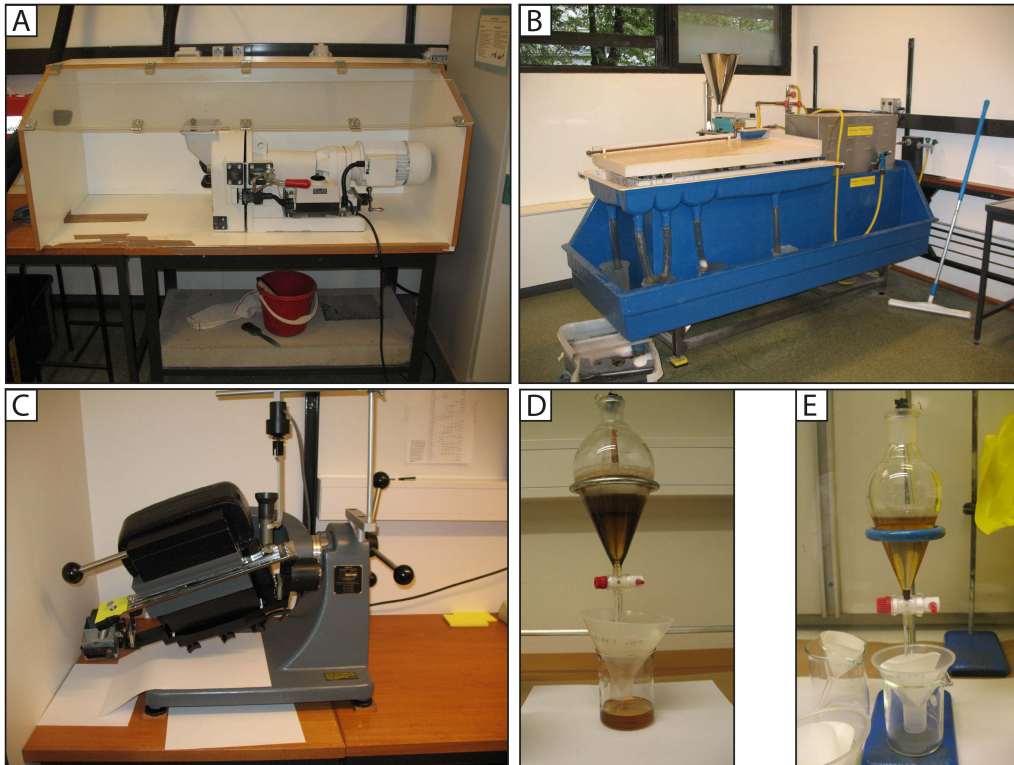


Fig. 14. Techniques applied in the following order for crushing and mineral separation at the University of Bergen: A: Fritsch Pulverisette 13 discmill. B: Holman-Wilfley shaking table. C: Frantz Magnetic Separator D: LST heavy-liquid. E: DIM heavy-liquid.

Zircon Imaging and Spot Identification

Cathodoluminescence (CL), transmitted light (TL) and reflected light (RL) imaging was done at the University of Bergen. In preparation for CL-imaging, the polished mount was coated with gold. Zircons were photographed with a Zeiss Supra 55VP Scanning Electron Microscope with CL detector to reveal internal textures. TL- and RL- images were taken with a Olympus BX51 optical microscope to identify inclusions and fractures in the grains. Spots for SIMS analysis were identified comparing all three different images to allow textural interpretations and to avoid inclusions and fractures.

4.2.2 SIMS Analysis

Before analysis, the gold coating from CL-imaging was removed, the mount was carefully cleaned and a fresh gold coating applied. Zircon U-Pb geochronology and scanning ion imaging was performed using a CAMECA IMS1280 large geometry ion microprobe at the Nordsim facility, Stockholm (Fig. 15). Geochronological analyses follow routine protocols outlined by Whitehouse et al. (1999) and Whitehouse and Kamber (2005). A ca. 6 nA, -13 kV O_2 -primary beam (imaged aperture of 150 μm corresponding to a spot diameter on the sample of ca. 15 μm) was used to generate +10 kV secondary ions which were admitted to the mass spectrometer and detected in a peak-hopping sequence using a single ion-counting electron multiplier. The mass spectrometer was operated at a mass resolution ($M/\Delta M$) of 5400, sufficient to separate all species of interest from molecular interferences. Each analysis comprised a 90 second pre-sputter to remove the

Au-coating and allow the secondary beam to stabilize, centering of the secondary beam in the field aperture, energy optimization in the 45 eV energy window, mass calibration adjustment using the $^{90}\text{Zr}_2^{16}\text{O}$ peak, and 12 cycles through the species of interest. Groups of analyses were performed in fully automated sequences, regularly interspersing standard analyses with those of the sample zircon grains. Data reduction utilized an in-house developed suite of software. Pb-isotope ratios were corrected for common Pb estimated from measured ^{204}Pb assuming the present-day terrestrial Pb isotope composition estimated from the model of Stacey and Kramers (1975); where the ^{204}Pb count was statistically insignificant relative to the long-term background on the EM, no correction was applied. U/Pb ratios were calibrated using an empirical power-law relationship between $\frac{^{206}\text{Pb}}{^{238}\text{U}}$ and $\frac{^{238}\text{U}^{16}\text{O}_2}{^{238}\text{U}}$ assuming the 1065 Ma age of the 91500 zircon (Wiedenbeck et al., 1995). Age calculations assume the decay constant recommendations of Steiger and Jäger (1977) and utilize the routines of Isoplot-Ex (Ludwig, 2003).

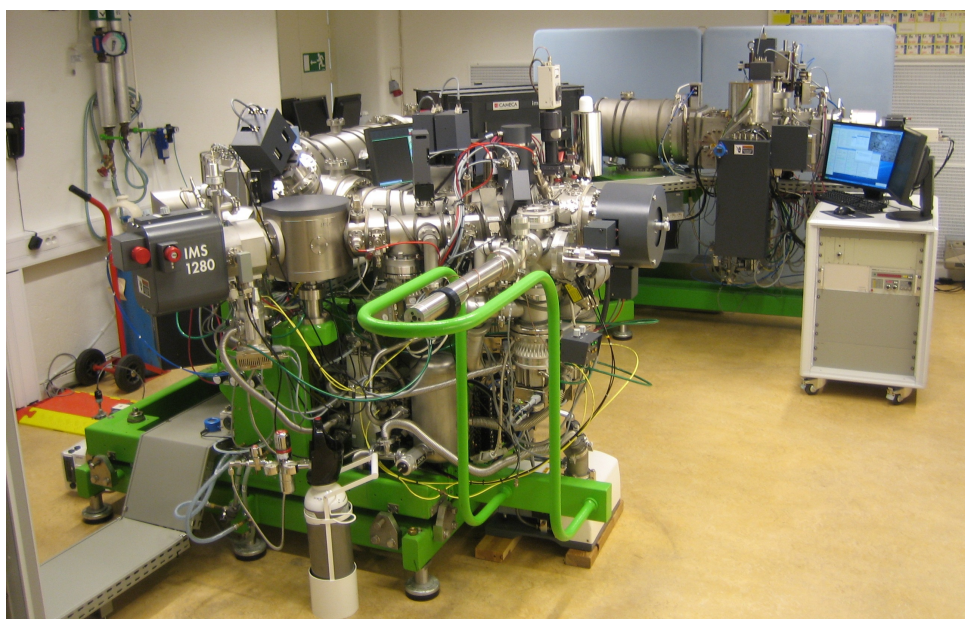


Fig. 15. CAMECA IMS1280 large geometry ion microprobe at the Nordsim facility, Stockholm. Image provided by Martin Whitehouse.

Data Evaluation

Single spot concordia ages were calculated for all analyses using Isoplot (Ludwig, 2003). If possible, a common concordia age was calculated for the entire sample. Alternatively, a weighted mean of concordia ages or discordia intercepts were calculated. All figures in the geochronology part were created using Isoplot (Ludwig, 2003). If not further specified, presented ages in this text are concordia ages with 2σ errors. It should be noted, that negative discordance values correspond to normal discordance.

5 Results

5.1 Mapping

The results from field mapping are presented in a geological map of Lyderhorn (Appendix 4), accompanying N-S cross section (Appendix 5) as well as a three-dimensional geological model (Appendix 8). Separate maps are provided for structural measurements (Appendix 6 and 7). Fig. 16A shows geographic domains of the working area that are used in the text as references together with outcrop numbers (Appendix 2 and 3).

Lyderhorn has a prominent geomorphology (Fig. 16B). The mountain itself is N-S elongated and most steep surfaces are N-S oriented. Three massifs form exceptions from the rule: Ørnafjellet (329 m.a.s.l.) in the north, Skarpafjellet (183 m.a.s.l.) in the south and the cone-shaped peak of Lyderhorn itself (396 m.a.s.l.). The steep western side of the mountain has many inaccessible cliffs and represents a natural N-S cross-section (Fig. 17). The NE-slope has a consistent moderate dip and is covered by tight vegetation. The SE-slope below the peak of Lyderhorn is steep and rugged. The morphology of the southern part is controlled by E-W trending granite bodies that stick out of the vegetation cover.

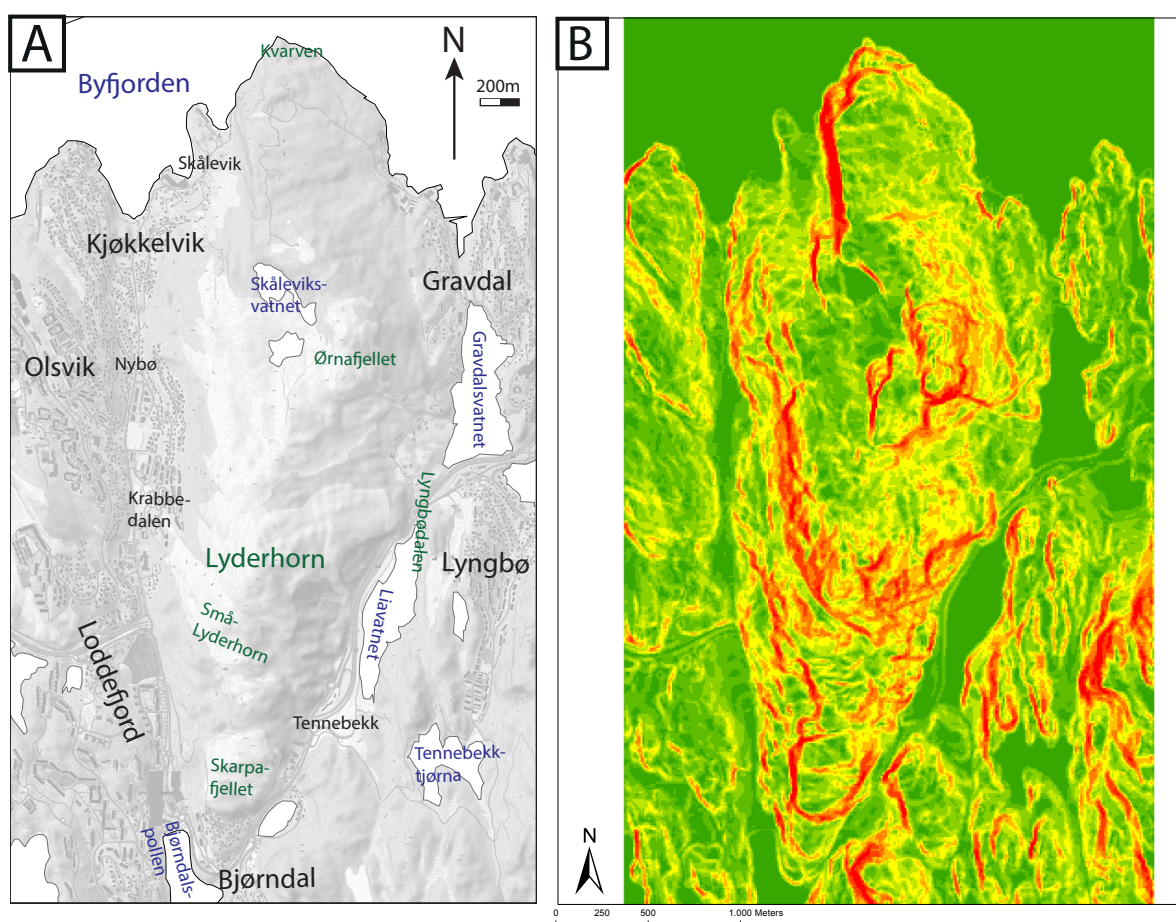


Fig. 16. A: Geographic map of Lyderhorn with specification of subareas. Map from norgeskart.no. B: Map of the topographic slope calculated from a DEM with a horizontal resolution of 10 m x 10 m. The steepness of the slope is shown by colors: green: 0 - 20°, yellow: 20 - 45°, red: 45 - 90°.

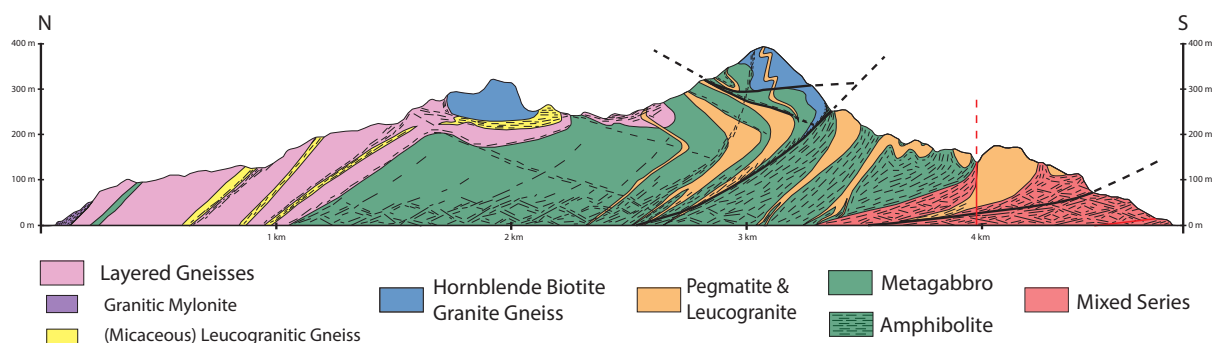


Fig. 17. Schematic N-S cross section through Lyderhorn. The mapped lithologies are grouped in five units. Dashes indicate orientation and intensity of deformation. In the gabbroic unit dashes distinguish vaguely between metagabbro and amphibolite. Thick black lines show representative shallowly NE-dipping shear zones. Note, that they localize along contacts but also cut fold structures. The red line marks a major steep brittle fault. Two times vertical exaggeration.

5.1.1 Petrology

Gabbroic Rocks

A major body of gabbroic rocks forms the core of Lyderhorn. Gabbroic rocks are in general relatively poorly exposed, occupy topographic lows and are covered by vegetation. A small lense of more or less unaltered gabbro forms a hill at Olsvik (Fig. 18A). On Lyderhorn itself, gabbroic rocks are transformed into metagabbros or amphibolites.

Metagabbros have a characteristic appearance in rounded outcrops with green hornblende and white plagioclase (Fig. 18B). Other constituents are relict orthopyroxene. Accessories are titanite-rutile aggregates and opaque minerals. The contacts between metagabbros and amphibolites are transitional. Amphibolites (Fig. 18C) are defined by finer grain size due to dynamic recrystallization of plagioclase and metamorphic growth of aligned amphiboles. Based on this relation, amphibolites are regarded as the more deformed equivalents of metagabbros. Garnet-bearing amphibolites occur at the west face of Lyderhorn at the intrusive contact of a pegmatite (45). White tonalitic veins occur in all kinds of gabbroic rocks (Fig. 18D). These veins might represent late differentiates of the gabbroic magma. However, due to the intrusion of granitic rocks of varying composition it cannot be ruled out that the tonalitic veins belong to this later magmatic episode.

The gabbroic rocks on Lyderhorn show many similarities to gabbroic lithologies on Askøy (Askvik, 1971) and have therefore been correlated by Kolderup and Kolderup (1940).

Hornblende Biotite Granite Gneiss

Two bodies of gneissic hornblende biotite granite form the peaks of Lyderhorn and Ørnafjellet. The Lyderhorn body is intruded by numerous pegmatites which are absent on Ørnafjellet. Minor bodies of hornblende biotite granite occur within the gabbroic rocks (e.g. at Nybø, 199). The gneissic granite forms massive outcrops especially where it is intruded by pegmatites (Fig. 19A). Textures are inequigranular medium grained. Compositions are mostly melanocratic and syenogranitic but grade towards granodioritic or tonalitic at the rims of the bodies. The



Fig. 18. Field appearance of gabbroic rocks. A: Weakly altered gabbro (Olsvik, 198). B: Metagabbro in a section perpendicular to stretching lineation (Lyderhorn, 50). Note semi-brittle deformation of granitic vein along small, subhorizontal faults. C: Amphibolite in a section parallel to mineral stretching lineation (Krabbedalen, 35). D: Heterogenously deformed amphibolite with white tonalitic veins and intrusive pegmatite (Krabbedalen, 36).



Fig. 19. A: Massive hornblende biotite granite gneiss intruded by a one meter wide, subvertical, pinkish pegmatite in the center of the picture (Lyderhorn peak, 197). B: Deformation of both lithologies in a mesoscale NE-dipping shear zone (Lyderhorn peak, 191).

characteristic appearance of hornblende biotite granite gneisses comes from centimetre-size bright patches of pinkish K-feldspar and minor plagioclase and dark patches consisting of large blueish-green hornblende phenocrysts as well as fine grained biotite, quartz and feldspar.

The gneissic granites are in general poorly foliated but discrete shear zones transform both, granites and intruding pegmatites, into heterogeneous mylonitic gneisses (Fig. 19B). Partly recrystallized K-feldspar crystals form augen textures but more often, aggregates of recrystallized feldspar have diffuse shapes.

The contact between gabbroic rocks and hornblende biotite granite is usually a several metre wide zone where both lithologies are interlayered without clear intrusive relationships (Fig. 20D). Inside this zone patches of both lithologies grade diffusively into each other (Fig. 20E). Other localities exhibit intrusive relationships. Fig. 20 shows white medium grained, hornblende biotite granite that intrudes and brecciates amphibolite (dark). Angular as well as rounded, lobate fragments of amphibolite are enclosed by granite (Fig. 20B). Fig. 20C shows irregular xenoliths of amphibolite within hornblende biotite granite. The xenoliths have an internal foliation that mimics the outer shape. Euhedral K-feldspar crystals occur within the amphibolite. The contacts are partly sharp and partly diffuse. The described findings indicate that the hornblende biotite granite intruded the gabbro before the latter was entirely crystallized.

Previously, hornblende biotite granite gneisses have been mapped inconsistently as 'granitic augen gneiss to flaser gneiss' (Fossen and Ragnhildstveit, 2008).

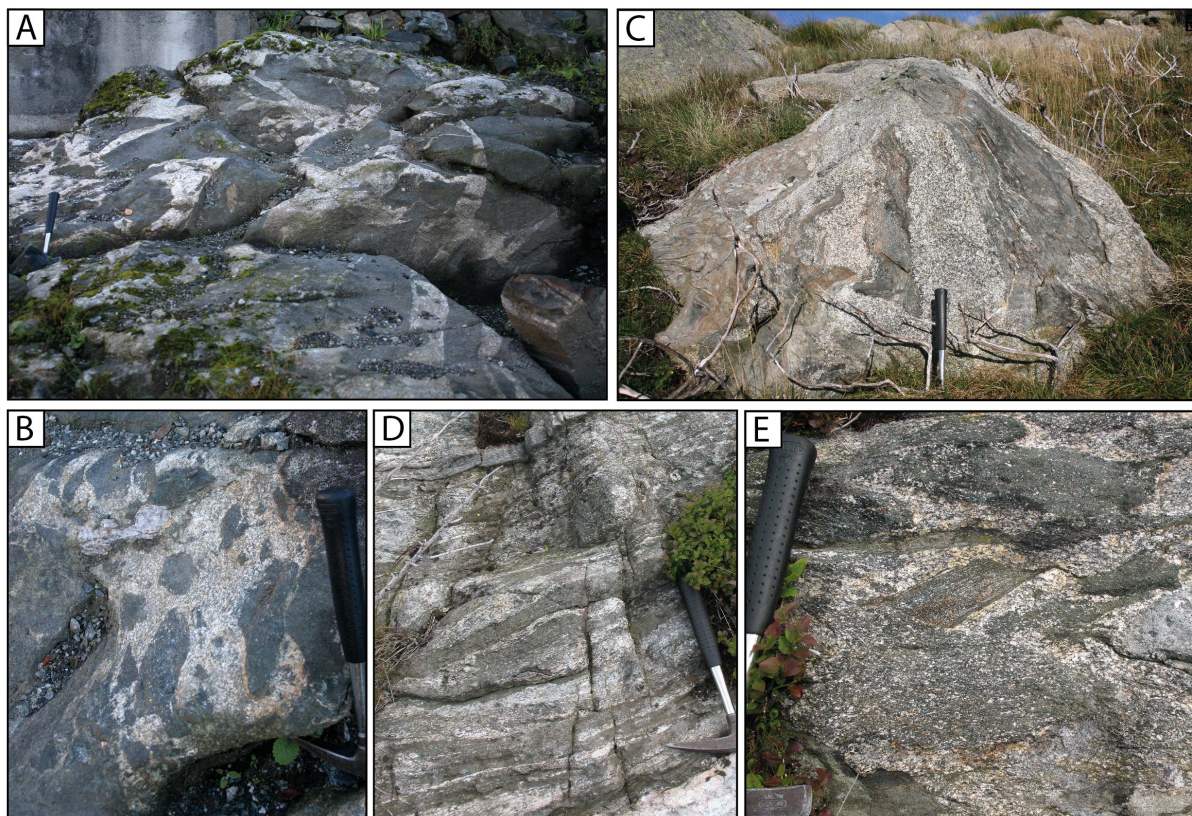


Fig. 20. A: White, hornblende biotite granite intruding amphibolite (Nybø, 200). B: Detail from the same outcrop: Angular and lobate fragments of amphibolite are contained within granite. C: Irregular xenoliths of amphibolite in hornblende biotite granite (Lyderhorn, 46). D: Interlayering of gabbro and granite in the contact zone (Lyderhorn, 50). E: Detail from the same outcrop: Xenoliths and diffuse gradational contacts coexist.

Layered Gneisses

Alternating layers of granitic and tonalitic gneisses mantle the gabbroic body on Lyderhorn to the north. This unit is well exposed along the northern ridge of the mountain and at Gravdal. Main components are granitic augen gneisses (protomylonites) with large K-feldspar augen surrounded by a fine grained matrix of recrystallized quartz, feldspar and biotite. Apparent intrusive contacts exist with fine to medium grained, uniform, bright-grey granitic gneiss (Fig. 21B). Several tens of metres thick granite layers have coarse grained to pegmatitic textures, similar to rocks in the leucogranite and pegmatite unit. Two thin dykes of amphibolites could be mapped over some distance. They are parallel to the foliation and show no clear cross-cutting relationships. In zones of high strain, augen gneisses are transformed into mylonitic gneisses (Fig. 21A). Apparent intrusive contacts have been identified, but due to the layered structure and the lithological heterogeneity a metavolcanic origin could also be possible.

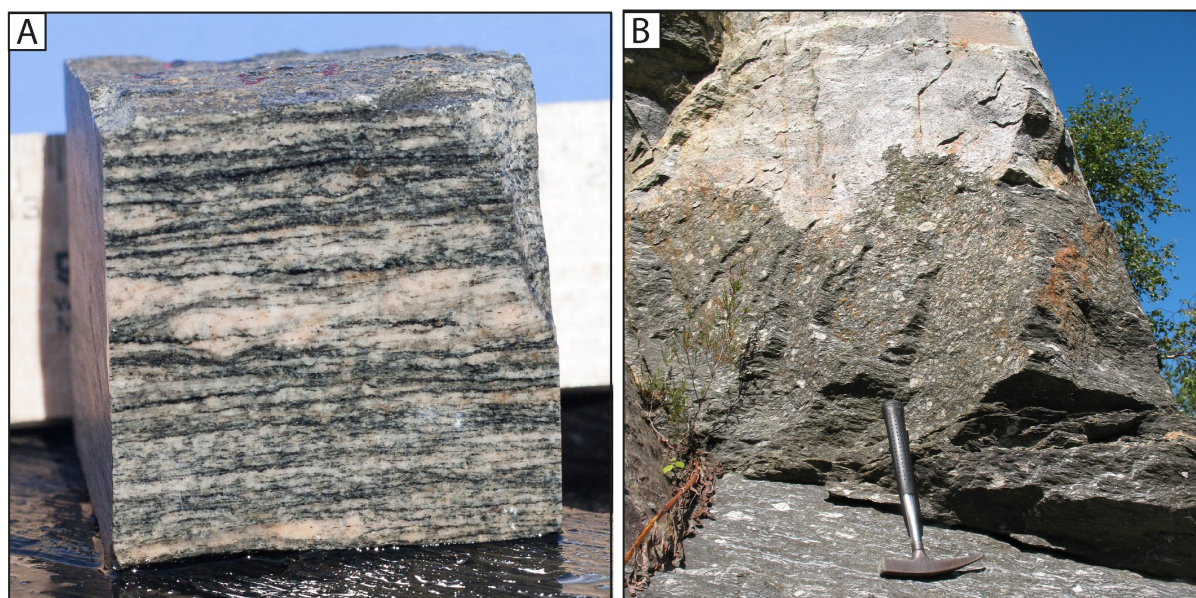


Fig. 21. Field appearance of the heterogeneous group of layered gneisses. A: Hand specimen of granitic S-L tectonite cut parallel to the E-plunging mineral lineation (Skåleviksvatnet, 151). B: Apparent intrusive contact of darker, protomylonitic augen gneiss with medium grained, bright-grey granitic gneiss (Gravdal, 103).

Leucogranites and Pegmatites

Leucogranites and pegmatites intrude all the previously described units. They appear as E-W elongated dykes south of Ørnafjellet and get more and more voluminous towards the south. Around Skarpafjellet, they occupy most of the area. The thickness of individual bodies ranges from centimetres to several tens of metres. The lithologies within this unit are very heterogenous. Textures vary within outcrops from pegmatitic to medium grained granite with diffuse transitions (Fig. 22A).

A major part of the unit is made up of pegmatites with alkali feldspar granitic composition. Individual K-feldspar crystals can reach sizes of more than 30 cm (Fig. 22B). The second constituent of the unit are medium grained, equigranular, leucocratic, gneissic granites with

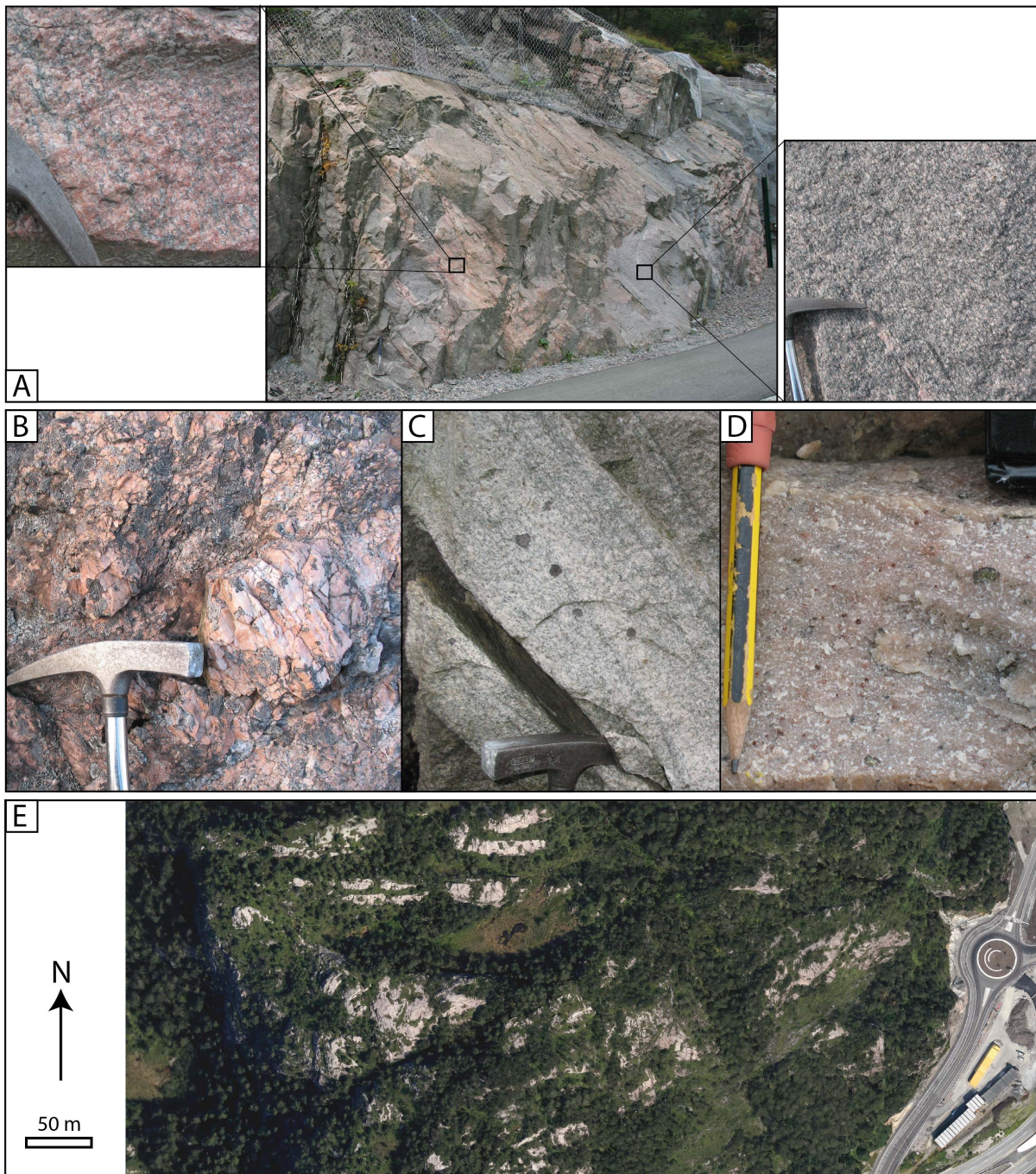


Fig. 22. Field appearance of leucogranites and pegmatites. The lithologies in the unit are very heterogeneous. A: Pegmatitic and medium grained textures grade diffusively into each other (Liavatnet, 163). B: K-feldspar megacryst (Skarpafjellet, 182). C: White, medium grained gneissic granite (Skarpafjellet, 183). D: Garnet-bearing aplite (Krabbedalen, 35). E: Folded, E-W-elongated pegmatite dykes (bright) stick out on orthophotos. Surrounding amphibolites are weathered away and covered by vegetation. Area between Skarpafjellet and Små-Lyderhorn. Image from Google Earth.

syeno- to monzogranitic composition (Fig. 22C). Garnet and titanite are common accessory minerals in pegmatites as well as in aplitic dykes (Fig. 22D). Common to all lithologies is their occurrence as confined, E-W striking bodies. These are well visible where pegmatite dykes intrude amphibolite and stick out because of their resistance towards weathering (Fig. 22E).

The mapped occurrence of this unit shows an accurate coincidence with highly radiogenic gamma-spectrometry measurement carried out by Rudlang (2011). This relationship allows a direct correlation between lithology and heat production in the area that did not become clear from earlier lithological subdivisions. What is commonly referred to as the 'Løvstakken granite' consists of different constituents. Of these, only the granite and pegmatite unit is highly radiogenic.

Mixed Series

The unit that covers the area around Loddefjord, consists basically of a mix of the previously described lithologies. The major component are irregularly shaped bodies of pegmatites with variable dimensions, compositions and textures. Lenses of amphibolite and metagabbro are contained within networks of pegmatite veins (Fig. 23A). Mafic rocks alternate on a metre-scale with layers of hornblende biotite granite gneiss and banded mylonitic gneisses (Fig. 23B). Only the pegmatites show clear intrusive relationships with the other lithologies. The deformation of the unit is heterogeneous but in general strong. Granitic and amphibolitic protoliths have been tectonically transposed into banded gneisses. Layers of different composition alternate on the meso- and microscale. The mapped extent of the unit corresponds to the 'layered series' by Weiss (1977).

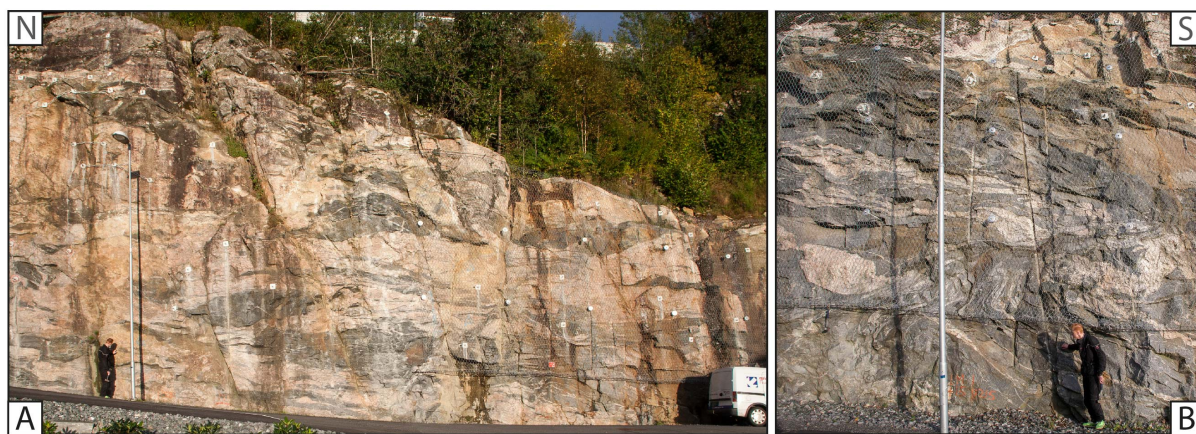


Fig. 23. Roadcut exposing the mixed series (Bjørndal, 169). A: Intrusive vein network of pegmatites encloses lenticular bodies of amphibolite and metagabbro. B: Granitic gneiss in the same outcrop intruded by irregular pegmatite bodies. Both lithologies are affected by a mesoscale shear zone.

5.1.2 Structure

Penetrative Ductile Deformation

Penetrative ductile deformation in the Lyderhorn area is recorded from amphibolite facies to the brittle-plastic transition with clear retrograde overprinting relationships. ENE-plunging mineral stretching lineations formed with identical orientations indifferent of metamorphic grade or lithology (Appendix 7). However, along the N-S cross section the trend of linear fabrics rotates towards ESE in the Loddefjord area (Fig. 24A). Further south, outside of the study area, lineations plunge towards ENE (Weiss, 1977; Fossen and Ragnhildstveit, 2008). The observed pattern shows a relationship with the shape of the gabbroic body that forms the core of Lyderhorn. The mean trend of the stretching lineations is 82° and thereby identical with the mean trend of measured fold axes (Fig. 25A). The penetrative mylonitic foliation is commonly parallel to lithological contacts. Planar fabrics dip in general shallowly to moderately towards the NE but steep dip occurs in restricted E-W striking zones.

Depending on their mineral composition, different rock types were transformed into L-S and S-L tectonites, respectively. Restricted domains within the gabbroic body escaped penetrative deformation but most gabbroic rocks were metamorphosed into metagabbros and amphibolites, showing deformation at amphibolite facies conditions. Associated fabrics show a strong anisotropy (Fig. 26 A and B). Recrystallization of plagioclase and metamorphic growth of amphiboles produced a pronounced ENE-plunging linear fabric. The development of a mylonitic foliation depends on the presence of biotite. Extensional C-C' structures are well developed on the meso- and microscale and show consistently top-to-E sense of shear (Fig. 26B and C).

In the various granitic rock types, greenschist facies fabrics prevail. Linear fabrics are formed by elongated rods of recrystallized quartz and feldspar. They plunge consistently to ENE with identical orientation as amphibolite facies lineations. Kinematic indicators are well developed in mylonitic gneisses and show consistently top-to-E shear-sense (Fig. 27 A - D). The layered gneiss unit and the mixed series are dominated by granitic rocks. Here, S-L fabrics are strongly developed and the granitic protoliths are transformed into banded gneisses. The degree of mylonitization increases in general from north to south. Protomylonites prevail in the layered gneiss unit, mylonites and ultramylonites are more common in the mixed series. Clastomylonites formed from heterogeneous lithologies in steep, E-W striking shear zones. Phyllonites are abundant in shallowly NE- and SE-dipping shear zones. Granitic bodies from the leucogranite and pegmatite unit are commonly contained within gabbroic rocks and have a dominant linear fabric. The ductile deformation of this unit is heterogeneous. Close to contacts, mylonitic to ultramylonitic foliations can be well developed and ultramylonitic leucogranites can be found (Fig. 27E). Within pegmatite bodies, lower greenschist facies deformation formed spectacular microfabrics showing synchronous brittle fracturing of large feldspars and crystal-plastic deformation of quartz (Fig. 27F).

Penetrative deformation continued below greenschist facies conditions. Synchronous plastic and brittle deformation of quartz shows major deformation at the brittle-plastic transition. Cataclastic fabrics are to a limited degree penetrative but occur mostly localized in discrete shear zones.

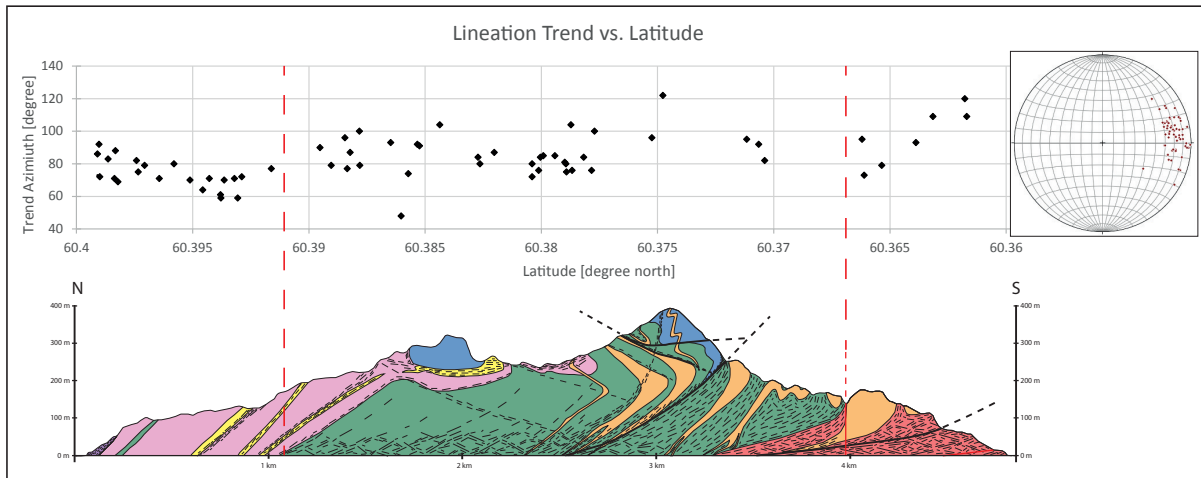


Fig. 24. The trend of mineral stretching lineations show a slight rotation along the N-S cross-section from ENE in the north to ESE in the south. Different orientations show a relationship with the extent and shape of the main gabbroic body (marked by red dashed lines).

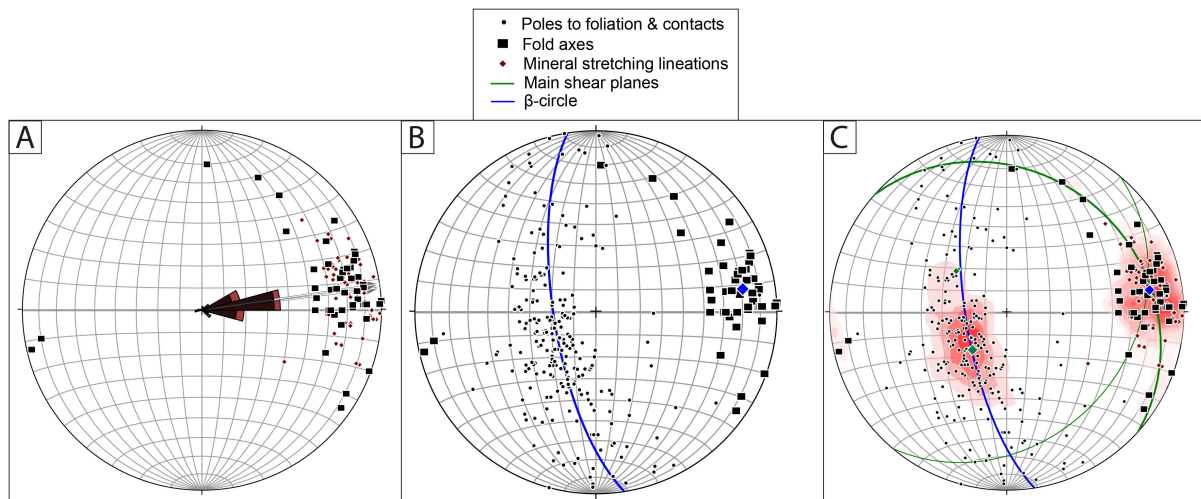


Fig. 25. Stereoplots of structural data acquired in this study. A: Rose diagrams and calculated mean trends (grey arrows) show identical orientations of mineral stretching lineations (red dots, $n = 64$) and fold axes (black squares, $n = 52$). The mean trend of both is 82° . B: Poles to foliations and contacts ($n = 232$) plot along one great circle (blue). The corresponding fold axis (blue diamond) plots in the center of measured fold axes (black squares). C: Stereoplot of all ductile to semi-brittle fabrics in the Lyderhorn Gneiss. Contour plots are shown for poles to planar fabrics, lineations and fold axes. Green great circles and corresponding poles (green diamonds) represent the two major orientations of shallowly NE- and SE-dipping shear zones and intersect in the centre of fold axes and mineral lineations. The predominant shear plane dips to the NE.

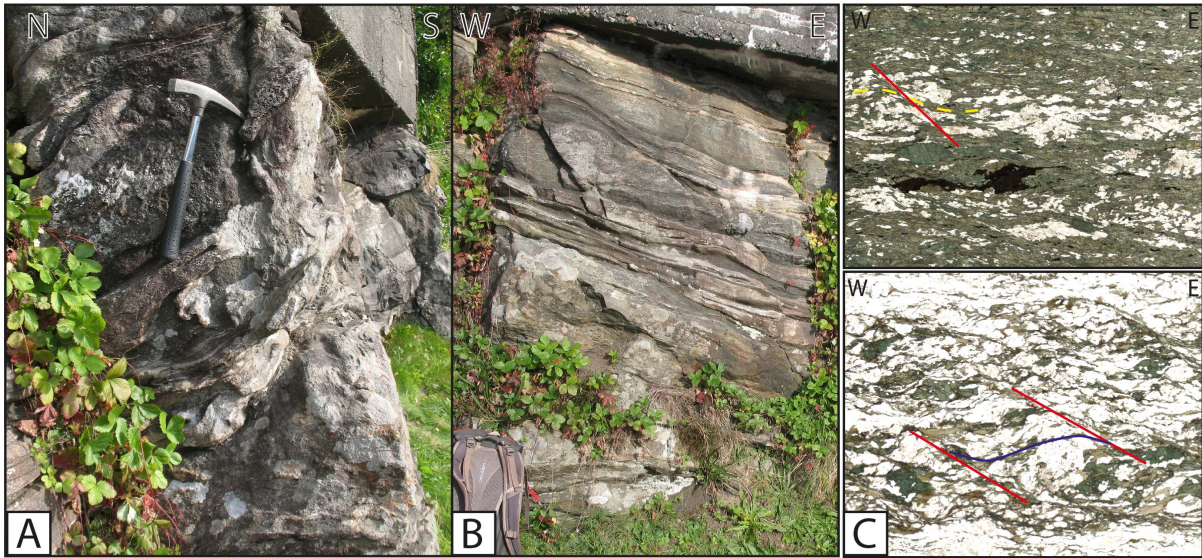


Fig. 26. Amphibolite facies fabrics. A and B: Two perpendicular outcrop faces expose anisotropic mylonitic amphibolite. The mineral lineation plunges shallowly towards E (Bjørndal, 168). A: The N-S face (perpendicular to the lineation) exhibits heterogeneously folded granitic veins. B: On the E-W face (parallel to the lineation) fabrics are subparallel and strongly stretched-out. Downward-cutting C'-shear bands deflect the mylonitic foliation and indicate extensional top-to-E kinematics (Van der Pluijm and Marshak, 2004; Fossen and Rykkelid, 1990). Backpack for scale. C: Photomicrographs of C-C' structures in amphibolite (C': red, S: yellow; Krabbedalen, 35) and an amphibole-rich layer in banded gneiss (C': red, C: blue; Bjørndal, 170). Both show top-to-E sense of shear. Width of view in both pictures is ~ 1 cm; plain polarized light.

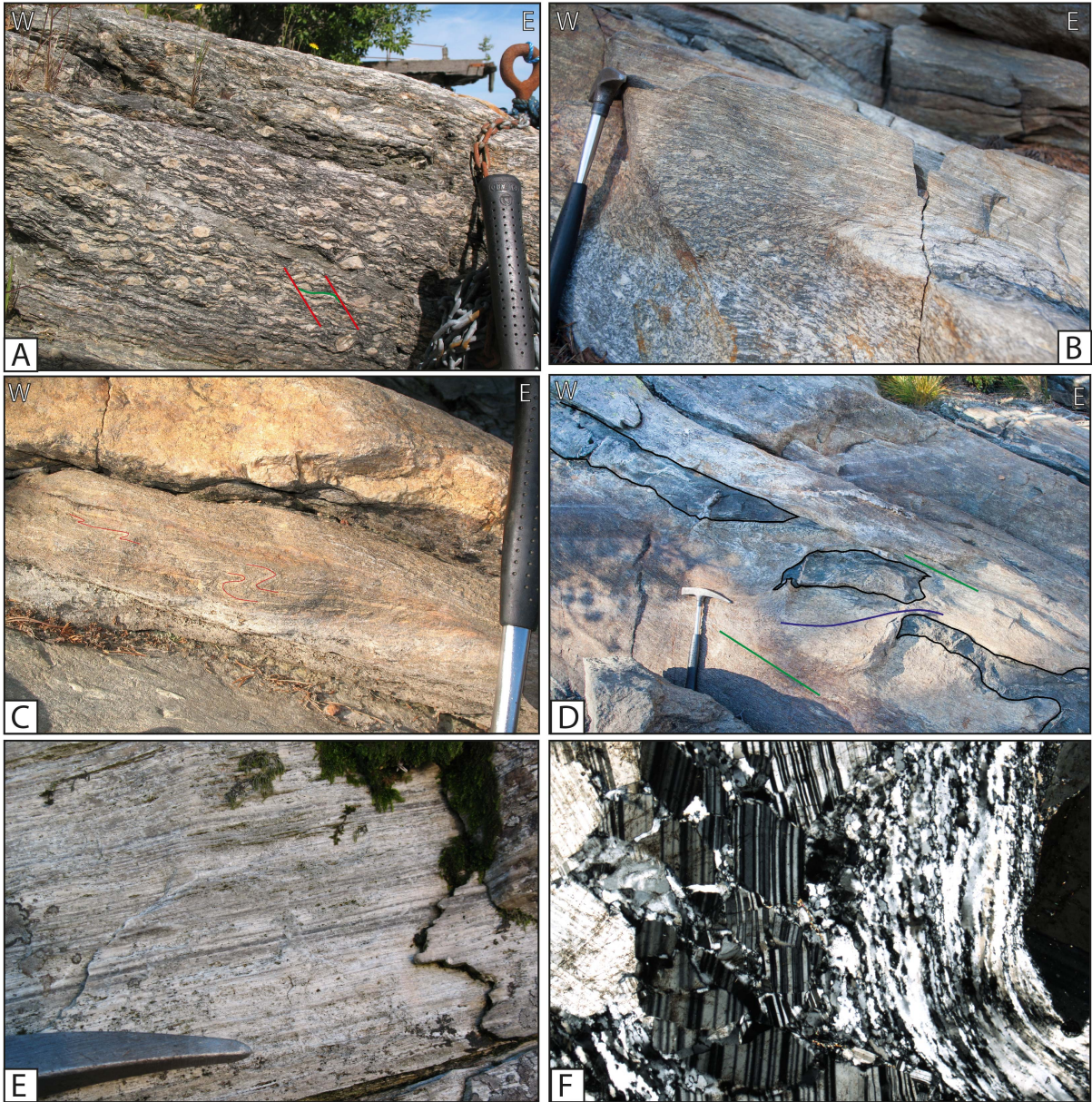


Fig. 27. Greenschist facies fabrics in granitic rocks. Kinematic indicators (A - D) show consistently top-to-E sense of shear: A: Feldspar δ -type grain-tail complexes and C-C' structures (C': red, C: green) in granitic augen gneiss (Gravdal, 83). B: Deflection of foliation at a mesoscale mylonitic shear zone in granitic gneiss (Skåleviksvatnet, 133). C: Tight to isoclinal, E-verging folds in mylonitic granitic gneiss (Skåleviksvatnet, 132). D: Disrupted amphibolite dyke contained in mylonitic granitic gneiss. Together with the NE-dipping mylonitic foliation, the fragments are rotated into a S-C structure (C: green, S: blue; Skåleviksvatnet, 133). E: Ultramylonitic leucogranite (Lyderhorn, 75). F: Photomicrograph showing brittle fracturing of feldspar and dynamic recrystallization of quartz in pegmatite (Lyderhorn, 197; see also Fig. 50). Width of view is ~ 2 mm; cross-polarized light.

Folding

Folding of the mylonitic foliation and lithological contacts can be found on different scales and in all lithologies. In Fig. 25B, all planar fabrics plot along one great circle. The corresponding fold axis plots together with measured, shallowly ENE-plunging fold axes. The general NE plunge of planar fabrics reflects the position of the Lyderhorn Gneiss in the northern limb of an upright, E-plunging megafold. Observable micro-, meso- and macrofolds in all lithologies are tight to isoclinal, shallowly E-plunging, recumbent folds (Fig. 28). Their fold axes are (sub-)parallel with mineral stretching lineations, what classifies them as curtain folds (or oblique folds; Passchier and Trouw, 2005). The dip of the axial surfaces varies between moderate dip to the S and shallow dip to the N (Fig. 28), but the general structure implies N-vergent 'christmas-tree' fold geometries (compare with Fig. 17) and implies vertical shortening.

Folded amphibolites and granitic gneisses indicate that folding occurred at amphibolite to greenschist facies conditions. Fig. 29 shows strain variations around an E-plunging fold in granitic gneiss. Constrictional strain in the hinge area formed an augen gneiss L-tectonite with E-plunging lineation (Fig. 29A). In the limbs, the same lithology was transformed into a banded mylonitic gneiss (Fig. 29B). A weak, thin layer of biotite-rich amphibolite with small, irregular granitic veins has flown into the hinge area, acting as a lubricant during folding (Fig. 29C).

Fold transposition of pegmatite bodies can be observed in high-strain zones (Fig. 30). At the east face of Lyderhorn a shear zone localized at contact between hornblende biotite granite gneiss and amphibolite. Within the E-dipping shear zone, several metre thick pegmatite bodies are intensely folded along N-S trending fold axes (Fig. 31A), whereby the wavelength of folds reflects the layer thickness. Complex fold patterns formed in this zone due to the heterogeneous behaviour of strongly contrasting rheologies. Opposed fold vergence of isoclinal folds can be explained by fold transposition under continuous top-to-E shear with a component of vertical shortening (Fig. 30). Pegmatite dykes in amphibolite show thinning and boudinage followed by tight folding (Fig. 31C). Extension followed by shortening can not occur under steady-state deformation (Fossen, 2010b), but the case of this shear zone it is probably a result of strong rheological heterogeneity under continuous retrograde deformation.

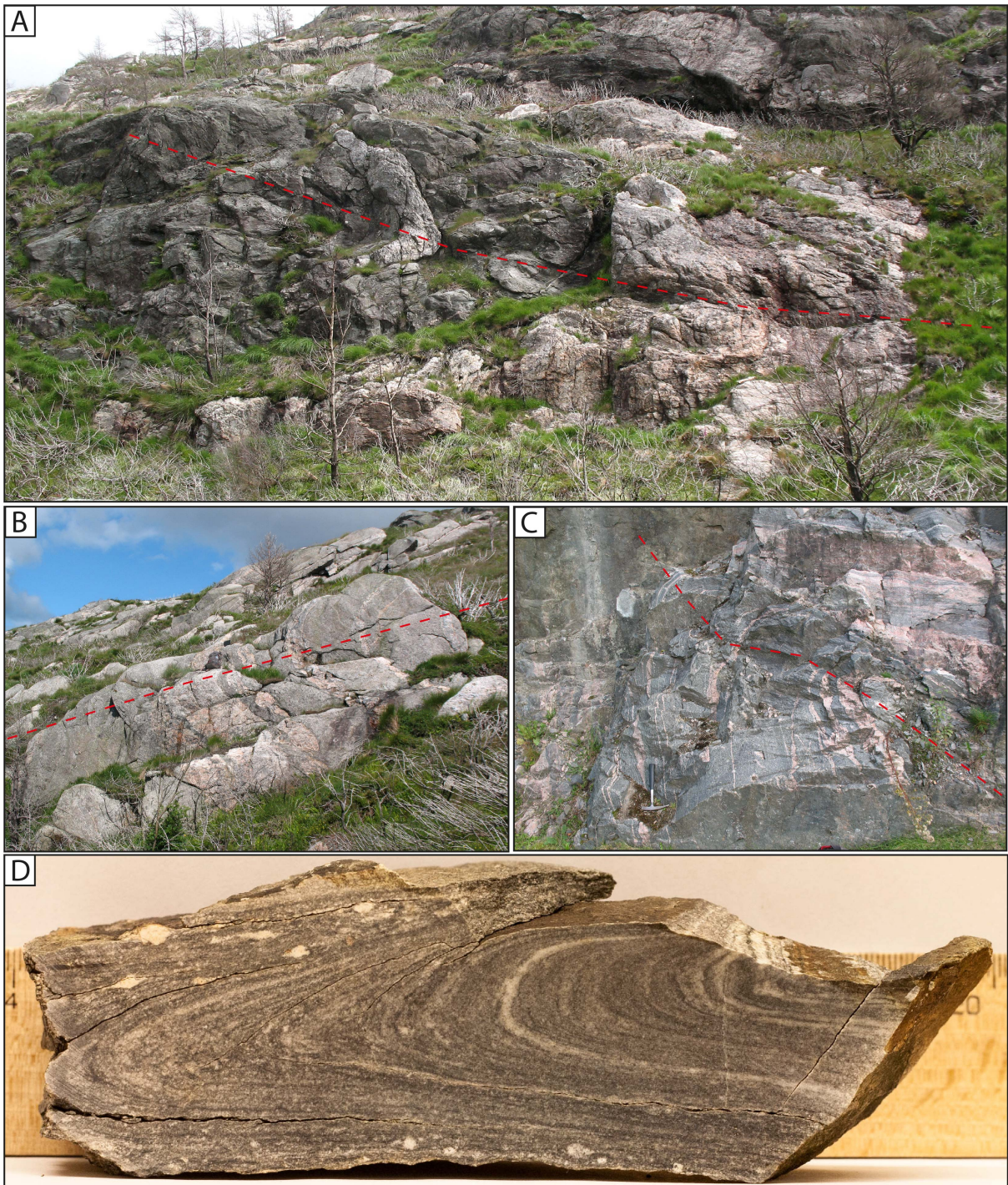


Fig. 28. Tight to isoclinal E-plunging folds. All images have the same orientation with N on the left and S on the right side. The trace of axial surfaces is marked with dashed red lines. A: Tight recumbent fold in pegmatite and garnet-bearing amphibolite (Lyderhorn, 45). Fold axis: $10 \rightarrow 082$. Width of view is ~ 15 m. B: Tight, recumbent fold in hornblende biotite granite gneiss and pegmatite (Lyderhorn, 52). Fold axis: $10 \rightarrow 069$. The fold is N-vergent but the axial surface dips shallowly to the N. Width of view is ~ 8 m. C: Folded granitic gneiss in the mixed series (Loddefjord, 171). Fold axis: $36 \rightarrow 084$. Thinning of the upper limb (right part of the picture) causes a strong asymmetry. The fold gets tighter towards the right side and has a curved, S-dipping axial surface. Hammer for scale. D: Cut hand specimen of an isoclinal, recumbent fold in mylonitic granitic gneiss (Lyderhorn, 75). The orientation of the fold axis is $15 \rightarrow 074$. The foliation dips moderately to the NE ($048/25$). Width of hand specimen is ~ 15 cm.

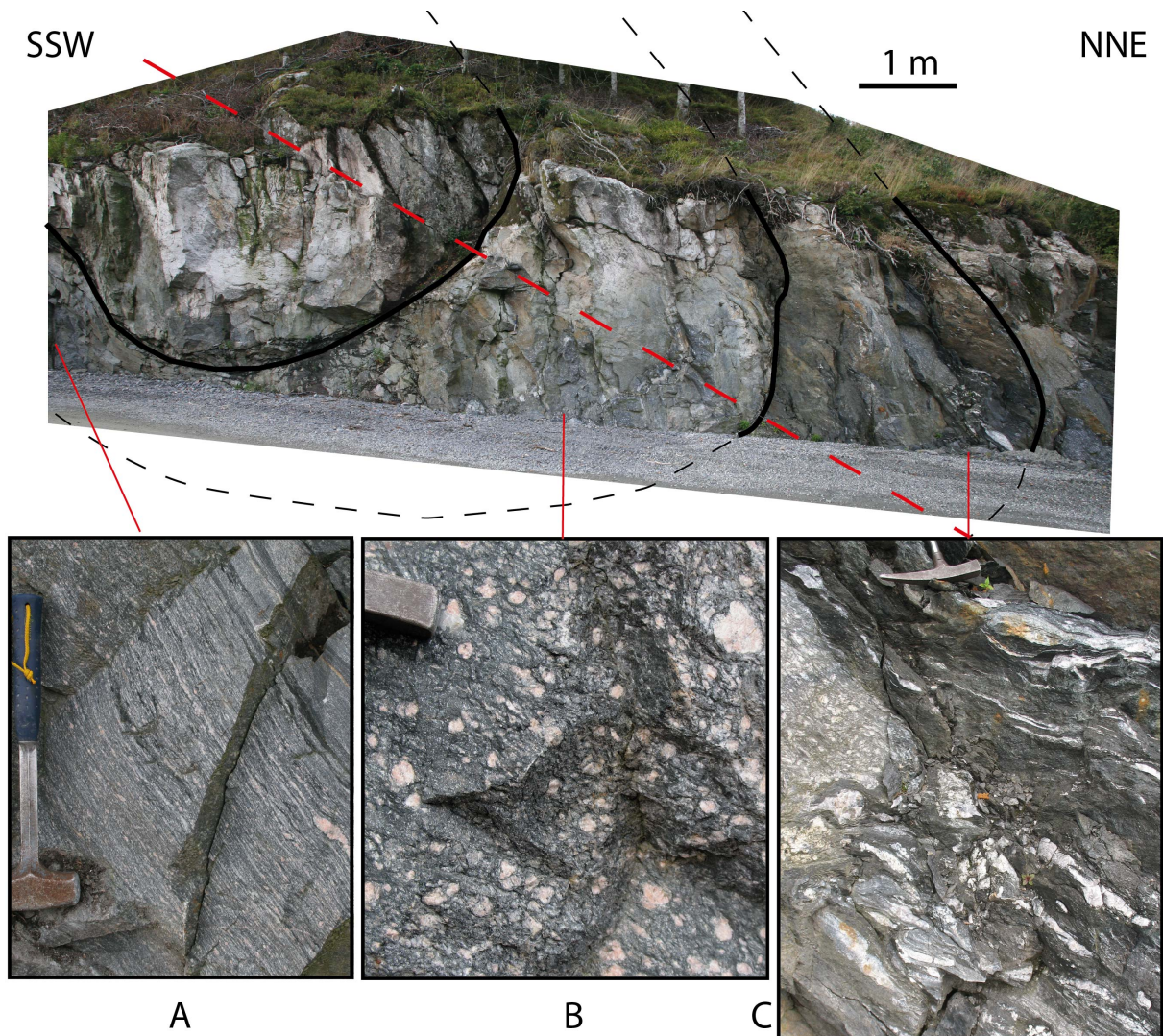


Fig. 29. Roadcut exposing the hinge area of a tight fold in granitic gneiss (Gravdal, 83). The axial surface (dashed red line) is inclined towards NNE. Strain varies around the fold. Flattening strain in the lower limb formed mylonitic gneiss (A). Constrictional strain in the hinge developed an augen gneiss texture with several centimetre large K-feldspar augen (B). A thin layer of biotite-rich amphibolite which contains small, white granitic veins acted as a lubricant during folding (C). Orientation of fold axis is $29 \rightarrow 090$.

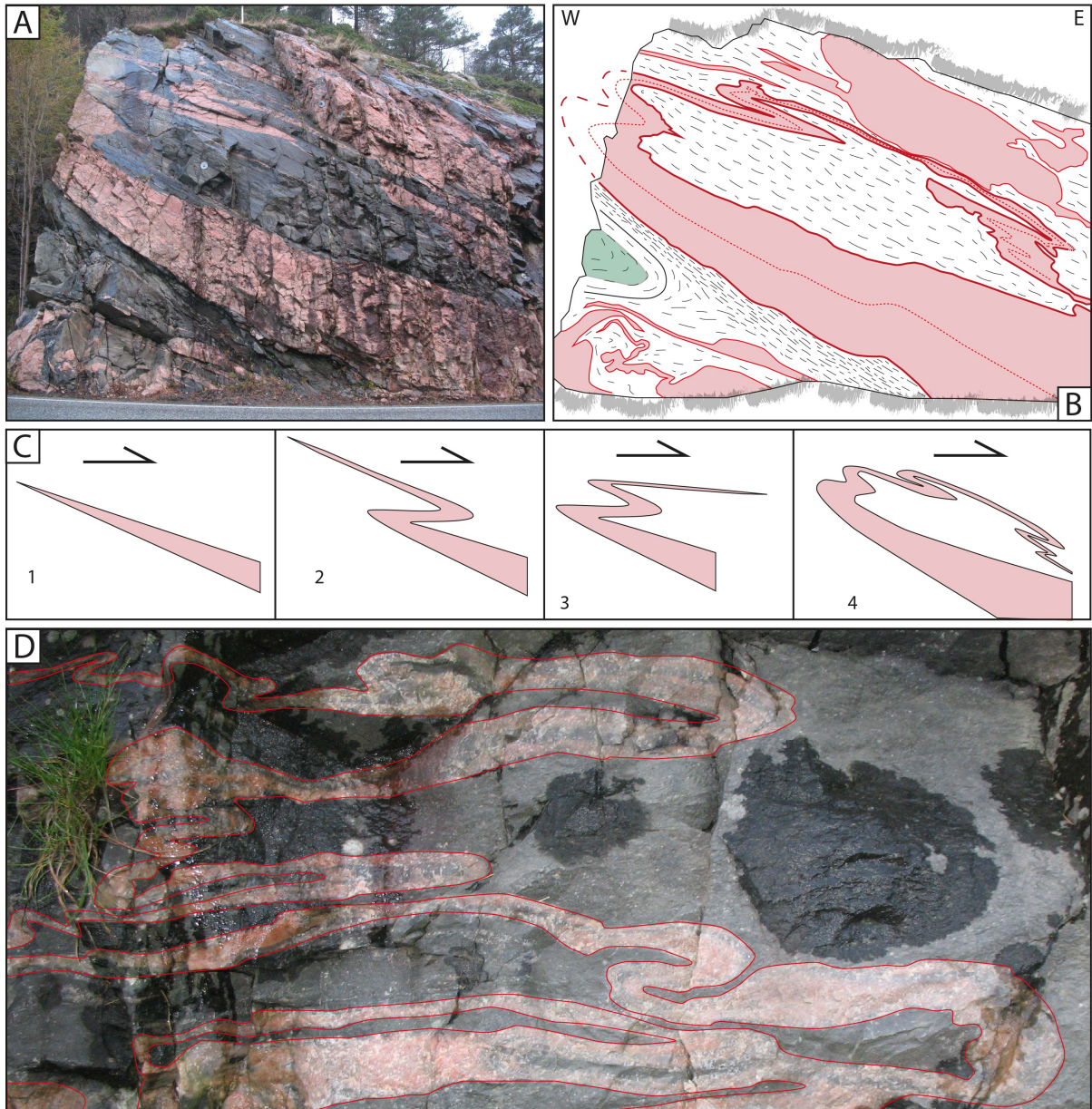


Fig. 30. Fold transposition in a E-dipping shear zone at the contact between granitic gneiss and amphibolite (Lyngbødalen, 1). The width of the picture (A) is ~ 10 m. The schematic sketch (B) outlines the main features: The outcrop consists of mylonitic granitic gneiss (white), pegmatite (pink) and amphibolite (green). Fold transposition of a large pegmatite body produced isoclinal folds with opposed vergence (dark red outline; the internal folding is indicated by a dashed red line). The intensity of folding is dependent on layer thickness. Thin pegmatite veins within granitic gneiss in the lower left corner of the outcrop, show complex fold patterns that are probably related to space problems in the hinge of the major fold (fold axis: $20 \rightarrow 002$). A low-grade shear zone has localized at the lower contact of the large pegmatite. C: The schematic sketch explains how the complex fold geometry could have formed by fold transposition under continuous top-to-E simple shear and a component of vertical shortening. D: Detail photo from the same outcrop shows multiply folded pegmatite vein implying vertical shortening. Width of view is ~ 0.8 m.

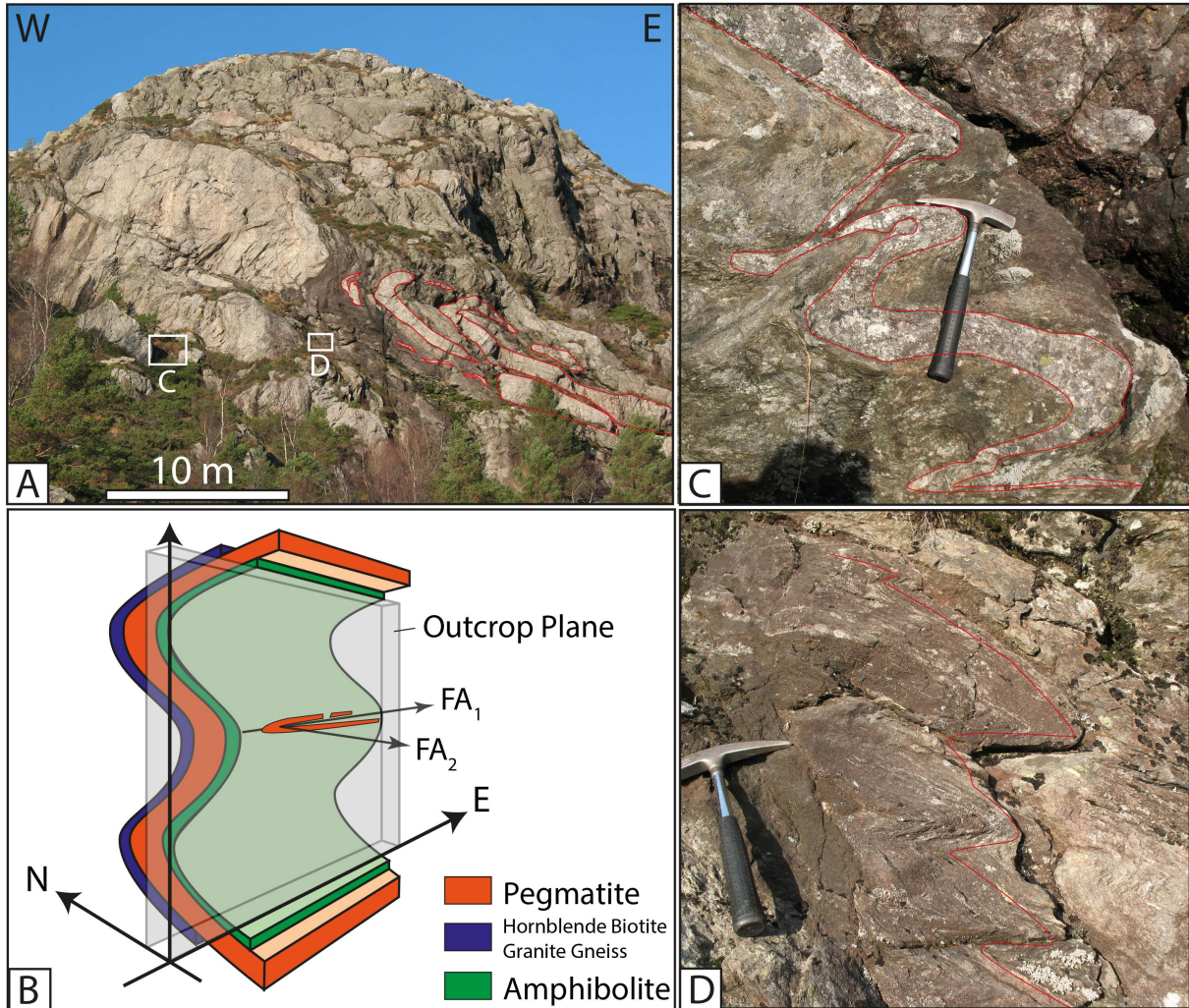


Fig. 31. Complex folding below the peak of Lyderhorn (190). The outcrop represents the upper part of the high-strain zone shown in Fig. 30. A: The outcrop is a roughly 50 m wide and 30 m high, S-facing cliff. It exposes the contact between hornblende biotite granite gneiss (medium grey, upper part) and amphibolite (dark grey, right part). Both are intruded by pegmatites (bright grey). The isoclinally folded pegmatite dykes in the right part of the picture (red outline) are several metres thick. They show thinning, boudinage and disruption as it is typical for fold transposition in lithologies with contrasting competence (Van der Pluijm and Marshak, 2004). White boxes indicate the location of detail photos. B: The schematic 3D-sketch shows that the entire outcrop is located in the hinge area of an E-plunging, recumbent macrofold (FA_1). The bright pegmatite that occupies most of the left part of the outcrop surface is no more than two metres thick. It seems more massive because the outcrop surface follows the orientation of the dyke. Within the shear zone, N-S-trending fold axes (FA_2) are developed. C: Pegmatite vein in amphibolite shows thinning followed by tight folding of the attenuated parts. D: Kink-like, recumbent folds in heterogeneous mylonitic amphibolite indicate top-to-E sense of shear.

Discrete Shear Zones

Strain localization at lithological contacts formed numerous discrete shear zones. A network of anastomosing shear zones dissects Lyderhorn and the surrounding area into angular segments (Fig. 32, compare with Fig. 17). Two types of shear zones can be distinguished: Subvertical, E-W-striking shear zones reflect the steep dip of folded contacts in the hinge of E-plunging macrofolds. High-angle shear zones can be found north of the peaks of Lyderhorn (e.g. outcrop 28) and Ørnafjellet (outcrop 124), respectively. They exhibit amphibolite- to greenschist facies fabrics and developed clastomylonites with decimetre-large, feldspar-rich, pegmatitic fragments contained in a fine-grained, mylonitic matrix.

More frequent are shallowly NE- and subordinate SE-dipping shear zones. Two main shear planes were identified (045/25 and 130/30) that intersect in the centre of measured lineations and fold axes (Fig. 25C). Low-angle shear zones show a high- to medium-grade history but earlier fabrics are commonly obliterated by a strong low-grade overprint. Different types of low-grade fault rocks formed from granitic and gabbroic protoliths, respectively. Both types imply fluids to have played an important role during deformation around the plastic-brittle transition. Two representative shear zones with different fault rocks are explained in detail:

At Loddefjord, a major shear zone in the mixed series occurs on several levels below Skarpafjellet (Fig. 33A). A high- to medium-grade history is recorded in mylonitic amphibolites and banded gneisses. The lower-grade deformation in the heterogeneous unit has paradoxically localized in amphibolite lenses. In such lenses, amphibole is almost completely replaced by biotite and chlorite (Fig. 34A). Tonalitic veins and layers of granitic gneiss are tectonically brecciated and are contained in a matrix of chlorite phyllonite (Fig. 34B - D). Kolderup and Kolderup (1940) described the fault rocks because of the rounded granitic fragments as 'tectonic conglomerates'. Fig. 33B shows an spectacular and easy accessible locality that exposes the up to 10 m thick, lenticular deformation zone of the Loddefjord shear zone. The deformation zone is dissected by thin, low-angle brittle faults and the rim of the deformation zone is reactivated as a brittle fault plane. E-plunging quartz-striations on the fault plane are parallel to ductile mineral stretching lineations; only epidote-mineralized fault planes show a distinct oblique plunge to the N.

Unlike the exposures shown in Fig. 33 and Fig. 34, outcrop 174 is parallel to the E-plunging mineral lineations (Fig. 35). Kinematic indicators in mylonitic granitic rocks and chlorite phyllonites indicate consistent top-to-E sense of shear and are associated with retrograde overprinting relationships (Fig. 35A - C). Aggregates of actinolite overgrow granitic fragments (Fig. 35D). The retrograde mineral reactions (hornblende \rightarrow biotite \rightarrow chlorite) and the actinolite aggregates give evidence for the presence of hydrothermal fluids in the shear zone during deformation from greenschist facies down to the brittle-ductile transition. The alteration into chlorite phyllonites implies considerable strain weakening of amphibolites and allows low-grade deformation to localize in mafic layers.

Corresponding processes can be observed in felsic rocks. Figure 36 shows an example at the summit of Lyderhorn. A mylonitic shear zone follows the folded contact between metagabbro and hornblende biotite granite, but cuts through the granite body at the hinge of the fold (Fig. 36A). The shear zone branches out to follow the contact of a large pegmatite body. The feldspar-rich pegmatite is transformed into a felsic phyllonite (Fig. 36B). In the fault rock, feldspar is

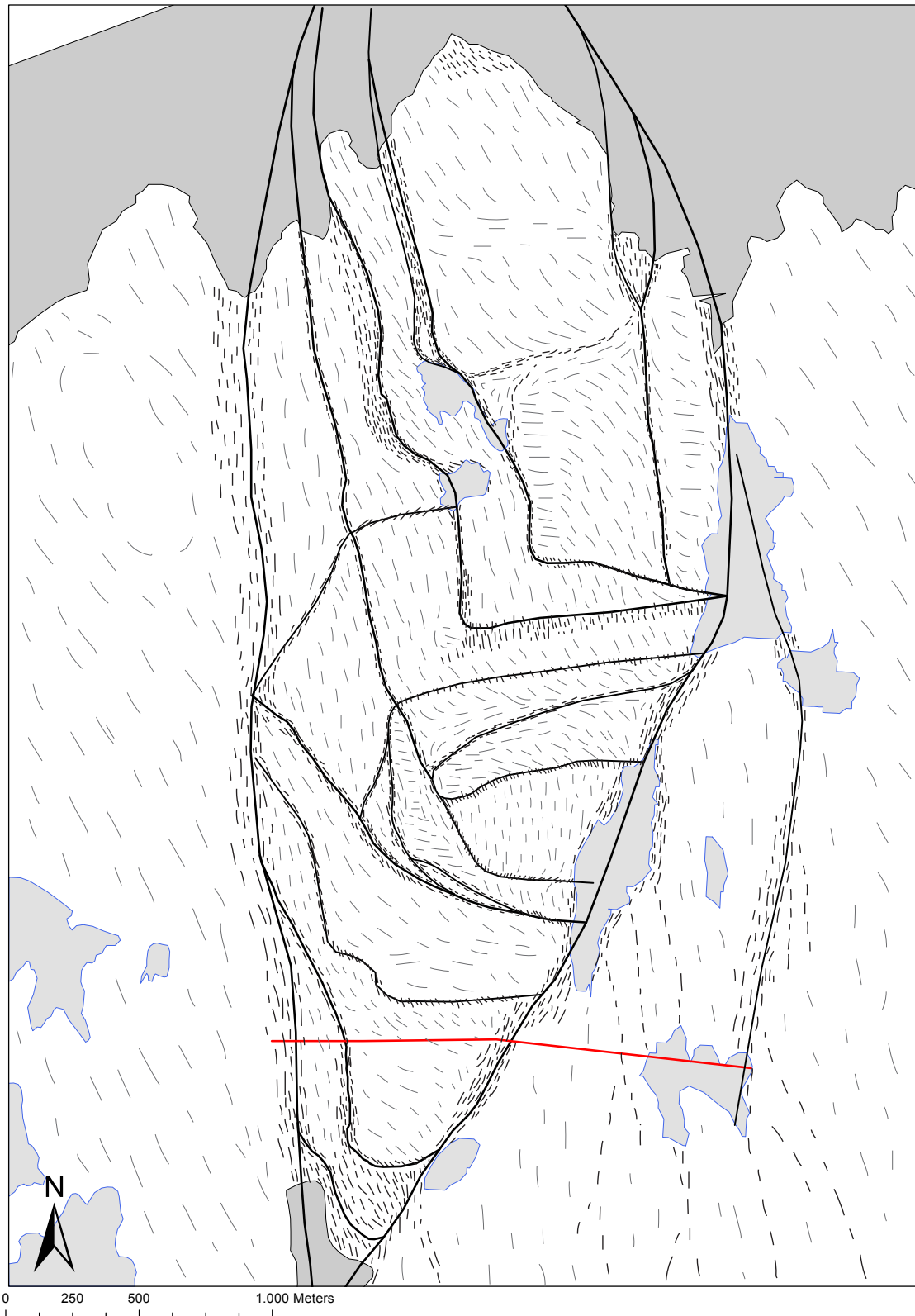


Fig. 32. Schematic map showing discrete shear zones (solid black lines) and the trace of foliation. Anastomosing, shallowly NE- and SE-dipping shear zones cut the entire area into angular segments (compare with Fig. 17). Steep, E-W striking fabrics are preserved inside these blocks. High-angle shear zones formed in hinge areas. Most surfaces on the eastern slope of Lyderhorn are E-dipping low-angle shear zones.

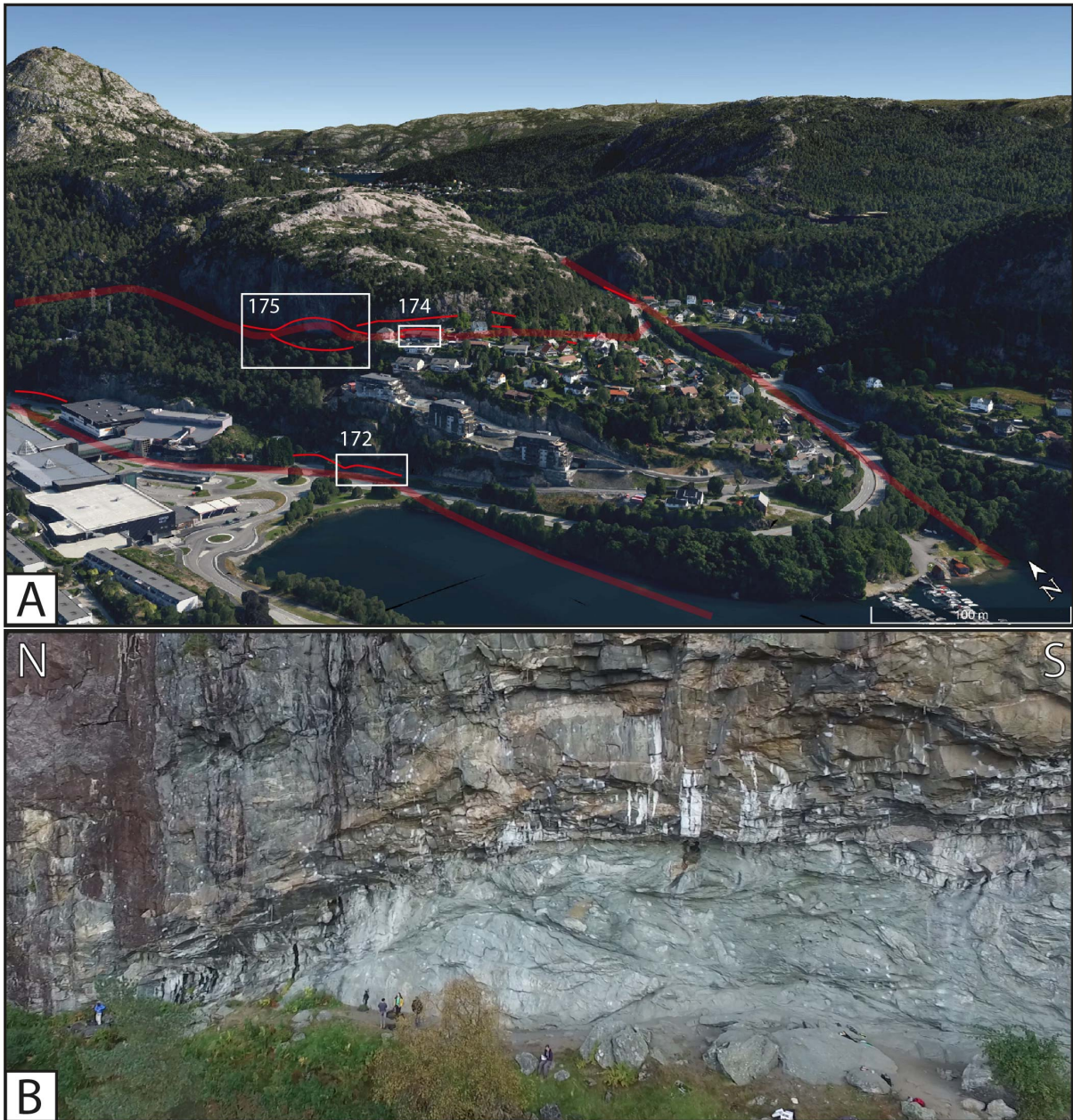


Fig. 33. Loddefjord shear zone: A: The anastomosing shear zone appears on several levels below Skarpafjellet (solid red lines: exposure; transparent red lines: interpretation). White boxes and numbers mark different outcrops. Image from Google Earth. B: Outcrop 175 is the most spectacular exposure of the lenticular, up to 10 m thick deformation zone of the Loddefjord Shear Zone. The section is perpendicular to the mineral lineation. Lenticular, angular and rounded clasts of plagiogranite and granitic gneiss swim in a greenish-grey matrix of chlorite phyllonite. The size of the clasts ranges from millimetres to several metres. The largest granitic lenses is 5 m high and almost 10 m wide (close to where people are standing). Image from Robert Sasak.

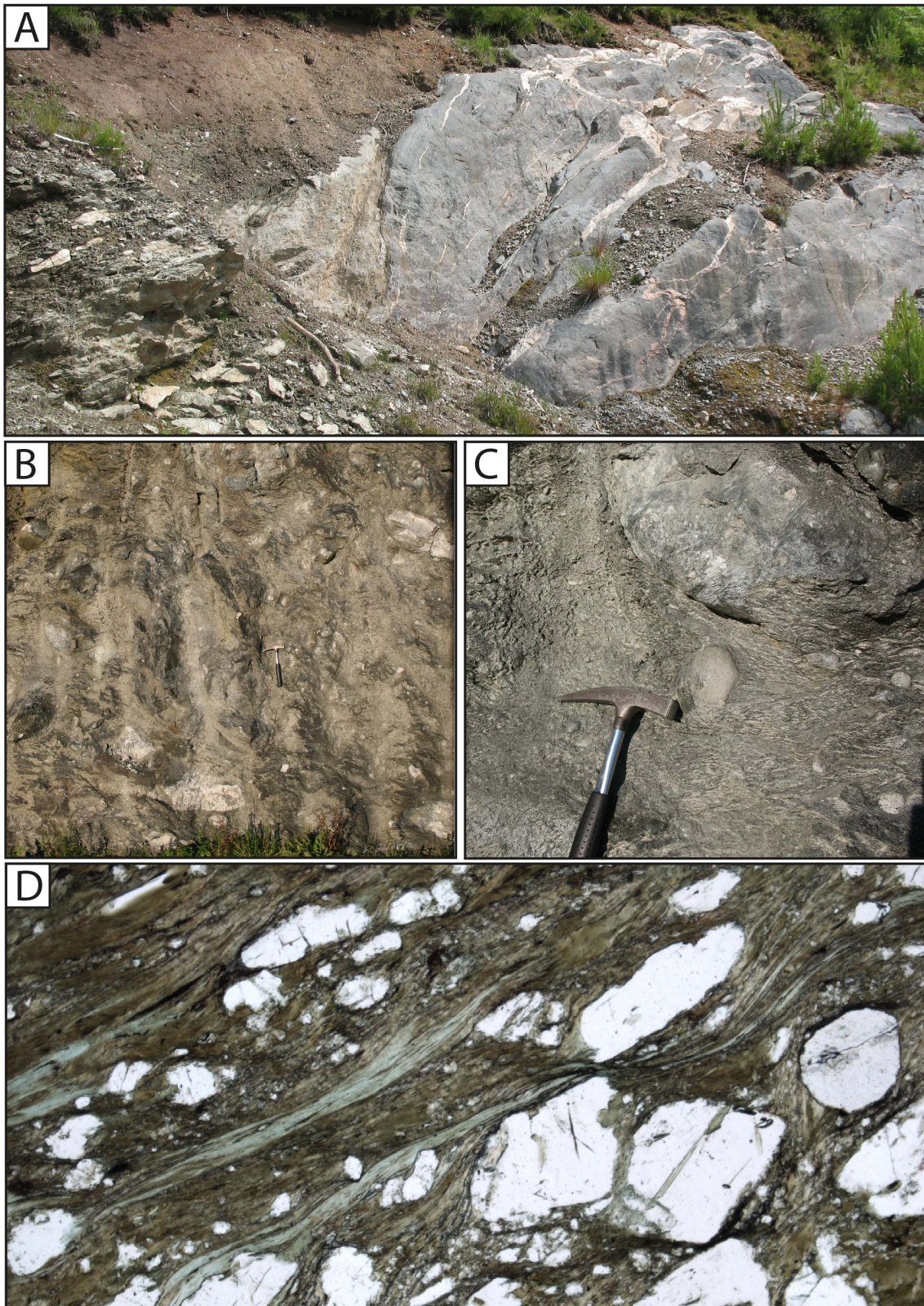


Fig. 34. A: Amphibolite with white tonalitic veins (right side) is transformed into chlorite phyllonite (left side) in a NE-dipping shear zone (Krabbedalen, 37). Width of image is ~ 10 m. B: Road cut exposing a lower branch of the Loddefjord shear zone (172). Angular and rounded granitic fragments float in a matrix of greenish-grey chlorite phyllonite. Hammer for scale. C: Detail from the same outcrop: The strong rounding of granitic clasts comes from transposed isolated fold hinges. D: Microphotograph of the phyllonitic matrix from the same outcrop. Fragmented feldspar clasts (colorless) are transposed in a mylonitic matrix of biotite (brown) and chlorite (green). Width of image is ~ 5 mm. Plain polarized light.

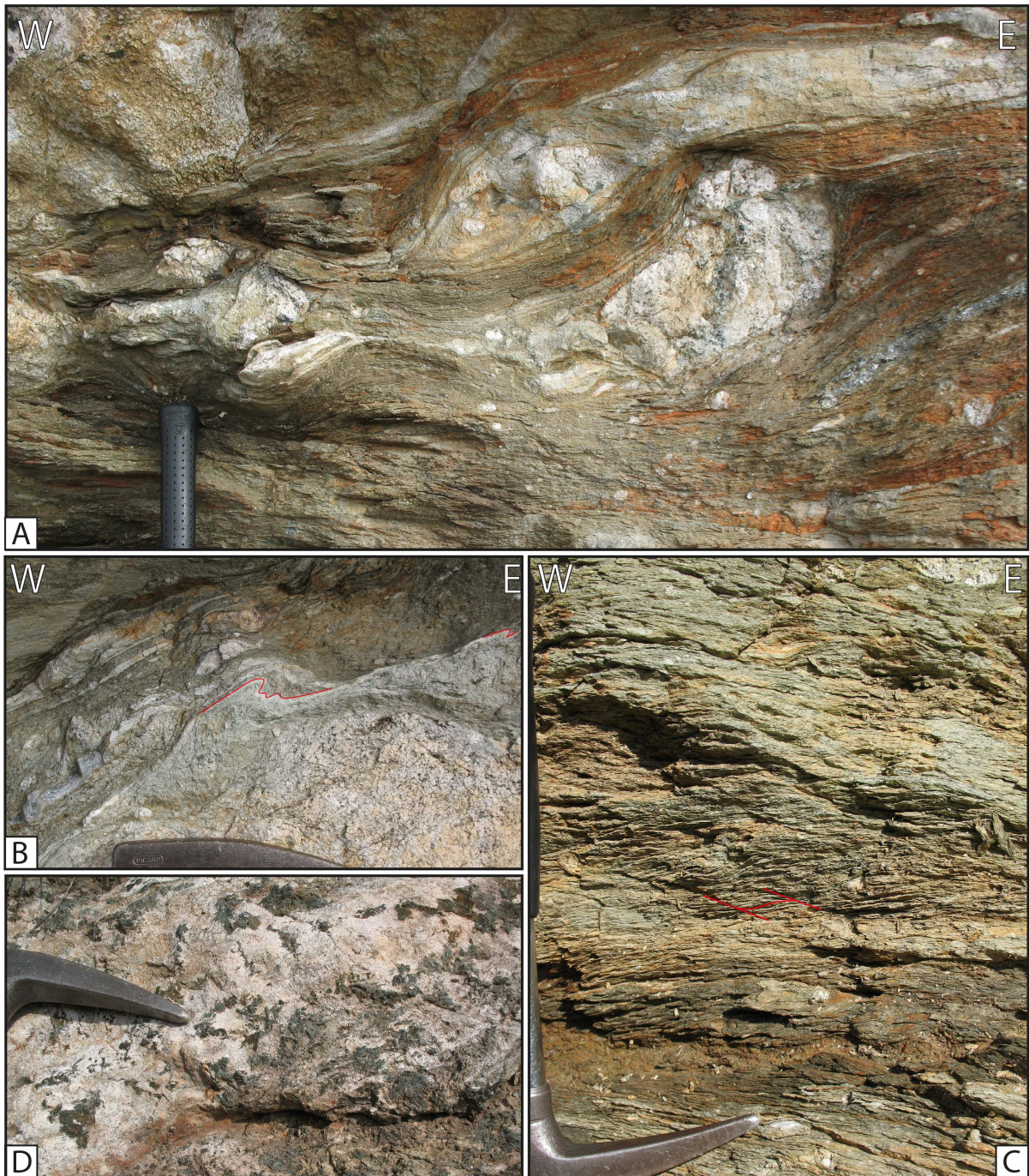


Fig. 35. Outcrop 174 (A - C and E) exposes the Loddefjord shear zone parallel to mineral lineations. A: Asymmetrically sheared, white granitic clasts in chlorite phyllonite matrix. The mylonitic fabric within the granitic clasts follows the asymmetric outer shape. Asymmetries imply top-to-E sense of shear. B: Mylonitization and isoclinal folding (red outline) at the rim of a large granitic clast. Granitic fragments get detached from the main block and swim in the phyllonite matrix. C: C-C' structures in chlorite phyllonite indicate top-to-E shear-sense at low-grade conditions. D: Hydrothermal actinolite aggregates overgrow a white granitic block.

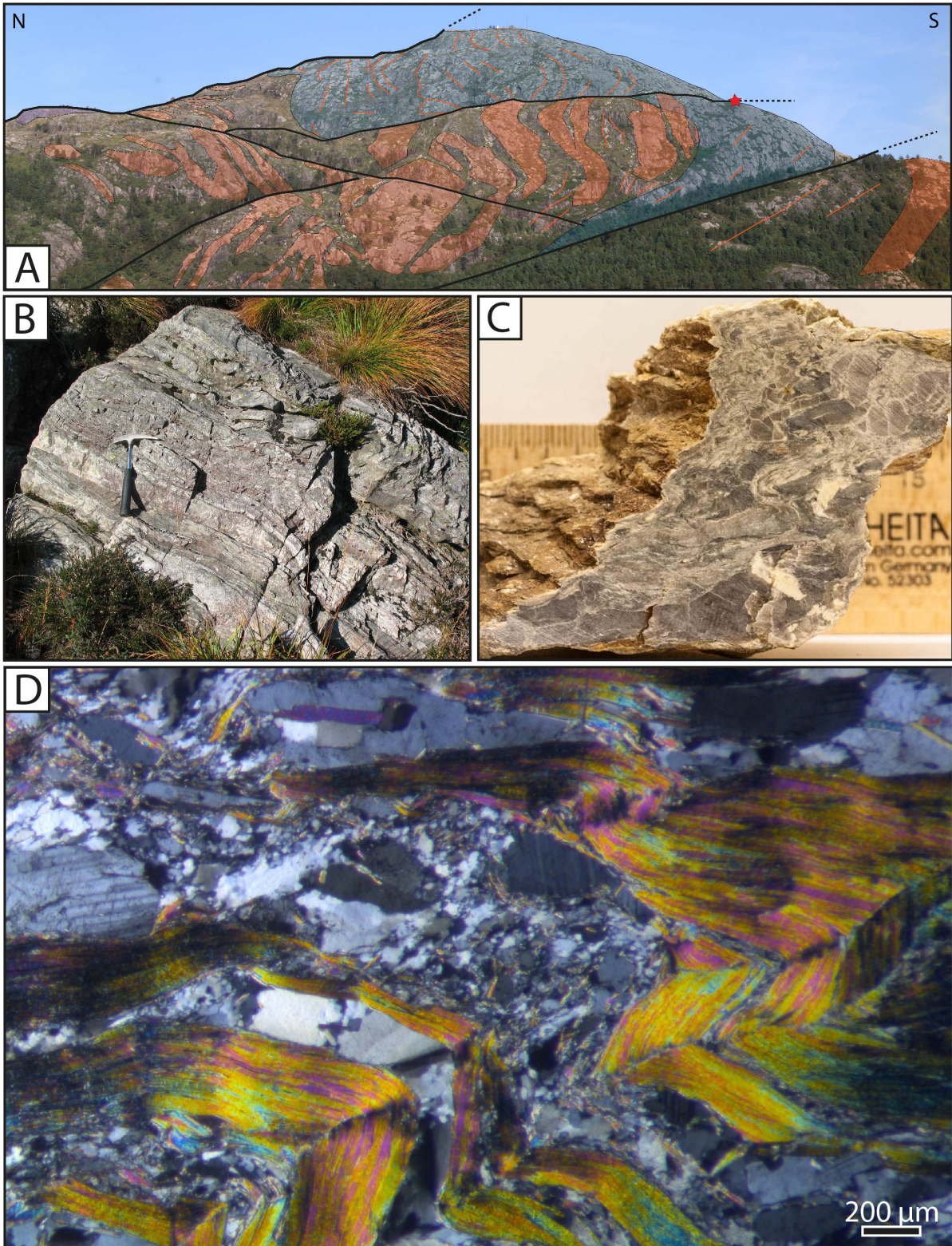


Fig. 36. Felsic phyllonite in mylonitic shear zone. A: Interpretative photo of the peak of Lyderhorn, seen from the W. Width of view is ~ 600 m. Lithologies are: Hornblende biotite granite (blue); pegmatite (orange) and metagabbro (no color). Several NE- and SE-dipping shear zones transect the peak (black lines). A mylonitic shear zone follows the contact between hornblende biotite granite and metagabbro. It cuts through the granite in the hinge of the isoclinal folded body (red star). On the south face, the shear zone transforms a feldspar-rich pegmatite into a felsic phyllonite. B: Outcrop 17 exposes the phyllonitic shear zone. C: Cut hand specimen of the fault rock. K-feldspar (yellowish-white) is almost completely replaced by muscovite and quartz. Width of image is 9 cm. D: Photomicrograph showing alteration of K-feldspar into quartz and muscovite and Kink-folding. Crossed-polarized light.

almost entirely replaced by muscovite and quartz (Fig. 36C and D). This retrograde mineral reaction also implies the presence of aqueous fluids during shearing and involves considerable strain weakening of the original granite rheology (Wintsch et al., 1995, Bos and Spiers, 2002). Other shear zones developed flinty, silica-rich fault rocks from quartz-rich protoliths that were deformed at the brittle-plastic transition. Abundant cataclasites show that low-angle deformation continued at brittle conditions (Fig. 37). Some fault rocks show a complex history with growth of hydrothermal garnet that acted as porphyroclasts during cataclastic flow (Fig. 37C and D). Many lithological contacts are reactivated as shallowly E-dipping brittle faults that show typical mullion-like corrugations and pronounced striations.

Based on the described geometries (E-dipping), displacements (normal to oblique-normal) and fault rocks, low-angle shear zones in the Lyderhorn area can be classified as detachments. These structures continue outside of the study area. Askvik (1971) mapped a mylonitic shear zone on SE Askøy that consists in fact mostly of cataclasites. The Loddefjord shear zone continues most likely in Bjørndalspollen towards the south. Numerous E-dipping, low-angle shear zones occur all over the Laksevåg peninsula (e.g. at Nygård: 60.390° N; 5.278° E). E-dipping brittle detachment faults are well exposed at Hesjaholten (60.345° N; 5.260° E).

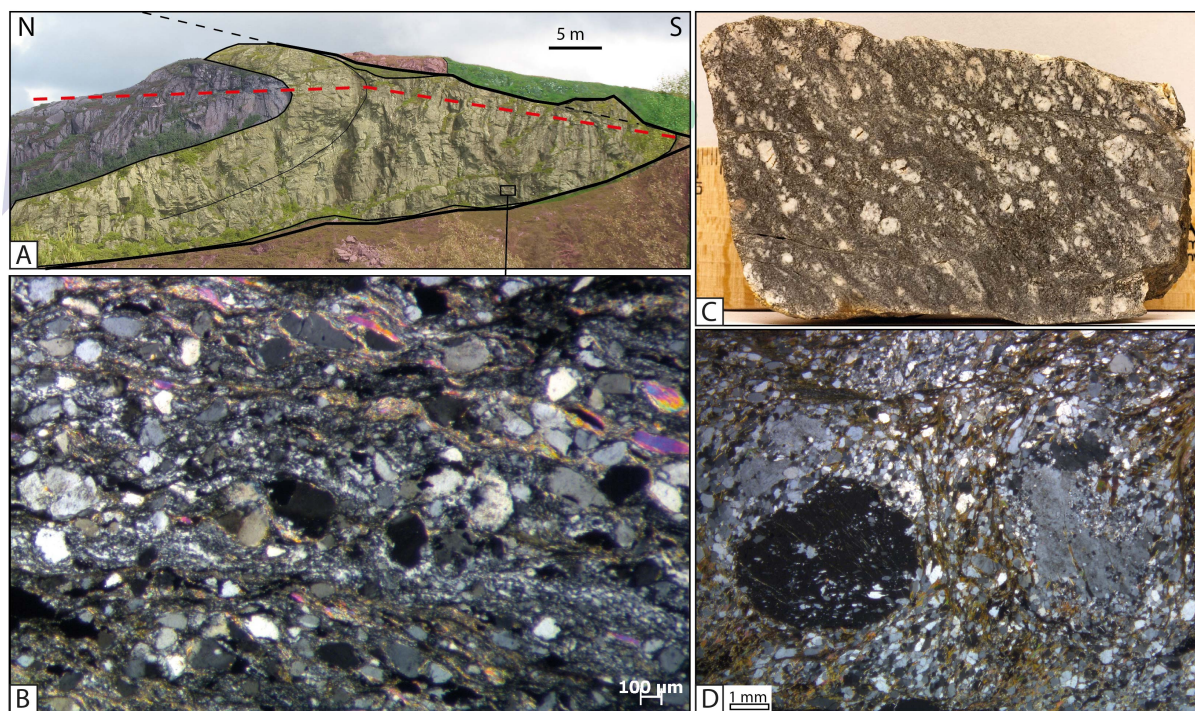


Fig. 37. A: Outcrop 79 (S of Ørnafjellet) exposes the hinge of an isoclinal, recumbent macrofold (dashed red line marks axial surface). The core of the hinge consists of hornblende biotite granite gneiss (blue). Granitic gneiss (yellow) has a strong cataclastic overprint. The fold structure is cut by shallowly NE- and SE-dipping shear zones (solid black lines) that juxtapose the granitic gneiss with amphibolite (green) and heterogeneous gneiss (pink). B: Photomicrograph of the cataclastic granitic gneiss with a mylonitic history. C: Hand specimen of complex granitic fault rock with up to 1 cm large idiomorphic red garnets (Ørnafjellet, 94). Width of image is 10 cm. D: Photomicrograph showing a large K-feldspar crystal on the right side that is unstable and replaced by muscovite and quartz, while the idiomorphic garnet on the left side overgrows quartz and feldspar. This could indicate the presence of fluids during faulting and probable porphyroblast growth of hydrothermal garnet. Brittle microfaults localize along mica crystals and flow around the intact garnet crystal. This indicates that the garnet acted as a porphyroclast during brittle deformation.

Summary of Structural Results

All described structures show a genetical interdependence which implies that they formed in one single deformation event. Figure 38 schematically summarizes the style of ductile deformation: Penetrative ductile deformation formed L-S-tectonites with characteristically different N-S and E-W outcrop faces. Mineral stretching lineations plunge indifferent of metamorphic grade to the ENE. Planar fabrics dip mostly to NE. Oblique, E-plunging, recumbent meso- and macrofolds developed simultaneously with top-to-E shearing. Fold axes have statistically the same orientation as mineral stretching lineations of all metamorphic grades. Fold geometries record a component of vertical shortening. The observable mesofolds and macrofolds are part of the northern limb of an upright, E-plunging megafold that is reflected in the shape of the Laksevåg peninsula and the entire Bergen Arc. Their geometrical relationship can be described as christmas-tree or alternatively cascading folds.

Overprinting relationships imply continuous retrograde deformation from amphibolite facies down to the brittle-plastic transition. One of the most important findings of this study is the intensity of low-grade top-to-E deformation. Retrograde hydration reactions formed phyllonites. The induced strain weakening assisted deformation to localize NE- and SE-dipping detachment shear zones that cut and overprint earlier fold structures. Cataclastic fault rocks have similar fabric orientations as earlier formed tectonites. They give evidence for severe low-angle deformation at and below the brittle-plastic transition.

This study did not investigate steep brittle structures in detail. Major steep lineaments strike N-S and E-W, respectively. Just the most pronounced vertical, E-W striking structure that forms Grøvdalen N of Skarpafjellet is shown on the map and the cross section. Minor fractures with oblique orientations are abundant, especially in the rigid pegmatites. Mathiesen (2013) gave a more detailed description of fracture orientations in the area but did not distinguish consistently between shallow and steep structures. Fault surfaces in pegmatites and feldspar-rich granitic rocks show commonly K-feldspar alteration and epidote-mineralization, similar to what has been described from other parts of the Øygarden Complex (Larsen et al., 2003; Fossen et al., 2016).

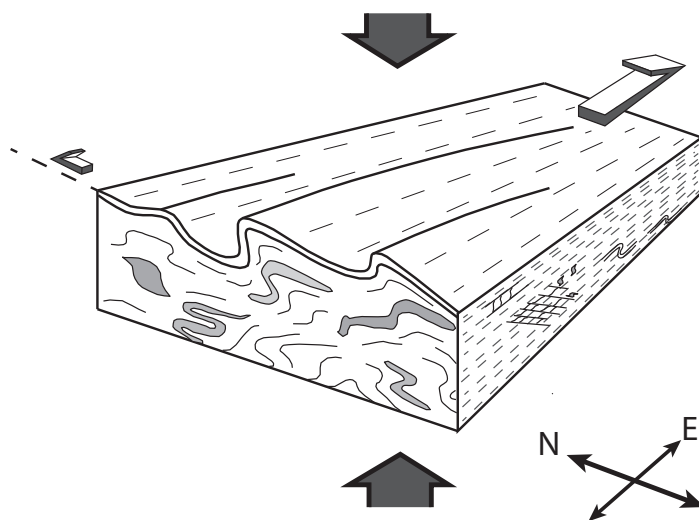


Fig. 38. Schematic sketch illustrating the style of ductile deformation. See text for discussion.

5.2 U-Pb Zircon Geochronology

Seven samples were analysed by SIMS U-Pb zircon geochronology (Table 1 and Fig. 39).

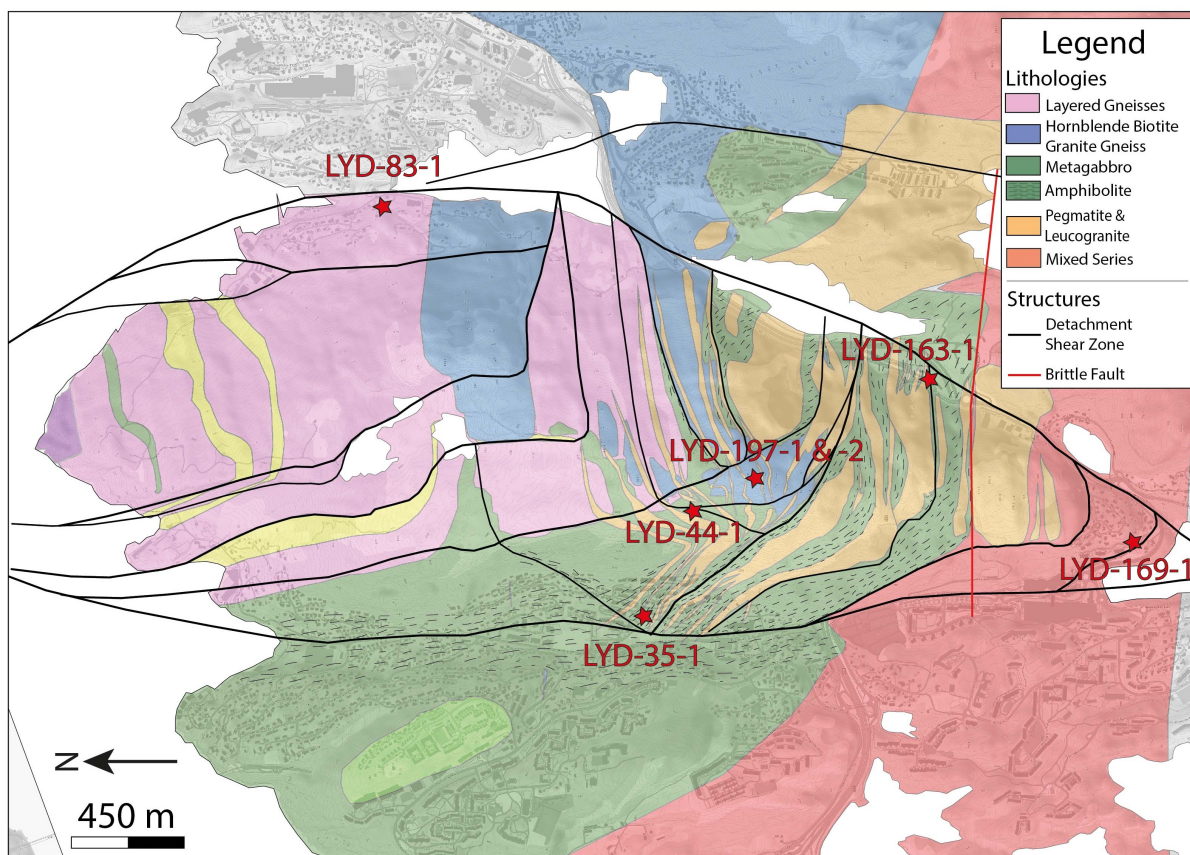


Fig. 39. Geological map of Lyderhorn showing sample localities for U-Pb zircon geochronology.

Table 1. Overview over samples taken for U-Pb zircon geochronology

Sample	Unit	Lithology	GPS Position	Altitude	Outcrop description
LYD-35-1	Gabbroic rocks	Amphibolite	5°13'53,6"E 60°22'37,7"N	83 m	Road cut Lyderhornslie
LYD-44-1	Gabbroic rocks	Metagabbro	5°14'20,9"E 60°22'31,9"N	290 m	Natural cliff along hiking trail
LYD-83-1	Layered gneisses	Banded, mylonitic granitic gneiss	5°15'35,7"E 60°23'14,5"N	25 m	Road cut Gravidalslie
LYD-163-1	Pegmatites and leucogranites	Leucogranite	5°14'58,5"E 60°22'4,5"N	49 m	Road cut Lyderhornsvie
LYD-169-1	Mixed series	Banded, mylonitic granitic gneiss	5°14'18,8"E 60°21'37,5"N	45 m	Road cut Bjørndalsbakken
LYD-197-1	Hornblende biotite granite gneiss	Hornblende biotite granite gneiss	5°14'30,7"E 60°22'24,9"N	392 m	Natural cliff; below antenna
LYD-197-2	Pegmatites and leucogranites	Pegmatite	5°14'30,7"E 60°22'24,9"N	392 m	Natural cliff; below antenna

5.2.1 Sample LYD-197-1

Hornblende biotite granite gneiss was sampled on the peak of Lyderhorn (Fig. 40A). In the outcrop, weakly foliated hornblende biotite granite gneiss intruded by subvertical pinkish pegmatites. The sample corresponds to the lithological description of the unit in section 5.1.1.

Zircon is an abundant accessory phase in the sample. Crystals are commonly euhedral and relatively large (100 - 300 μm). Most grains are elongated with an aspect ratio between 3 - 4. Zircons are clear with a brownish tone, have small inclusions and are only weakly fractured. Oscillatory zoning, typical for zircons growing from granitic melts (Corfu et al., 2003), is very common (Fig. 41C). Some cores have more complex zoning and a few xenocrystic cores exist.

Twenty-seven spots were analysed on 24 different grains. All analyses are concordant (less than 5% discordant). Twenty-six analyses give a common concordia age of 1042 ± 3 Ma with a MSWD of 0.78 (Fig. 41A). The normal distribution of single analysis concordia ages (Fig. 41B) is only disturbed by a single outlier age that comes from a diffuse, U-rich zone (spot 09-2). U measured in this spot (1399 ppm) is considerably higher than in all other analyses which range from 100 - 600 ppm (Appendix 1). Th/U ratios cluster around 0.3. Only spot 09-2 has a much lower ratio of 0.03.

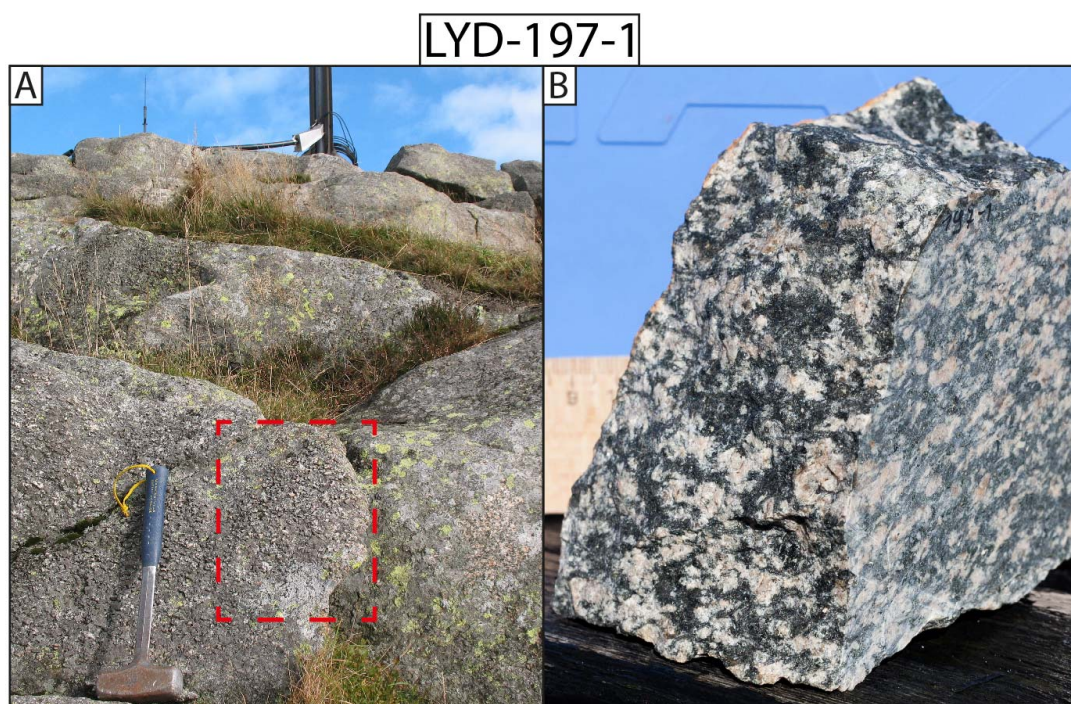


Fig. 40. Sample LYD-197-1: A: Sample locality of weakly foliated, massive hornblende biotite granite gneiss at the peak of Lyderhorn. The red rectangle marks the sampled corner of the outcrop. Hammer for scale. B: Hand specimen of the sampled lithology. Width of image is ~ 10 cm.

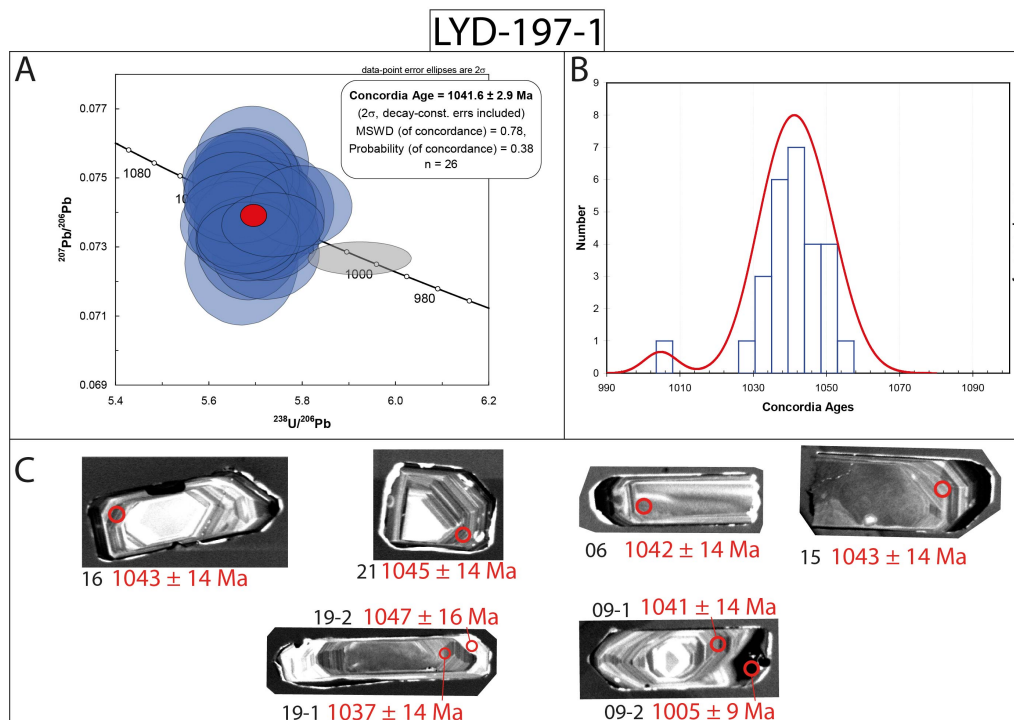


Fig. 41. Results LYD-197-1: A: Tera-Wasserburg plot with common concordia age. One analysis (spot 09-2) was excluded from the calculation (grey error ellipse). B: Relative probability plot and histogram of single grain concordia ages. C: Cathodoluminescence images of representative zircon grains. Red circles mark analysed spots (black numbers) with a diameter of $20 \mu\text{m}$. Single grain concordia ages (red) are given with 2σ -errors.

5.2.2 Sample LYD-44-1

Metagabbro was sampled in the inner part of the mafic body at the west face of Lyderhorn. The outcrop is of low relief, with typical rounded corners and white weathering color (Fig. 42A). The metagabbro is weakly foliated (114/45) and intruded by a large, white pegmatite body that is concordant with the foliation. The lithology consists mostly of bright, blueish-green amphiboles that form an intergranular texture with weakly recrystallized plagioclase (Fig. 42B). Other constituents are minor orthopyroxene and biotite. Chlorite and is a secondary phase. Abundant titanite, few opaque minerals and rare zircon are accessory minerals.

Most zircon crystals are subhedral and elongated (aspect ratios 2 - 5). Some grains are fragmented. The most euhedral grains are relatively large with long sides between $200 - 300 \mu\text{m}$. The crystals are clear, colorless and have only few inclusions and fractures. Most crystals show oscillatory zoning with broad zones parallel to the c-axis (Fig. 43C). Some complex zoning patterns do occur. In general the zircons are typical for the appearance of magmatic zircons grown from a gabbroic melt (Corfu et al., 2003).

Nineteen grains were analysed in sample LYD-44-1. Eighteen analyses give a common concordia age of 1041 ± 3 Ma (Fig. 43A). One reversly discordant analysis (spot 17) was excluded for the calculation. Single grain concordia ages have a perfect normal distribution with a pronounced peak at 1041 Ma (Fig. 43B). All measured U are below 500 ppm (Appendix 1). Th/U ratios are typically for magmatic rocks between $0.6 - 1.05$. The reversly discordant spot 17 has the highest concentrations of U and Th analysed in this sample.

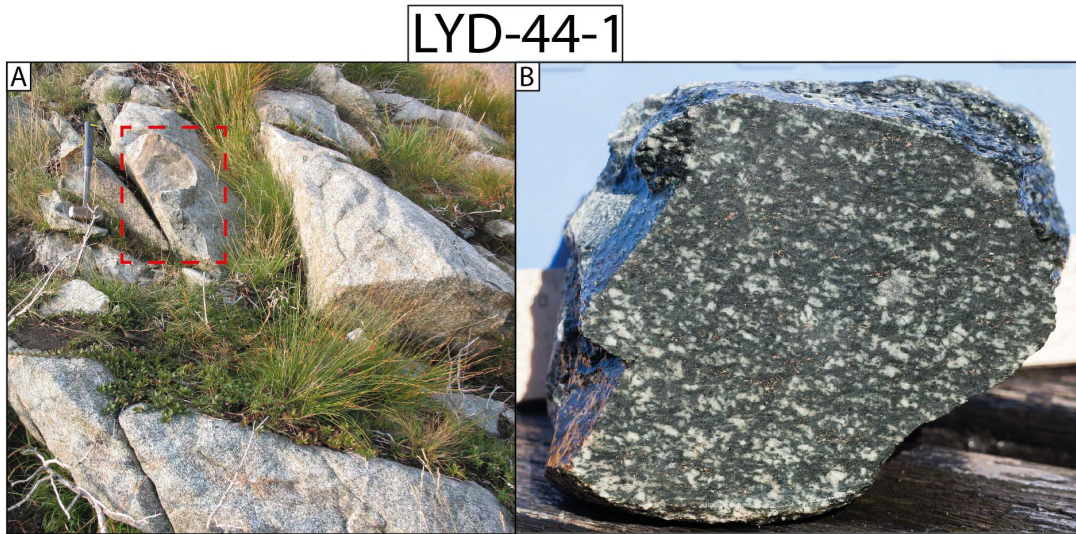


Fig. 42. Sample LYD-44-1: A: Sample locality of weakly foliated metagabbro at the west face of Lyderhorn. The red rectangle marks the sampled corner of the outcrop. Hammer for scale. B: Hand specimen of the sample. Width of image is ~ 10 cm.

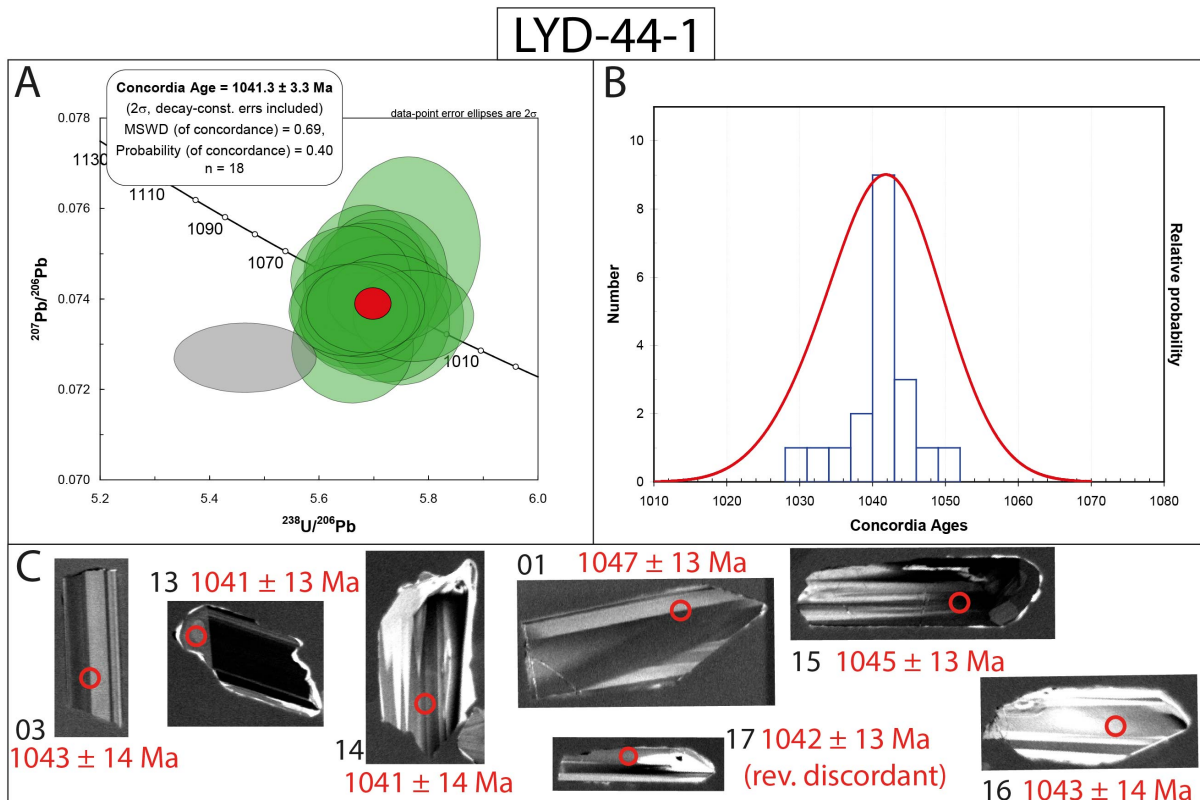


Fig. 43. Results LYD-44-1: A: Tera-Wasserburg plot with common concordia age. One analysis (spot 17) was excluded from the calculation (grey error ellipse). B: Relative probability plot and histogram of single grain concordia ages. C: Cathodoluminescence images of representative zircon grains. Red circles mark analysed spots (black numbers) with a diameter of $20 \mu\text{m}$. Single grain concordia ages (red) are given with 2σ -errors.

5.2.3 Sample LYD-35-1

An amphibolite from the gabbroic unit was sampled at Krabbedalen. The amphibolite has no distinct contact with the metagabbro from the same unit. The sampled outcrop consists of layered amphibolite with slight variations in composition (Fig. 44A). Thin, white granitic veins are parallel with the foliation. The amphibolite is intruded by subvertical pinkish pegmatites with sharp contacts. The sample consists almost entirely of hornblende, plagioclase and minor opaque minerals. Aligned amphiboles and dynamically recrystallized plagioclase form a pronounced L-S-fabric (Fig. 44B). The most felsic part of the outcrop was sampled (Fig. 44A). A thin, white granitic vein could not entirely be avoided. The granitic material was afterwards removed from the sample as good as possible.

Zircon is a very rare accessory phase in the sample. The few grains that could be separated can be divided into two subpopulations (Fig. 45B). The first consists of six fragments of subhedral to anhedral grains. The sizes vary between 100 - 200 μm . The crystals are colorless clear and have oscillatory zoning (e.g. spot 05; Fig. 45B). Some grains show more complex internal structures (e.g. spot 07). The second group consists of four smaller, stubby grains with rounded corners. These crystals are more brownish, fractured and partly metamict. On CL-images they are almost black (e.g. spot 04; Fig. 45B). Oscillatory zoning is weakly visible.

Only ten grains could be analyzed in sample LYD-35-1. Several analyses are either reversely or normally discordant (Fig. 45A). They poorly define a discordia with an upper intercept at 1026 ± 7 Ma and a poorly constrained lower intercept (260 ± 170 Ma). The four oldest grains are from the first described subpopulation and give a weighted mean age of 1040 ± 15 Ma. U range from 200 - 1500 ppm (Appendix 1). The two previously described subpopulations are also reflected in uranium concentrations. The low-luminescent, rounded grains are considerably higher in uranium which is reflected in younger and more discordant ages. Figure 55A (brown) shows a weak correlation between U and concordia ages. Th/U ratios spread between 0.4 and 1.1.

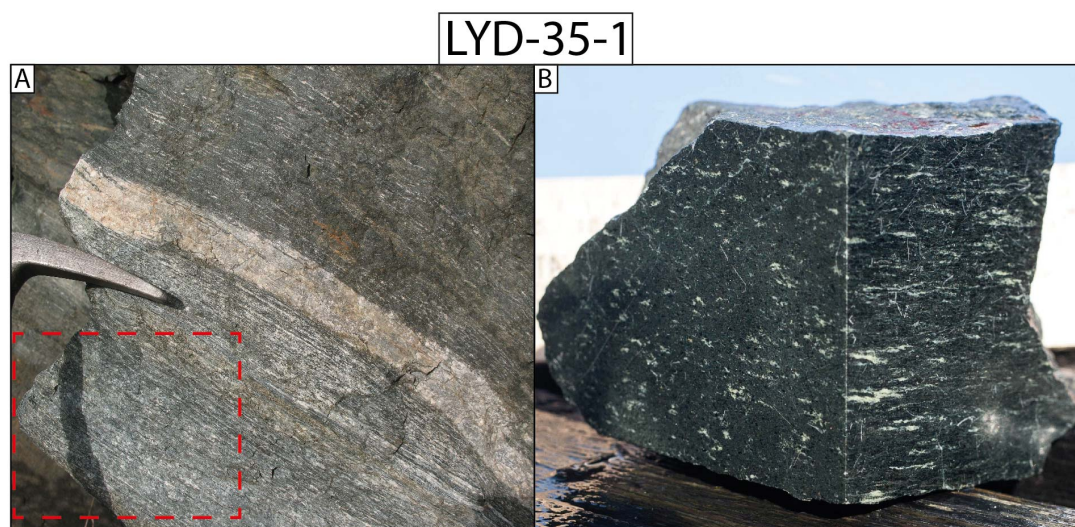


Fig. 44. Sample LYD-35-1: A: Sample locality of amphibolite with lithological layering and white granitic vein. The most felsic part of the outcrop was sampled (red rectangle) and the granitic vein avoided. Hammer for scale. B: Hand specimen from the more mafic part of the outcrop. Width of image is ~ 10 cm.

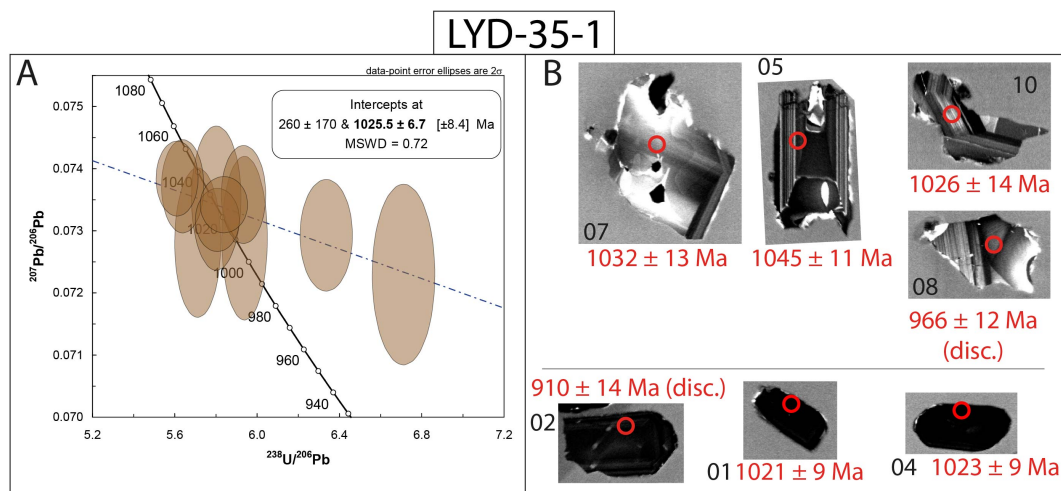


Fig. 45. Results LYD-35-1: A: Tera-Wasserburg plot of all analyses. A discordia is poorly defined by two discordant analyses. B: Cathodoluminescence images of representative zircon grains. Two subpopulations of zircons have been identified. Red circles mark analysed spots (black numbers) with a diameter of 20 μm . Single grain concordia ages (red) are given with 2σ -errors. Note that discordant ages are of no geological significance.

5.2.4 Sample LYD-169-1

A banded, mylonitic granitic gneiss in the mixed series was sampled in a fresh road cut at Bjørndal (Fig. 46A). The several hundred metre long outcrop exposes all the heterogeneous lithologies and deformation that are characteristic for the mixed series. Pink pegmatite bodies with various shapes and dimensions intrude the granitic gneiss. Heterogeneous domains of the outcrop show strong folding of the granitic gneiss and pegmatites along moderately E-plunging fold axes (Fig. 46B). The composition of the gneiss is leucogranitic. The gneissic banding is made of finely laminated, grey layers and pink bands of K-feldspar. The width and textures of K-feldspar bands varies. These bands seem to be deformed small pegmatite veins and were therefore avoided for sampling. The grey layers consist of fine grained quartz, feldspar (K-feldspar more frequent than plagioclase) and minor biotite. Quartz and feldspar are dynamically recrystallized and form a mylonitic to ultramylonitic L-S-fabric (076/30; 18 \rightarrow 081). Biotite is commonly replaced by chlorite. Accessories are epidote, titanite, zircon and apatite.

Zircon is abundant as an accessory phase in this sample. The crystals are euhedral or subhedral. The size of most grains is around 100 - 150 μm . Shapes are mostly stubby with an aspect ratio around 2. Some grains have subrounded corners. Grains are commonly brownish, semi-transparent and have abundant inclusions. On CL-images zircons appear relatively dark. Oscillatory zoning is visible but blurred (Fig. 47C). Some grains have xenocrystic cores. A characteristic feature of the zircon population are thin, irregular, high-luminescent rims. These rims are too thin to be analysed.

Eighteen grains were analysed in sample LYD-169-1. Single grain concordia ages cluster around 1025 Ma with a weighted mean age of 1026 ± 4 Ma (Fig. 47A). Ten concordant analyses give an identical common concordia age (Fig. 47B). All analyses have high U (800 - 2000 ppm; Appendix 1) but no direct correlation is found between U and concordia age. Th/U-ratios are between 0.6 - 1.2.

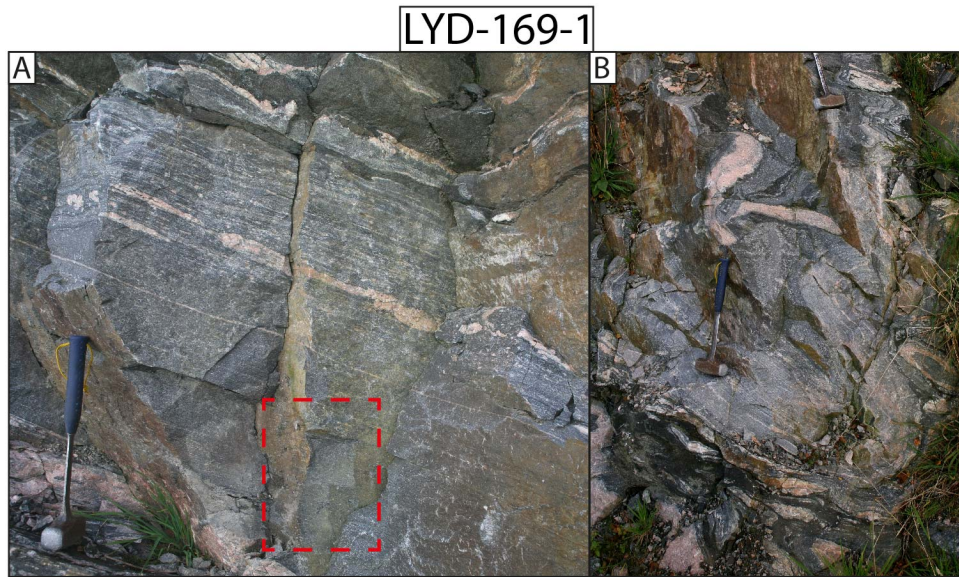


Fig. 46. Sample LYD-169-1: A: Sample locality of mylonitic granitic gneiss in the mixed series. The red rectangle marks the sampled part of the outcrop. Hammer for scale. B: In the same outcrop the mylonitic gneiss is ptygmatically folded (fold axis: 30 \rightarrow 082). Here, the lithology is very heterogeneous with layers of amphibolite (bottom) and intrusive pink pegmatite bodies of various size and dimension. C: Hand specimen cut perpendicular to the stretching lineation. Width of image is \sim 10 cm.

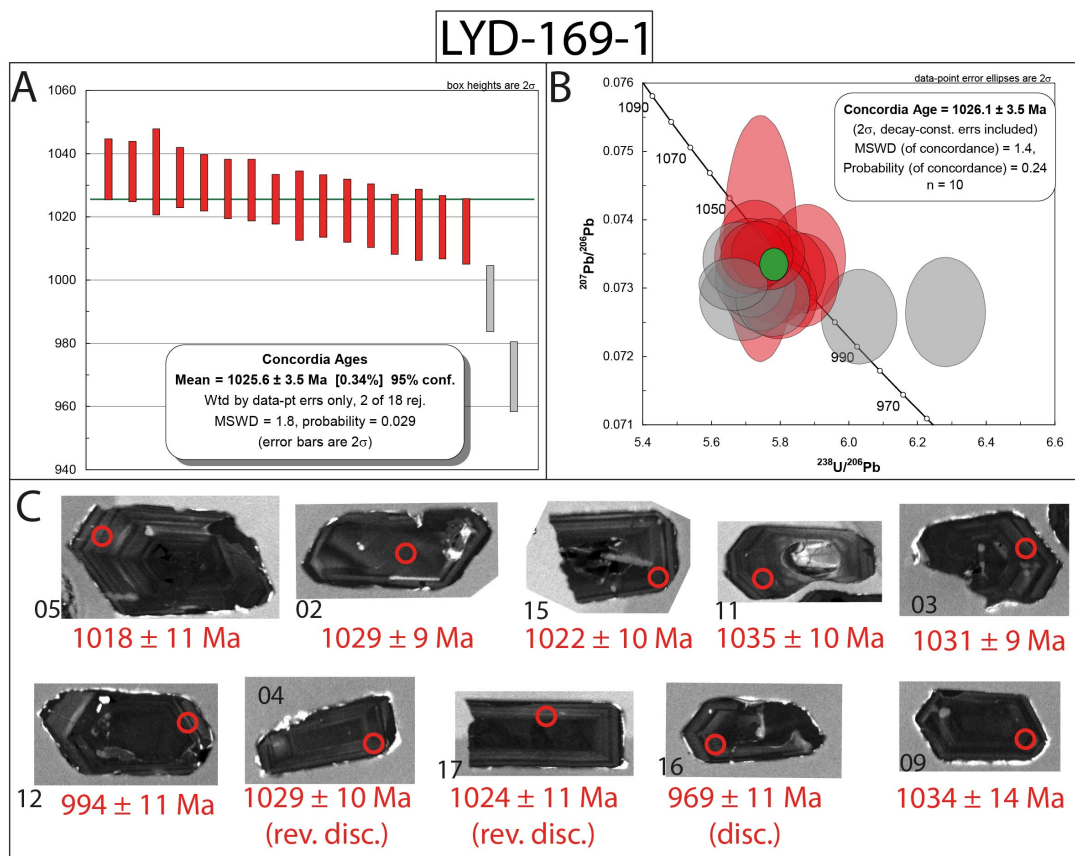


Fig. 47. Results LYD-169-1: A: The weighted mean age of single grain concordia ages is 1025.6 ± 3.5 Ma. Two discordant analyses are rejected. B: Tera-Wasserburg plot and calculation of common concordia age. C: Cathodoluminescence images of representative zircon grains. Red circles mark analysed spots (black numbers) with a diameter of $20 \mu\text{m}$. Single grain concordia ages (red) are given with 2σ -errors. Note that discordant ages are of no geological significance.

5.2.5 Sample LYD-83-1

A banded mylonitic granitic gneiss from the layered gneiss unit was sampled at a new road cut in Gravdal (Fig. 48A). The sample represents the lower limb of a previously described fold (Fig. 29). Finely laminated, dark layers of fine grained quartz, feldspar and biotite alternate with bright, pinkish K-feldspar layers (Fig. 48B). Fine grained quartz and feldspar are dynamically recrystallized and have very uneven grain boundaries. The thickness and texture of the K-feldspar bands varies. Fine grained layers of K-feldspar are mylonitic but also coarse grained and pegmatitic bands occur. The mineral stretching lineation plunges shallowly to ENE ($14 \rightarrow 073$).

Zircon is a common accessory mineral in the sample. The crystals are euhedral to subhedral and have commonly rounded corners. Shapes are often stubby (aspect ratio 2) but more elongated grains exist (aspect ratio > 4). The size of most grains is around $100 \mu\text{m}$ and rarely exceeds $200 \mu\text{m}$. Most crystals are clear, some have a brownish tint. Inclusions are very common but fractures are rare, especially in smaller grains. The internal zoning is variable (Fig. 49D). Euhedral grains show oscillatory zoning (e.g. spot 05). Others have convolute zoning (spot 14) or sector zoning (spot 07-1). A large number of grains shows distinct cores and rims. The cores are commonly lower in uranium and have oscillatory zoning while the rims are rich in uranium and homogeneous (e.g. spots 03, 04, 07-2 and 12). Some grains have thin, discontinuous high-luminescent rims.

Twenty-two spots were analysed on 21 different grains. In the concordia diagram most analyses plot around 1500 Ma (Fig. 49A). Three strongly discordant analyses define a discordia line with an upper intercept age of 1488 ± 7 Ma and a lower intercept of 485 ± 31 Ma. The 5%-discordance filtered single spot concordia ages have a bimodal distribution (Fig. 49B) that reflects two distinct textural domains in the zircon population. Spots with clear oscillatory zoning have uranium concentrations below 400 ppm and give a precise weighted mean age of 1504 ± 4 Ma (Fig. 49C). Weakly discordant ages between 1450 - 1480 Ma are associated with dark rims or diffuse textural domains and high U between 400 - 1000 ppm. Three strongly discordant analyses (spot 04, 12, 07-2) reveal even higher U (up to 1600 ppm). Figure 55A (violet) shows a clear correlation between U and concordia age. Th/U ratios are between 0.2 and 0.4.

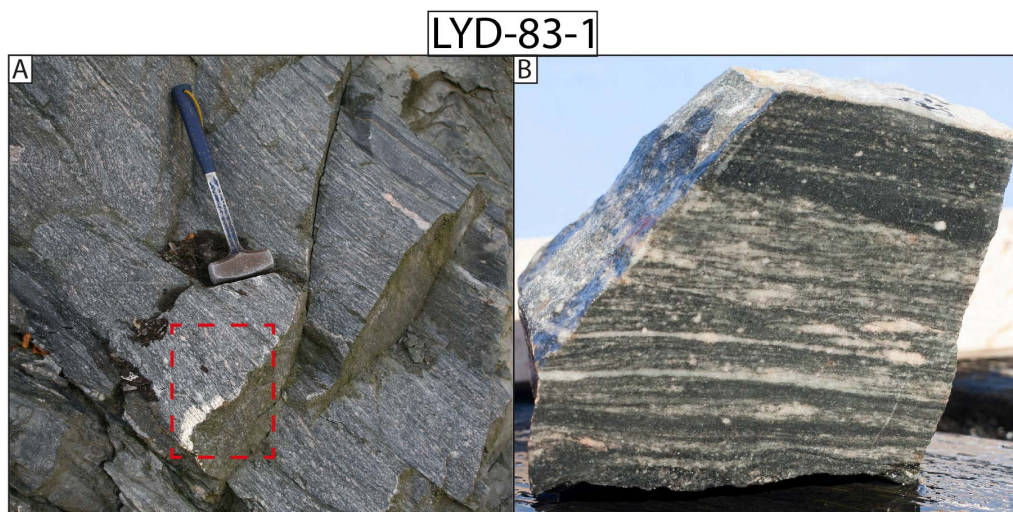


Fig. 48. Sample LYD-83-1: A: Sample locality of mylonitic granitic gneiss. The red rectangle marks the sampled corner of the outcrop. Hammer for scale. B: Hand specimen cut parallel to the mineral lineation. Width of image is ~ 7 cm.

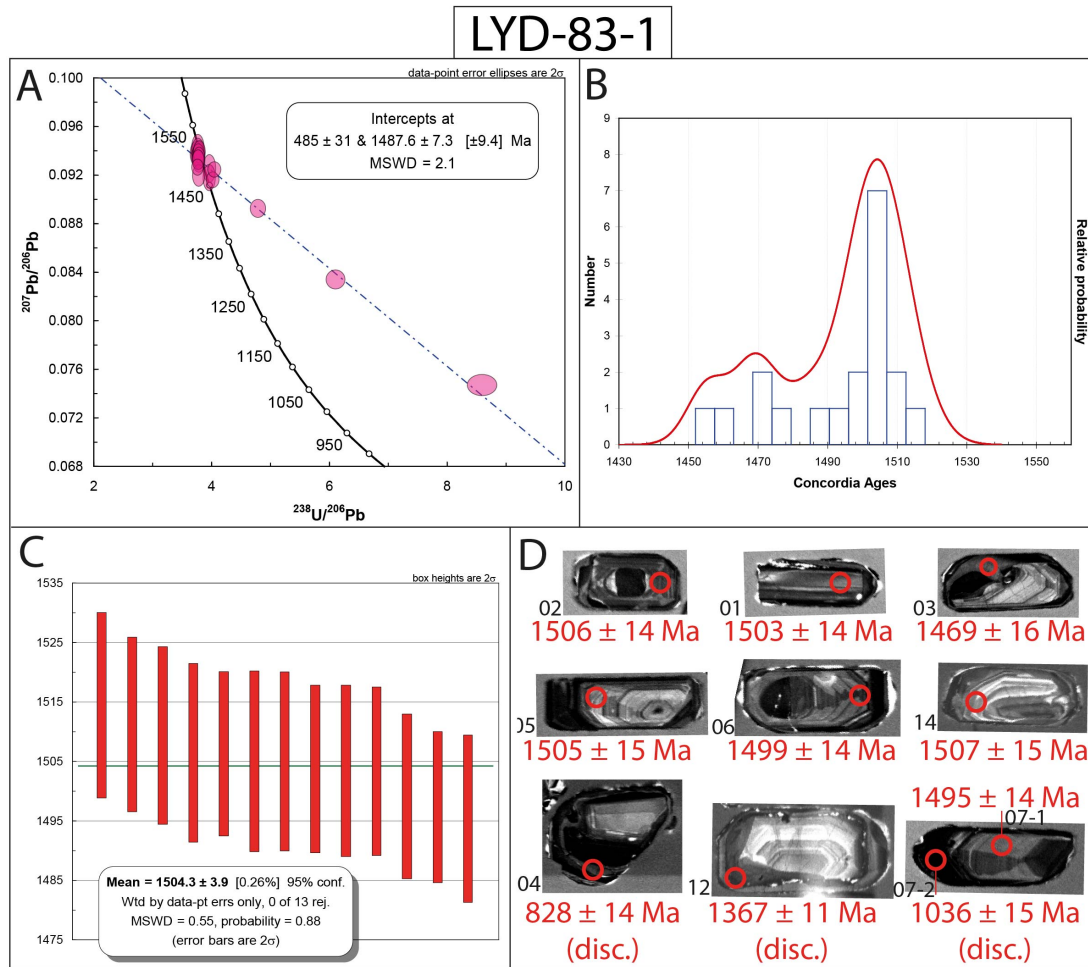


Fig. 49. Results LYD-83-1: A: Tera-Wasserburg plot of all analyses. A discordia is well defined by three strongly discordant analyses. B: Relative probability plot and histogram of 5% discordance-filtered single spot concordia ages. C: Weighted mean of 13 single spot concordia ages from spots with clear oscillatory zoning and relatively low U (< 400 ppm). D: Cathodoluminescence images of representative zircon grains. Red circles mark analysed spots (black numbers) with a diameter of $20 \mu\text{m}$. Single spot concordia ages (red) are given with 2σ -errors. Note that discordant ages are of no geological significance.

5.2.6 Sample LYD-197-2

Pegmatites and leucogranites were mapped as one unit but two individual samples were analysed. A pegmatite was sampled at the peak of Lyderhorn where it intrudes hornblende biotite granite gneiss. The sample locality is the same as for LYD-197-1 (Fig. 50A). The intruding pinkish pegmatite body is one metre wide and has subvertical, SW-NE-striking contacts (307/72). The lithology consists mostly of pinkish K-feldspar, white plagioclase, grey quartz and subordinate red garnet (Fig. 50B). Larger feldspar grains are marginally recrystallized but deform mostly by brittle fracturing while quartz dynamically recrystallized into elongated rods.

Zircon is present as an accessory phase. The entire zircon population is extremely metamict and original crystal shapes are mostly destroyed (Fig. 51B). Grains are commonly $100 - 200 \mu\text{m}$ long and elongated (aspect ratio around 3) and euhedral. The internal zoning is largely obliterated. In few grains relics of oscillatory zoning are visible. In transmitted light the grains are entirely non-transparent.

Out of c. 150 picked grains only eight spots could be analysed. One grain (spot 03) differs strongly from the rest of the zircon population and has an age and element concentrations that are typical for sample LYD-197-1 from the same outcrop. It could represent assimilation from the host rock but is here not further considered. The remaining seven analyses define a discordia with an upper intercept of 964 ± 25 Ma and a lower intercept of 488 ± 21 Ma (Fig. 51A). Both, the upper and the lower intercepts are fixed by concordant analyses (spot 01 and 09). U is in all spots extremely high (1000 - 3500 ppm; Appendix 1) which explains the strong metamictization. Figure 55A (red) shows a strong correlation between U and concordia age. All measured Th/U-ratios are below 0.05 except for spot 11.

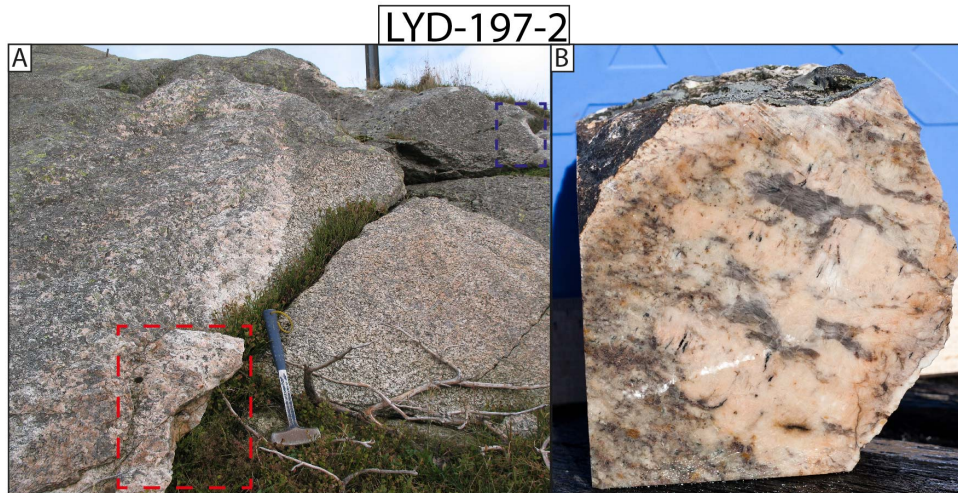


Fig. 50. Sample LYD-197-2: A: Sample locality of pinkish pegmatite intruding hornblende biotite granite at the peak of Lyderhorn. The red rectangle marks the sampled corner of the outcrop. The sample locality of sample LYD-197-1 is marked with a blue rectangle in the background (upper right corner). Hammer for scale. B: Hand specimen of the sample. Width of image is ~ 10 cm.

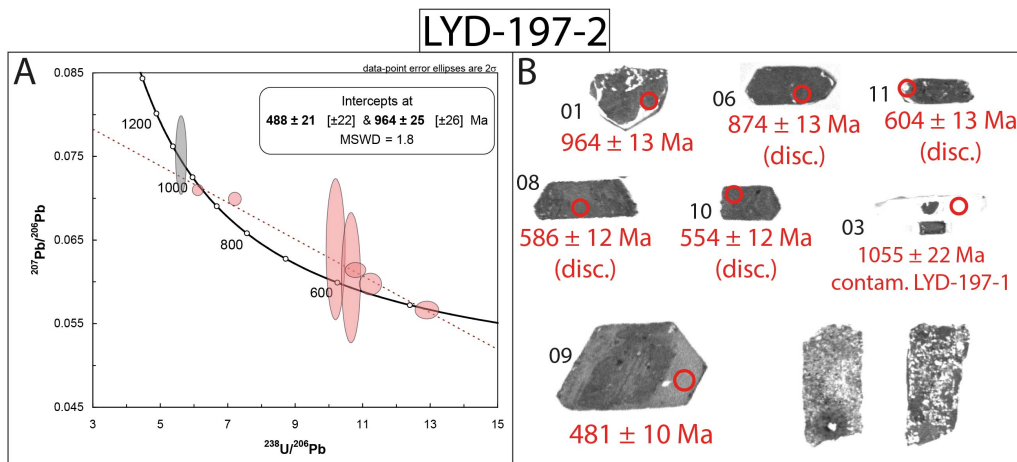


Fig. 51. Results LYD-197-2: A: Tera-Wasserburg plot of all analyses. Most analyses are strongly discordant, but two concordant analyses fix the upper and lower intercepts. One analysis (spot 03) is contamination from sample LYD-197-1 in the same outcrop and excluded (grey error ellipse). B: Cathodoluminescence images of representative zircon grains. Red circles mark analysed spots (black numbers) with a diameter of $20 \mu\text{m}$. Single grain concordia ages (red) are given with 2σ -errors. Note that discordant ages are of no geological significance. Only eight grains could be analysed as most zircons in the sample are extremely metamict (see examples in lower right corner).

5.2.7 Sample LYD-163-1

The leucogranite from the same unit was sampled at a fresh road cut close to Liavatnet. The roughly 20 m wide body intrudes amphibolite. The NE-SW-striking contacts are subvertical (150/82). Inside the granite body textures vary with diffuse contacts between pegmatitic and medium grained granite (Fig. 52A). The pegmatitic parts were avoided for sampling. The lithology consists mainly of pinkish-red K-feldspar, smaller amounts of plagioclase and quartz as well as minor mica (Fig. 52B). Flame perthites are abundant in K-feldspar and myrmekites occur. Biotite is the only mafic constituent and is mostly altered to chlorite. Quartz and feldspar are dynamically recrystallized into a weak L-S-fabric.

Zircon is an abundant accessory mineral. Most grains are euhedral and have a rather stubby shape. A large number of crystals are broken. Elongation ratios are between 2 and 3. Sizes range mainly from 100 - 200 μm . Moderate to strong metamictization obliterates internal textures. Figure 53C shows a number of grains that reveal oscillatory zoning or at least remnants of it (e.g. spot 06, 04, 16). More complex zoning patterns can also be observed (e.g. spot 09). Many grains have xenocrystic cores, some of which are rounded.

Only the least metamict grains were analysed. Sixteen spots were analysed on 15 individual grains. With the exception of one outlier, the analyses define a discordia with an upper intercept at 1013.8 ± 11 Ma and a lower intercept at 462 ± 18 Ma (Fig. 53A). The outlier spot 05 has an (discordant) older age of 1166 ± 13 Ma. It comes from a grain that is texturally difficult to interpret. The most concordant analyses cluster between 1050 Ma and 1000 Ma. Six analyses weakly define a plateau, with a weighted mean age of 1024 ± 10 Ma (Fig. 53B).

Most analyses have very high U, ranging up to 4500 ppm (Appendix 1). Figure 55A (yellow) shows a strong correlation between U and concordia age. Th/U ratios are mostly between 0.4 and 0.7. Spot 07 and 17-2 have Th/U ratios higher than 1.

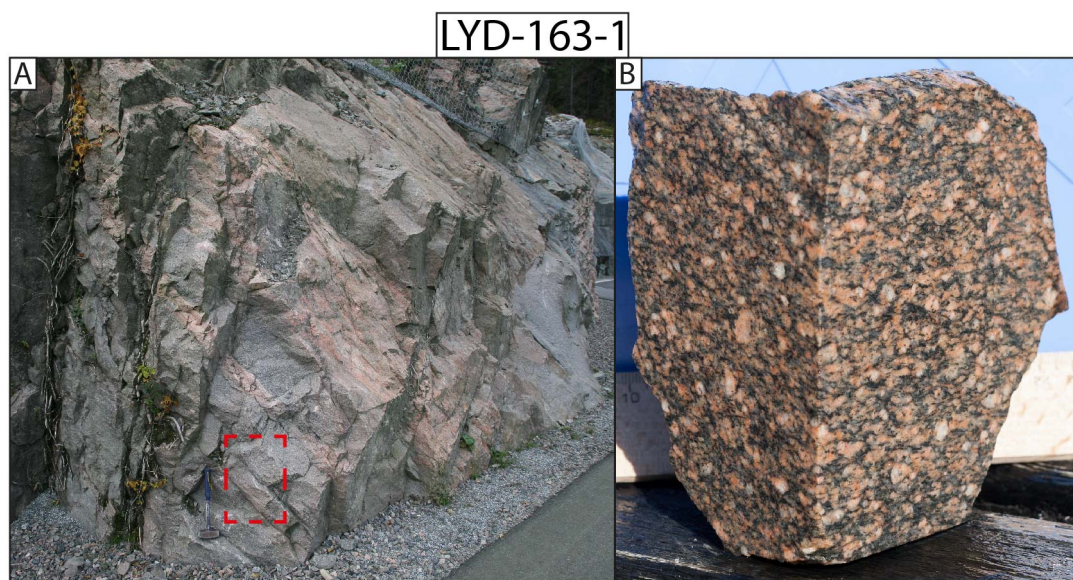


Fig. 52. Sample LYD-163-1: A: Sample locality of leucogranite with diffuse veins of pinkish pegmatite. The red rectangle marks the sampled part of the outcrop. Hammer for scale. B: Hand specimen of the sample. Width of image is ~ 10 cm.

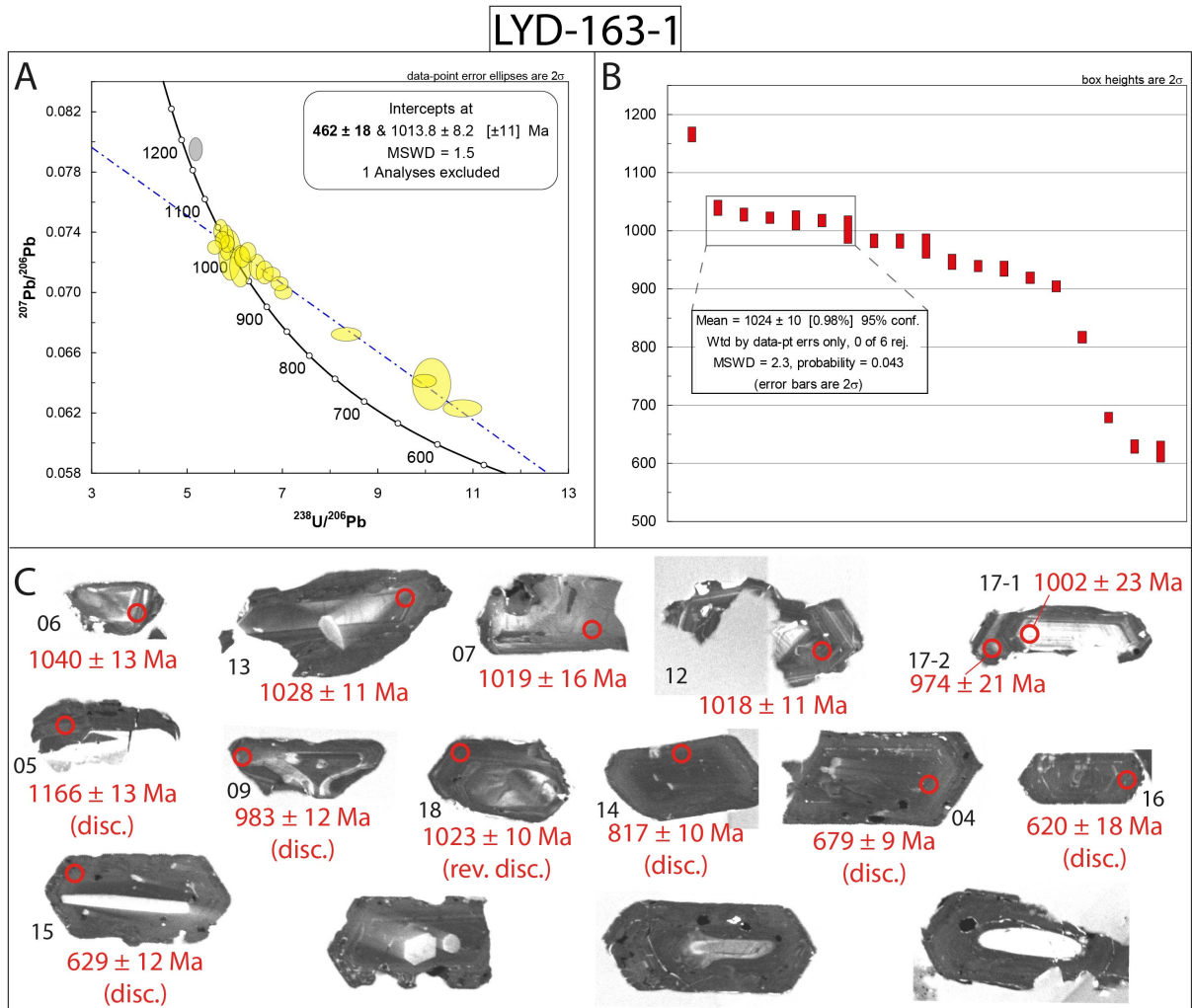


Fig. 53. Results LYD-163-1: A: Tera-Wasserburg plot of all analyses. A discordia is defined by a large number of discordant analyses. One analyses (spot 05) has a considerably older age and is excluded for the calculation of intercept ages (grey error ellipse). B: Overview over single grain concordia ages. Six analyses that form a small plateau can be used to calculate a weighted mean age. C: Cathodoluminescence images of representative zircon grains. Red circles mark analysed spots (black numbers) with a diameter of $20 \mu\text{m}$. Single grain concordia ages (red) are given with 2σ -errors. Note that discordant ages are of geological significance.

5.2.8 Summary of Geochronological Results

Fig. 54 shows the distribution of all acquired single spot concordia ages. The probability distribution of 5% discordance-filtered ages (right column) illustrates that concordant analyses form two age-plateaus (marked by purple and green) and are separated by curved 'tails' of discordant analyses. The older plateau (purple) is defined by sample LYD-83-1 with a clear probability peak at 1505 Ma. The majority of concordant ages define a pronounced probability peak at 1041 Ma (green). Concordant ages get slightly younger before they bend into a tail of discordant ages. One single analysis in sample LYD-197-1 defines the latest concordance-peak at 485 Ma (red).

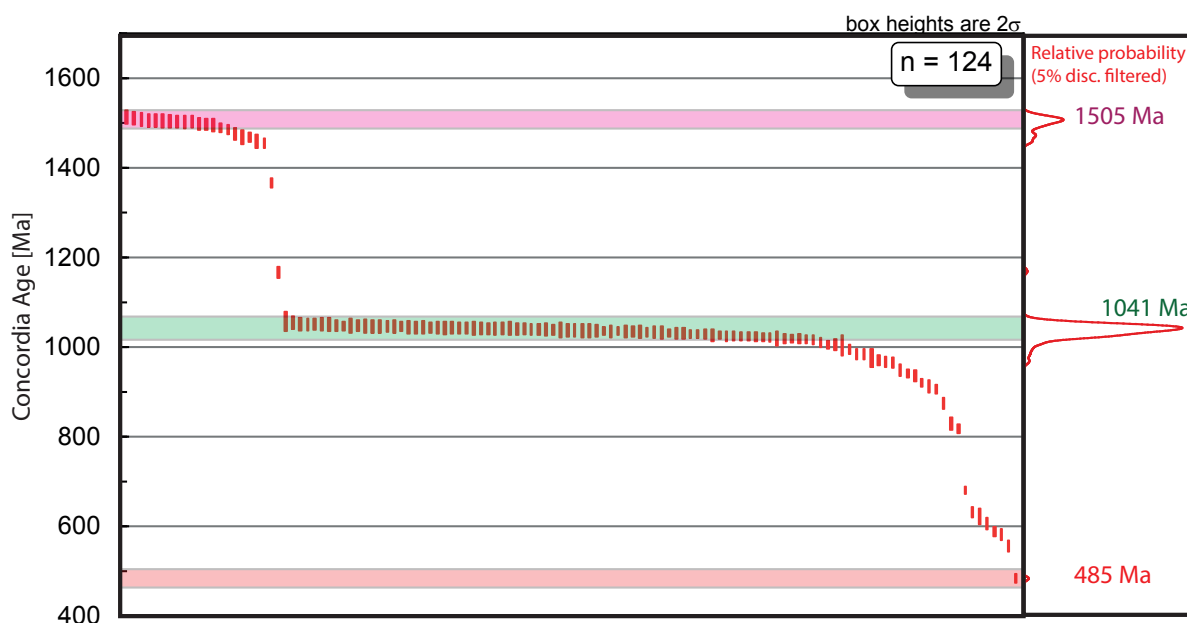


Fig. 54. Distribution of all concordia ages acquired in this study. Ages are shown as 2σ -bars. The relative probability of 5% discordance-filtered concordia ages is shown in the right column. It shows that concordant ages occur in three distinct episodes at 1505 Ma (purple), 1041 Ma (green) and 485 Ma (red) that are separated by discordant analyses.

Samples with high uranium concentrations show a clear correlation with resulting concordia ages (Fig. 55A). The oldest ages in each sample are associated with low uranium concentrations (below 500 ppm). Figure 55B shows Th/U ratios plotted against respective concordia ages. Most analyses plot between 0.1 and 1.2, typical for magmatic zircons (e.g. Wu and Zheng, 2004). The analyses of individual samples define distinct clusters with few outliers. The pegmatite sample LYD-197-2 reveals very low Th/U-ratios (< 0.1) spread over a wide range of ages (500 My). Figure 56 shows the relationship between uranium concentration and discordance. Concordant analyses and reversely discordant analyses (positive discordance) are independent of uranium concentration. On the other hand, a moderate correlation can be found for normally discordant analyses. The higher the uranium concentration the more discordant are the analyses. The relationship between common lead and discordance is more complex. Reversely discordant and concordant analyses are in general poor in common lead. Normally discordant analyses are relatively rich in common lead but there is no clear correlation.

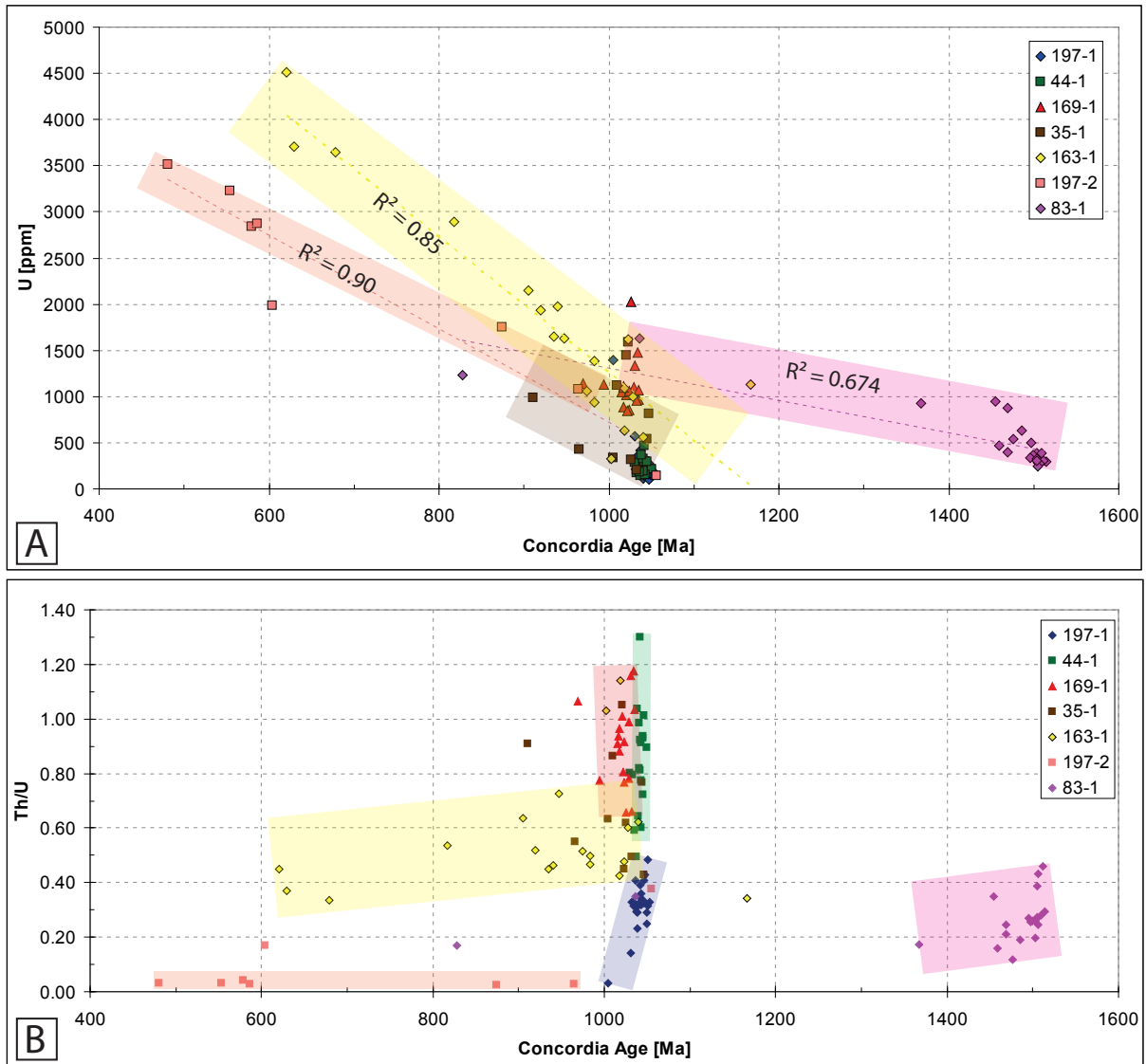


Fig. 55. A: Uranium concentrations of different samples plotted against concordia ages. Four samples show a negative correlation (significant for three samples) that is highlighted by coloured bars. Determination coefficients are given. B: Th/U-ratios plotted against concordia ages. The analyses of individual samples define distinct clusters that are highlighted by colors.

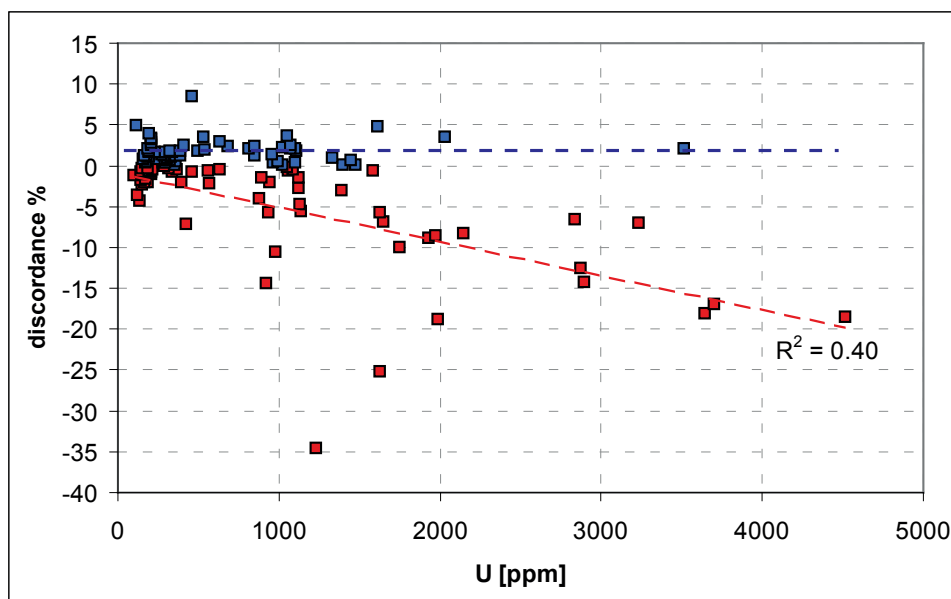


Fig. 56. Discordance plotted against uranium concentration of all analyses. Reversely discordant and concordant analyses show no correlation with uranium concentration (blue). Normally discordant analyses (negative values, red) are moderately correlated with uranium concentration ($R^2 = 0.4$). Note, that the correlation is in fact positive which is easy to confuse due to negative values for normal discordance.

6 Discussion

The discussion of the results is split into two parts that follow the chronological order of geologic events. Based on the interpretation of U-Pb zircon geochronology results, an igneous formation history for the Lyderhorn Gneiss and lithological correlations to the surrounding area are proposed. Afterwards, the structural evolution of the Lyderhorn Gneiss is assessed. To explain inconsistencies with the established tectonic model of the Bergen area, an alternative model for the Devonian exhumation of the Øygarden Complex is discussed.

6.1 Geochronology

6.1.1 Interpretation of Acquired Ages

LYD-197-1 and LYD-44-1

Based on zircon textures, Th/U ratios, concordance and normal distributions of ages, I interpret the common concordia age of each of the samples and as the magmatic crystallization age. Hornblende biotite granite gneiss (LYD-197-1) as well as metagabbro (LYD-44-1) crystallized around 1041 ± 3 Ma. Their exact age relationship is not distinguishable because the age difference is within uncertainties. The two samples have texturally distinct zircon populations but their ages conform statistically to one single population with a perfect normal distribution and a weighted mean age of 1041 ± 2 Ma (Fig. 57). Field relationships imply that the hornblende biotite granite intruded the gabbro. Diffuse contacts suggest that the gabbro was not entirely crystallized before the granite intruded. This field interpretation is confirmed by geochronology. A noteworthy result is that amphibolite facies regional metamorphism had no effect on the zircon U-Pb zircon system in neither of the samples.

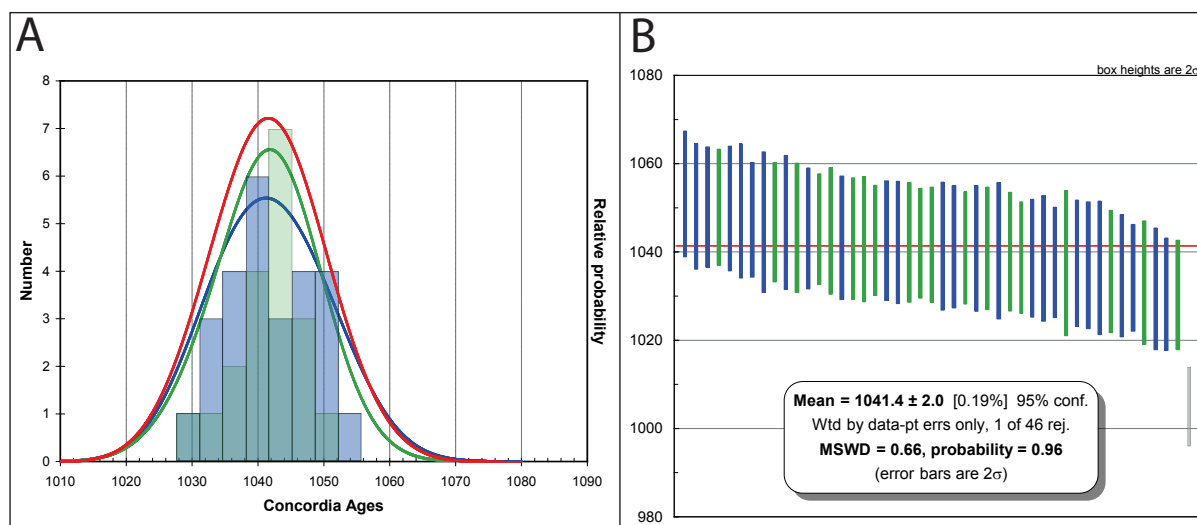


Fig. 57. Ages from sample LYD-197-1 (blue) and LYD-44-1 (green) form statistically one single population. A: Probability density plots and histograms of the two individual samples (blue/green). The relative probability of ages from both samples together (red) shows a perfect normal distribution. One outlier analyses (spot 09-2) from sample LYD-197-1 was excluded. B: Single spot concordia ages from the different samples show an evenly distributed occurrence. All analyses together have a MSWD-age of 1041 ± 2 Ma. The MSWD of 0.66 with a probability of 0.96 implies that the ages conform statistically to one population.

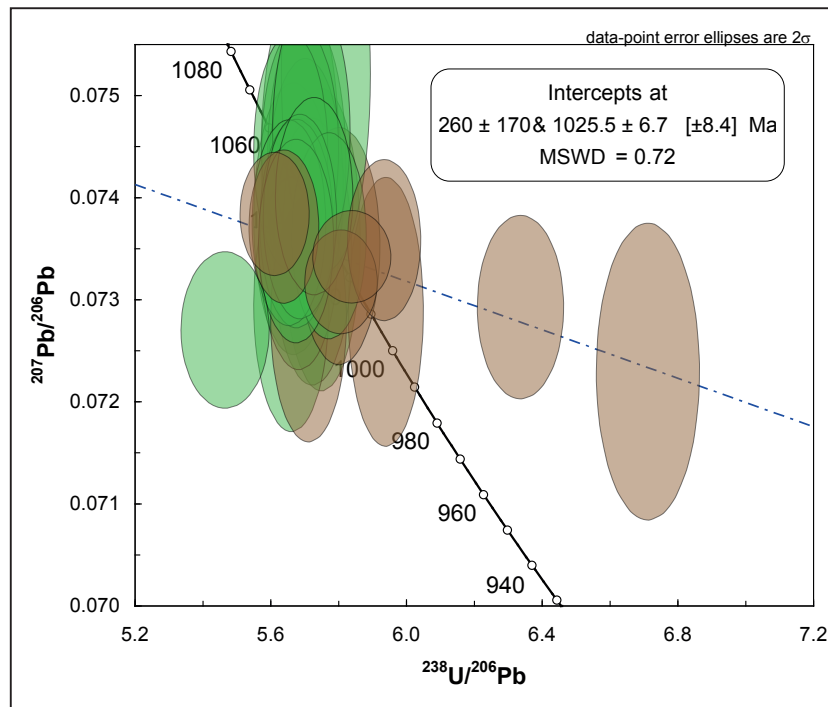


Fig. 58. Collective Tera-Wasserburg plot of samples from the gabbroic unit. The ages from the amphibolite (LYD-35-1; brown) show a close relation to the concordant analyses from the metagabbro (LYD-44-1; green). The upper intercept age is therefore not interpreted as the protolith age of the amphibolite. See text for discussion.

LYD-35-1

Because of a limited number of analyses and two distinct zircon subpopulations the interpretation of sample LYD-35-1 is complex. Discordance of U-rich analyses implies that episodic Pb-loss occurred. The lower intercept is meaningless because of its large error. The interpretation of the upper intercept age (1026 ± 7 Ma), as the igneous protolith age of the amphibolite, would imply two distinct episodes of gabbroic magmatism at 1041 Ma and 1026 Ma, respectively. Anchoring of the lower intercept at 483 ± 13 Ma (lower intercept age of other discordant samples; see below), does not change the upper intercept. Zircon from the amphibolite has considerably higher U than zircon from the metagabbro (LYD-44-1). High U correlates weakly with younger and more discordant ages. Th/U ratios are very similar in both gabbroic samples and typical for igneous zircon. The most concordant analyses from the amphibolite plot within the scatter of the metagabbro (Fig. 58A). The four oldest zircons from the amphibolite with clear igneous textures have a mean age of 1040 ± 15 Ma that corresponds to the crystallization age of the gabbro (1041 ± 3 Ma). The discordia line is mainly defined by the second subpopulation of U-rich zircon. The upper intercept age is similar to ages from granitic samples with high-U zircon (LYD-169-1, LYD-163-1). Therefore, the upper intercept age is likely to represent the crystallization age of the small granitic vein that is contained within the amphibolite. Field relationships suggest that the amphibolite is the high-strain equivalent of the metagabbro. I interpret the crystallization age of the metagabbro (1041 ± 3 Ma), to represent also the crystallization age of the gabbroic protolith of the amphibolite.

LYD-169-1

The zircon population of the mylonitic granitic gneiss from the mixed series is characterized by high U and moderate metamictization. Textures and Th/U ratios conform with magmatic zircons. The weighted mean age of 1026 ± 4 Ma is interpreted as the igneous crystallization age of the granitic protolith. Six slightly reversely discordant and two normally discordant analyses show a minor disturbance of the U-Pb system in metamict grains. This disturbance is interpreted to reflect a low grade thermal resetting similar to other samples with metamict grains (LYD-163-1, LYD-197-2 and LYD-83-1). The intense ductile deformation of the mylonitic gneiss is most likely recorded in thin, discontinuous rims but had no further effect on the U-Pb system.

LYD-83-1

The igneous protolith age of the mylonitic granitic gneiss could be represented either by the upper intercept age of 1488 ± 7 Ma or the weighted mean age of 1504 ± 4 Ma that comes from 13 grains with low U and magmatic textures. Slightly discordant ages that are within the 5% discordance limit form a subpopulation of ages at 1480 - 1450 Ma. All such younger ages come from texturally homogeneous rims with U above 400 ppm. The population of concordant ages around 1505 Ma, comes entirely from spots with U below 400 ppm and clear oscillatory zoning. Th/U ratios that are typical for magmatic zircons, imply that distinct textural domains formed together in one episode of zircon growth. None of the xenocrystic cores in the sample, that could represent an even older generation of zircon, has been analysed. The correlation between age

and U implies that minor Pb-loss affected zircon domains with more than 400 ppm U. Therefore, the 1480 - 1450 Ma age population is not interpreted as a distinct phase of zircon crystallization. The younger ages are better explained by slight resetting due to the thermal effect of nearby gabbro and granite intrusions at 1041 Ma or by the Ordovician thermal event that caused severe Pb-loss in strongly metamict grains. I therefore interpret the weighted mean age of 1504 ± 4 Ma to represent the crystallization age of the granite protolith.

LYD-197-2 and LYD-163-1

The lithological unity of pegmatites (sample LYD-197-2) and leucogranites (sample LYD-163-1) is confirmed by geochronology. Zircon populations in both samples have very high U, are strongly metamict and revealed similar discordance patterns with a large number of strongly discordant analyses. Two conceivable alternatives exist for the interpretation of the intercepts: 1. The lower intercept represents the age of intrusion and the upper intercept represents zircon inheritance, respectively. 2. The upper intercept represents the age of intrusion and the lower intercept is caused by thermal resetting. To answer this question it is helpful to compare lower intercepts of different samples (Fig. 59). The discordia lines of LYD-197-2 and LYD-163-1 are perfectly parallel. The leucogranite has a younger lower intercept age (462 ± 18 Ma) than the pegmatite (488 ± 21 Ma). A concordant analysis from the pegmatite fixes the lower intercept even more precisely to 481 ± 10 Ma.

The mylonitic gneiss sample LYD-83-1 has a corresponding lower intercept age of 485 ± 31 Ma. Discordant analyses in all three samples show a strong correlation between concordia age and U (Fig. 55A). Th/U ratios in the pegmatite are below 0.1 but the metamict zircons show relict magmatic textures and no sign of metamorphic recrystallization. The clear correlation between age and U explains the lower intercepts by partial or complete resetting of extremely U-rich and metamict zircon due to a thermal event in Ordovician times. Intrusion ages in the leucogranite and pegmatite unit must therefore be represented by the upper intercepts of sample LYD-197-2 and LYD-163-1.

Due to the severe metamictization, only seven grains could be successfully analysed in sample LYD-197-2 that give a very poorly constrained upper intercept age of 964 ± 21 Ma. Far more successful analyses from sample LYD-163-1 give a well constrained upper intercept age of 1014 ± 8 Ma.

As the samples represent the same lithological unit it seems legitimate to treat their ages as one population. Figure 60A shows that the samples complement each other in their distribution of concordia ages. Regression of both samples together gives an upper intercept of 1011 ± 13 Ma. One reversely discordant analysis occurs in each of the samples that 'drag' the discordia towards younger intercepts. Excluding the two reversely discordant analyses improves the statistical correlation of the discordia regression significantly (Fig. 60B). The alternative upper intercept of 1022 ± 9 Ma is identical with the weighted mean age of the six most concordant ages from sample LYD-163-1 (1024 ± 10 Ma) and the crystallization age of the lithological similar sample LYD-169-1 (1026 ± 4 Ma). The alternative lower intercept age of 483 ± 13 Ma is identical with the lower intercept age of sample LYD-83-1 (485 ± 31 Ma) and the concordant analyses LYD-197-2-09 (481 ± 10 Ma). I therefore interpret the intercept ages in Figure 60B to be the

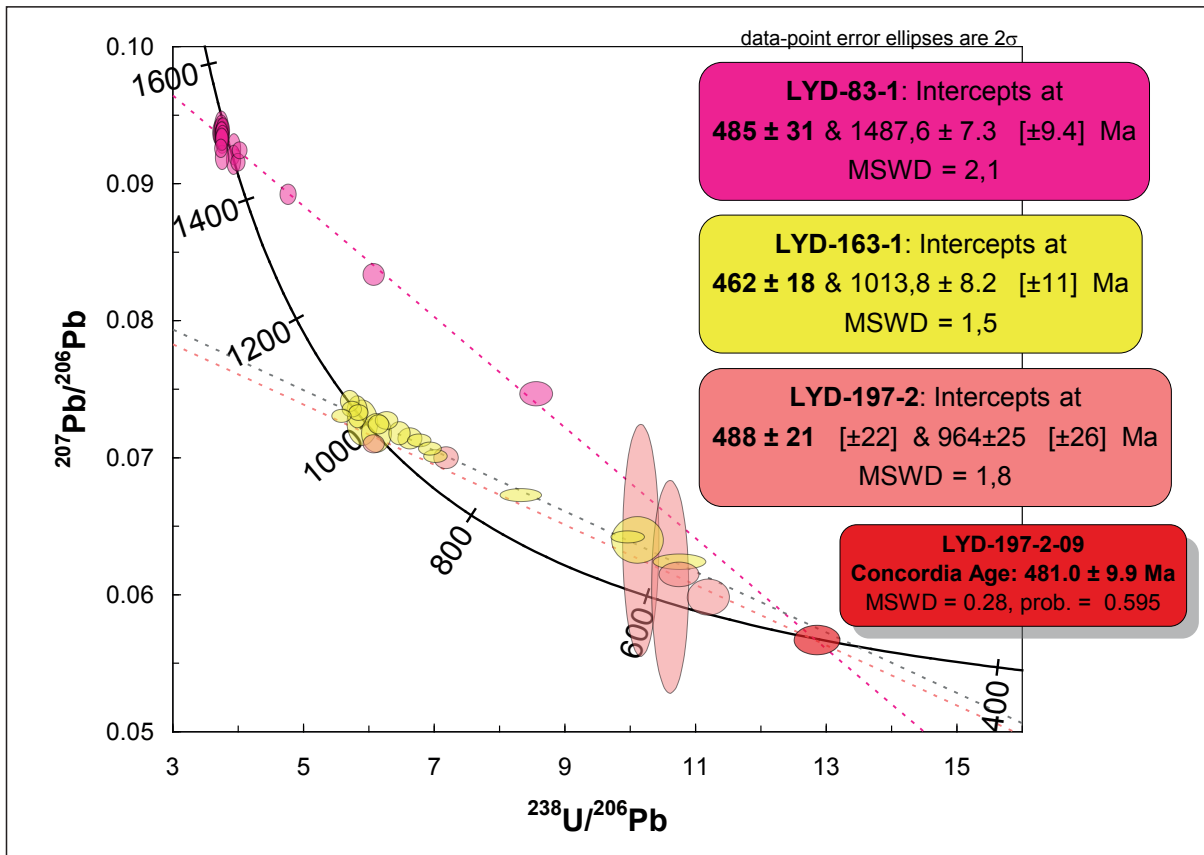


Fig. 59. Discordia lines of three discordant samples intersect in the lower intercept that is furthermore fixed by the concordant analysis LYD-197-2-09 at 481 ± 10 Ma.

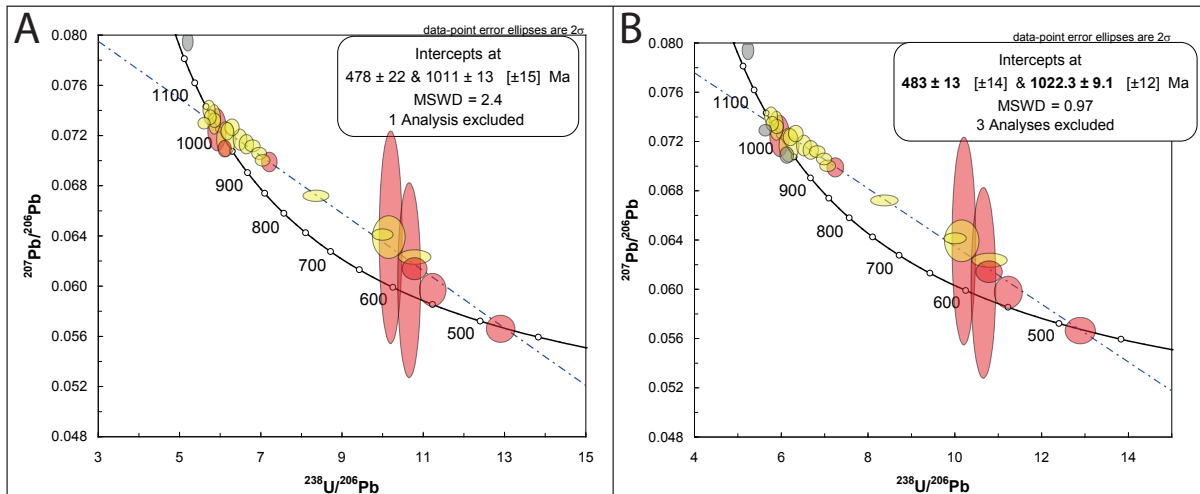


Fig. 60. Comparison of ages from the Pegmatite and Leucogranite unit. A: Joint Tera-Wasserburg plot of sample LYD-197-1 and LYD-163-1. Both samples together define a discordia with intercepts at 1011 ± 15 Ma and 478 ± 22 Ma. One older age outlier is excluded. B: The correlation of the regression is strongly improved when two reversely discordant analyses are excluded. The alternative intercept ages are: 1022 ± 9 Ma and 483 ± 13 Ma. These ages are seen as the best estimation for the age igneous crystallization and thermal resetting of the pegmatite and leucogranite unit.

best estimation for both, the age of intrusion and the age of thermal resetting in the pegmatite and leucogranite unit.

6.1.2 Igneous Formation of the Lyderhorn Gneiss and Regional Correlations

Fig. 61 summarizes the magmatic formation ages found in this study. The oldest constituents of the Lyderhorn Gneiss are layered granitic gneisses with an igneous crystallization age of 1504 ± 4 Ma. A large gabbroic body intruded into the gneisses at 1041 ± 3 Ma. Before it was entirely crystallized, the gabbro was intruded by smaller bodies of hornblende biotite granite. Subsequently, all lithologies were intruded by numerous pegmatite and leucogranite dykes that crystallized between 1026 ± 4 Ma and 1022 ± 9 Ma. The leucocratic intrusives get more and more voluminous towards the south.

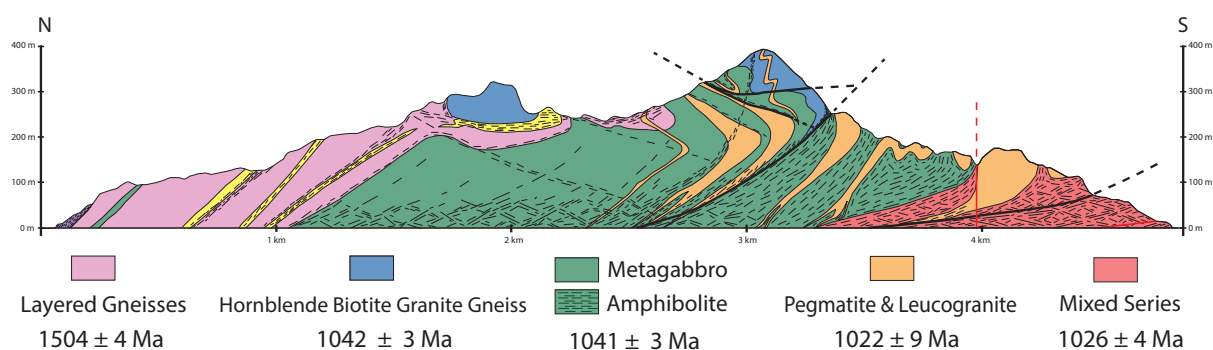


Fig. 61. Magmatic crystallization ages of the igneous protoliths of the Lyderhorn Gneiss. See text for discussion.

The lithologies in the Lyderhorn Lyderhorn Gneiss can be correlated with lithologies in the surrounding area. Fig. 62 shows a simplified geological map which combines the results from this study with brief investigations in other areas on the Laksevåg Peninsula and southern Askøy as well as previously published mapping results.

A relatively thin layer of hornblende biotite granite gneiss follows the strongly bent contact between Øygarden Complex and Minor Bergen Arc. The lithology, that forms the peaks of the mountains Damsgårdsfjellet, Gravdalsfjellet and Løvstakken is identical with the hornblende biotite granite gneiss that has been dated on the peak of Lyderhorn (sample LYD-197-1). Previous, unpublished U-Pb zircon geochronology studies from the Løvstakken area dated this lithology to 1084 ± 13 Ma and 1045 ± 14 Ma (Fig. 10). These ages agree more or less with the more precise dating of sample LYD-197-1. The granite-dominated mixed series was mapped by Weiss (1977) as 'layered series' but the unit is not shown consistently on the geological map of Bergen (Fig. 11). A massive body of leucocratic, gneissic granite occupies most of Fyllingsdalen. The granite has an extraordinary high radiogenic heat production (Schulze, 2014). Within the mapping area, leucogranites and pegmatites tend to get more voluminous from north towards south. They constitute a major part of the mixed series which grades into the massive granite further south. Obvious similarities in composition, texture and high concentration of radiogenic elements suggest that the Fyllingsdalen granite is of similar age as the dated leucogranitic samples LYD-197-2, LYD-163-1 and LYD-169-1 (1026 - 1022 Ma). The geological correlation of southern Askøy and

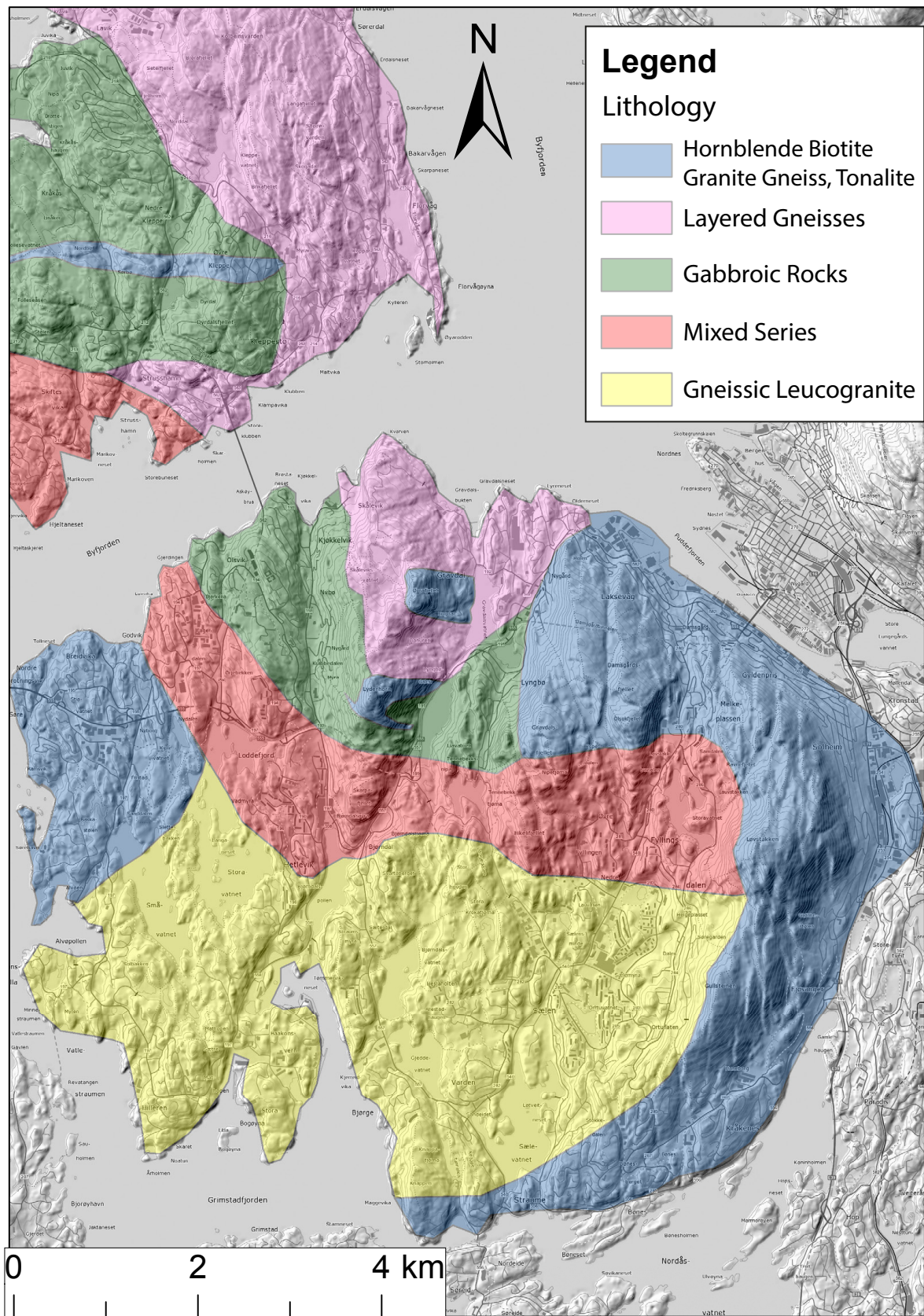


Fig. 62. Simplified geological map of the Laksevåg Peninsula and southern Askøy combining results from this study with previous mapping by Askvik (1971), Weiss (1977) and Fossen and Ragnhildstveit (2008).

the Laksevåg peninsula by Kolderup and Kolderup (1940), is supported by my own investigations. Like the gabbro on Lyderhorn, the gabbroic body on Askøy is mantled by layered granitic gneisses. It contains an E-W-striking dyke that Askvik (1971) mapped as tonalite (quartz diorite). New road cuts NW of Strusshamnvatnet ($5^{\circ}11'34''\text{E}$, $60^{\circ}24'51''\text{N}$) expose a granitic core of the body. Closer to the contact the composition in the dyke grades towards tonalite and shows intensive magmatic brecciation of the gabbro. The intrusive relationships are very similar with the hornblende biotite granite gneiss on Lyderhorn. I therefore assume that the granite-tonalite dyke on Askøy corresponds to the folded granite body on Lyderhorn.

I propose that the magmatic ages from the Lyderhorn Gneiss (Fig. 61) are also valid for corresponding lithologies shown on Fig. 62. The intrusive formation history of the area can be recognized on this map: gabbroic melts intruded at 1041 Ma into Telemarkian (1504 Ma) layered gneisses. The gabbro body was directly afterwards intruded by various dykes and sills ranging in composition from hornblende biotite granite to tonalite. At 1026 - 1022 Ma, voluminous leucogranites intruded in the southern part of the Laksevåg Peninsula. The mixed series represents the contact zone between the granite intrusion and other lithologies.

6.1.3 Significance of Ages for the Regional Geology of SW Norway

SIMS U-Pb zircon geochronology revealed ages that range over more than 1000 My. The geochronological dataset of the Lyderhorn Gneiss covers a large part of the geological history of SW Norway and records three major orogenic periods. Fig. 63 shows a cyclic discordance pattern. Concordant 'peaks' are separated by roughly 500 My long 'troughs' of discordant ages. The concordant peaks correspond to the Gothian-Telemarkian, Sveconorwegian and Caledonian orogenic periods, respectively (compare with Fig. 2). This implies that the cyclic discordance of the geochronological dataset represents two entire supercontinent-cycles with their typical 500 My periodicity (e.g. Torsvik and Cocks, 2005).

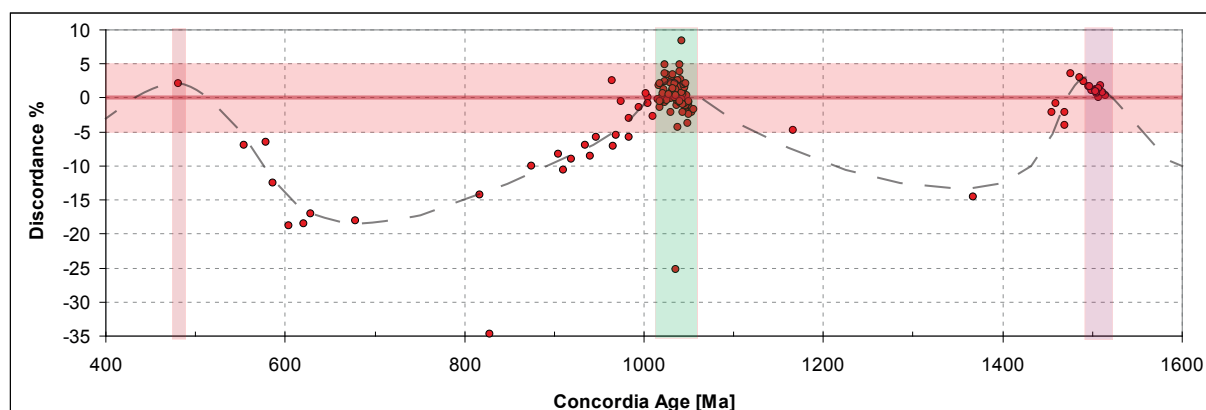


Fig. 63. Discordance of U-Pb zircon ages plotted against concordia age. Negative values correspond to normal discordance. The discordance shows a cyclic pattern with three concordant peaks that correspond to the Gothian-Telemarkian, Sveconorwegian and Caledonian orogenic periods, respectively. The cycles in this geochronological dataset represent as such two entire supercontinent-cycles.

Correlating the Øygarden Complex with Baltican Basement

So far, no U-Pb zircon ages have been published from the Øygarden Complex (Fig. 10). Most authors refer to the Øygarden Complex as parautochthonous Baltican basement (e.g. Larsen et al., 2003) but also an allochthonous tectonostratigraphic position has been discussed (e.g. Bering, 1984, Fossen and Rykkelid, 1990 and Fossen, 1988b). The magmatic formation of the Lyderhorn Gneiss corresponds exactly with the Gothian-Telemarkian and Sveconorwegian orogenic episodes, the two most important phases of crustal formation in the Baltican basement (Fig. 64; compare with Fig. 2; Roberts and Slagstad, 2015). This correspondence assigns the Øygarden Complex clearly to the Telemarkian domain of the Baltican basement and makes an allochthonous tectonostratigraphic position improbable.

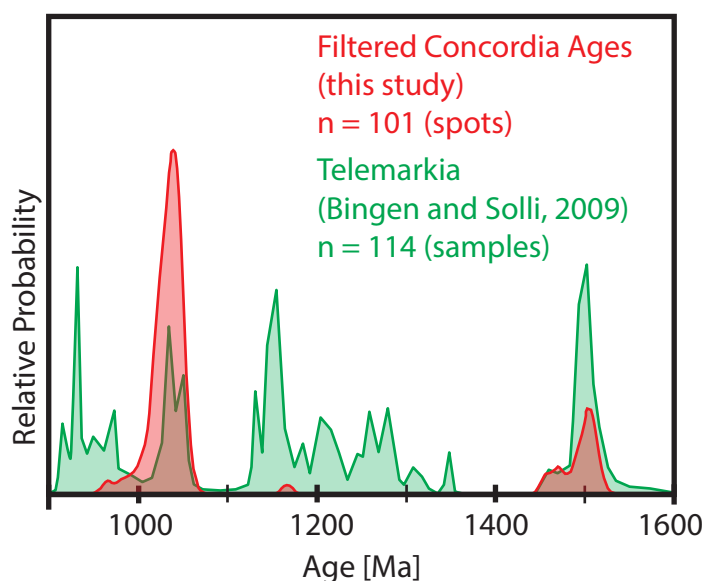


Fig. 64. Comparison of 5% discordance-filtered concordia ages from this study (red) with the probability of magmatic ages in the Telemarkia domain of the Baltican basement (green; modified from Bingen and Solli (2009), their Fig. 4). The number of ages from this study corresponds to individual spots while it represents entire samples for the published data.

Implications of 1040 - 1020 Ma Magmatism for Sveconorwegian Orogeny

Six out of seven igneous protoliths of the Lyderhorn Gneiss formed in the Sveconorwegian orogenic period. Sveconorwegian magmatism in the Lyderhorn Gneiss occurred in two distinct magmatic phases: Gabbro and hornblende biotite granite magmatism at 1041 Ma was succeeded by leucocratic granite magmatism between 1026 - 1022 Ma. The timing of Sveconorwegian magmatism in the Lyderhorn Gneiss shows a strong overlap with the Sirdal Magmatic Belt (SMB) in southern Norway (Fig. 65A). The ages of voluminous SMB granitoids form two clusters at 1050 and 1030 Ma (Coint et al., 2015). They resemble the ages of the two distinct magmatic phases that were found in the Lyderhorn Gneiss. Diffuse textural variations in leucogranites and xenolith-rich zones are some of the lithological similarities between granites in the eastern part of the Øygarden Complex and the SMB (Coint et al., 2015). Highly radiogenic granites and the strong Caledonian overprint are found in the Øygarden Complex but are absent in

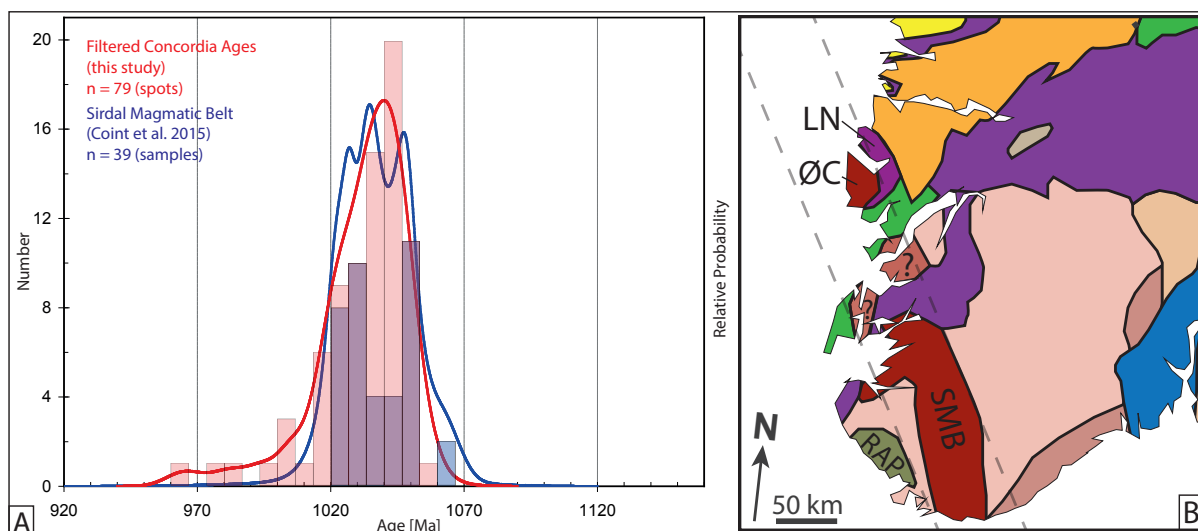


Fig. 65. A: Comparison of Sveconorwegian magmatic ages from the Lyderhorn Gneiss and the Sirdal Magmatic Belt (SMB; Coint et al., 2015, their Table 1). The number of ages from this study corresponds to individual spots while it represents entire samples for the published data. B: Simplified geological map of SW Norway showing the Øygarden Complex (ØC) as a possible northern continuation of the Sirdal Magmatic Belt (SMB). See Fig. 3 for legend. Basement areas in Sunnhordland with that are marked by question marks, might link the two areas. A NNW-trend of the SMB (shown as dashed line) is in agreement with the general strike of Sveconorwegian domain boundaries in southern Norway. It would support the correlation of anorthosite complexes in the Caledonian, eastwards-thrust Lindås Nappe (LN) and the Rogaland Anorthosite Province (RAP) as proposed by Bingen et al. (2001).

the SMB. Coint et al. (2015) described only granitic SMB-age magmatism but unpublished data prove contemporaneous gabbroic magmatism in southern Norway (T. Slagstad, personal communication). The map in Fig. 65B shows the geographic relationship of Øygarden Complex and SMB. Based on the similarity of ages and lithologies as well as the geographic relationship, it is tempting to correlate the Øygarden Complex with the SMB. Such a correlation is in agreement with the general orientation of Sveconorwegian domain boundaries in southern Norway that have a NNW-SSE-strike (Fig. 3; Bingen et al., 2008b). Several basement domains in Sunnhordland, with lithologies similar to the Øygarden Complex (e.g. Rosendal area), could link the two areas. Future geochronological studies will have to show whether or not the Øygarden Complex represents a direct northern continuation of the SMB.

Contemporaneous gabbroic and granitic magmatism at 1041 Ma has vague implications for the nature of the Sveconorwegian Orogen. The dated hornblende biotite granite corresponds in lithology and age to the Feda augen gneiss suite in southern Telemarkia that Bingen and Van Breemen (1998) interpreted to have formed in a subduction-setting. In an alternative model, Bingen et al. (2008b) explained the Feda Suite magmatism by crustal thickening. Slagstad et al. (2013) proposed another reinterpretation of the Feda suite and see it as a constituent of the SMB that was formed by arc-magmatism. The lack of geochemical data allows no clear geodynamical interpretation of the dated lithologies in the Lyderhorn Gneiss. However, identical ages of gabbroic and granitic magmatism are better explained by a subduction setting at 1041 Ma than by crustal thickening due to continent-continent collision. Only geochemical analyses can show, whether distinct leucogranitic magmatism in the Lyderhorn Gneiss at 1026 - 1022 Ma is more consistent with syn-collisional magmatism (Bingen et al., 2008b) or a continued

accretionary setting (Slagstad et al., 2013).

Did the Lyderhorn Gneiss Experience Sveconorwegian Metamorphism?

The entire deformation of the Lyderhorn Gneiss is identified to be of Caledonian age (see discussion below). A small number more or less concordant analyses (Fig. 65A) falls in the time period after 1020 Ma in which widespread Sveconorwegian high-grade metamorphism is proposed (Bingen et al., 2008b). Younger ages in the Lyderhorn Gneiss correlate systematically with high U and metamictization and should therefore not be interpreted as a distinct phase of zircon crystallization. The time period between igneous crystallization and proposed metamorphism is furthermore too short for enough metamictization to accumulate that thermal resetting due to diffusional Pb-loss could have played an important role at this time (Cherniak and Watson, 2003). Undisturbed magmatic samples from Lyderhorn (e.g. LYD-197-1 and LYD-44-1) and 'wet', unaltered gabbroic as well as granitic rocks in the surrounding area contradict furthermore the occurrence of widespread Sveconorwegian high-T metamorphism after 1020 Ma in the Øygarden Complex. This result is in agreement with the findings in the SMB that have led to the proposal of a non-collisional, accretionary Sveconorwegian Orogen (Slagstad et al., 2013).

Pre-Caledonian Architecture of the Baltican Basement

The pre-Caledonian structure of the Baltican basement is of great importance for the understanding of Caledonian continental subduction and exhumation. Sveconorwegian granulite facies metamorphism is a common assumption made for the entire Baltican basement to explain the extraordinary strength of the WGR during sustained Caledonian UHP metamorphism (e.g. Butler et al., 2015). Yet, recent work in the basement of southern Norway (Slagstad et al., 2013, Coint et al., 2015) and this study show, that this general assumption might be wrong. Widespread Sveconorwegian high-grade metamorphism that is held responsible for an entirely dry Baltican crust is in fact absent in large parts of the basement of southern Norway.

Based on the geochronology of polymetamorphic Caledonian nappes, Roffeis et al. (2013) recently proposed the identification of an E-W-trending Sveconorwegian domain boundary that separates the Telemarkian domain in southern Norway from the Gothian domain in the WGR. The orientation of this proposed domain boundary deviates considerably from the general NNW-SSE strike in the Sveconorwegian province as well as the NW-trending limit of Sveconorwegian overprint in the WGR (Fig. 3: SF). The domain boundary Roffeis et al. (2013) propose in their Fig. 7 splits the Øygarden Complex in a northern Gothian and a southern Telemarkian half. This boundary is in conflict with the NNW-trending correlation of the Øygarden Complex and the SMB, proposed in Fig. 65B. Even if the currently available information does not clearly rule out any of the possible orientations, a NNW-trend is more consistent with the overall structure of the Sveconorwegian belt. A continuous NNW-trend of Sveconorwegian domain boundaries would further support the correlation of anorthosite complexes in the Lindås Nappe and the Rogaland Anorthosite Province as proposed by Bingen et al. (2001). Caledonian, SE-directed thrusting of the Lindås Nappe explains the inverted arrangement of Øygarden Complex and Lindås Nappe (Fig. 65B). Their original Sveconorwegian constellation could be analogous to Rogaland Anorthosite Province and SMB in southern Norway. A pre-Caledonian demarcation of

Øygarden Complex and WGR would furthermore define the northern branch of the Bergen Arc Shear Zone as a reactivated Sveconorwegian domain boundary.

Constraints from U-Pb Discordance on the Early Caledonian Thermal Evolution of the Øygarden Complex

Early Ordovician (483 ± 13 Ma) resetting of strongly metamict grains is the only sign the entire Caledonian Orogeny left in the zircon U-Pb system of the Lyderhorn Gneiss. This result is only at first sight surprising, because it actually reflects the characteristic behaviour of the U-Pb diffusion system in zircon: robustness to high temperatures and vulnerability to Pb-loss at low temperatures because of metamictization (Mezger and Krogstad, 1997).

The discordance of several samples in the Lyderhorn Gneiss can be explained by the following thermal evolution: U-rich zircons in Telemarkian granitic rocks accumulated radiation damage after their igneous formation at 1500 Ma. Sveconorwegian intrusion of voluminous gabbroic and granitic magmas caused minor diffusional Pb-loss. After its igneous formation, the Lyderhorn Gneiss must have resided over several hundred million years below the 'critical amorphization temperature' of ~ 360 °C (Cherniak and Watson, 2003). This allowed U-rich grains to accumulate severe metamictization. A rapid increase in temperature lead to partial or complete resetting of metamict grains at 483 ± 13 Ma. Above 360 °C radiation damage is healed, but recovery of strong metamict zircon is a slower process than Pb diffusion (Cherniak and Watson, 2003). The Øygarden Complex must have resided at elevated temperatures over a sustained period of time, so that all metamictization was annealed and further radiation damage prevented. The U-Pb system remained closed during penetrative Caledonian deformation of the Øygarden Complex with temperatures in excess of 600 °C (Boundy et al., 1996).

The 483 Ma lower intercept age falls in the poorly understood Early Caledonian phase. The timing of temperature increase in the Lyderhorn Gneiss is coincident with the Trondheim event (Roberts, 2003). The dominating tectonic regime of this period is controversially discussed: Andersen et al. (2012) proposed the formation of a hyperextended passive margin, while Slama and Pedersen (2015) argued for an active margin that signifies the onset of the Caledonian Orogeny. A temperature increase in the Baltican margin is compatible with both, extensional as well as convergent tectonic regimes. Sustained elevated temperatures in the Øygarden Complex, however, might be better explained by the onset of Caledonian convergence. Post-Caledonian processes did not further modify the U-Pb system in zircon.

6.2 Structure

6.2.1 Comparison of Structural Data with Selected Previous Studies

Mineral lineations in most parts of the Øygarden Complex have a gentle plunge towards ESE (Fossen and Rykkelid, 1990). Lineations in the Lyderhorn Gneiss deviate from this trend and plunge towards ENE (Fig. 66A). Structural mapping by Weiss (1977) has shown that the ENE-trend prevails in the entire Laksevåg Peninsula (Fig. 66B). This trend is oblique to the main NW-SE trend assumed for Scandian thrusting and extensional backmovement in SW Norway (Fig. 7A and references therein, but resembles what Braathen et al. (2000) described for the

central Norway basement window below the Kollstraumen detachment (Fig. 66C). The Lyderhorn Gneiss and the Kollstraumen detachment are located far apart but have many similarities in structural style (compare Fig. 38 from this work and Fig. 2 from Braathen et al., 2000). Both are dominated by constrictional strain forming ENE-trending L-S to L-tectonites with top-to-ENE sense of shear. The north-eastern footwall of the Bergen Arc Shear Zone is part of the southern WGR. Lineations in the footwall of the concave W-dipping detachment shear zone trend exactly E-W (Fig. 66D). Further inland to the NE, the trend of lineations rotates towards NE-SW (Fig. 7A).

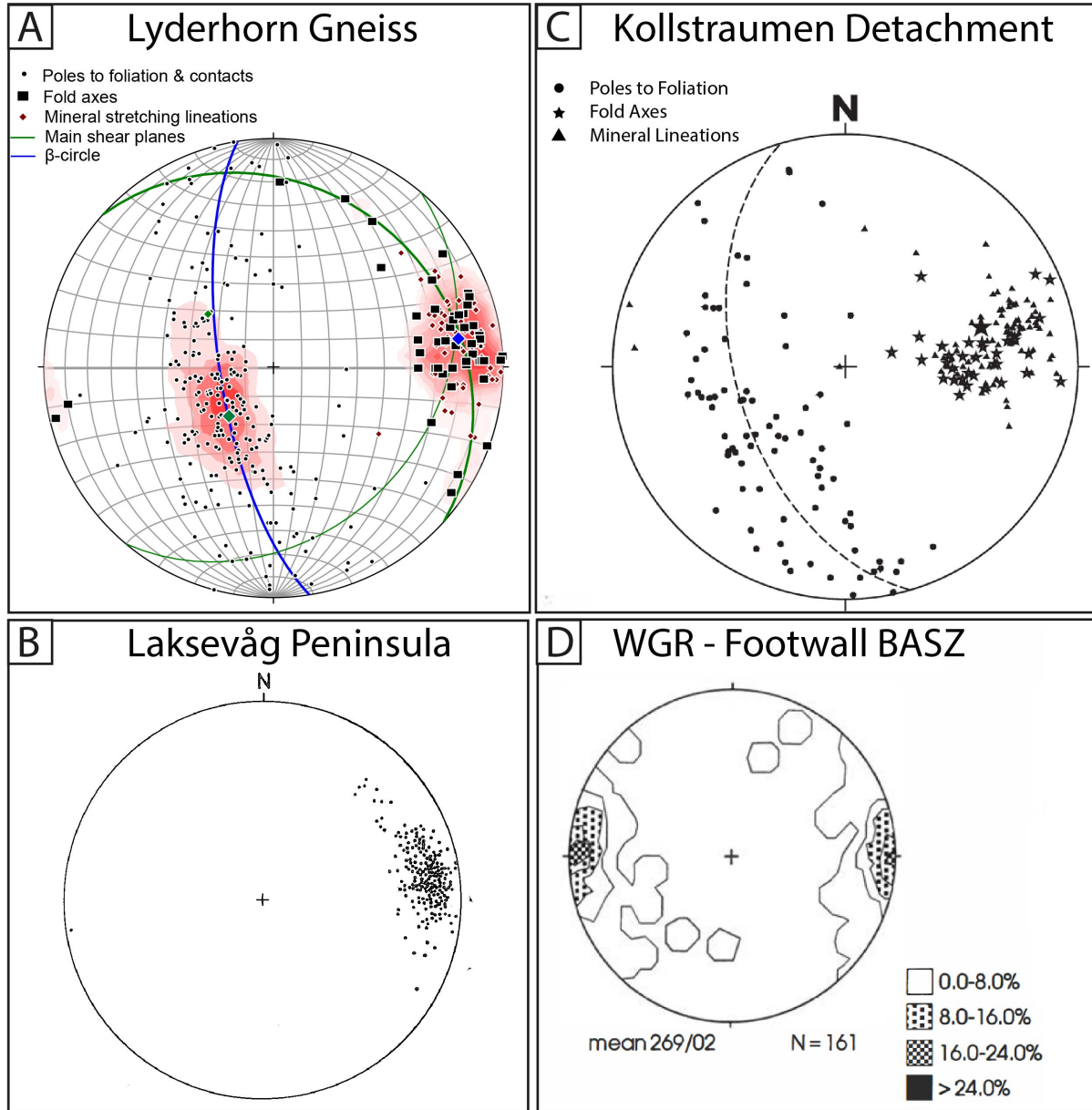


Fig. 66. Comparison of structural data from this study (A) with previously published studies: B: Stereoplot of lineations on the Laksevåg peninsula. Modified from Weiss (1977). C: Stereoplot of structural data from the Kollstraumen detachment. Modified from Braathen et al. (2000). D: Contour stereoplot of stretching lineations from the WGR in the footwall of the northern BASZ. Modified from Wennberg et al. (1998).

6.2.2 Structure of the Lyderhorn Gneiss in the Caledonian Orogeny

Age of Deformation in the Lyderhorn Gneiss

During the Scandian phase of the Caledonian Orogeny (430 - 405 Ma) the Øygarden Complex experienced at least upper amphibolite facies conditions (Fig. 67). In the Early Devonian, the Øygarden Complex cooled extremely rapidly (~ 30 °C/My) through lower amphibolite facies (408 - 404 Ma) and greenschist facies (401 Ma) before it reached the brittle-plastic transition at 396 Ma (see references in Fig. 67). This exhumational development is dated in the western part of the Øygarden Complex, but it corresponds exactly to the retrograde metamorphic evolution that is recorded in the Lyderhorn Gneiss: This study has found that the structure of the Lyderhorn Gneiss formed in one single, continuous deformation event. Phyllonites, formed at the brittle-plastic transition, have identical fabric orientations than amphibolite facies fabrics. Such hydrous, low-grade fault rocks cannot have experienced Scandian temperatures in excess of 600 °C (Boundy et al., 1996), implying that the deformation of the Lyderhorn Gneiss cannot be older than Scandian. If one further assumes, that the Øygarden Complex is a coherent unit, the thermal history of the Lyderhorn Gneiss must correspond to the evolution dated on Øygarden. This constrains the deformation of the Lyderhorn Gneiss to the Early Devonian.

Opposed Shear-Senses in the Øygarden Complex

The interpretation of Early Devonian deformation in the Lyderhorn Gneiss is complicated by the fact that mineral cooling ages from the western Øygarden Complex are associated with top-to-W kinematics (Fossen and Dunlap, 1998), while top-to-E shear-sense prevails in the Lyderhorn Gneiss.

Two opposed senses of shear are found within the stack of E-dipping gneissic tectonites in the Øygarden Complex and form two distinct domains (Fig. 68; compare with Fig. 9). The domains correlate vaguely with different lithologies and states of deformation: Top-to-E fabrics are commonly associated with augen gneisses and gneissic granites (Ragnhildstveit and Helliksen, 1997). The top-to-W domain consists mainly of migmatitic gneisses that were transformed into layered gneiss tectonites (Rykkeliid and Fossen, 1992). Top-to-E fabrics in the eastern part of the Øygarden Complex are hitherto seen to be contractional, formed during Scandian nappe emplacement in the Bergen Arc System (e.g. Fossen and Dunlap, 1998). Top-to-W fabrics in the lower part of the stack of layered tectonites are assigned to Devonian extension. The Lyderhorn Gneiss is located in the top-to-E domain but its structural record is incompatible with formation during Scandian contraction.

Structural Incompatibility of the Lyderhorn Gneiss with Scandian Thrusting

Extensional meso- and micro-shear bands in the Lyderhorn Gneiss indicate extensional top-to-E shear strain from amphibolite facies conditions down to the brittle-plastic transition (Fig. 26 and 35C). The strong overprint of shallowly E-dipping low-grade deformation with top-to-E kinematics on earlier formed fabrics is difficult to explain by Scandian thrusting.

Retrograde overprinting relationships, fault rocks and displacement classify the Loddefjord shear zone as a detachment (here termed Loddefjord Detachment Shear Zone). It shows striking

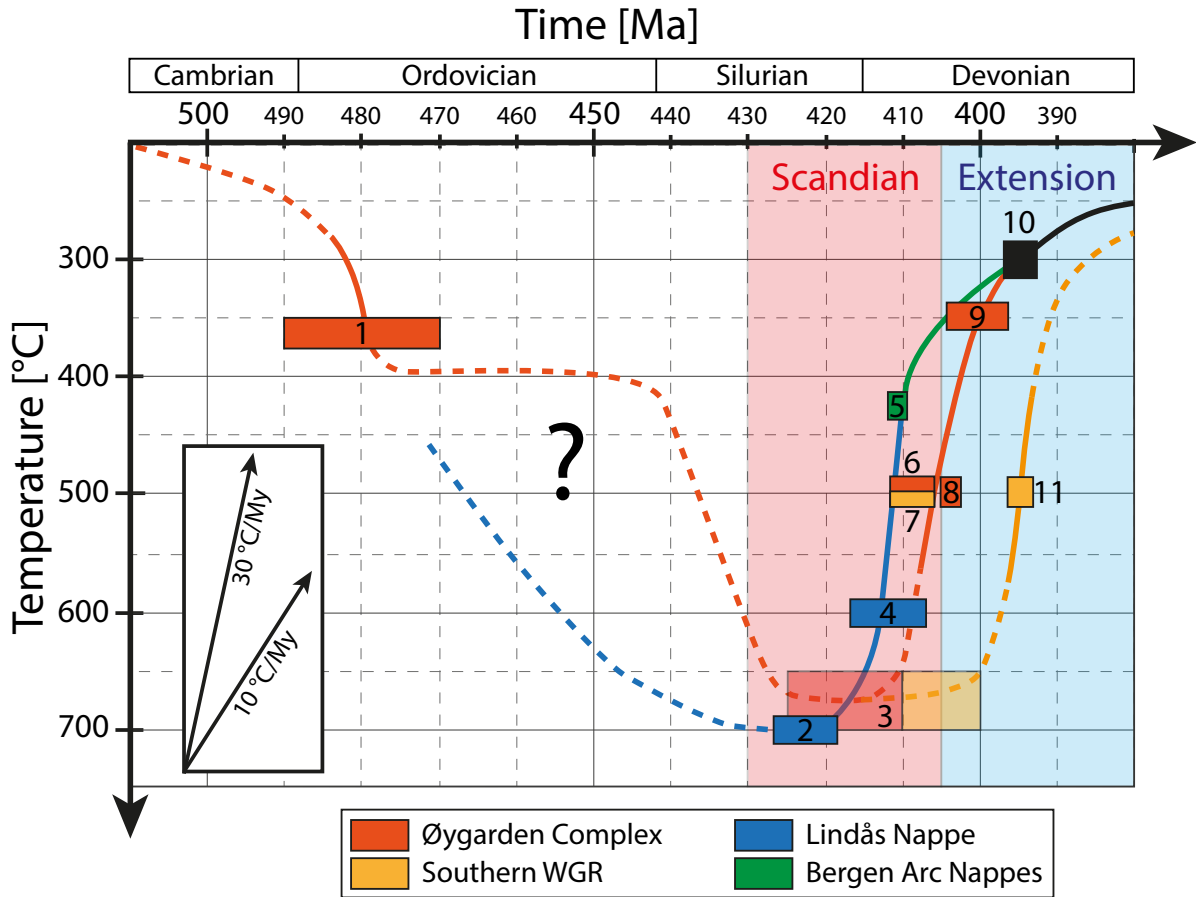


Fig. 67. Caledonian T-t paths for different units in the Bergen Arc System. Solid and dashed lines reflect well and poorly constrained paths, respectively. Representative cooling rates are indicated. Constraints sorted by age: 1 - U-Pb resetting of metamict zircon (483 ± 13 Ma; this study); 2 - U-Pb zircon eclogite (423 ± 4 Ma; Bingen et al., 2004); 3 - Hornblende-plagioclase thermobarometry (no age; Boundy et al., 1996); 4 - Rb-Sr Amphibolite (409 ± 8 Ma; Bingen et al., 2001); 5 - Ar-Ar muscovite (411 ± 2 Ma; Fossen and Dunlap, 1998; ~ 410 Ma; Fossen and Dunlap, 2006); 6 - Ar-Ar hornblende (408 ± 3 Ma; Boundy et al., 1996); 7 - Ar-Ar hornblende (409 ± 3 Ma; Boundy et al., 1996); 8 - Ar-Ar hornblende (404 ± 1 Ma; Fossen and Dunlap, 1998); 9 - Ar-Ar biotite (401 ± 5 Ma; Boundy et al., 1996); 10 - U-Pb sphene (~ 396 Ma; Larsen et al., 2003); 11 - Ar-Ar hornblende (395 ± 2 Ma; Boundy et al., 1996). Controversial white mica Ar-Ar ages in the Lindås Nappe (433 - 430 Ma; Boundy et al., 1996; Fossen and Dunlap, 1998) that pre-date the timing of eclogite formation are not shown. Temperature estimates of different methods: U-Pb sphene: ~ 300 °C (Larsen et al., 2003); Ar-Ar biotite: ~ 350 °C (Fossen and Dunlap, 1998); U-Pb zircon resetting: ~ 360 °C (Cherniak and Watson, 2003); Ar-Ar muscovite: ~ 425 °C (Harrison et al., 2009); Ar-Ar hornblende: ~ 500 °C (Boundy et al., 1996); Rb-Sr amphibolite: ~ 600 °C (Bingen et al., 2001); U-Pb zircon eclogite: ~ 700 °C (Bingen et al., 2004);

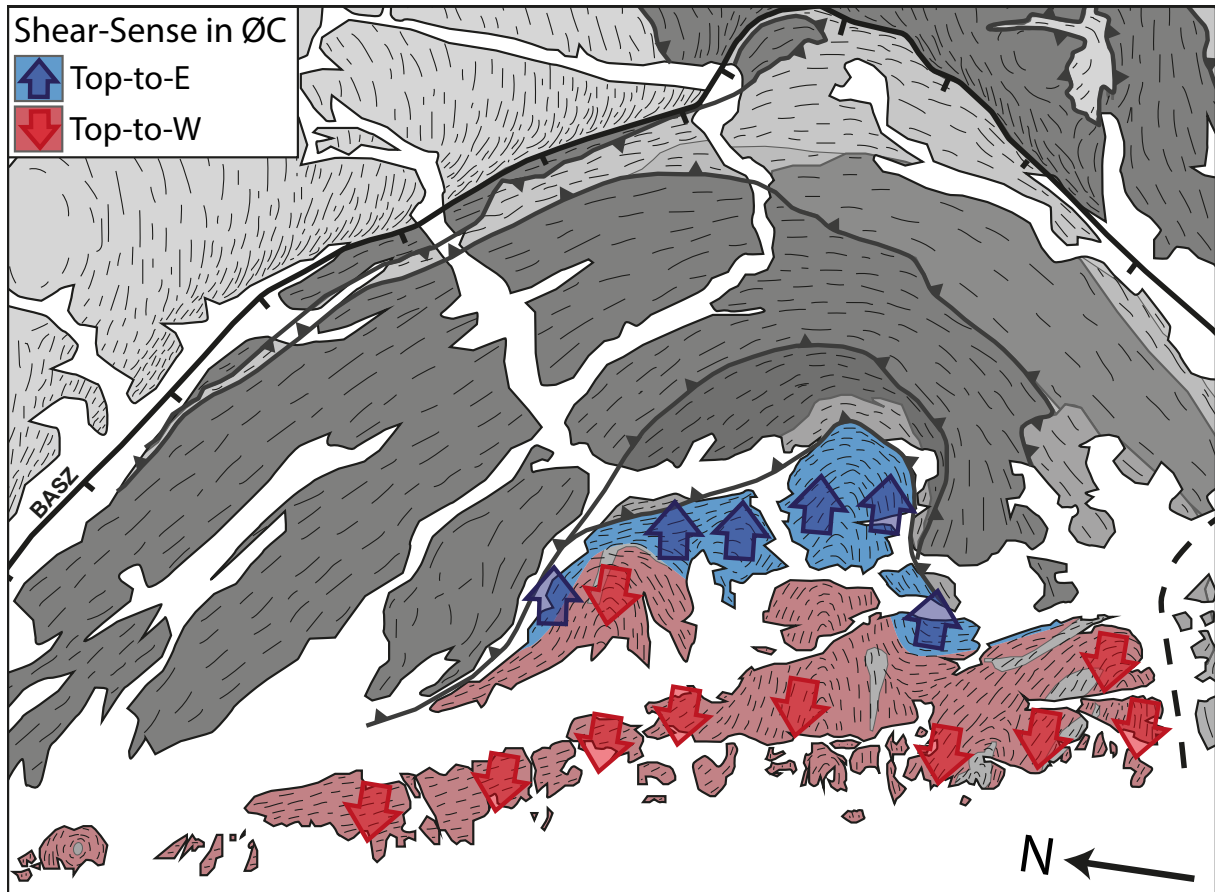


Fig. 68. Two opposed senses of shear coexist in the stack of E-dipping gneiss tectonites that form the Øygarden Complex. Blue arrows indicate top-to-E and red arrows top-to-W kinematics. Modified from Fossen and Rykkelid (1990). The shown demarcation of two kinematic domains within the Øygarden Complex correlates with distinct lithologies and deformation states (Ragnhildstveit and Helliksen, 1997).

similarities in fault rock development with other structures in the Devonian detachment system. Braathen et al. (2004) highlighted the low shear strength of phyllonites, as they are found in the Loddefjord Detachment Shear Zone. The current tectonic model assumes that Scandian top-to-E fabrics are preserved in the eastern part of the Øygarden Complex (e.g. Larsen et al., 2003). Scandian fabrics in the western part of the Øygarden Complex on the other hand, are assumed to be overprinted by Devonian top-to-W deformation. If one assumes that phyllonites with top-to-E sense of shear in the Lyderhorn Gneiss would have formed during Scandian thrusting, they should have inevitably become overprinted by Devonian extensional deformation because of their weak rheology. They bear, however, no sign of a top-to-W overprint.

Another contradiction is found in the sequence of structural events recorded in the Lyderhorn Gneiss: Penetrative top-to-E shearing is synchronous with folding along E-W-trending fold axes. Discrete, E-dipping detachment shear zones cut fold structures. This observed structural sequence reverses the currently valid tectonic model, where open folding along E-W trending fold axes is interpreted to post-date ductile top-to-W shearing, reflecting Devonian crustal extension (Larsen et al., 2003). Within the Lyderhorn Gneiss, the intensity of ductile top-to-E shearing increases from top to bottom and north to south. That means, strain increases away from the Basal Caledonian Thrust (Larsen et al., 2003) and argues against formation of the Lyderhorn Gneiss during Scandian thrusting.

Cooling Ages and Fault Geometries in the Bergen Arc System

Published Ar-Ar cooling ages in the Bergen Arc System show a distinct distribution (Fig. 69). All dated ages in the nappes are older than 410 Ma. Cooling ages in the footwall of the Bergen Arc Shear Zone (WGR and Bergsdalen Nappe) are younger than 410 Ma. This offset is explained by the Bergen Arc Shear Zone, a Devonian detachment. Cooling ages in the Øygarden Complex are identical to the WGR, i.e. also younger than 410 Ma. The current tectonic model interprets the contact between Øygarden Complex and Minor Bergen Arc as the Basal Caledonian Thrust (e.g. Larsen et al., 2003). If the Øygarden Complex would have been finally juxtaposed with the nappes in the Bergen Arc System by Scandian thrusting, both units should show identical post-Scandian cooling histories. Fossen and Dunlap (2006) dated the change from Scandian contraction to extension in the Bergen area to 405 Ma. At this time, published mineral ages show still separated cooling paths for the nappes and the Øygarden Complex (Fig. 67). Hence, the distribution of cooling ages implies a Devonian exhumational structure to juxtapose Øygarden Complex and Minor Bergen Arc.

The Basal Caledonian Thrust dips with 30 - 40° to the east and has top-to-E kinematics (Fig. 9). Thus, its present geometry and displacement define the structure as a normal fault. The Loddefjord Detachment Shear Zone is parallel to the Basal Caledonian Thrust and its continued northern branch on Askøy links the two structures. It seems therefore likely, that both structures were active at the same time and that the 'basal Caledonian thrust' was reactivated as a detachment (here termed the Bergen Detachment Shear Zone; Fig. 69). This reinterpretation would explain the observed fault geometries as well as the distribution of cooling ages in the Bergen Arc System.

Fossen (1989) described E-dipping low-angle shear zones in the Minor Bergen Arc with

'flinty ultramylonitic mica schists' that cut earlier mylonitic fabrics. The description resembles detachments in the Lyderhorn Gneiss and could be expression of corresponding E-directed detachment faulting in the Minor Bergen Arc. The distinction, if earlier formed fabrics are in fact Scandian or related to Devonian extensional deformation is probably impossible, because of identical shear sense in both phases. It should however be noted that top-to-W overprint, as it is typical for the reactivated basal décollement zone (Fossen, 2000), is absent and that the tectonostratigraphy in the Bergen Arc System is reversed.

At first glance, it seems surprising that shallowly E-dipping semi-brittle deformation apparently localized in the strong basement and not in the weak nappes. Yet, this observation is in accordance with Devonian E-directed detachment faulting, exhuming relatively warm basement that is weakened by fluids. A further extensional structure could separate the Fenns fjorden Devonian Basin from the nappes and/or the Øygarden Complex, because the latter resided at the beginning of the Middle Devonian still at the brittle-plastic transition (Fig. 67).

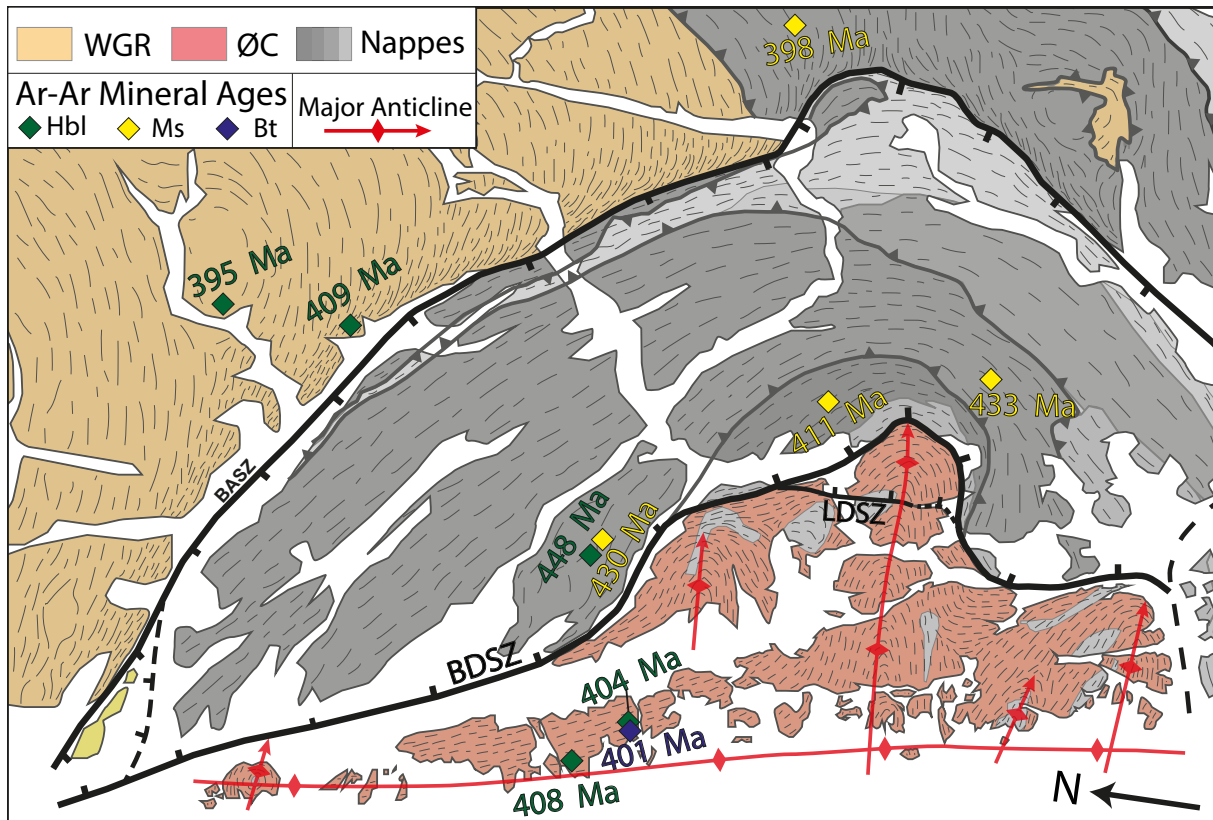


Fig. 69. Simplified map showing the distribution of previously published Ar-Ar cooling ages in the Bergen Arc System (Boundy et al., 1996; Fossen and Dunlap, 1998; Fossen and Dunlap, 2006). Based on the identification of the Loddefjord Detachment Shear Zone (LDSZ), the contact between Øygarden Complex and Minor Bergen Arc is reinterpreted as a Devonian detachment that is termed in the text Bergen Detachment Shear Zone (BDSZ). See text for discussion. This reinterpretations explains the age difference cooling ages in the Scandian nappes (grey) and the Øygarden Complex (bright red) as well as identical ages in the Øygarden Complex and the WGR (bright orange). Further shown are hinge lines of large scale anticlines in the the Øygarden Complex modified from Larsen (1996) and Larsen et al. (2003). The perpendicular anticlines formed simultaneously in the Early Devonian. They intersect on the island Fedje, defining the Fedje Dome (Larsen, 1996).

Fold Geometries in the Øygarden Complex

The ductile structure of the Øygarden Complex is defined by two perpendicular sets of fold axes (Fig. 69). The layered gneiss tectonites in the Øygarden Complex are intensely folded into upright, E-plunging folds. The structural analysis of the Lyderhorn Gneiss revealed numerous E-plunging recumbent folds on the northern limb of an upright megafold. This special fold geometry is either described as Christmas-tree folds, related to vertical shortening of a preexisting upright antiform (Fossen, 2010b) or cascading folds a characteristic feature of gneiss domes (Whitney et al., 2004).

Upright, E-W trending folds are a governing element in the structure of the Devonian extensional system (e.g. Chauvet and Séranne, 1994). In the Nordfjord-Sogn detachment zone these folds formed in a transtensional regime (Fossen et al., 2013) contemporary with the deposition of Devonian sediments e.g. (Fossen et al., 2016). Based on the correlation of Bergen Arc Shear Zone and Nordfjord-Sogn detachment zone (Wennberg et al., 1998), E-plunging upright folds in the Øygarden Complex should be of identical age. Early Devonian folding is also in accordance with the thermal evolution of the Øygarden Complex. This study has shown that E-plunging recumbent folds in the Lyderhorn Gneiss developed together with amphibolite and greenschist facies fabrics and are thereby constrained to the Early Devonian (compare Fig. 67). Thus, recumbent meso- and macrofolds in the Lyderhorn Gneiss formed at the same time as upright megafolds in the Øygarden Complex. Thus, their geometry is best explained as cascading folds.

Fabrics in the entire Øygarden Complex and large parts of the Bergen Arc dip to the east, reflecting the eastern limb of the N-S-trending Sotra-Fedje culmination. Larsen et al. (2003) constrained folding along N-S axes to be post-Scandian. As the Øygarden Complex reached the brittle-plastic transition by the beginning of the Middle Devonian, they must be Early Devonian, thus contemporaneous with E-W-trending folds. The perpendicular anticlines intersect on the island Fedje, where they define the Fedje Dome (Larsen, 1996; Fig. 69). Perpendicular, contemporaneous folding define the exposed part of the Øygarden Complex as a half-dome. In the westernmost part of the Øygarden Complex the foliation is close to horizontal but further west it dips to the W (Fossen, 1998). Together with the part that is today below sea level, the general ductile structure of the Øygarden Complex defines a dome. Following the example of the Fedje Dome, E-plunging anticlines in the the Øygarden Complex could be regarded as the eastern parts of E-W elongated subdomes, as they are typical for larger gneiss dome systems (Yin, 2004).

Bidirectional Devonian Extension in the Øygarden Complex

To summarize the previous discussion, Fig. 70 illustrates schematically three tectonic models that are tested to explain opposed shear-senses in the Øygarden Complex, published mineral cooling ages, the structural sequence of the Lyderhorn Gneiss and other features of the Bergen Arc System.

At an earlier stage, some researchers proposed that top-to-W fabrics reflect an early Caledonian event that later became overprinted by Scandian thrusting ((Fig. 70): Model A; Bering, 1984; Fossen and Rykkelid, 1990). Mineral cooling ages have shown that top-to-W fabrics in the western Øygarden Complex formed during Devonian crustal extension (Fossen and Dunlap, 1998)

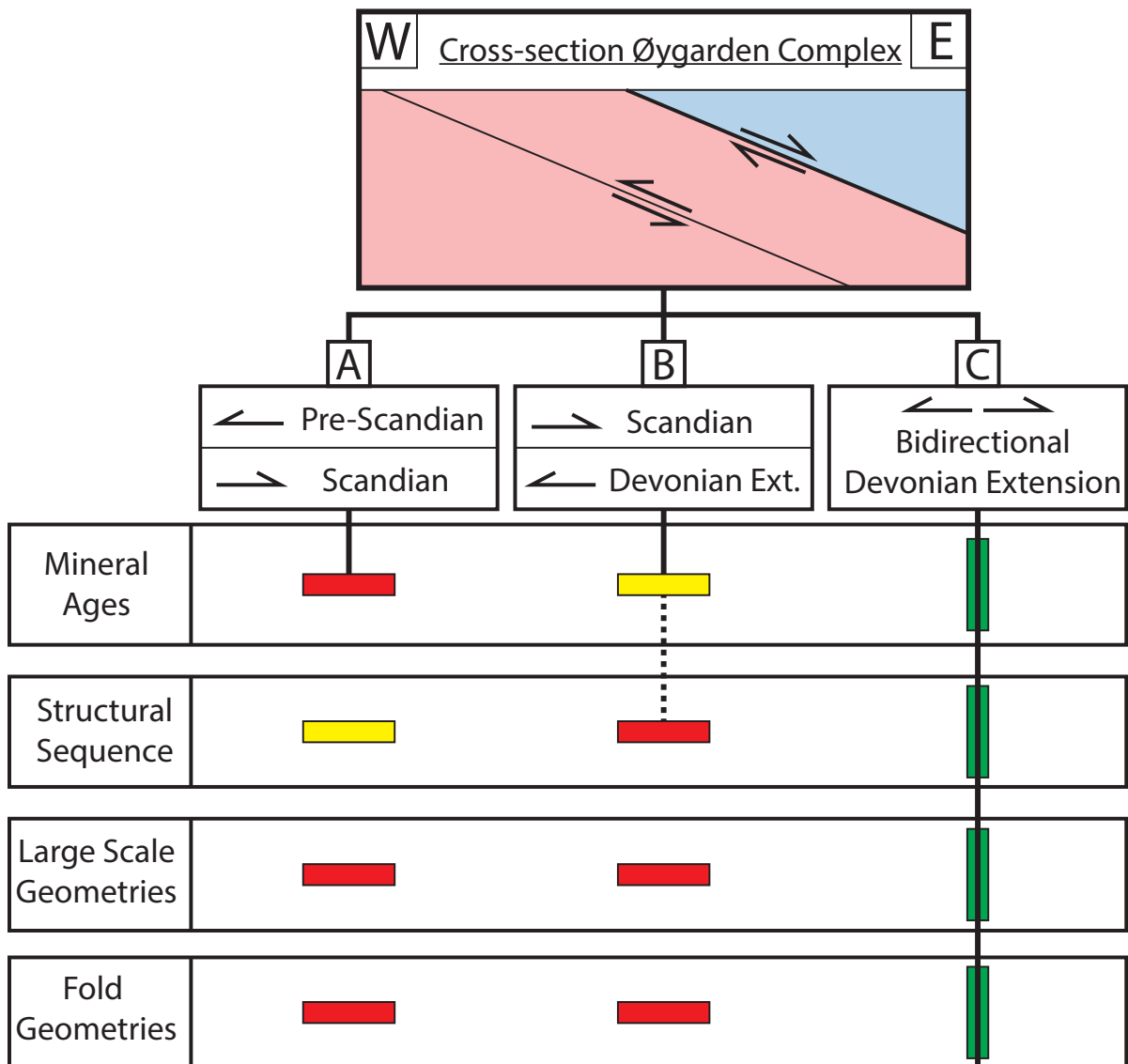


Fig. 70. Schematic flow chart to compare different tectonic models. The upper sketch shows a strongly simplified E-W cross-section of E-dipping tectonites in the Øygarden Complex. In the eastern part prevails top-to-E shear-sense (blue) and in the western part top-to-W (red; compare with Fig. 68). Three models are tested to explain opposed shear sense in agreement with mineral ages (compare Fig. 67 and 69), the structural sequence of the Lyderhorn Gneiss and other structural features of the Bergen Arc System. Model A is based on Fossen and Rykkeliid (1990) and interprets top-to-W fabrics as pre-Scandian and top-to-E fabrics as Scandian. Model B is the established tectonic model based on Rykkeliid and Fossen (1992) and Larsen et al. (2003). Scandian top-to-E fabrics are overprinted by Devonian extension (top-to-W). I propose a new model (C) that explains opposed shear-senses by bidirectional Devonian extension. Rectangles in the flow chart illustrate the consistence of tested models with observed structural features. Different colors and orientations imply: Red - inconsistent; yellow - limited consistence; green - consistent. Only bidirectional Devonian extension explains consistently all tested features. See text for discussion.

and Model A can therefore be ruled out.

The established tectonic model of the Bergen Area assumes that top-to-E fabrics in the eastern part of the Øygarden Complex formed during Scandian thrusting (Fig. 70: model B). This model is contradicted by the structural record of the Lyderhorn Gneiss. Neither large scale fault and fold geometries nor the distribution of cooling ages in the Bergen Arc System are consistently explained by model B.

The thermal history of the Øygarden Complex constrains the structural evolution of the Lyderhorn Gneiss to the Early Devonian. Fabrics, structures and the metamorphic development in the Lyderhorn Gneiss imply exhumation by extensional deformation. As the structure of the Lyderhorn Gneiss formed in a single deformation event, it must have entirely formed during Devonian extension. Previous studies have shown that the western part of the Øygarden Complex experienced contemporaneous top-to-W deformation (Boundy et al., 1996; Fossen and Dunlap, 1998). Hence, Devonian extension in the Øygarden Complex was bidirectional.

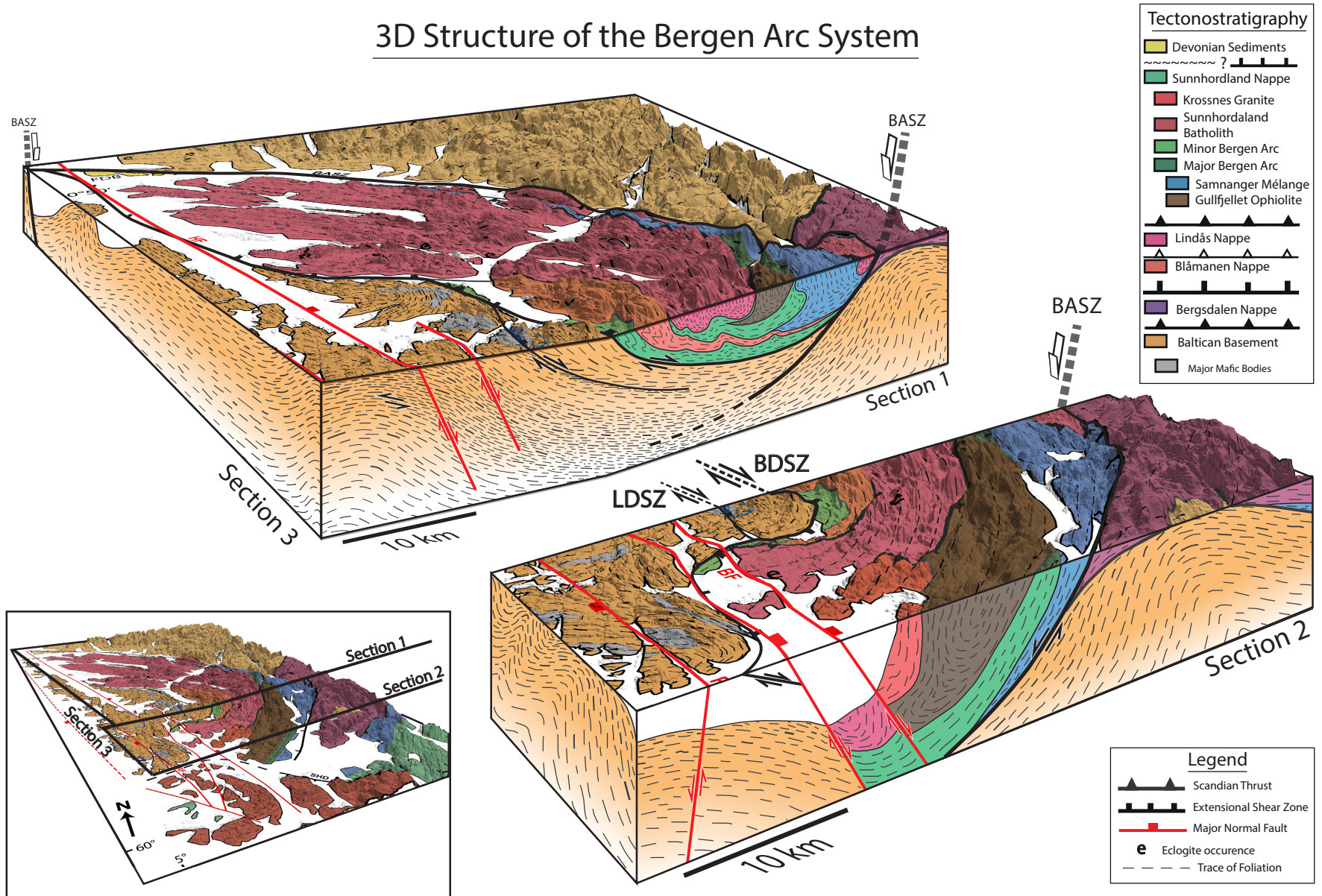
6.2.3 Reinterpretation of the Øygarden Complex as a Devonian Extensional Gneiss Dome

Based on the previous discussion, I suggest that the Øygarden Complex could be reinterpreted as a Devonian extensional gneiss dome. Bidirectional Devonian extension in the Øygarden Complex can be explained by a symmetrical core complex style of exhumation, with many similarities to the Central Norway basement window (Braathen et al., 2000).

The schematic block diagram in Fig. 71 illustrates the main features of this newly proposed model: Opposed senses of shear within the Øygarden Complex can be explained by lateral inward flow of hot and viscous crust, below a more rigid crust that is extended by detachment faulting (compare Fig. 71 and 72). Fossen et al. (2016) described low-angle Devonian fabrics that could represent a shallowly W-dipping detachment. Yet, it can only be speculated whether the Øygarden Complex is bound by a Devonian detachment shear zone only to the E, or also to the W. Fossen et al. (2014) presented evidence for viscous flow of lower crust in this part of the Caledonides during the Devonian. A pending question is whether temperatures were high enough for partial melting to occur. The age of migmatization in the Øygarden Complex is so far not constrained by U-Pb zircon geochronology.

Fig. 71. (Next page): This schematic block diagram of the Bergen Arc System reinterprets the Øygarden Complex as a Devonian extensional gneiss dome. The map in Figure 8 is rendered on a DEM (2.7 vertical exaggeration) and shown in perspective view from SSE. The 3D map is cut open along three section lines (see inlet): Section 1 corresponds to the cross section in Figure 9 (see references there). Section 2 is based on regional cross sections (Ragnhildstveit and Helliksen, 1997, Fossen and Rykkelid, 1992, Fossen, 1992, Færseth et al., 2011) and own interpretations. Section 3 is based on Larsen (1996) and interpretations of the observed foliation pattern and fold axes shown in Fig. 69. This model is based on the identification of the E-dipping Loddefjord Detachment Shear Zone (LDSZ) and the reinterpretation of the Bergen Detachment Shear Zone (BDSZ; compare with Fig. 69). In this proposed model, lateral inward flow of hot and viscous crust explains opposed shear-senses in the Øygarden Complex as shown in Fig. 68. Major normal faults are only shown schematically without precise geometries and offsets. Note the similarity of with idealized models of extensional gneiss domes (Fig. 72).

3D Structure of the Bergen Arc System



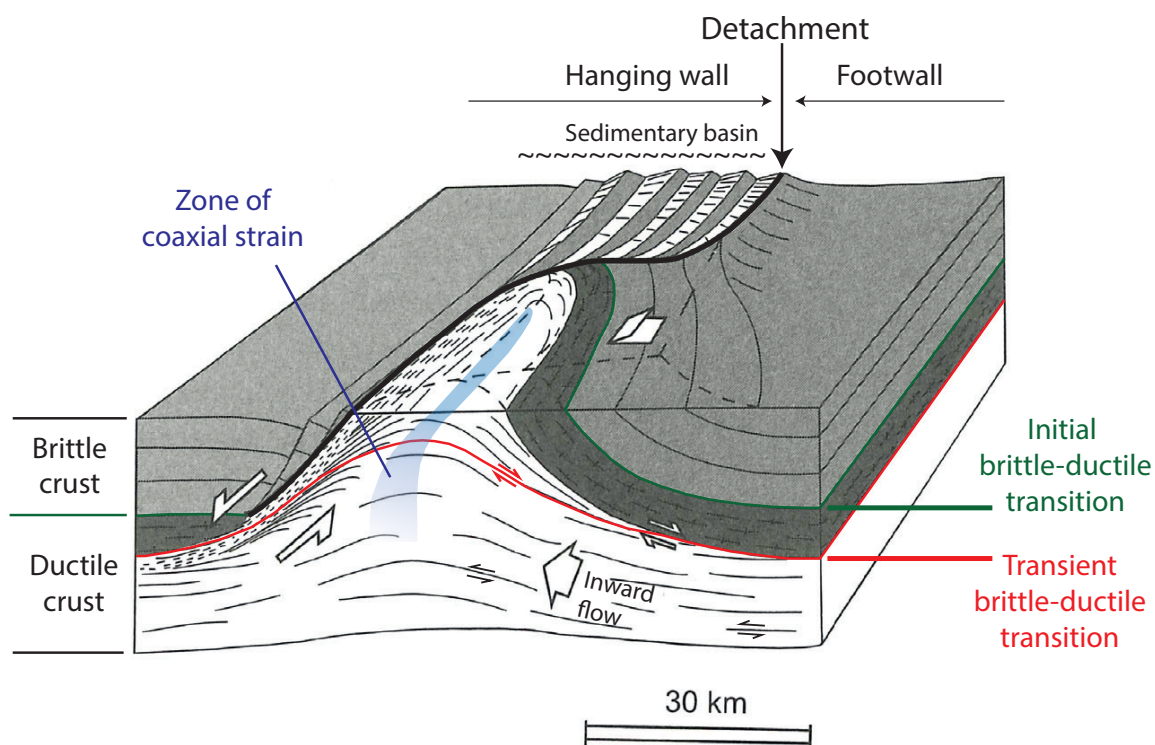


Fig. 72. Idealized block diagram of an extensional gneiss dome. Lateral inward flow of viscous crust causes opposed shear-senses and a zone of coaxial strain at the apex of the dome. Due to rapid cooling, the brittle-plastic transition migrates downwards and ductile fabrics become overprinted by (semi-)brittle deformation. Syntectonic sediments are deposited in hanging-wall basins. Modified from Tirel et al. (2004).

Tirel et al. (2004) have shown that extensional gneiss domes can form regardless of the presence of melt. A granitic density anomaly, contained within a thickened crust of quartz-dioritic composition, is enough to trigger dome formation at extension rates between 0.66 - 2 cm/yr. Numerous leucocratic granites mapped in this study could represent such a density anomaly (Rudlang, 2011). Their extreme radiogenic heat production (Schulze, 2014), could play a role in the model of extensional gneiss dome formation. The complex deformation of granitic bodies in the Lyderhorn Gneiss corresponds to the typical fold pattern found in gneiss domes (Tirel et al., 2004). They correspond to cascading folds that form due to vertical shortening during diapiric ascent (Whitney et al., 2004).

Fault rocks in the Loddefjord Detachment Shear Zone correspond to chloritic fault breccias that are typical of cordilleran core complexes (Van der Pluijm and Marshak, 2004). The downward migration of the transient brittle-plastic transition, due to rising of the dome (Fig. 72), is well exposed in the Lyderhorn Gneiss. It leads to the formation of strongly corrugated semi-brittle detachment fault surfaces, that are further typical features of extensional core complexes (Braathen et al., 2000).

Since the first identification of Devonian core-complexes in the Norwegian Caledonides by Norton (1986), this exhumation model was applied to several basement culminations in central Norway (e.g. Osmundsen et al., 2003). Osmundsen et al. (2005) classified two different types of extensional, gneiss-cored culminations (Fig. 73). Type 2 culminations resemble metamorphic core complexes and are defined by the following characteristics. All of them apply to the Øygarden

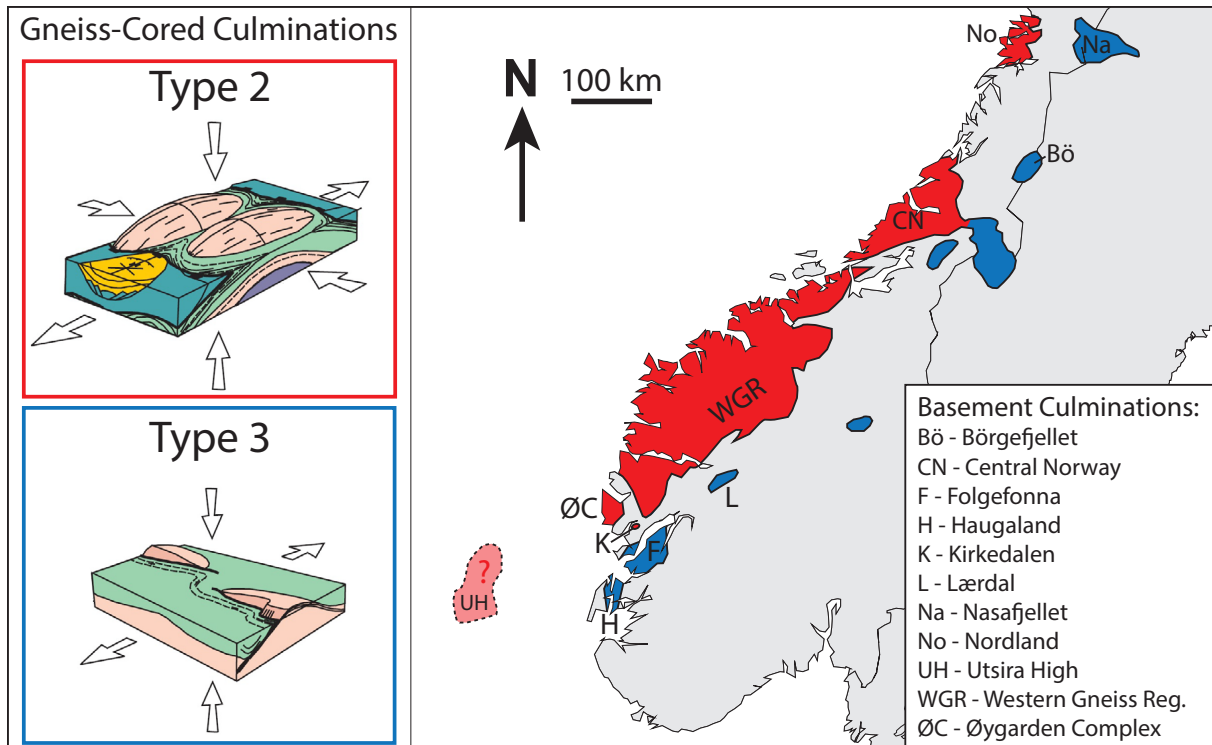


Fig. 73. Classification of Devonian, extensional gneiss-cored culminations along the Mid-Norwegian margin from Osmundsen et al. (2005) expanded onto SW Norway. The Øygarden Complex and the southern WGR qualify as type 2 culminations (red). Geometries of basement culminations in the footwall of the Hardangerfjord Shear Zone (compare with Fig. 74) resemble Type 3 culminations (blue). The offshore Utsira High could represent another Type 2 core complex.

Complex:

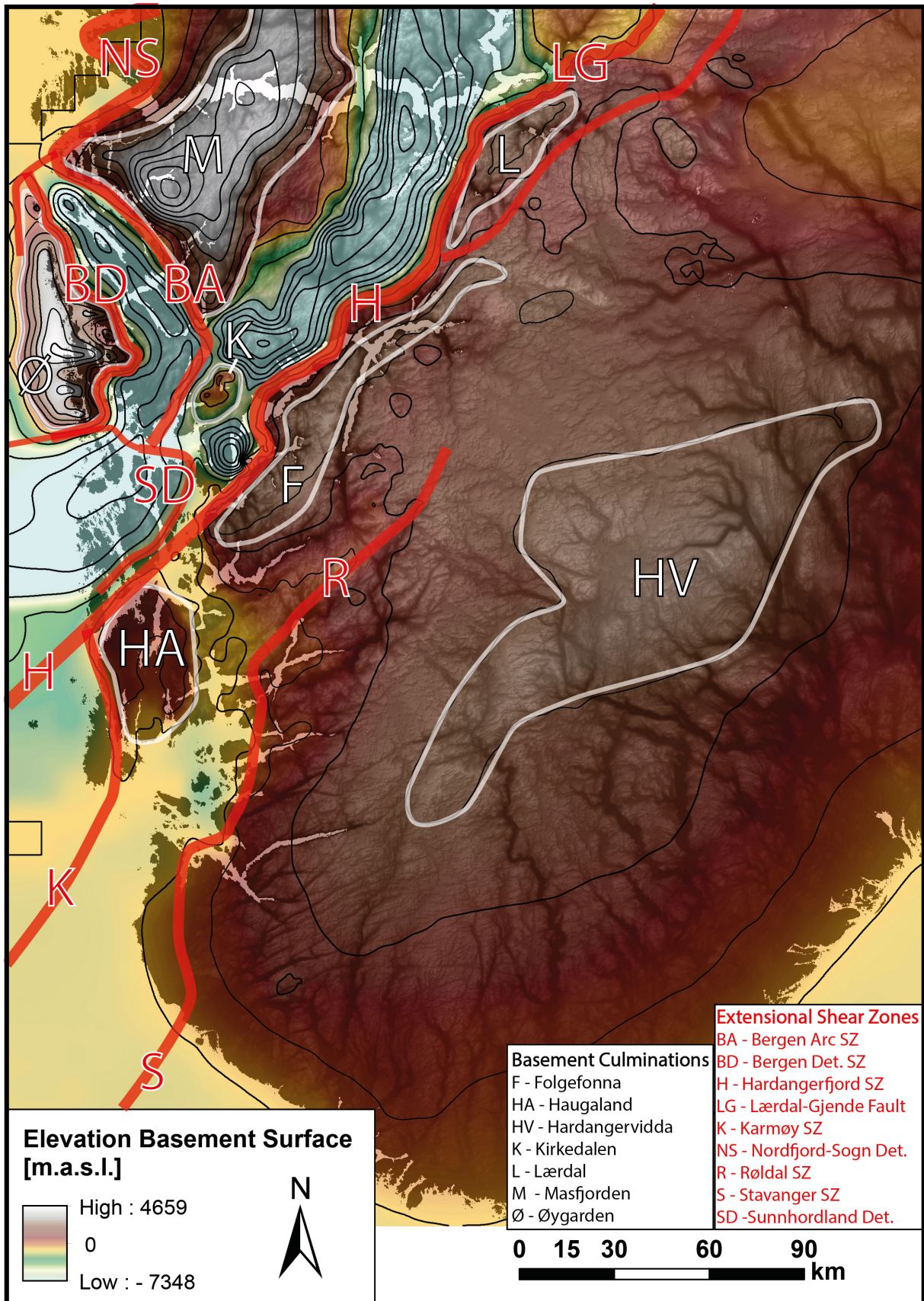
- flanked by extensional detachments
- capped by brittle detachments
- characterised by extension-parallel folds
- formed in constrictional strain field
- juxtaposed against Devonian sedimentary basin

Domal structures are abundant in the basement of SW Norway and show a spatial association with Devonian detachment shear zones (Fig. 74). The Kirkedalen Window is a dome-shaped basement window in the SE footwall of the Bergen Arc Shear Zone (BASZ). In the corresponding NE footwall, migmatitic gneisses define a domal foliation pattern around Masfjorden. Published hornblende Ar-Ar ages from the core of the domal structure (395 Ma) are 14 Myr younger than equivalent ages within the nearby BASZ (409 Ma; Fig. 69; Boundy et al., 1996). The age difference could reflect dome formation in the footwall of the BASZ during Devonian extension. Indirect evidence for the presence of partial melt is given by nearby Caledonian eclogites that were interpreted to be hosted by 'undeformed lenses of Precambrian granite' (Winsvold, 1996). This interpretation contradicts the modern understanding of eclogite formation (e.g. Austrheim et al., 1997) and the relationship might rather indicate that eclogite formation in the southern WGR was contemporaneous with partial melting, just like in other parts of the WGR (e.g. Gordon et al., 2013, Gordon et al., 2015).

Osmundsen et al. (2005) applied their classification of gneiss-cored culminations no further south than the central WGR. Here, I propose that the Øygarden Complex and probably also the southern WGR (south of Sognefjorden) could be classified as Devonian type 2 core complexes (Fig. 73). The geometry of basement culminations in the footwall of the Hardangerfjord Shear Zone, is furthermore recognised to be very similar to type 3 culminations (e.g. Folgefonna- and Lærdal-High Fig. 73 and 74). The two types of basement culminations define linear, orogen-parallel belts (Fig. 73) that correspond to the 'geanticlines' Ramberg (1981) defined in his Fig. 2. The linear array has implications for onshore-offshore correlations. Fossen et al. (2016) described an E-dipping Devonian detachment shear zone on the eastern flank of the Utsira High in the northern North Sea. The position of the Utsira High coincides with the linear belt of type 2 culminations onshore (Fig. 73). Core complex formation could be tested as a possible model to explain the Utsira High and the opposed polarity of the Utsira Shear Zone.

The proposed reinterpretation of the Øygarden Complex suggests a possible link between the exhumation of the Øygarden Complex and the syn-orogenic decoupling and exhumation of the Lindås Nappe (Jolivet et al., 2005). Fluid-induced mineral reactions and deformation played an important role in both of the units, even though, at very different metamorphic grades. The fabrics that define the shape of the Bergen Arc range from eclogite facies to the brittle-plastic condition. This might indicate that the Bergen Arc itself could be a product of prolonged exhumational crustal flow.

Fig. 74. (Next page): Map of the reconstructed post-Caledonian basement surface in SW Norway. The elevation of the interpolated surface is shown by transparent colors and contour lines, overlaying a DEM. Contour intervals are 1000 m below sea level and 500 m above sea level. The basement surface SE of the Hardangerfjord Shear Zone (HSZ), is directly based on Fossen and Hurich (2005), Fig. 8 and corresponds to the sub-Cambrian peneplain. The basement surface NW of the HSZ, is reconstructed from regional cross sections (e.g. Ragnhildstveit and Helliksen, 1997; Fossen and Rykkelid, 1992; Fossen, 1992) and corresponds to the contact between basement and Caledonian nappes. The elevation was reconstructed with the assumption that the Caledonian foliation approximates the orientation of the basement surface. Further shown are Devonian detachment shear zones (red), based on Fossen et al. (2016); Fossen and Hurich (2005) and the results of this study. Domal basement culminations (white outline) in the footwall of Devonian extensional shear zones have distinct shapes that correspond to the classification by Osmundsen et al. (2005) (Fig. 73). An abrupt change in surface curvature coincides with the Hardangerfjord Shear Zone (HSZ) that marks the transition from cold and rigid Baltican crust in the foreland, to relatively hot viscously flowing crust in the hinterland (Fossen et al., 2014). Note that the western part of the Øygarden Complex is poorly constrained and the northern edge of the map is perturbed by the spatial limit of the interpolation. See Appendix 9 for a 3D visualization.



7 Conclusion

Based on the findings of this study, I propose the following evolution of the Lyderhorn Gneiss and corresponding implications:

Evolution of the Lyderhorn Gneiss

- Telemarkian Orogeny
 - 1504 Ma: Granitic magmatism
- Sveconorwegian Orogeny
 - 1041 Ma: Gabbro and hornblende biotite granite magmatism.
 - 1026 - 1022 Ma: Intrusion of voluminous leucocratic granites with high radiogenic heat production.
 - No record of Sveconorwegian high-grade metamorphism and deformation.
- Neoproterozoic to Early Paleozoic: Residence at low temperatures accumulates severe metamictization of U-rich zircon.
- Caledonian Orogeny
 - 483 Ma: Resetting of strongly metamict zircons.
 - Ordovician (to Silurian?): Sustained elevated temperatures anneal radiation damage and prevent further Pb-loss.
 - Early Devonian: Top-to-ENE shear deformation, synchronous with oblique, isoclinal recumbent folding at amphibolite facies and greenschist facies conditions. Fluid-assisted formation of E-dipping detachment shear zones and semi-brittle detachment faults.

Implications

- Igneous protolith ages correlate the Øygarden Complex with the Telemarkian domain of the Baltican basement (Bingen and Solli, 2009).
- Sveconorwegian magmatism suggests a relation between Øygarden Complex and Sirdal Magmatic Belt. This correlation implies a continuous NNW-trend of Sveconorwegian domain boundaries into the 'caledonized' part of the Baltican basement.
- The absence of Sveconorwegian high-grade metamorphism is compatible with a recently proposed accretionary style of the Sveconorwegian Orogeny (Slagstad et al., 2013), and contradicts the common assumption of an entirely 'dry' pre-Caledonian Baltican basement (e.g. Butler et al., 2015).
- The rapid temperature increase marks probably the onset of Caledonian convergence in the Early Ordovician. The Lyderhorn Gneiss must have resided long enough at elevated temperatures to anneal metamictization.

- During the Caledonian Orogeny, the Lyderhorn Gneiss was highly metamorphosed and strongly deformed but the U-Pb zircon system remained closed.
- Scandian peak metamorphism was followed by very rapid exhumation in the Early Devonian. Bidirectional Devonian extension in the Øygarden Complex is explained by exhumation as an extensional gneiss dome. The proposed symmetrical core complex exhumation style is analogous to the Central Norway basement window (Braathen et al., 2000) and other basement culminations along the mid-Norwegian margin (Osmundsen et al., 2005).
- Onshore-offshore correlations suggest the Utsira High as a possible Devonian core complex.

8 Future Work

This study has raised far more questions than it answered. Future PhD and M.Sc. projects at the University of Bergen would be well suited to address pending questions in the regional geology of Bergen.

Sveconorwegian Framework

So far, the lack of geochemical data from the Lyderhorn Gneiss prevents geodynamic interpretations of Sveconorwegian magmatism in the Øygarden Complex. Major and trace element analyses of the dated lithologies could reveal, whether Sveconorwegian magmatism in the Lyderhorn Gneiss is syn-collisional, as proposed by Bingen et al. (2008b), or represents a continuous accretionary setting (Slagstad et al., 2013).

The proposed correlation of Øygarden Complex and Sirdal Magmatic Belt could be tested by U-Pb zircon geochronology of largely undated basement complexes in Sunnhordland (e.g. Kvinnherad, Haugaland). Precise, in-situ dating techniques need to be applied in the southern WGR to distinguish the Caledonian overprint from the igneous formation history. This would allow for a clear reconstruction of Sveconorwegian domain boundaries and a better understanding of the pre-Caledonian configuration of the Baltican basement.

Caledonian Framework

The proposed exhumation model for the Øygarden Complex is based on a number of observations, but none of them is a 'hard fact' corresponding to deformed Devonian pegmatite dikes in the Central Norway basement window (Braathen et al., 2000). The following next steps could be taken to test the model:

High-precision, in-situ U-Pb zircon geochronology of migmatitic gneisses in the western part of the Øygarden Complex and in the footwall of the BASZ could show, whether migmatization in these areas is Proterozoic, as commonly assumed, or in fact Caledonian. Previous field mapping will be necessary to determine suitable sample localities to date the migmatization. However, it is commonly problematic to date the timing of doming by U-Pb

zircon geochronology (Whitney et al., 2004), so other high-temperature geochronometers should be applied as well.

To validate the proposed model, it will be very important to precisely constrain the cooling histories of different units in the Bergen Arc System and the surrounding basement. Further studies of Ar-Ar mineral cooling ages are needed, to test the significance of distinct cooling paths, used in the previous argumentation. Thermal modelling could be applied to distinguish the effect of highly radiogenic granitic rocks in the basement from cooling resulting from the tectonic denudation.

Another important question is, if a major Devonian detachment shear zone is located west offshore the Øygarden Complex. Such a structure is indicated by low-angle Devonian fabrics and detachments (Fossen et al., 2016), but previous studies were uncertain about its existence (e.g. Fossen and Hurich, 2005, Fig.1).

Because of its position in the hanging wall of the BASZ (which again is located in the hanging wall of the HSZ), the interaction of detachments in the Bergen Arc System must be much more complex than shown in the simplified illustration in Fig. 72. Fault rock dating (e.g. chlorite phyllonite in the Loddefjord Detachment Shear Zone) could help to understand the interaction of strongly curved detachment shear zones with opposed polarity. Integrated structural and geochronological investigations of the Øygarden Complex and other domal culminations in the basement of SW Norway (e.g. Kirkedalen, Folgefonna, Masfjorden, etc.) are necessary, to establish a detailed sequence of Early Devonian detachment faulting and possible dome forming mechanisms.

Osmundsen et al. (2005) described, how core complexes at the mid-Norwegian margin control the location of major domain boundaries in the Mesozoic rift. Following this example, it could be tested if similar onshore-offshore correlations can be drawn at the SW Norwegian margin. The spatial relationship between the Utsira High and onshore basement culminations as well as the opposed polarity of the Utsira Shear Zone, could be taken as a starting point, to test core complex exhumation as a possible formation mechanism for the Utsira High.

The validation (or falsification) of the proposed exhumation model for the Øygarden Complex, is of more than regional importance. Its validation would imply that rates of viscous flow in the basement of SW Norway would have been previously underestimated. A reevaluation could provide significant implications for the governing exhumation mechanism of the warmer basement in the WGR.

Methods

In this study, three-dimensional reconstructions and visualisation techniques have been applied in a rudimentary manner, to illustrate complex shapes and structures. It would be desirable, to develop such techniques to a level that satisfies scientific standards. Two-dimensional integration of foliation datasets could be a powerful tool to reconstruct shapes of large-scale geological structures. Mathematical methods already exist for shape reconstruction by two-dimensional integration of gradient data and are in industry use

(e.g. Huang et al., 2015). Their application to structural geology could be developed, for example through an interdisciplinary M.Sc. thesis in cooperation with the department of mathematics.

References

- Allègre, C. J. (2008). *Isotope geology*. Cambridge University Press Cambridge.
- Allmendinger, R. W., Cardozo, N., and Fisher, D. M. (2011). *Structural geology algorithms: Vectors and tensors*. Cambridge University Press.
- Andersen, T. B., Corfu, F., Labrousse, L., and Osmundsen, P.-T. (2012). Evidence for hyper-extension along the pre-Caledonian margin of Baltica. *Journal of the Geological Society* 169, pp. 601–612.
- Andersen, T. B., Jamtveit, B., Dewey, J., and Swensson, E. (1991). Subduction and eduction of continental crust: major mechanism during continent-continent collision and orogenic extensional collapse, a model based on the south Caledonides. *Terra Nova* 3, pp. 303–310.
- Andersen, T. B. and Jamtveit, B. (1990). Uplift of deep crust during orogenic extensional collapse: A model based on field studies in the Sogn-Sunnfjord Region of western Norway. *Tectonics* 9, pp. 1097–1111.
- Andersen, T. B. and Jansen, Ø. J. (1987). The Sunnhordland Batholith, W. Norway: regional setting and internal structure, with emphasis on the granitoid plutons. *Norsk geologisk tidsskrift* 67, pp. 159–183.
- Askvik, H. (1971). *Gabbroic and quartz dioritic intrusions in gneisses on southern Askoy, West Norwegian Caledonides*. Universitetsforlaget, pp. 3–38.
- Austrheim, H., Erambert, M., and Engvik, A. K. (1997). Processing of crust in the root of the Caledonian continental collision zone: the role of eclogitization. *Tectonophysics* 273, pp. 129–153.
- Austrheim, H. and Griffin, W. L. (1985). Shear deformation and eclogite formation within granulite-facies anorthosites of the Bergen Arcs, western Norway. *Chemical Geology* 50, pp. 267–281.
- Barth, N. C., Hacker, B. R., Seward, G. G., Walsh, E. O., Young, D., and Johnston, S. (2010). Strain within the ultrahigh-pressure Western Gneiss region of Norway recorded by quartz CPOs. *Geological Society, London, Special Publications* 335, pp. 663–685.
- Bell, R. E., Jackson, C. A.-L., Whipp, P. S., and Clements, B. (2014). Strain migration during multiphase extension: Observations from the northern North Sea. *Tectonics* 33, pp. 1936–1963.
- Bering, D. (1984). Tektono-metamorf utvikling av det vestlige gneiskompleks i Sund, Sotra. Cand. real. thesis. University of Bergen.
- Bingen, B., Austrheim, H., Whitehouse, M. J., and Davis, W. J. (2004). Trace element signature and U–Pb geochronology of eclogite-facies zircon, Bergen Arcs, Caledonides of W Norway. *Contributions to Mineralogy and Petrology* 147, pp. 671–683.
- Bingen, B., Davis, W. J., and Austrheim, H. (2001). Zircon U–Pb geochronology in the Bergen arc eclogites and their Proterozoic protoliths, and implications for the pre-Scandian evolution of the Caledonides in western Norway. *Geological Society of America Bulletin* 113, pp. 640–649.
- Bingen, B., Davis, W. J., Hamilton, M. A., Engvik, A. K., Stein, H. J., Skar, O., and Nordgulen, O. (2008a). Geochronology of high-grade metamorphism in the Sveconorwegian belt, S. Norway: U–Pb, Th–Pb and Re–Os data. *Norsk Geologisk Tidsskrift* 88, p. 13.
- Bingen, B., Demaiffe, D., Hertogen, J., Weis, D., and Michot, J. (1993). K-rich calc-alkaline augen gneisses of Grenvillian age in SW Norway: mingling of mantle-derived and crustal components. *The Journal of geology*, pp. 763–778.
- Bingen, B., Nordgulen, O., and Viola, G. (2008b). A four-phase model for the Sveconorwegian orogeny, SW Scandinavia. *Norsk Geologisk Tidsskrift* 88, p. 43.
- Bingen, B., Skår, Ø., Marker, M., Sigmond, E. M., Nordgulen, Ø., Ragnhildstveit, J., Mansfeld, J., Tucker, R. D., and Liégeois, J.-P. (2005). Timing of continental building in the Sveconorwegian orogen, SW Scandinavia. *Norwegian Journal of Geology* 85, pp. 87–116.
- Bingen, B. and Solli, A. (2009). Geochronology of magmatism in the Caledonian and Sveconorwegian belts of Baltica: synopsis for detrital zircon provenance studies. *Norwegian Journal of Geology/Norsk Geologisk Forening* 89.

- Bingen, B. and Van Breemen, O. (1998). Tectonic regimes and terrane boundaries in the high-grade Sveconorwegian belt of SW Norway, inferred from U–Pb zircon geochronology and geochemical signature of augen gneiss suites. *Journal of the Geological Society* 155, pp. 143–154.
- Bogdanova, S., Bingen, B., Gorbatshev, R., Kheraskova, T., Kozlov, V., Puchkov, V., and Volozh, Y. A. (2008). The East European Craton (Baltica) before and during the assembly of Rodinia. *Precambrian Research* 160, pp. 23–45.
- Bos, B. and Spiers, C. J. (2002). Frictional-viscous flow of phyllosilicate-bearing fault rock: Microphysical model and implications for crustal strength profiles. *Journal of Geophysical Research: Solid Earth* 107.
- Boundy, T. M., Essene, E. J., Hall, C. M., Austrheim, H., and Halliday, A. (1996). Rapid exhumation of lower crust during continent-continent collision and late extension: Evidence from $^{40}\text{Ar}/^{39}\text{Ar}$ incremental heating of hornblendes and muscovites, Caledonian orogen, western Norway. *Geological Society of America Bulletin* 108, pp. 1425–1437.
- Boundy, T. M., Mezger, K., and Essene, E. J. (1997). Temporal and tectonic evolution of the granulite-eclogite association from the Bergen Arcs, western Norway. *Lithos* 39, pp. 159–178.
- Braathen, A., Nordgulen, Ø., Osmundsen, P.-T., Andersen, T. B., Solli, A., and Roberts, D. (2000). Devonian, orogen-parallel, opposed extension in the Central Norwegian Caledonides. *Geology* 28, pp. 615–618.
- Braathen, A., Osmundsen, P. T., and Gabrielsen, R. H. (2004). Dynamic development of fault rocks in a crustal-scale detachment: An example from western Norway. *Tectonics* 23.
- Braathen, A., Osmundsen, P. T., Nordgulen, O., Roberts, D., and Meyer, G. B. (2002). Orogen-parallel extension of the Caledonides in northern Central Norway: an overview. *Norsk Geologisk Tidsskrift* 82, pp. 225–242.
- Brueckner, H. K. and Cuthbert, S. J. (2013). Extension, disruption, and translation of an orogenic wedge by exhumation of large ultrahigh-pressure terranes: Examples from the Norwegian Caledonides. *Lithosphere* 5, pp. 277–289.
- Brueckner, H. K., Van Roermund, H. L., and Pearson, N. J. (2004). An Archean (?) to Paleozoic evolution for a garnet peridotite lens with sub-baltic shield affinity within the Seve Nappe Complex of Jämtland, Sweden, Central Scandinavian Caledonides. *Journal of Petrology* 45, pp. 415–437.
- Butler, J. P., Beaumont, C., and Jamieson, R. A. (2015). Paradigm lost: Buoyancy thwarted by the strength of the Western Gneiss Region (ultra) high-pressure terrane, Norway. *Lithosphere*, pp. L426–1.
- Bybee, G., Ashwal, L., Shirey, S., Horan, M., Mock, T., and Andersen, T. (2014). Pyroxene megacrysts in Proterozoic anorthosites: Implications for tectonic setting, magma source and magmatic processes at the Moho. *Earth and Planetary Science Letters* 389, pp. 74–85.
- Centrella, S., Austrheim, H., and Putnis, A. (2015). Coupled mass transfer through a fluid phase and volume preservation during the hydration of granulite: An example from the Bergen Arcs, Norway. *Lithos* 236, pp. 245–255.
- Chauvet, A. and Séranne, M. (1994). Extension-parallel folding in the Scandinavian Caledonides: implications for late-orogenic processes. *Tectonophysics* 238, pp. 31–54.
- Cherniak, D. J. and Watson, E. B. (2003). Diffusion in zircon. *Reviews in mineralogy and geochemistry* 53, pp. 113–143.
- Coint, N., Slagstad, T., Roberts, N., Marker, M., Røhr, T., and Sørensen, B. E. (2015). The Late Mesoproterozoic Sirdal Magmatic Belt, SW Norway: Relationships between magmatism and metamorphism and implications for Sveconorwegian orogenesis. *Precambrian Research*.
- Condon, D. J., McLean, N., Noble, S. R., and Bowring, S. A. (2010). Isotopic composition ($^{238}\text{U}/^{235}\text{U}$) of some commonly used uranium reference materials. *Geochimica et Cosmochimica Acta* 74, pp. 7127–7143.

- Corfu, F., Andersen, T., and Gasser, D. (2014). The Scandinavian Caledonides: main features, conceptual advances and critical questions. *Geological Society, London, Special Publications* 390, pp. 9–43.
- Corfu, F., Hanchar, J. M., Hoskin, P. W., and Kinny, P. (2003). Atlas of zircon textures. *Reviews in mineralogy and geochemistry* 53, pp. 469–500.
- Davis, D. W., Krogh, T. E., and Williams, I. S. (2003). Historical development of zircon geochronology. *Reviews in mineralogy and geochemistry* 53, pp. 145–181.
- Doré, A., Lundin, E., Fichler, C., and Olesen, O. (1997). Patterns of basement structure and reactivation along the NE Atlantic margin. *Journal of the Geological Society* 154, pp. 85–92.
- Doré, A., Lundin, E., Jensen, L., Birkeland, Ø., Eliassen, P., and Fichler, C. (1999). Principal tectonic events in the evolution of the northwest European Atlantic margin. *Geological society, london, petroleum geology conference series*. Vol. 5. Geological Society of London, pp. 41–61.
- Dunning, G. and Pedersen, R. (1988). U/Pb ages of ophiolites and arc-related plutons of the Norwegian Caledonides: implications for the development of Iapetus. *Contributions to Mineralogy and Petrology* 98, pp. 13–23.
- Duretz, T., Gerya, T., Kaus, B., and Andersen, T. (2012). Thermomechanical modeling of slab eduction. *Journal of Geophysical Research: Solid Earth* 117.
- Eide, E. A., Torsvik, T. H., and Andersen, T. B. (1997). Absolute dating of brittle fault movements: Late Permian and late Jurassic extensional fault breccias in western Norway. *Terra Nova* 9, pp. 135–139.
- Essex, R., Gromet, L., ANDRÉASSON, P.-G., and Albrecht, L. (1997). Early Ordovician U-Pb metamorphic ages of the eclogite-bearing Seve nappes, Northern Scandinavian Caledonides. *Journal of Metamorphic Geology* 15, pp. 665–676.
- Færseth, R. B., Gjelberg, J., and Martinsen, O. J. (2011). Structural geology and sedimentology of Silurian metasediments in the Ulven area, Major Bergen Arc, SW Norway. *Norwegian Journal of Geology/Norsk Geologisk Forening* 91.
- Fauconnier, J., Labrousse, L., Andersen, T. B., Beyssac, O., Duprat-Oualid, S., and Yamato, P. (2014). Thermal structure of a major crustal shear zone, the basal thrust in the Scandinavian Caledonides. *Earth and Planetary Science Letters* 385, pp. 162–171.
- Fayon, A. K., Whitney, D. L., and Teyssier, C. (2004). Exhumation of orogenic crust: Diapiric ascent versus low-angle normal faulting. *Geological Society of America Special Papers* 380, pp. 129–139.
- Fossen, H. (1988a). Metamorphic history in the Bergen Arcs, Norway, as determined from amphibole chemistry. *Norsk geologisk tidsskrift* 68, pp. 223–239.
- (1988b). The Ulriken gneiss complex and the Rundemanen Formation: a basement-cover relationship in the Bergen Arcs, West Norway. *Norges Geologiske Undersøkelse Bulletin* 412, pp. 67–86.
- (1989). Geology of the minor Bergen arc, west Norway. *Bulletin Norges geologiske undersøkelse* 416, pp. 47–62.
- (1992). The role of extensional tectonics in the Caledonides of south Norway. *Journal of structural geology* 14, pp. 1033–1046.
- (1993). Linear fabrics in the Bergsdalen Nappes, southwest Norway: implications for deformation history and fold development. *Norsk geologisk tidsskrift* 73, pp. 95–108.
- (1998). Advances in understanding the post-Caledonian structural evolution of the Bergen area, West Norway. *Norsk Geologisk Tidsskrift* 78, pp. 33–46.
- (2000). Extensional tectonics in the Caledonides: Synorogenic or postorogenic. *Tectonics* 19, pp. 213–224.
- (2010a). Extensional tectonics in the North Atlantic Caledonides: a regional view. *Geological Society, London, Special Publications* 335, pp. 767–793.
- (2010b). *Structural geology*. Cambridge University Press.
- (2015). Field Guide for the Brazil-Norway Summer school in West Norway.

- Fossen, H. and Austrheim, H. (1988). Age of the Krossnes granite, west Norway. *Norges Geologiske Undersøkelse Bulletin* 413, pp. 61–65.
- Fossen, H. and Dunlap, W. J. (1998). Timing and kinematics of Caledonian thrusting and extensional collapse, southern Norway: evidence from 40 Ar/39 Ar thermochronology. *Journal of structural geology* 20, pp. 765–781.
- (2006). Age constraints on the late Caledonian (Scandian) deformation in the Major Bergen Arc, SW Norway. *Norsk Geologisk Tidsskrift* 86, p. 59.
- Fossen, H., Gabrielsen, R. H., Faleide, J. I., and Hurich, C. A. (2014). Crustal stretching in the Scandinavian Caledonides as revealed by deep seismic data. *Geology* 42, pp. 791–794.
- Fossen, H. and Holst, T. B. (1995). Northwest-verging folds and the northwestward movement of the Caledonian Jotun Nappe, Norway. *Journal of Structural Geology* 17, pp. 3–15.
- Fossen, H. and Hurich, C. A. (2005). The Hardangerfjord Shear Zone in SW Norway and the North Sea: a large-scale low-angle shear zone in the Caledonian crust. *Journal of the Geological Society* 162, pp. 675–687.
- Fossen, H., Khani, H. F., Faleide, J. I., Ksienzyk, A. K., and Dunlap, W. J. (2016). Post-Caledonian extension in the West Norway–northern North Sea region: the role of structural inheritance. *Geological Society, London, Special Publications* 439, SP439–6.
- Fossen, H., Mangerud, G., Hesthammer, J., Bugge, T., and Gabrielsen, R. (1997). The Bjoroy Formation: a newly discovered occurrence of Jurassic sediments in the Bergen Arc System. *Norsk Geologisk Tidsskrift* 77, pp. 269–287.
- Fossen, H. and Ragnhildstveit, J. (2008). Berggrunnskart Bergen 1115 I, M 1:50.000. *Norges Geologiske Undersøkelse*.
- Fossen, H. and Rykkelid, E. (1990). Shear zone structures in the Øygarden area, West Norway. *Tectonophysics* 174, pp. 385–397.
- (1992). The interaction between oblique and layer-parallel shear in high-strain zones: observations and experiments. *Tectonophysics* 207, pp. 331–343.
- Fossen, H., Teyssier, C., and Whitney, D. L. (2013). Transtensional folding. *Journal of Structural Geology* 56, pp. 89–102.
- Furnes, H., Dilek, Y., and Pedersen, R. B. (2012). Structure, geochemistry, and tectonic evolution of trench-distal backarc oceanic crust in the western Norwegian Caledonides, Solund-Stavfjord ophiolite (Norway). *Geological Society of America Bulletin* 124, pp. 1027–1047.
- Gabrielsen, R. H., Faleide, J. I., Pascal, C., Braathen, A., Nystuen, J. P., Etzelmüller, B., and O’Donnell, S. (2010). Latest Caledonian to Present tectonomorphological development of southern Norway. *Marine and Petroleum Geology* 27, pp. 709–723.
- Gabrielsen, R. H., Nystuen, J. P., Jarsve, E. M., and Lundmark, A. M. (2015). The Sub-Cambrian Peneplain in southern Norway: its geological significance and its implications for post-Caledonian faulting, uplift and denudation. *Journal of the Geological Society* 172, pp. 777–791.
- Gee, D. G., Fossen, H., Henriksen, N., and Higgins, A. K. (2008). From the early Paleozoic platforms of Baltica and Laurentia to the Caledonide Orogen of Scandinavia and Greenland. *Episodes* 31, pp. 44–51.
- Geisler, T., Schaltegger, U., and Tomaschek, F. (2007). Re-equilibration of zircon in aqueous fluids and melts. *Elements* 3, pp. 43–50.
- Glodny, J., Kühn, A., and Austrheim, H. (2008). Geochronology of fluid-induced eclogite and amphibolite facies metamorphic reactions in a subduction–collision system, Bergen Arcs, Norway. *Contributions to Mineralogy and Petrology* 156, pp. 27–48.
- Gordon, S. M., Whitney, D. L., Teyssier, C., and Fossen, H. (2013). U–Pb dates and trace-element geochemistry of zircon from migmatite, Western Gneiss Region, Norway: significance for history of partial melting in continental subduction. *Lithos* 170, pp. 35–53.

- Gordon, S. M., Whitney, D. L., Teyssier, C., Fossen, H., and Kylander-Clark, A. (2015). Geochronology and geochemistry of zircon from the northern Western Gneiss Region: Insights into the Caledonian tectonic history of western Norway. *Lithos*.
- Hacker, B. R., Andersen, T. B., Johnston, S., Kylander-Clark, A. R., Peterman, E. M., Walsh, E. O., and Young, D. (2010). High-temperature deformation during continental-margin subduction & exhumation: The ultrahigh-pressure Western Gneiss Region of Norway. *Tectonophysics* 480, pp. 149–171.
- Hacker, B. R. and Gans, P. B. (2005). Continental collisions and the creation of ultrahigh-pressure terranes: Petrology and thermochronology of nappes in the central Scandinavian Caledonides. *Geological Society of America Bulletin* 117, pp. 117–134.
- Harley, S. L. and Kelly, N. M. (2007). Zircon tiny but timely. *Elements* 3, pp. 13–18.
- Harrison, T. M., C el erier, J., Aikman, A. B., Hermann, J., and Heizler, M. T. (2009). Diffusion of 40 Ar in muscovite. *Geochimica et Cosmochimica Acta* 73, pp. 1039–1051.
- Harrison, T. M., Watson, E. B., and Aikman, A. B. (2007). Temperature spectra of zircon crystallization in plutonic rocks. *Geology* 35, pp. 635–638.
- Huang, L., Idir, M., Zuo, C., Kaznatcheev, K., Zhou, L., and Asundi, A. (2015). Comparison of two-dimensional integration methods for shape reconstruction from gradient data. *Optics and Lasers in Engineering* 64, pp. 1–11.
- Ireland, T. R. and Williams, I. S. (2003). Considerations in zircon geochronology by SIMS. *Reviews in Mineralogy and Geochemistry* 53, pp. 215–241.
- Johnston, S. M., Hacker, B. R., and Andersen, T. B. (2007). Exhuming Norwegian ultrahigh-pressure rocks: Overprinting extensional structures and the role of the Nordfjord-Sogn Detachment Zone. *Tectonics* 26.
- Jolivet, L., Raimbourg, H., Labrousse, L., Avigad, D., Leroy, Y., Austrheim, H., and Andersen, T. B. (2005). Softening triggered by eclogitization, the first step toward exhumation during continental subduction. *Earth and Planetary Science Letters* 237, pp. 532–547.
- Kolderup, C. F. and Kolderup, N. H. (1940). Geology of the Bergen Arc System. *Bergen Museums Skrifter* 20, p. 137.
- Ko ler, J. and Sylvester, P. J. (2003). Present trends and the future of zircon in geochronology: laser ablation ICPMS. *Reviews in Mineralogy and Geochemistry* 53, pp. 243–275.
- Krabbendam, M. and Wain, A. (1997). Late-Caledonian structures, differential retrogression and structural position of (ultra) high-pressure rocks in a Nordfjord-Stadlandet area, Western Gneiss Region. *Norges Geologiske Unders kelse* 432, pp. 127–139.
- Krabbendam, M. and Dewey, J. F. (1998). Exhumation of UHP rocks by transtension in the Western Gneiss Region, Scandinavian Caledonides. *Geological Society, London, Special Publications* 135, pp. 159–181.
- Ksienzyk, A. K., Dunkl, I., Jacobs, J., Fossen, H., and Kohlmann, F. (2014). From orogen to passive margin: constraints from fission track and (U–Th)/He analyses on Mesozoic uplift and fault reactivation in SW Norway. *Geological Society, London, Special Publications* 390, SP390–27.
- K hn, A., Glodny, J., Austrheim, H., and Raheim, A. (2002). The Caledonian tectono-metamorphic evolution of the Lindas Nappe: constraints from U–Pb, Sm–Nd and Rb–Sr ages of granitoid dykes. *Norsk Geologisk Tidsskrift* 82, pp. 45–58.
- Labrousse, L., Het nyi, G., Raimbourg, H., Jolivet, L., and Andersen, T. B. (2010). Initiation of crustal-scale thrusts triggered by metamorphic reactions at depth: Insights from a comparison between the Himalayas and Scandinavian Caledonides. *Tectonics* 29.
- Labrousse, L., Jolivet, L., Andersen, T., Agard, P., H bert, R., Maluski, H., and Sch rer, U. (2004). Pressure-temperature-time deformation history of the exhumation of ultra-high pressure rocks in the Western Gneiss Region, Norway. *Geological Society of America Special Papers* 380, pp. 155–183.

- Larsen, Ø. (1996). Fedjedomens tektoniske utvikling (Øygarden gneiskompleks, vest Norge) - en alternative model for dannelse av gneisdomer. Cand. real. thesis. University of Bergen.
- Larsen, Ø., Fossen, H., Langeland, K., and Pedersen, R.-B. (2003). Kinematics and timing of polyphase post-Caledonian deformation in the Bergen area, SW Norway. *Norsk Geologisk Tidsskrift* 83, pp. 149–166.
- Li, Z.-X., Bogdanova, S., Collins, A., Davidson, A., De Waele, B., Ernst, R., Fitzsimons, I., Fuck, R., Gladkochub, D., Jacobs, J., et al. (2008). Assembly, configuration, and break-up history of Rodinia: a synthesis. *Precambrian research* 160, pp. 179–210.
- Ludwig, K. R. (1998). On the treatment of concordant uranium-lead ages. *Geochimica et Cosmochimica Acta* 62, pp. 665–676.
- (2003). *User's manual for Isoplot 3.00: a geochronological toolkit for Microsoft Excel*. Kenneth R. Ludwig.
- Lundmark, A. and Corfu, F. (2007). Age and origin of the Årdal dike complex, SW Norway: False isochrons, incomplete mixing, and the origin of Caledonian granites in basement nappes. *Tectonics* 26.
- Mathiesen, T. (2013). Bruddanalyse i vestre Bergensområdet med konsekvenser for geotermisk utvinning. MA thesis. University of Bergen.
- Maystrenko, Y. P., Slagstad, T., Elvebakk, H. K., Olesen, O., Ganerød, G. V., and Rønning, J. S. (2015). New heat flow data from three boreholes near Bergen, Stavanger and Moss, southern Norway. *Geothermics* 56, pp. 79–92.
- Mezger, K. and Krogstad, E. (1997). Interpretation of discordant U-Pb zircon ages: An evaluation. *Journal of metamorphic Geology* 15, pp. 127–140.
- Milnes, A., Wennberg, O., Skår, Ø., and Koestler, A. (1997). Contraction, extension and timing in the South Norwegian Caledonides: the Sognefjord transect. *Geological Society, London, Special Publications* 121, pp. 123–148.
- Nielsen, A. T. and Schovsbo, N. H. (2011). The Lower Cambrian of Scandinavia: depositional environment, sequence stratigraphy and palaeogeography. *Earth-Science Reviews* 107, pp. 207–310.
- Nielsen, S. B., Gallagher, K., Leighton, C., Balling, N., Svenningsen, L., Jacobsen, B. H., Thomsen, E., Nielsen, O. B., Heilmann-Clausen, C., Egholm, D. L., et al. (2009). The evolution of western Scandinavian topography: a review of Neogene uplift versus the ICE (isostasy–climate–erosion) hypothesis. *Journal of Geodynamics* 47, pp. 72–95.
- Norton, M. (1986). Late Caledonide extension in western Norway: a response to extreme crustal thickening. *Tectonics* 5, pp. 195–204.
- Osmundsen, P. T., Braathen, A., Sommaruga, A., Skilbrei, J. R., Nordgulen, Ø., Roberts, D., Andersen, T. B., Olesen, O., and Mosar, J. (2005). Metamorphic core complexes and gneiss-cored culminations along the Mid-Norwegian margin: an overview and some current ideas. *Norwegian Petroleum Society Special Publications* 12, pp. 29–41.
- Osmundsen, P. and Andersen, T. (2001). The middle Devonian basins of western Norway: sedimentary response to large-scale transtensional tectonics? *Tectonophysics* 332, pp. 51–68.
- Osmundsen, P., Braathen, A., Nordgulen, Ø., Roberts, D., Meyer, G., and Eide, E. (2003). The Devonian Nesna shear zone and adjacent gneiss-cored culminations, North–Central Norwegian Caledonides. *Journal of the Geological Society* 160, pp. 137–150.
- Passchier, C. W. and Trouw, R. A. (2005). *Microtectonics*. Vol. 2. Springer.
- Pease, V., Daly, J., Elming, S.-Å., Kumpulainen, R., Moczydlowska, M., Puchkov, V., Roberts, D., Saintot, A., and Stephenson, R. (2008). Baltica in the Cryogenian, 850–630Ma. *Precambrian Research* 160, pp. 46–65.
- Pedersen, R., Bruton, D., and Furnes, H. (1992). Ordovician faunas, island arcs and ophiolites in the Scandinavian Caledonides. *Terra Nova* 4, pp. 217–222.

- Pedersen, R. B. and Dunning, G. R. (1997). Evolution of arc crust and relations between contrasting sources: U-Pb (age), Nd and Sr isotope systematics of the ophiolitic terrain of SW Norway. *Contributions to Mineralogy and Petrology* 128, pp. 1–15.
- Ragnhildstveit, J. and Helliksen, D. (1997). Geologisk kart over Norge, berggrunnskart Bergen - M 1:250.000. *Norges Geologiske Undersøkelse*.
- Ramberg, H. (1981). The role of gravity in orogenic belts. *Geological Society, London, Special Publications* 9, pp. 125–140.
- Ramberg, I., Bryhni, I., Nøttvedt, A., and Rangnes, K., eds. (2008). *The making of a land - Geology of Norway*. Norsk Geologisk Forening.
- Rino, S., Kon, Y., Sato, W., Maruyama, S., Santosh, M., and Zhao, D. (2008). The Grenvillian and Pan-African orogens: world's largest orogenies through geologic time, and their implications on the origin of superplume. *Gondwana Research* 14, pp. 51–72.
- Roberts, D. and Gee, D. G. (1985). The Caledonide orogen–Scandinavia and related areas. Ed. by D. Gee and B. Sturt. Chichester: Wiley. Chap. An introduction to the structure of the Scandinavian Caledonides, pp. 55–68.
- Roberts, D. (2003). The Scandinavian Caledonides: event chronology, palaeogeographic settings and likely modern analogues. *Tectonophysics* 365, pp. 283–299.
- Roberts, N. M. and Slagstad, T. (2015). Continental growth and reworking on the edge of the Columbia and Rodinia supercontinents; 1.86–0.9 Ga accretionary orogeny in southwest Fennoscandia. *International Geology Review*, pp. 1–25.
- Robinson, P., Roberts, D., Gee, D. G., and Solli, A. (2014). A major synmetamorphic Early Devonian thrust and extensional fault system in the Mid Norway Caledonides: relevance to exhumation of HP and UHP rocks. *Geological Society, London, Special Publications* 390, pp. 241–270.
- Roffeis, C. and Corfu, F. (2014). Caledonian nappes of southern Norway and their correlation with Sveconorwegian basement domains. *Geological Society, London, Special Publications* 390, pp. 193–221.
- Roffeis, C., Corfu, F., and Austrheim, H. (2012). Evidence for a Caledonian amphibolite to eclogite facies pressure gradient in the Middle Allochthon Lindås Nappe, SW-Norway. *Contributions to Mineralogy and Petrology* 164, pp. 81–99.
- Roffeis, C., Corfu, F., and Gabrielsen, R. (2013). A Sveconorwegian terrane boundary in the Caledonian Hardanger–Ryfylke Nappe Complex: The lost link between Telemarkia and the Western Gneiss Region? *Precambrian Research* 228, pp. 20–35.
- Rohr, T., Corfu, F., Austrheim, H., and Andersen, T. B. (2004). Sveconorwegian U-Pb zircon and monazite ages of granulite-facies rocks, Hisaroya, Gulen, Western Gneiss Region, Norway. *Norsk* 84, pp. 251–256.
- Root, D. B., Hacker, B., Mattinson, J., and Wooden, J. L. (2004). Zircon geochronology and ca. 400 Ma exhumation of Norwegian ultrahigh-pressure rocks: an ion microprobe and chemical abrasion study. *Earth and Planetary Science Letters* 228, pp. 325–341.
- Root, D. and Corfu, F. (2012). U–Pb geochronology of two discrete Ordovician high-pressure metamorphic events in the Seve Nappe Complex, Scandinavian Caledonides. *Contributions to Mineralogy and Petrology* 163, pp. 769–788.
- Root, D., Hacker, B., Gans, P., Ducea, M., Eide, E., and Mosenfelder, J. (2005). Discrete ultrahigh-pressure domains in the Western Gneiss Region, Norway: implications for formation and exhumation. *Journal of Metamorphic Geology* 23, pp. 45–61.
- Rudlang, T. (2011). Heat Flow and Deep Underground Temperature in the Bergen Region. MA thesis. NTNU - Trondheim.
- Rykkelid, E. and Fossen, H. (1992). Composite fabrics in mid-crustal gneisses: observations from the Øygarden Complex, West Norway Caledonides. *Journal of structural geology* 14, pp. 1–9.

- Schulze, K. (2014). Radiogenic Heat Production in the Bed Rock of Bergen, Norway with Gamma-Spectrometry and its Relevance for Geothermal Energy. MA thesis. Christian-Albrechts University Kiel.
- Seranne, M. and Seguret, M. (1987). The Devonian basins of western Norway: tectonics and kinematics of an extending crust. *Geological Society, London, Special Publications* 28, pp. 537–548.
- Skår, Ø. and Pedersen, R. B. (2003). Relations between granitoid magmatism and migmatization: U–Pb geochronological evidence from the Western Gneiss Complex, Norway. *Journal of the Geological Society* 160, pp. 935–946.
- Skjerlie, K. P., Pedersen, R. B., Wennberg, O. P., and De La Rosa, J. (2000). Volatile phase fluxed anatexis of metasediments during late Caledonian ophiolite obduction: evidence from the Sogneskollen Granitic Complex, west Norway. *Journal of the Geological Society* 157, pp. 1199–1213.
- Slagstad, T., Pin, C., Roberts, D., Kirkland, C. L., Grenne, T., Dunning, G., Sauer, S., and Andersen, T. (2014). Tectonomagmatic evolution of the Early Ordovician suprasubduction-zone ophiolites of the Trondheim Region, Mid-Norwegian Caledonides. *Geological Society, London, Special Publications* 390, pp. 541–561.
- Slagstad, T., Roberts, N. M., Marker, M., Røhr, T. S., and Schiellerup, H. (2013). A non-collisional, accretionary Sveconorwegian orogen. *Terra Nova* 25, pp. 30–37.
- Slama, J. and Pedersen, R. B. (2015). Zircon provenance of SW Caledonian phyllites reveals a distant Timanian sediment source. *Journal of the Geological Society*, pp. 2014–143.
- Spencer, C. J., Kirkland, C. L., and Taylor, R. J. (2015). Strategies towards statistically robust interpretations of in situ U–Pb zircon geochronology. *Geoscience Frontiers*.
- Stacey, J. t. and Kramers, I. (1975). Approximation of terrestrial lead isotope evolution by a two-stage model. *Earth and planetary science letters* 26, pp. 207–221.
- Steer, P., Huisman, R. S., Valla, P. G., Gac, S., and Herman, F. (2012). Bimodal Plio-Quaternary glacial erosion of fjords and low-relief surfaces in Scandinavia. *Nature Geoscience* 5, pp. 635–639.
- Steiger, R. and Jäger, E. (1977). Subcommittee on geochronology: convention on the use of decay constants in geo- and cosmo-chronology. *Earth and planetary science letters* 36, pp. 359–362.
- Sturt, B. A., Skarpenes, O., Pringle, I. R., and Ohanian, A. T. (1975). Reconnaissance Rb/Sr isochron study in the Bergen Arc System and regional implications. *Nature* 253, pp. 595–599.
- Sturt, B., Pringle, I., and Ramsay, D. (1978). The Finnmarkian phase of the Caledonian orogeny. *Journal of the Geological Society* 135, pp. 597–610.
- Tirel, C., Brun, J.-P., and Burov, E. (2004). Thermomechanical modeling of extensional gneiss domes. *Geological Society of America Special Papers* 380, pp. 67–78.
- Torsvik, T. H. and Cocks, L. R. M. (2005). Norway in space and time: a centennial cavalcade. *Norwegian Journal of Geology* 85, pp. 73–86.
- Tucker, R. D., Robinson, P., Solli, A., Gee, D. G., Thorsnes, T., Krogh, T. E., Nordgulen, Ø., and Bickford, M. (2004). Thrusting and extension in the Scandian hinterland, Norway: New U–Pb ages and tectonostratigraphic evidence. *American Journal of Science* 304, pp. 477–532.
- Van der Pluijm, B. and Marshak, S. (2004). *Earth Structure*. New York, London: WW Norton Company.
- Vander Auwera, J., Bogaerts, M., Liégeois, J.-P., Demaiffe, D., Wilmart, E., Bolle, O., and Duchesne, J. C. (2003). Derivation of the 1.0–0.9 Ga ferro-potassic A-type granitoids of southern Norway by extreme differentiation from basic magmas. *Precambrian Research* 124, pp. 107–148.
- Vander Auwera, J., Bolle, O., Bingen, B., Liégeois, J.-P., Bogaerts, M., Duchesne, J.-C., De Waele, B., and Longhi, J. (2011). Sveconorwegian massif-type anorthosites and related granitoids result from post-collisional melting of a continental arc root. *Earth-Science Reviews* 107, pp. 375–397.

- Vetti, V. V. and Fossen, H. (2012). Origin of contrasting Devonian supradetachment basin types in the Scandinavian Caledonides. *Geology* 40, pp. 571–574.
- Weiss, L. E. (1977). Structural Features of the Laksevåg Gneiss, Bergen, Norway. *Norges geologiske undersøkelse* 334, pp. 1–17.
- Wennberg, O. P., Milnes, A. G., and Winsvold, I. (1998). The northern Bergen Are Shear Zone an oblique-lateral ramp In the Devonian extensional detachment system of western Norway. *Norsk Geologisk Tidsskrift* 78, pp. 169–184.
- Whitehouse, M. J. and Kamber, B. S. (2005). Assigning dates to thin gneissic veins in high-grade metamorphic terranes: a cautionary tale from Akilia, southwest Greenland. *Journal of Petrology* 46, pp. 291–318.
- Whitehouse, M. J., Kamber, B. S., and Moorbath, S. (1999). Age significance of U-Th-Pb zircon data from early Archaean rocks of west Greenland - a reassessment based on combined ion-microprobe and imaging studies. *Chemical geology* 160, pp. 201–224.
- Whitehouse, M., Claesson, S., Sunde, T., and Vestin, J. (1997). Ion microprobe U-Pb zircon geochronology and correlation of Archaean gneisses from the Lewisian Complex of Gruinard Bay, northwestern Scotland. *Geochimica et Cosmochimica Acta* 61, pp. 4429–4438.
- Whitney, D. L., Teyssier, C., and Vanderhaeghe, O. (2004). Gneiss domes and crustal flow. *Geological Society of America Special Papers* 380, pp. 15–33.
- Wiedenbeck, M., Alle, P., Corfu, F., Griffin, W., Meier, M., Oberli, F., Quadt, A. v., Roddick, J., and Spiegel, W. (1995). Three natural zircon standards for U-Th-Pb, Lu-Hf, trace element and REE analyses. *Geostandards newsletter* 19, pp. 1–23.
- Winsvold, I. (1996). Tektonisk utvikling av Byrknesøy (Vest-Norge) - opphevingshistorie av eklogitter i sørvestlige del av Vestre gneiskompleks. MA thesis. University of Bergen.
- Wintsch, R., Christoffersen, R., and Kronenberg, A. (1995). Fluid-rock reaction weakening of fault zones. *Journal of Geophysical Research: Solid Earth* 100, pp. 13021–13032.
- Wu, Y. and Zheng, Y. (2004). Genesis of zircon and its constraints on interpretation of U-Pb age. *Chinese Science Bulletin* 49, pp. 1554–1569.
- Yin, A. (2004). Gneiss domes and gneiss dome systems. *Geological Society of America Special Papers* 380, pp. 1–14.
- Young, D. J., Hacker, B. R., Andersen, T. B., and Corfu, F. (2007). Prograde amphibolite facies to ultrahigh-pressure transition along Nordfjord, western Norway: Implications for exhumation tectonics. *Tectonics* 26.

Online Resources:

<http://geo.ngu.no/kart/berggrunn> (downloaded: 02.05.2016)

<http://www.ngu.no/nyheter/kart-viser-radioaktivitet-pa-vestlandet> (downloaded: 13.04.2016)

<https://shrimprg.stanford.edu/shrimp-rg> (downloaded: 20.05.2015)

9 Appendix

- **Appendix 1** - SIMS U-Pb Zircon Geochronology Results
- **Appendix 2** - List of Outcrops
- **Appendix 3** - Map of Outcrops
- **Appendix 4** - Geological Map of Lyderhorn - M 1:12.000
- **Appendix 5** - N-S Cross Section
- **Appendix 6** - Structural Map - Planar Fabrics
- **Appendix 7** - Structural Map - Linear Fabrics
- **Appendix 8** - 3D Geological Model of Lyderhorn
- **Appendix 9** - 3D Model of the Basement Surface in SW Norway

Appendix 2 - List of Outcrops

No.	Lithology	Structural	Foliation		Contact		Lineation		Fold Axis	
			Dip dir.	Dip	Dip dir.	Dip	Trend	Plunge	Trend	Plunge
1	mylonitic granitic gneiss, amphibolite intruded by pinkish pegmatite	fold transposition, pygmatic folds, catclasis	057	44	047	16				
2	granitic L-tectonite		034	35			076	21		
3	heterogeneous mylonitic gneiss									
4	pegmatite				157	84				
5	hornblende biotite granite gneiss intruded by pegmatite		041	46						
6	hornblende biotite granite gneiss		334	66						
7	hornblende biotite granite gneiss intruded by pegmatite		050	19			096	18		
8	metagabbro									
9	pegmatite					125	31			
10	pegmatite					132	30			
11	pegmatite									
12	pegmatite					016	74			
13	pegmatite intruding metagabbro		012	75						
14	hornblende biotite granite gneiss									
15	hornblende biotite granite gneiss intruded by aplitic granite		333	84						
16	hornblende biotite granite gneiss, minor pegmatite		001	86						
17	felsic phyllonite	phyllonitic shear zone	020	36						
18	hornblende biotite granite gneiss	mylonitic shear zone	050	40						
19	leucoranic L-tectonite						075	25		
20	leucoranic L-tectonite		115	35			085	18		
21	leucoranic S-L-tectonite		118	32			076	21		
22	pegmatite and heterogeneous gneiss	cataclastic	046	24			085	26		
23	heterogeneous gneiss	cataclastic	045	28						
24	protomylonitic gneiss		099	20						
25	heterogenous gneiss		064	22			084	19		
26	heterogenous gneiss, pegmatite	mylonitic	176	77						
27	metagabbro		170	90						
28	amphibolite	clastomylonitic shear zone	156	79						
29	hornblende biotite granite gneiss									
30	hornblende biotite granite gneiss		092	34						
31	heterogenous tonalitic gneiss	mylonitic, strongly folded	065	56						
32	metagabbro, medium grained		024	15						
33	amphibolite intruded by pegmatite		021	27						
34	amphibolite intruded by pegmatite	isoclinal folding	022	54						
35	amphibolite intruded by pegmatite	L-tectonite	055	47	035	58				
36	amphibolite intruded by pegmatite, white tonalitic veins	heterogeneous deformation	028	44						
37	amphibolite intruded by pegmatite	chlorite phyllonite shear zone			003	42				
38	amphibolite intruded by pegmatite		025	70						
39	heterogenous tonalitic gneiss	mylonitic	006	26						
40	hornblende biotite granite gneiss	mylonitic	271	26						
41	metagabbro intruded by pegmatite		086	15						
42	pegmatite									
43	pegmatite	sheared	123	45			122	45		
44	metagabbro		103	10						
45	garnet-bearing amphibolite intruded by pegmatite	isoclinal recumbent macrofold	146	43					075	20
46	hornblende biotite granite gneiss contact with metagabbro				161	42				
47	hornblende biotite granite gneiss intruded by pegmatite	mylonitic shear zone	052	28						
48	hornblende biotite granite gneiss intruded by pegmatite	mylonitic shear zone	037	30						
49	hornblende biotite granite gneiss contact with metagabbro	contact reactivated as mylonitic shear zone	059	29						
50	hornblende biotite granite gneiss contact with metagabbro									
51	pegmatite	mylonitic shear zone	058	69						
52	hornblende biotite granite gneiss intruded by pegmatite	tight recumbent fold	001	75					260	10
53	hornblende biotite granite gneiss	mylonitic	339	43						
54	amphibolite intruded by pegmatite		056	20			104	24		
55	pegmatite		069	42	067	50				
56	amphibolite	mylonitic, crenulation folding	068	25						
57	heterogenous tonalitic gneiss		070	25			080	24		
58	heterogenous tonalitic gneiss		017	34						
60	heterogenous tonalitic gneiss		059	30			084	14		
61	pegmatite and mylonitic tonalitic gneiss	recumbent fold	158	54						
62	pegmatite				154	55				

9 Appendix

63	metagabbro										
64	heterogenous tonalitic gneiss		134	39							
65	granitic S-L tectonite		119	31			072	27			
66	tonalitic gneiss		026	40							
67	amphibolite	complex folding	347	65							
68	metagabbro		119	41							
69	hornblende biotite granite gneiss contact with metagabbro				101	27					
70	hornblende biotite granite gneiss	mylonitic shear zone	083	30			100	26			
71	hornblende biotite granite gneiss contact with metagabbro	fold	174	79					090	30	
72	metagabbro, contact zone										
73	hornblende biotite granite gneiss, more tonalitic		054	20							
74	hornblende biotite granite gneiss	mylonitic shear zone	076	17			076	17			
75	hornblende biotite granite gneiss	mylonitic shear zone; oblique isoclinal recumbent fold	048	25			081	25			
76	amphibolite, contact zone		008	73							
77	heterogenous gneiss	semi-brittle shear zone; isoclinal folding	011	38							
78	cataclastic granitic gneiss	semi-brittle shear zone	064	30							
79	micaceous granitic gneiss	phyllonitic	080	15							
81	hornblende biotite granite gneiss										
82	hornblende biotite granite gneiss		082	15							
83	granitic gneiss	protomylonitic to mylonitic; strain variations around tight inclined fold	001	45					090	29	
84	granitic gneiss		010	38							
85	hornblende biotite granite gneiss										
86	tonalitic gneiss		084	20							
87	protomylonitic granitic gneiss		156	77							
88	pegmatite		186	29							
89	granitic gneiss	protomylonitic									
90	heterogeneous gneiss	mylonitic shear zone	026	57							
91	heterogeneous gneiss	protomylonitic; folding	010	51							
92	heterogeneous gneiss		181	87							
93	hornblende biotite granite gneiss		015	90							
94	garnet bearing granitic cataclastite										
95	hornblende biotite granite gneiss		030	45							
96	granitic augen gneiss										
97	granitic augen gneiss	large Fsp Augen	012	29							
98	granitic augen gneiss, amphibolite layer	protomylonite	092	37	107	40					
99	granitic cataclastite	brittle-plastic transition shear zone	102	15							
100	heterogenous gneiss		027	20							
101	layered gneiss		349	38			072	9			
102	granite mylonite	mylonite to ultramylonite, phyllonitic	067	17							
103	layered gneiss and granitic augen gneiss	top-to-NE	052	28			070	15			
104	heterogenous gneiss	protomylonitic	005	40			070	20			
105	granitic gneiss										
106	granitic gneiss		001	17			064	10			
107	granitic gneiss and amphibolite		032	30			079	20			
108	granitic augen gneiss	top-to-NE	072	28			075	29			
109	granitic augen gneiss	top-to-E	069	20			069	20			
110	granitic mylonite		094	35							
111	heterogeneous mylonitic gneiss	top-to-NE	146	46			072	24			
112	granitic mylonite		071	29			071	29			
113	granitic mylonite		150	35							
114	heterogeneous mylonitic gneiss	ptygmatic folding	082	26			086	14			
115	granitic mylonite		081	32							
116	granitic mylonite	top-to-NE	077	33			092	31			
117	granitic mylonite	isoclinal folds	042	23			088	17	088	17	
118	granitic augen gneiss	transition from mylonite to protomylonite	118	26							
119	granitic augen gneiss		041	36			082	25			
120	granitic augen gneiss		124	30							
121	granitic augen gneiss		068	24			071	24			
122	amphibolite		070	21							
123	granitic augen gneiss		077	12							
124	heterogenous mylonitic gneiss	clastomylonitic shear zone	001	84			087	10			
125	heterogenous mylonitic gneiss	clastomylonitic shear zone	300	27							
126	granitic augen gneiss		350	70							
127	granitic augen gneiss		041	16							
128	granitic augen gneiss	top-to-E	026	36			079	3			
129	heterogenous mylonitic gneiss										
130	heterogenous mylonitic gneiss		004	24			090	6			
131	heterogenous mylonitic gneiss	shear zone: ductile to brittle	062	27							

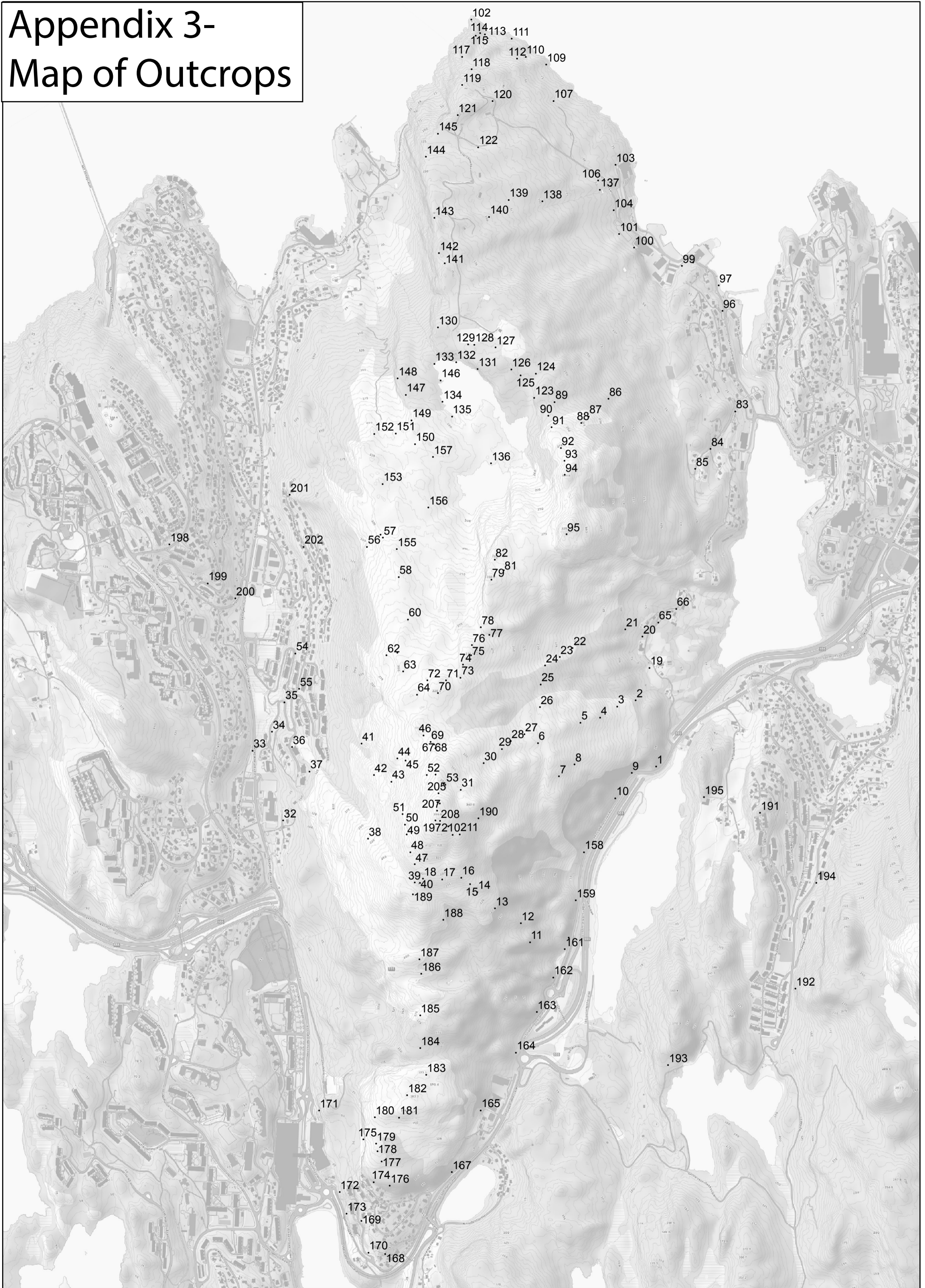
9 Appendix

132	mylonitic granitic gneiss	partly ultramylonitic	043	29			096	22		
133	mylonitic granitic gneiss	strongly non-cylindrical folding	023	32			077	26		
134	mylonitic granitic gneiss		012	36						
135	mylonitic granitic gneiss		042	30						
136	micaceous granitic gneiss	phyllonitic?	079	13			091	1		
137	granitic L-tectonite		087	10			071	10		
138	granitic L-tectonite		002	20			061	19		
139	granitic augen gneiss		034	24			059	19		
140	granitic L-tectonite						071	24		
141	granitic augen gneiss		035	18			077	22		
142	granitic L-tectonite									
143	granitic augen gneiss		040	29			059	26		
144	amphibolite, thin layer		075	19						
145	granitic augen gneiss	top-to-E	055	20			080	13		
146	mylonitic granitic gneiss		175	49			100	10		
147	mylonitic granitic gneiss		109	17						
148	mylonitic granitic gneiss	folding, top-to-E	070	24			079	16		
149	heterogenous mylonitic gneiss	shear zone	015	47			093	5		
150	mylonitic granitic gneiss		031	27			074	9		
151	mylonitic granitic gneiss		048	26			048	26		
152	heterogenous mylonitic gneiss		046	20						
153	metagabbro		052	37			104	21		
154	amphibolite	mylonitic, crenulation folding	041	20			084	10	095	13
155	heterogenous mylonitic gneiss		088	15						
156	heterogenous mylonitic gneiss		040	17						
157	mylonitic granitic gneiss	shear zone, top-to-E	050	42			092	7		
158	amphibolite intruded by pegmatite				109	30				
159	mylonitic tonalitic gneiss intruded by pegmatite	isoclinal recumbent fold	002	57						
160	mylonitic tonalitic gneiss intruded by pegmatite		062	39						
161	mylonitic tonalitic gneiss intruded by pegmatite		068	49						
162	leucogranite and pegmatite		005	25						
163	gneissic leucogranite	weakly foliated			150	82				
164	gneissic leucogranite				161	47				
165	pegmatite	semi-brittle shear zone	083	35						
166	gneissic granite				084	22				
167	layered series				342	50				
168	layered series	C-C shear bands in amphibolite	021	35						
169	layered series	ptygmatic folding	126	13						
170	layered series		050	37						
171	layered series	N-vergent fold, beginning amphibolite - chlorite phyllonite reaction	117	36					084	36
172	layered series; chlorite phyllonite	tectonic conglomerate	084	28						
173	layered series	strong folding	084	14					093	9
174	layered series; chlorite phyllonite	Loddefjord detachment shear zone, top-to-E	048	25			120	7		
175	layered series; chlorite phyllonite	Loddefjord detachment shear zone	018	27			109	8		
176	layered series	shear zone	052	16			109	10		
177	pegmatite		017	33						
178	pegmatite				178	35				
179	layered series (metagabbro)				184	81				
180	gneissic leucogranite						093	3		
181	layered series	fold	041	32	192	45			110	1
182	pegmatite									
183	pegmatite		019	22	033	60	079	16		
184	metagabbro	mylonitic	030	57			095	21		
185	pegmatite	fold			140	23			081	25
186	pegmatite		153	63						
187	pegmatite				027	50				
188	pegmatite	strong stretching lin - mullions?	070	25			082	29		
189	gneissic leucogranite		080	27			095	18		
190	pegmatite									
191	metagabbro intruded by pegmatite									
192	cataclastic gneissic leucogranite	semi-brittle shear zone								
193	gneissic leucogranite		100	32			073	23		
194	hornblende biotite granite gneiss									
195	heterogenous mylonitic gneiss									
196	hornblende biotite granite gneiss intruded by pegmatite	shear zone	103	20	352	62				
197	hornblende biotite granite gneiss intruded by pegmatite		079	20	307	72				
198	Gabbro (unaltered)						087	13		
199	amphibolite									
200	amphibolite	mylonitic, isoclinal folding, sheath fold?	350	36			080	9		

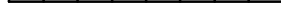
9 Appendix

201	amphibolite	folded, strong strain variation								085	20
	metagabbro intruded by hornblende										
202	biotite granite (intrusive breccia)	L-tectonite									
203	pegmatite				353	63					
204	pegmatite				165	89					
205	pegmatite										
206	pegmatite				320	58					
207	pegmatite				339	80					
208	pegmatite				350	85					
209	pegmatite				142	70					
210	pegmatite				340	83					
211	pegmatite				146	75					

Appendix 3- Map of Outcrops



0 105 210 420 Meters



Appendix 4 - Geological Map of Lyderhorn

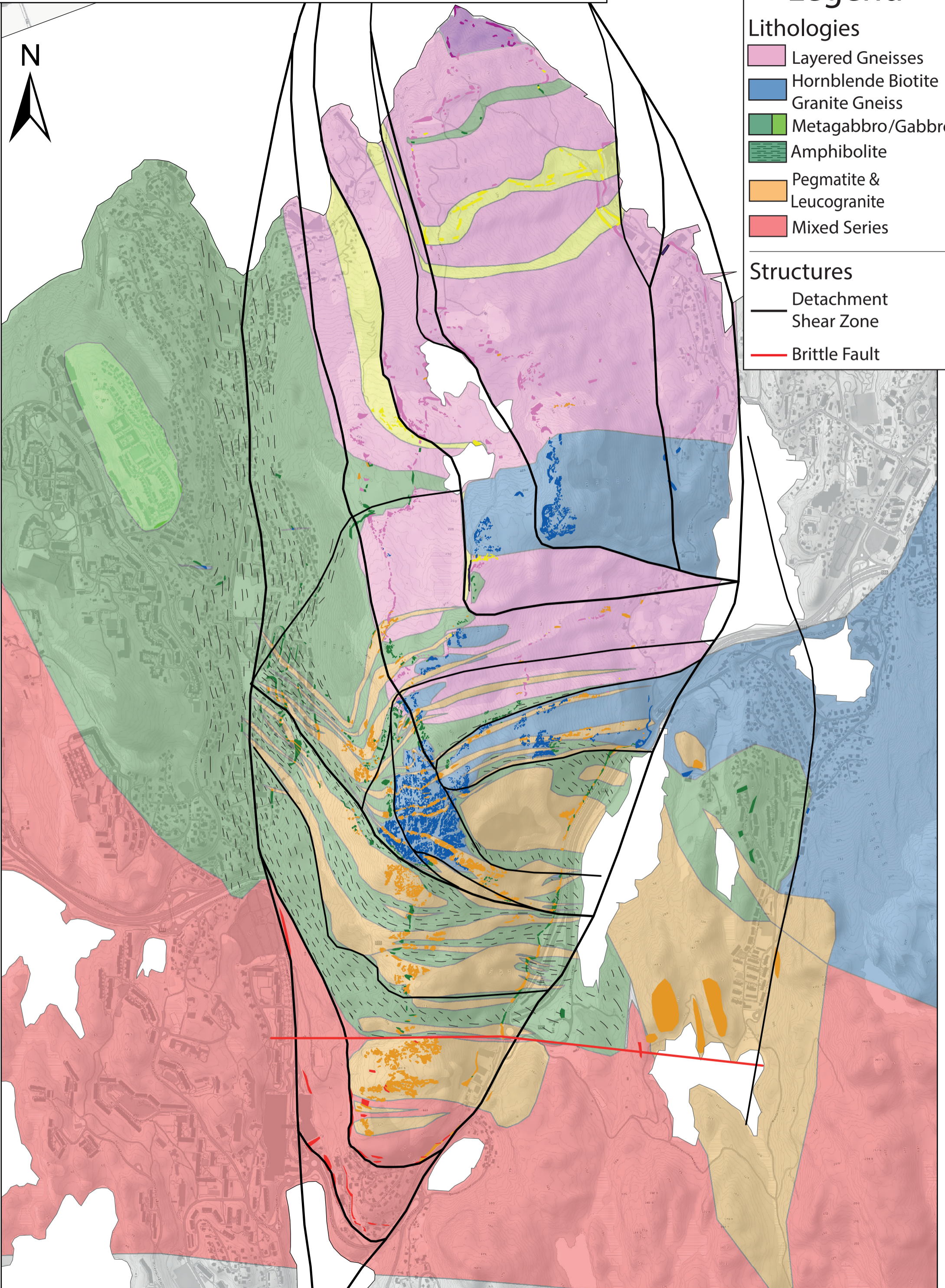
Legend

Lithologies

- Layered Gneisses
- Hornblende Biotite Granite Gneiss
- Metagabbro/Gabbro
- Amphibolite
- Pegmatite & Leucogranite
- Mixed Series

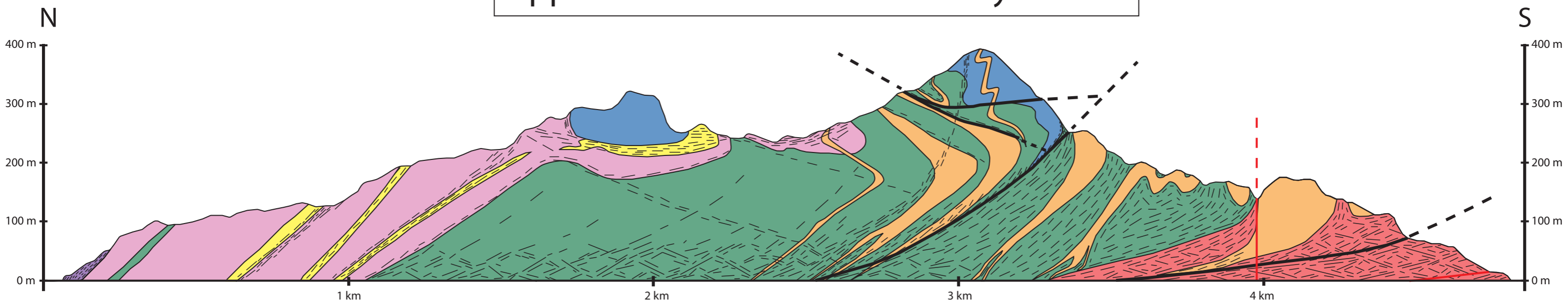
Structures






- Detachment
- Shear Zone
- Brittle Fault



0 250 500 1.000 Meters

Appendix 5 - N-S Cross Section Lyderhorn



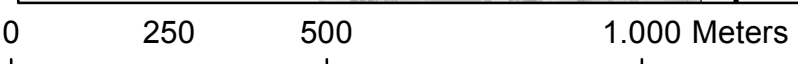
- | | | | | |
|---|--|--|---|--|
|  Layered Gneisses |  Hornblende Biotite Granite Gneiss |  Pegmatite & Leucogranite |  Metagabbro |  Mixed Series |
|  Granitic Mylonite | | |  Amphibolite | |
|  (Micaceous) Leucogranitic Gneiss | | | | |

Appendix 6



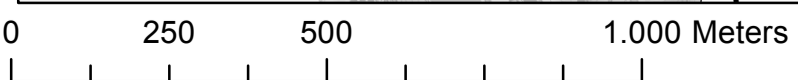
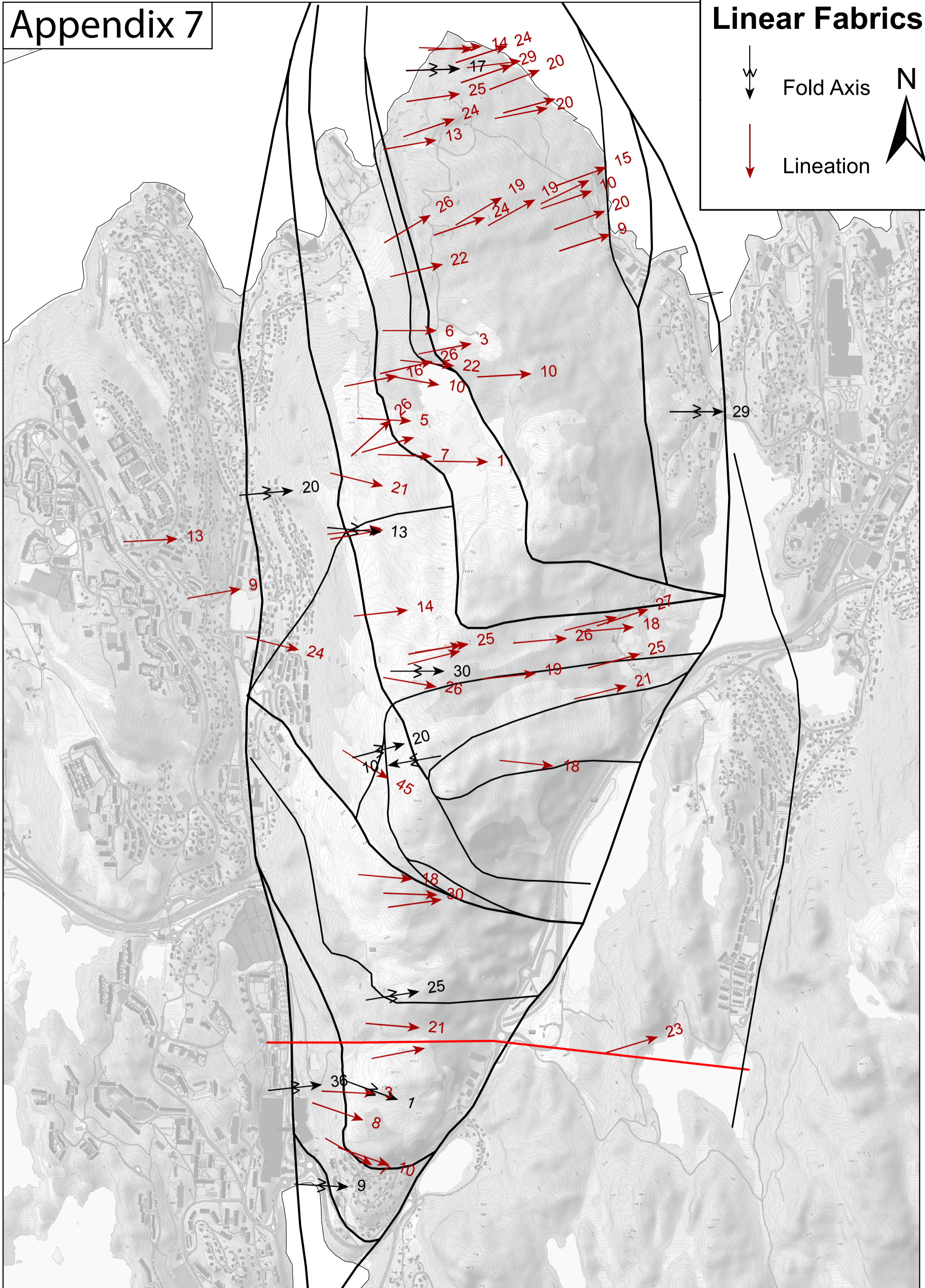
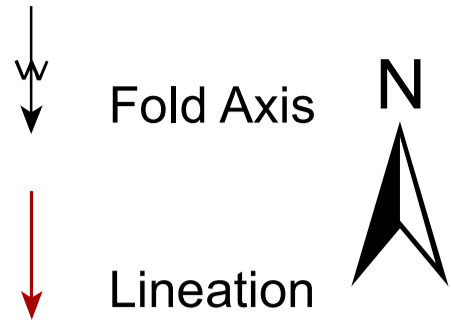
Planar Fabrics

-  Foliation
-  Contact

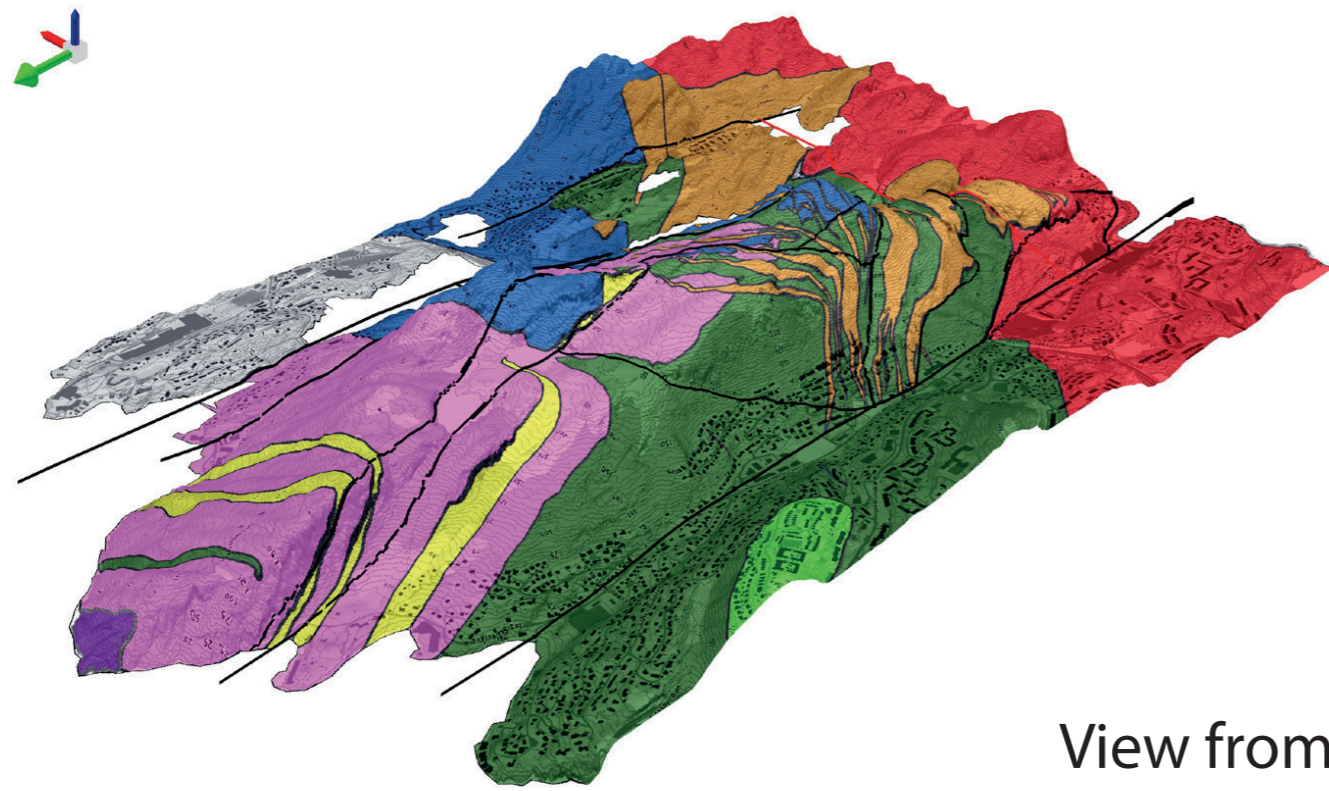


Appendix 7

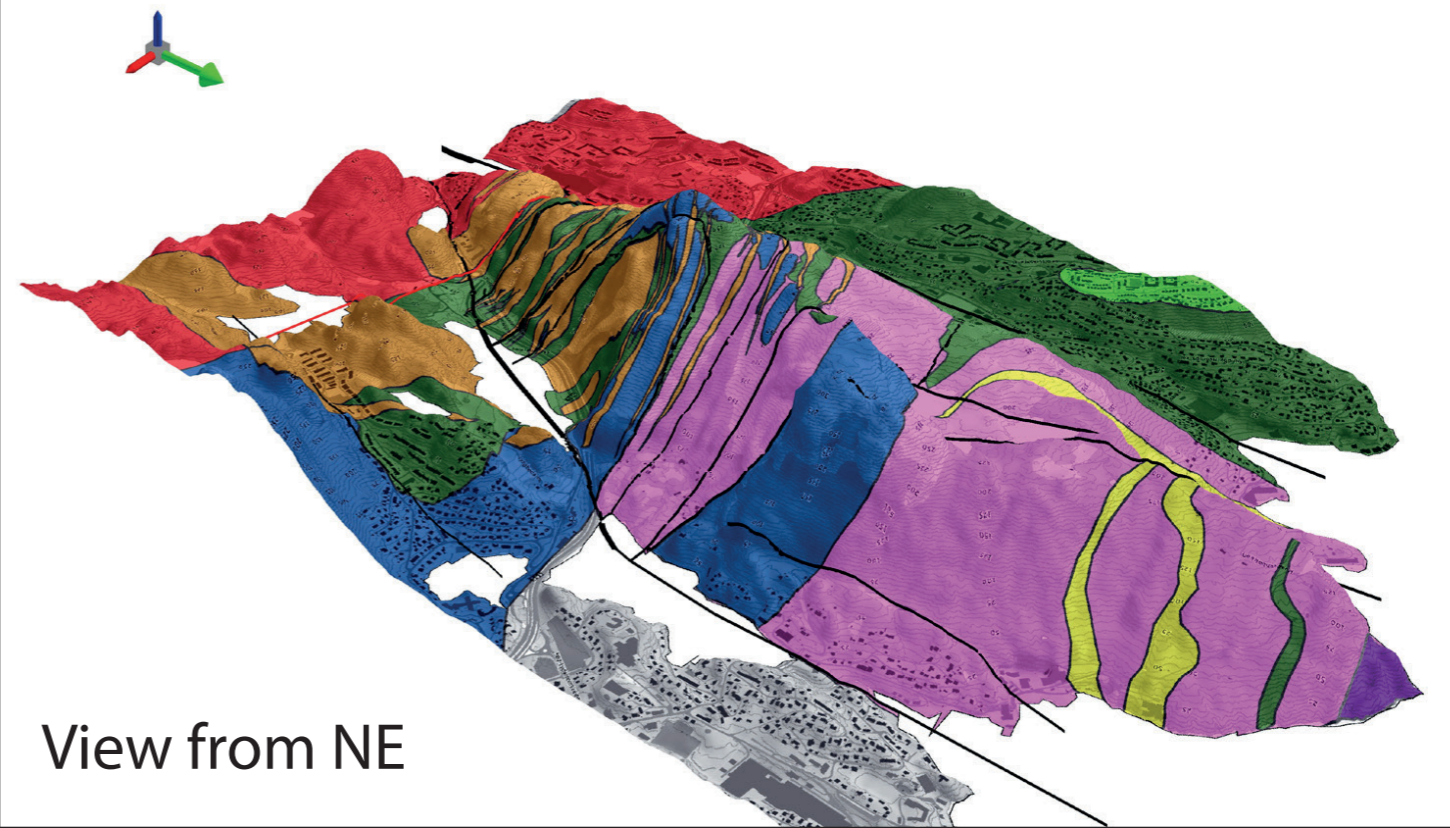
Linear Fabrics



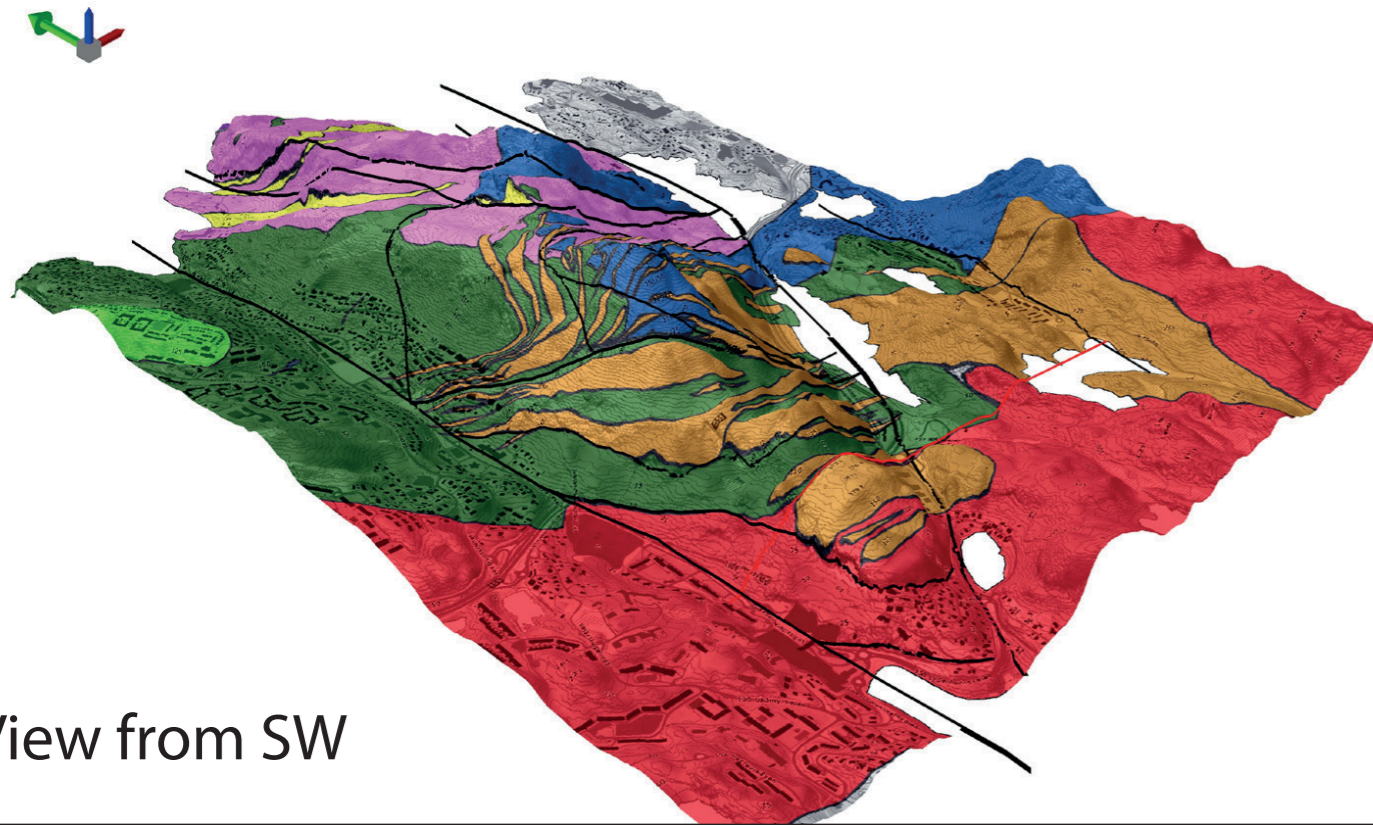
Appendix 8 - 3D Geological Model of Lyderhorn



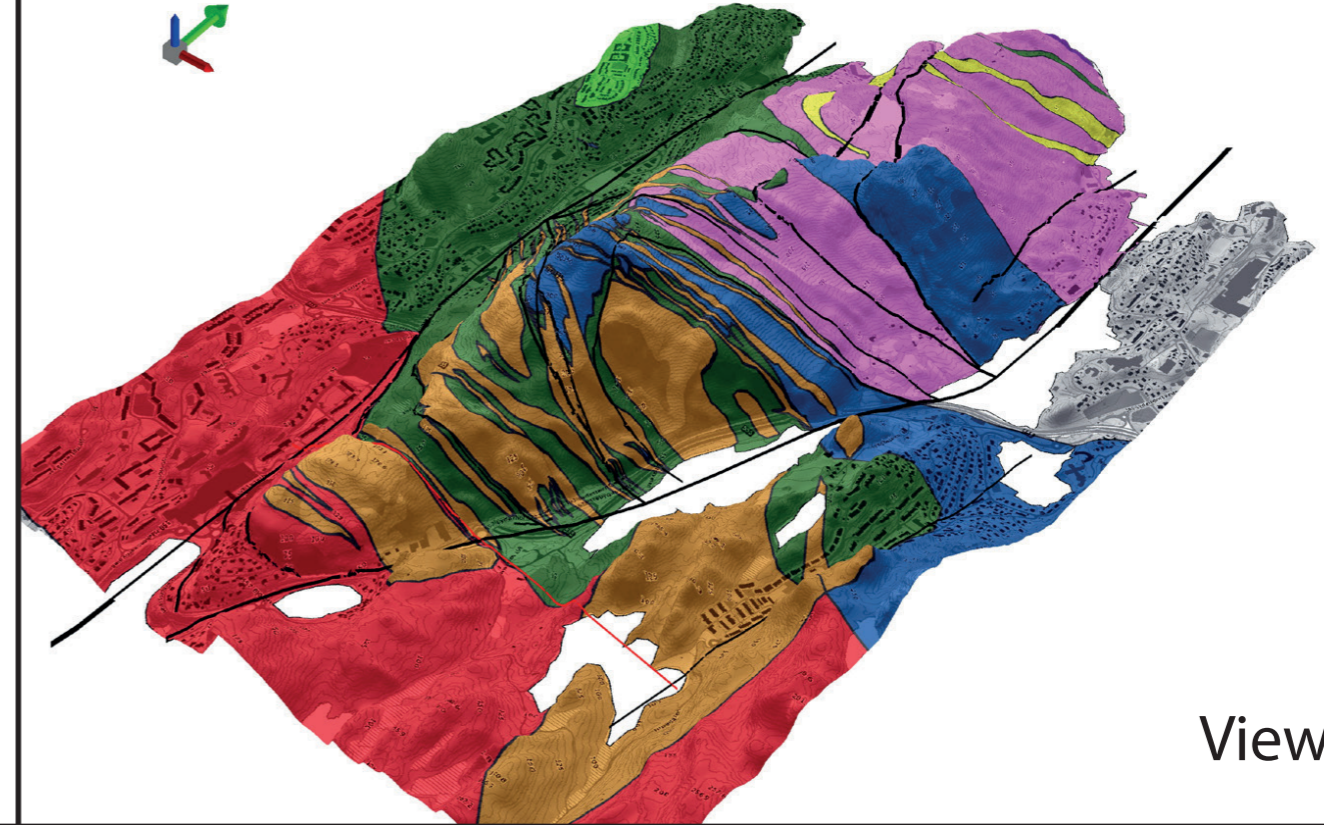
View from NW



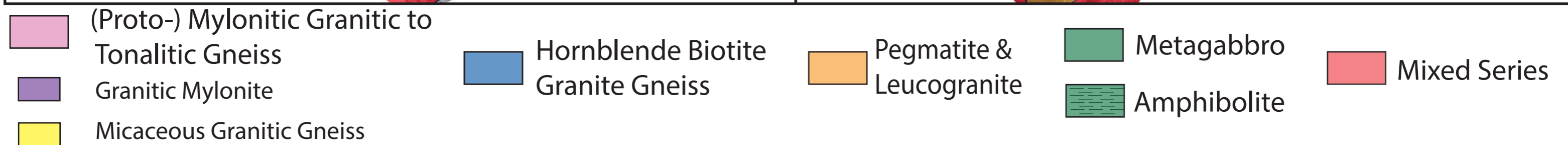
View from NE



View from SW

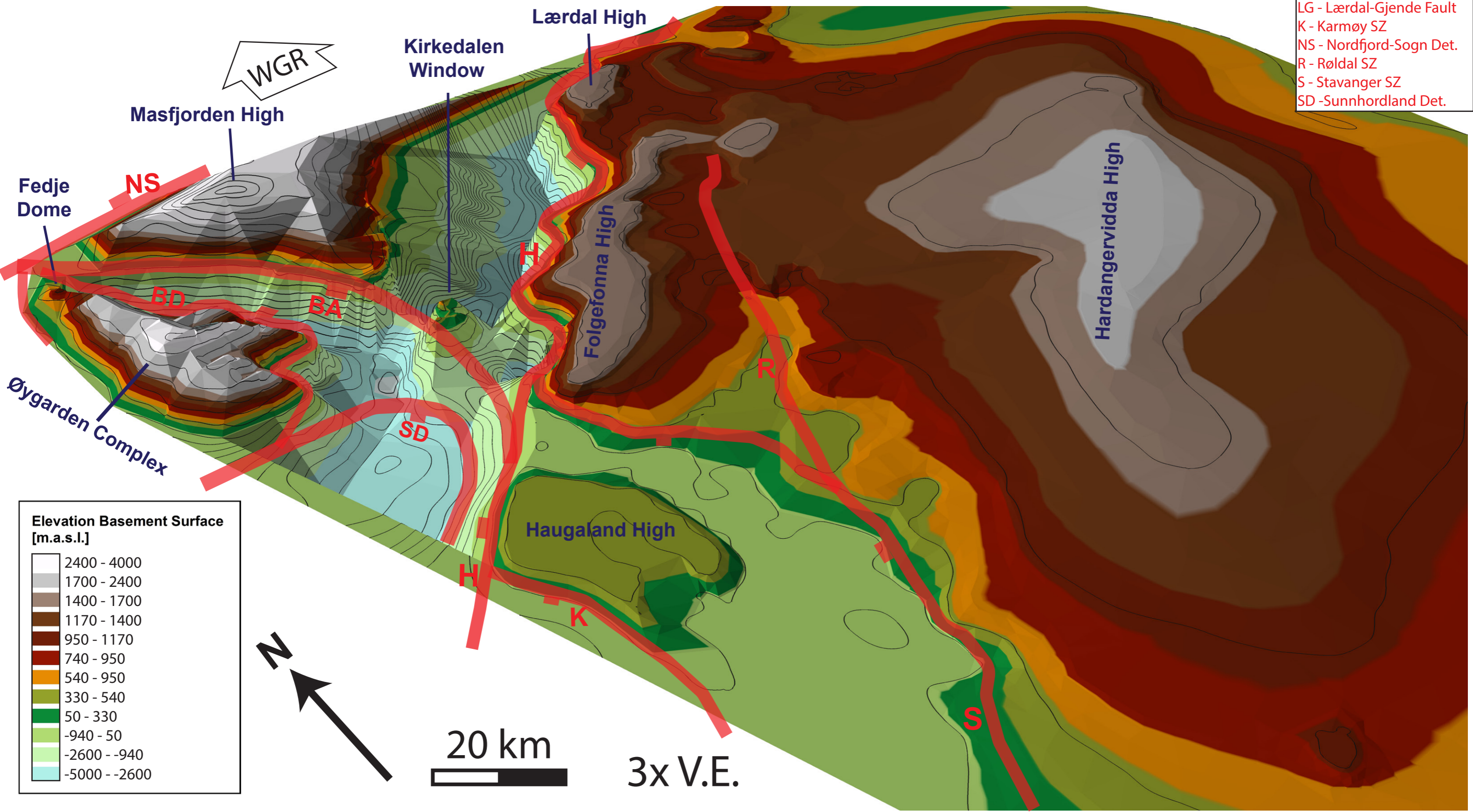


View from SE



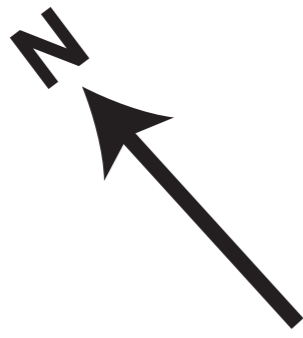
Appendix 9 - 3D Basement Surface in SW Norway

- Extensional Shear Zones**
- BA - Bergen Arc SZ
 - BD - Bergen Det. SZ
 - H - Hardangerfjord SZ
 - LG - Lærdal-Gjende Fault
 - K - Karmøy SZ
 - NS - Nordfjord-Sogn Det.
 - R - Røldal SZ
 - S - Stavanger SZ
 - SD - Sunnhordland Det.



Elevation Basement Surface [m.a.s.l.]

2400 - 4000
1700 - 2400
1400 - 1700
1170 - 1400
950 - 1170
740 - 950
540 - 950
330 - 540
50 - 330
-940 - 50
-2600 - -940
-5000 - -2600



3x V.E.